2012
Office of Fossil Energy Fuel Cell Program Portfolio

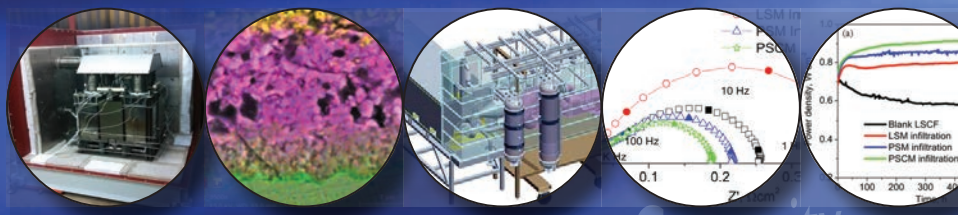

Increase Energy Security
Eliminate Carbon Footprint
Enhance Water Conservation

SECA
Solid State Energy Conversion Alliance

U.S. DEPARTMENT OF ENERGY

NETL

DOE/NETL-2012-1584

Office of Fossil Energy
Fuel Cell Program

2012 Portfolio

October 2012

Table of Contents

I. INTRODUCTION

I. Introduction

Competitive Innovation: Accelerating Technology Development

In 1999, the U.S. Department of Energy (DOE) Office of Fossil Energy, through the National Energy Technology Laboratory (NETL), founded the Solid State Energy Conversion Alliance (SECA) to develop low-cost, environmentally friendly solid oxide fuel cell (SOFC) technology suitable for diverse applications and fuels. The current focus is central electricity generation, with emphasis on the clean, efficient utilization of the nation's substantial coal reserves. More than one-third of the nation's electricity supply is generated from coal; developing technology to ensure environmentally clean and climate-friendly use of coal is of crucial national importance.

SECA fuel cells–a transformational technology–are a critical element of the Office of Fossil Energy's Advanced Energy Systems technology portfolio. The unique attributes of SOFC technology address environmental, climate change, and water concerns associated with fossil fuel–particularly coal–use, establishing a foundation for a secure energy future in the United States.

Why SOFC Technology?

Like most fuel cell technologies, SOFCs are scalable, efficient (not heat engines and therefore not subject to Carnot cycle limitations), and produce low emissions (NOx < 0.5 ppm) compared to combustion-based electrical power generation technologies (due to lower operating temperatures). However, there are a number of additional reasons why SOFCs were specifically chosen for focused development within SECA. First, relative to other fuel cell types, SOFCs are inherently fuel-flexible—they can reform methane internally, use carbon monoxide as a fuel, and tolerate some degree of common fossil fuel impurities such as hydrogen sulfide. Second, experimental data and analyses suggested that advanced SOFCs have an economically competitive cost entitlement relative to established commercial technologies and other fuel cell types. Anode-supported planar SOFCs using a thin ceramic (yttria stabilized zirconia, or YSZ) electrolyte could operate at lower temperatures (<800°C) than other SOFC types, thus allowing the use of lower-cost ferritic stainless steel interconnects, rather than the costly and difficult-to-process chromite interconnects required for higher-temperature SOFCs. Furthermore, the short conduction path (from the anode of one cell to the cathode of the next) results in lower ohmic losses and therefore higher stack efficiency and lower cost. Significantly, SOFCs are intrinsically well-suited for carbon capture in that the fuel and oxidant (air) streams are easily kept separate, thereby facilitating high levels of carbon capture without substantial additional cost.

NETL, SECA Industry Teams, and other organizations have conducted numerous system analyses for various integrated gasification fuel cell (IGFC) system configurations, with the most recent by NETL's Office of Program Planning and Analysis (OPPA) published in 2011. This work projects that SECA fuel cell technology can achieve 45% to 50% efficiency (based on higher heating value [HHV] of coal, including 99%+ CO_2 capture) with near-conventional (enhanced ConocoPhillips) gasifiers. With advanced catalytic gasification, efficiency potential is 60% HHV, with 97%+ CO_2 capture. These are near-zero emissions plants with significantly reduced water consumption relative to competing technologies due to the ability to capture and reuse the water produced within the fuel cell. The cost of electricity (COE) is competitive with or superior to (depending upon the CO_2 price) other advanced technologies under consideration (supercritical pulverized coal [SCPC], integrated gasification combined cycle [IGCC], all with carbon capture and sequestration [CCS]). Natural gas fuel cell (NGFC) systems utilizing SECA technology are also attractive alternatives to natural gas combined cycle (NGCC) with CCS. The first figure depicts both IGFC and NGFC power system configurations. The SOFC may also be pressurized, resulting in additional efficiency gains. The second and third figures compare the COE for IGFC and NGFC, respectively, over several enhancement scenarios. The fourth figure shows the significant reduction in water consumption for both IGFC and NGFC.

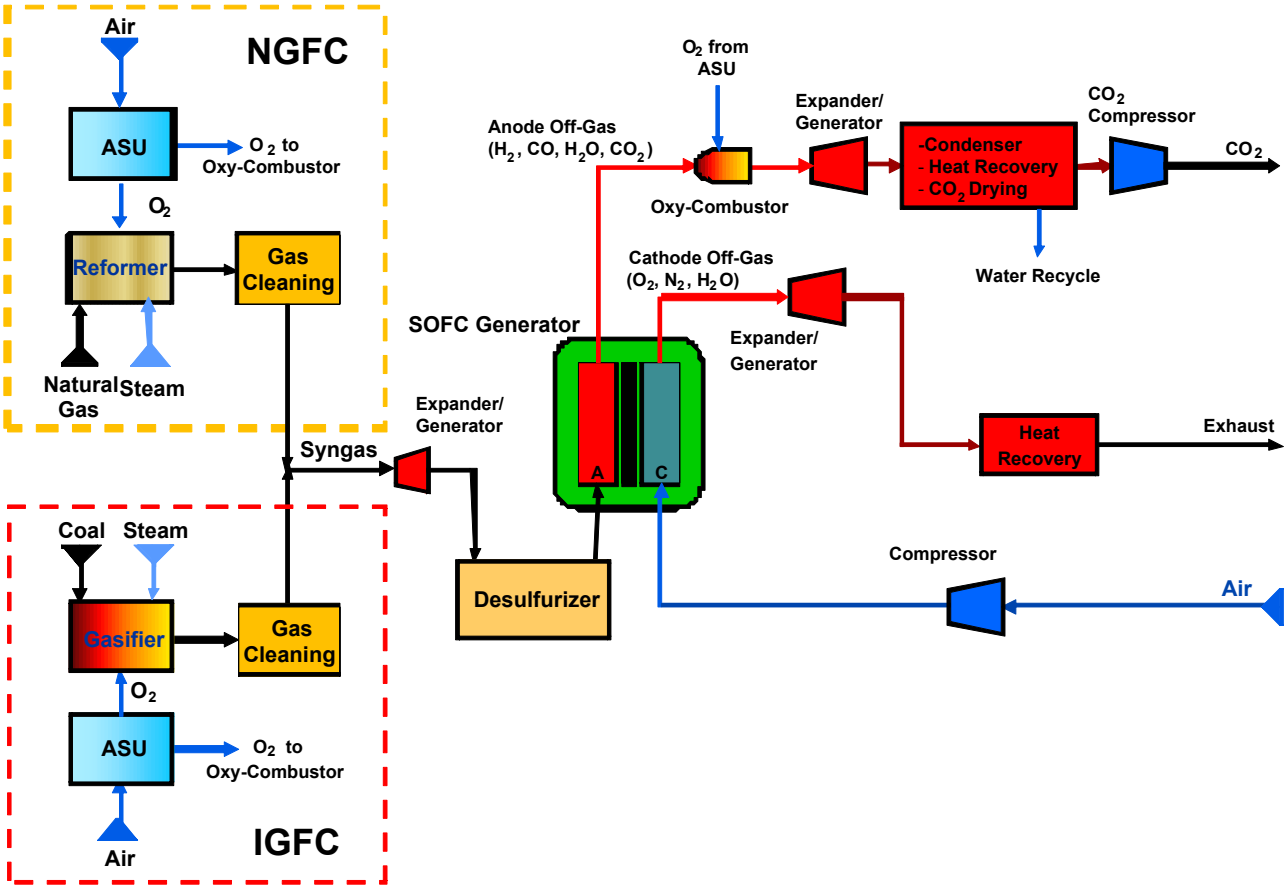

SOFC Plant Concepts: Common SOFC-based power block configuration shown, with alternative fuel supply configurations for NGFC and IGFC, respectively.

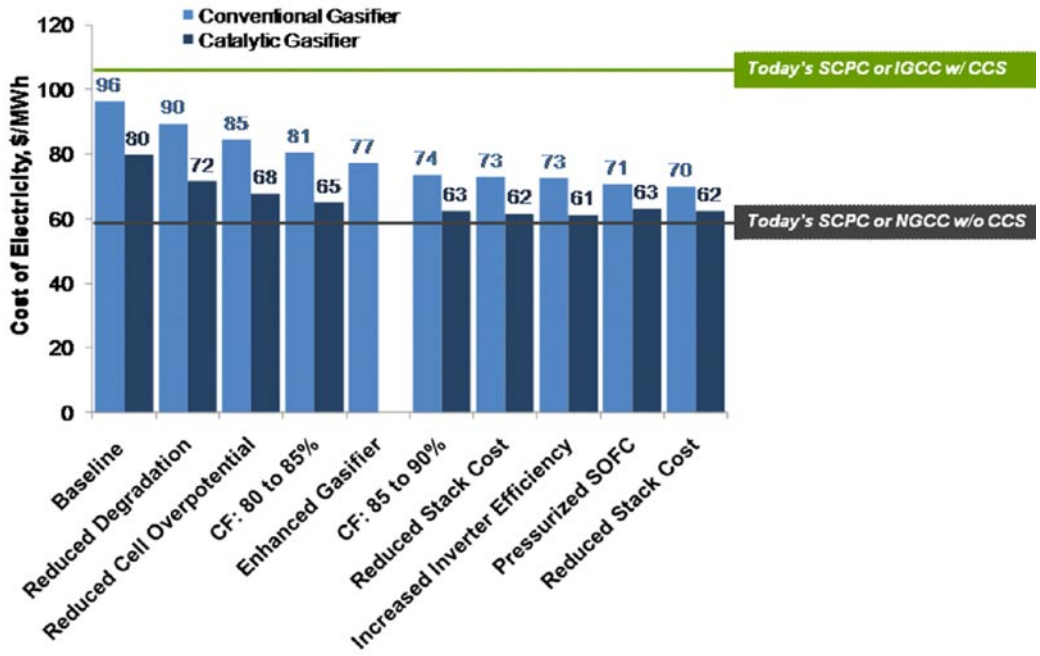

IGFC Pathway (97% - 99% CO_2 capture)

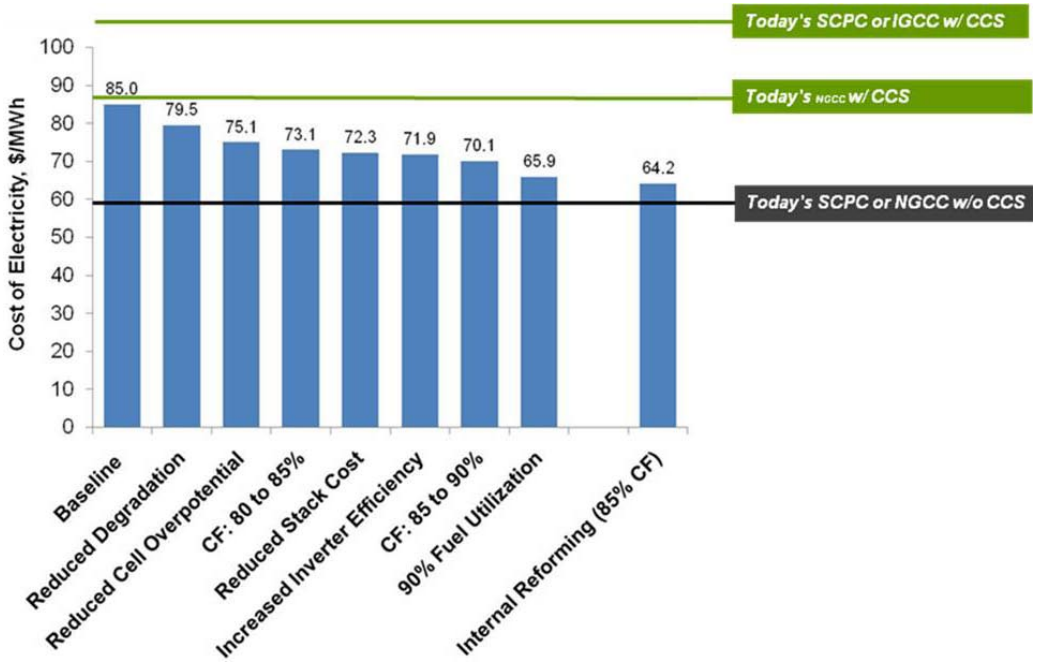

MWh = Megawatt hour

NGFC Pathway (99% CO_2 capture)

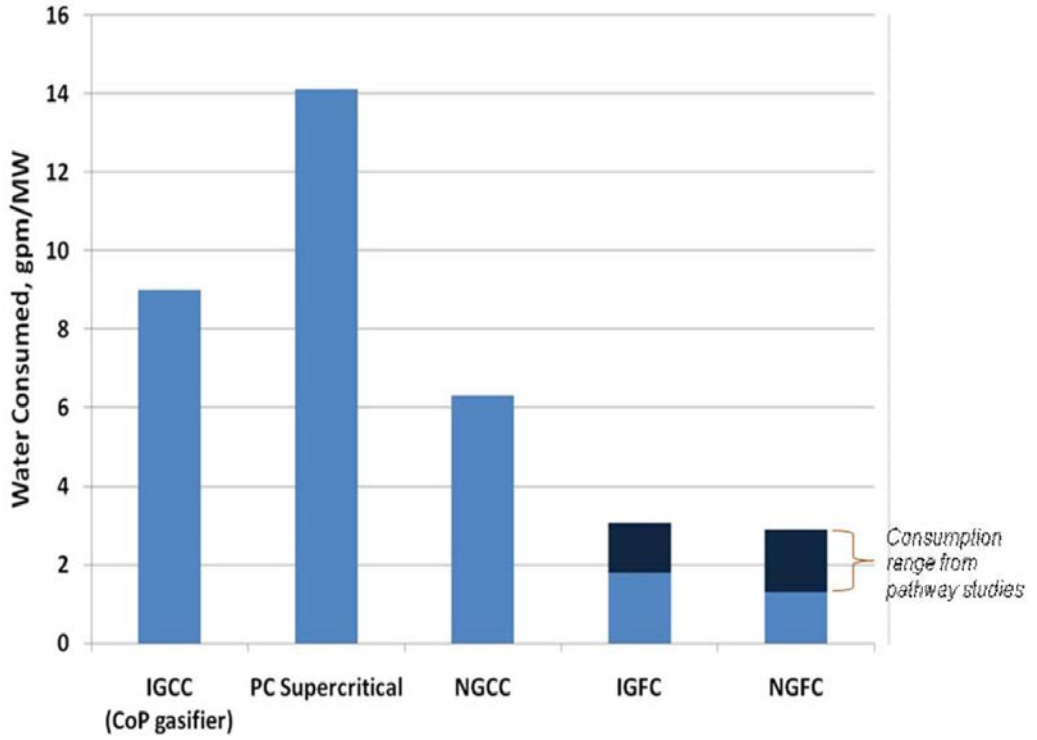

Net Water Consumption

History of the SECA Program

From its inception, SECA was structured as a unique alliance between government, industry and the scientific community. SECA is comprised of three groups: Industry Teams, Core Technology participants, and federal government (NETL) management. The Industry Teams design the fuel cell stacks and systems and are responsible for most hardware and market penetration issues. The Core Technology program element, made up of universities, national laboratories, small businesses, and other research and development (R&D) organizations, addresses applied technological issues common to multiple Industry Teams. Findings and inventions under the Core Technology program are made available to the Industry Teams, accelerating development progress. Federal government management facilitates interaction between Industry Teams and the Core Technology program element as well as establishes technical priorities and approaches. Program funding was established and maintained at approximately 65% for the Industry Teams and 35% for the Core Technology suite of projects. The inaugural SECA Industry Teams included General Electric (GE), Siemens Energy, Delphi Corporation, Cummins Power Generation/SOFCo, FuelCell Energy/Versa Power Systems (FCE/VPS), and Acumentrics Corp., all selected between 2001 and 2003.

At the time of its founding, SECA was part of the natural gas program, with an emphasis on distributed generation applications. The SECA concept was mass customization of a common 3–10 kW module that could address diverse markets—stationary power generation, military applications, and the transportation sector, e.g., auxiliary power units for Class 8 trucks. Primary fuels under consideration were natural gas and diesel. Office of Management and Budget (OMB) targets of $100/kW and $400/kW, in Year 2000 dollars, were established for stack and system costs, respectively, to be met in 2010, based upon a nominal production rate of 50,000 5-kW systems (250 MW total) per year. These 2010 targets reflected an approximately five-fold reduction in cost compared to the state of the technology that existed in 1999. Additional targets were established for other performance metrics, such as degradation (steady-state and transient). The program included rigorous periodic testing protocols to benchmark performance, with audits of the associated cost estimates.

The inaugural round of 3–10 kW Industry Team system tests was conducted between 2005 and 2007. All teams met the interim system cost ($800/kW) and steady-state degradation (4%/1,000 hours) targets over the required 1,500-hour test duration. The efficiency of these small simple-cycle systems ranged from 35% to 41% (based on the lower heating value [LHV] of natural gas [NG]).

The innovative SECA program structure, as well as the aforementioned successful testing, did not go unnoticed. In 2006, OMB cited the SECA program as leading the way in government-industry partnerships:

> *"The SECA program leverages private-sector ingenuity by providing Government funding to Industry Teams developing fuel cells, as long as the Teams continue to exceed a series of stringent technical performance hurdles. This novel incentive structure has generated a high level of competition between the Teams and an impressive array of technical approaches. The SECA program also develops certain core technologies that can be used by all the Industry Teams to avoid duplication of effort. The program exceeded its 2005 performance targets, and it is on track to meet its goal for an economically competitive technology by 2010."*

With the founding of SECA and its early success, the remaining legacy projects under the Vision 21 program and projects developing less competitive fuel cell technologies, e.g., molten carbonate fuel cell-turbine hybrids and tubular (cylindrical) SOFCs, were ended in the early- to mid-2000s.

In 2005, SECA transitioned from the natural gas program to the Strategic Center for Coal, with an emphasis on coal-fueled central electricity generation with carbon capture. New solicitations in 2005 and 2007 added projects to scale up the SECA fuel cells for application in large central electricity generation applications. Industry Team awardees included GE, Siemens, FCE/VPS, Rolls-Royce Fuel Cell Systems (RRFCS), and United Technologies Corporation (UTC)/ Delphi. Cummins withdrew from the program in 2006, as it did not have an interest at that time in the new program focus. GE scaled back from full Industry Team participation in 2006 to focus on what it saw as key SOFC technology hurdles through DOE-funded work at the Global Research Center. The Acumentrics project was transferred to DOE's Office of Energy Efficiency and Renewable Energy in 2008. By the end of 2008, there were four Industry Teams—Siemens, FCE/VPS, UTC/ Delphi, and RRFCS. The year 2008 saw another round of stack metric testing, with the interim cost ($600/kW, Year 2000 dollars) and degradation targets met by Siemens and FCE/VPS in 5,000-hour tests. UTC/Delphi and RRFCS did not test as they were both new projects.

In 2010, FCE/VPS met the ultimate $400/kW (Year 2000 dollars) target in testing of 120-cell 25-kW stacks comprised of scaled (550 cm^2) cells. By way of comparison, the typical planar SOFC stack at SECA's inception consisted of maximum 40 cells, each with an active area of ~100 cm^2, capable of perhaps 2 kW. At the

end of 2010, Siemens made a corporate decision to end its SOFC R&D program and withdrew from SECA.

Current Status of the SECA Program

The baseline for the SECA cost goals was informally updated in 2008 to $700/kW (power block) and $175/kW (stack), in Year 2007 dollars. This change was formally incorporated into the OMB targets in Fiscal Year (FY) 2011.

As mentioned above, FCE/VPS met the cost goal in 2010. In 2011 and 2012, the two later-awarded Industry Teams, UTC/Delphi and RRFCS, worked to complete SECA cost goal validation testing. In mid-2012, South Korea-based LG Electronics acquired 51 percent of RRFCS. The company will now be known as LG Fuel Cell Systems. All three industry teams are focusing on improving the reliability, robustness and endurance required for commercial central generation. This work will encompass materials R&D, design, failure analysis, and manufacturing development. It will also consist of considerable stack testing, including larger stacks, to validate performance and gather the required data to make further enhancements to the stack technology.

Fuel Cell Research and Development

The Office of Fossil Energy and NETL present this FY 2012 Fuel Cell Program Portfolio, a compilation of abstracts from the fuel cell projects managed through these offices. These abstracts are divided into subsections as detailed below.

SECA Industry Teams – Atmospheric Pressure Systems

This program element focuses on the applied R&D, scale-up, manufacturing and integration of SECA fuel cell technology operating at atmospheric pressure, ultimately resulting in fuel cell modules suitable to serve as the building-blocks for larger-scale power systems. Atmospheric pressure (relative to the SOFC stack) IGFC systems using advanced gasification technology have the potential to achieve efficiencies ≥50% with ≥99% carbon capture, near-zero emissions, and low water usage. Industry Teams will focus on large stack development and validation, and ultimately the development of 250 kW–1 MW fuel cell module prototypes that will serve as the basis for early commercial market entry and as components in central generation plants. Key R&D topics include cell and stack scaling, manufacturing, failure analysis, system integration, and materials. As the work progresses, it may extend to specialized balance of plant (BOP) hardware, controls, and instrumentation for prototype systems.

SECA Industry Teams—Pressurized Systems

This program element focuses on the applied R&D, scale-up, manufacturing and integration of SECA fuel cell technology operating at pressure (typically ≥4 bar), ultimately resulting in fuel cell modules suitable to serve as the building-blocks for larger-scale power systems. Pressurized (relative to the SOFC stack) IGFC systems using advanced gasification technology have the potential to achieve efficiencies of 60% with ≥97% carbon capture, near-zero emissions, and low water usage. Industry Teams will focus on large stack development and validation, and ultimately the development of 250 kW–1 MW fuel cell module prototypes that will serve as the basis for early commercial market entry and as components in central generation plants. Key R&D topics include cell and stack scaling, manufacturing, failure analysis, system integration, and materials. As the work progresses, it may extend to specialized BOP hardware, controls, and instrumentation for prototype systems.

SECA Core Technology R&D

The Core Technology R&D program element provides comprehensive applied research and development support in eight focus areas. This program structure reduces R&D cost by leveraging resources so that the Industry Teams do not engage in separate, redundant applied research programs, paying multiple times for the same technical solutions. Diligent NETL management of the Core Technology R&D program with this approach also ensures that only major issues are addressed. SECA's goal is to raise the technology bar in large strides rather than small steps. Core Technology R&D program areas of research are also augmented by special topics under the DOE's Experimental Program to Stimulate Competitive Research (EPSCoR) programs. The Core Technology R&D program is focused on the technologies critical to the commercialization of SOFCs:

- **Cathodes –** Improve the stability and performance of cathodes using state-of-the-art concepts and methodologies;
- **Anodes and Coal Contaminants –** Determine potential coal syngas contaminants and their impact on anode performance and stability;
- **Interconnects and Contact Materials –** Develop stable, low-cost metallic interconnects and interconnect contact materials operating in the temperature range of 650ºC to 850ºC with acceptably low area-specific resistance (ASR) and stability over the service lifetime;
- **Seals –** Develop materials and designs exhibiting adequate sealing performance with the requisite chemical and phase stability in long-term service;

- **Cross-Cutting Materials, Testing, and Manufacturing** – Develop materials and manufacturing technologies that improve fuel cell reliability, performance, and ability to tolerate fuel or air contaminants, and that achieve meaningful cost reduction;
- **Fuel Processing** – Develop fuel processing technologies that will meet application requirements such as zero water consumption, space and volume constraints, and transient capability;
- **Modeling and Simulation** – Create the tools to accelerate design cycles, predict performance, and determine the reliable operating envelope; and
- **Balance of Plant** – Develop high-temperature heat exchangers and blowers to enable high system efficiency and low cost.

Innovative Concepts

The Innovative Concepts program element evaluates and develops revolutionary advanced technologies to reduce costs and to enhance robustness, reliability, and endurance of fuel cell power systems for coal-fueled central generation, e.g., metal-supported SOFC concepts.

Small Business Innovation Research

Core Technology R&D program areas of research are also augmented by special topics under the DOE's Small Business Innovation Research/Small Business Technology Transfer (SBIR/STTR) programs.

A map of the projects described herein is shown below. The following page includes a chart of the projects by focus area. A list of all projects by state is provided in the summary at the end of this section.

Key Program Accomplishments

SECA Industry Teams—Atmospheric Pressure Systems

High Power Density 60 kW SOFC Module Successfully Developed. FCE/VPS developed a 60 kW fuel cell stack module consisting of an assembly of identical stacks to lay the foundation for scalable building blocks to be deployed in high-efficiency coal based power plants of the future. A stack module assembly includes non-repeat hardware such as the base structure, stack compression assembly, internal heat

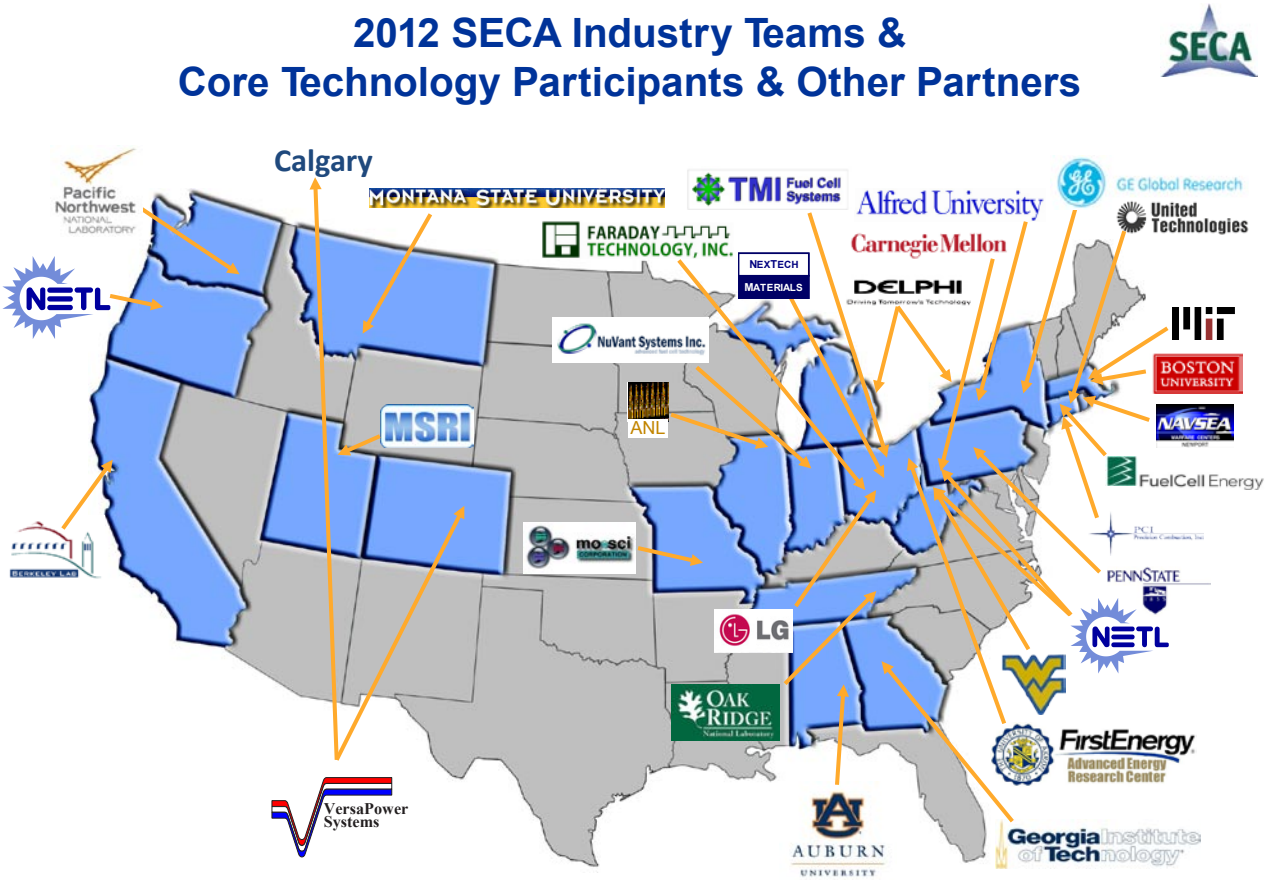

Map of focus areas of NETL projects

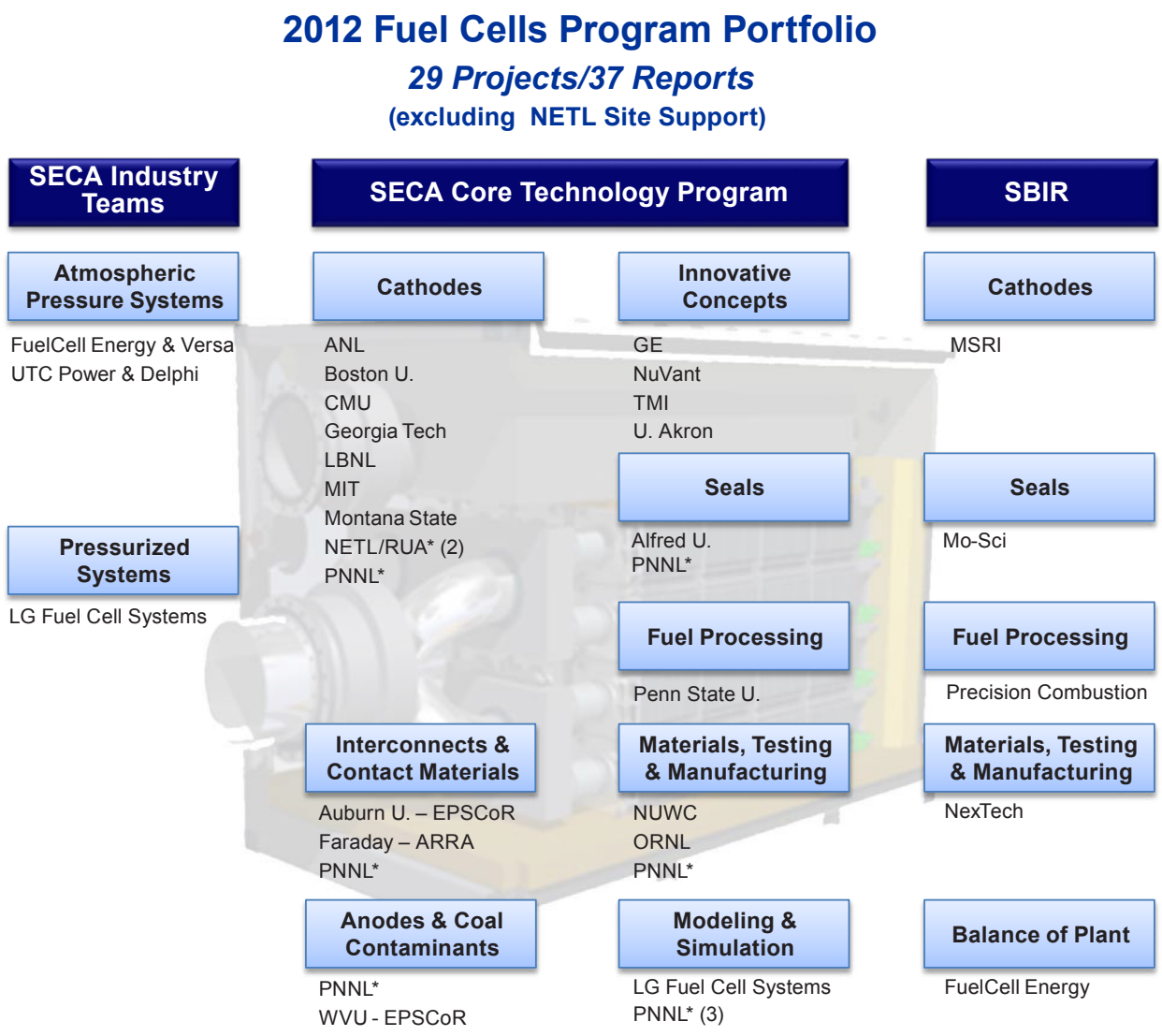

Chart of focus areas of NETL projects

exchangers for pre-heating anode inlet gas, and manifolds for distribution of anode and cathode gases to the individual stacks. A stack module assembly also includes instrumentation to provide for process control and data acquisition, as well as means for power collection and transferring direct current (DC) power from the module to the external power takeoff points. Other key non-repeat hardware includes an internally insulated enclosure to house the stacks and to provide the interface to the balance of plant equipment.

The key accomplishment included testing of the non-repeat hardware for a 60 kW proof of concept module using both cold-flow experiments as well as hot tests simulating the stack module operating environment. The tests showed that the module and the non-repeat component designs meet the system requirements under the actual operating conditions. The flow tests of the stack module verified a uniform cathode and anode flow distribution between the stacks (within 1%). The anode fuel heat exchanger tests showed better performance than predicted by yielding sufficient amount of heat to the anode gas at the operating flows. The electrical resistance measurements proved achievability of perfect dielectric isolation of stacks from the compression assembly and flow pipes at potentials up to 150% of the design value, as well as acceptable operation, i.e., low resistance, of all current collection equipment at operating temperature. The results of the tests verified the operability and robustness of the innovative features integrated in the 60 kW stack module design.

Improvements Realized in Glass Seals and Braze Seals, and Increased Endurance Leads to Increased Power on Button Cells. On the stack front, UTC/Delphi developed accelerated test strategies for the glass seal and the braze seal, and the seals successfully completed hundreds of thermal cycles. A 30-cell Gen 4 stack was built with several interfacial control concepts and was tested for 4,700 hours with the best treatment combinations degrading an average of 0.64% per 500 hours. Optimization of solids loading, firing parameters, and print screen mesh for the interlayer was completed, leading to an increase in power of greater than 50% on button cells. On the system front, Phase I endurance testing was completed after making substantial improvements to the test stand reliability. A system concept was selected for Phase II after extensive trade studies, and design of the 25 kW breadboard was completed. All balance of plant material was procured, and fabrication of the breadboard has been initiated. Finally, the design of the control strategy for the breadboard has been completed and the controls are being verified in the lab.

SECA Industry Teams—Pressurized Systems

LG's Fuel Cell Technology Meets Performance and Durability Expectations at the Block Scale Planned for Commercialization. LG Fuel Cell Systems Inc. (LGFCS), formerly known as Rolls-Royce Fuel Cell Systems (U.S.) Inc., has advanced the next generation of its integrated planar solid oxide fuel cells (IP-SOFCs) to block-scale testing. The block is the ~20 kW repeat unit designed to be the building block of MW-scale power generation systems. Block tests are being performed in specially designed test rigs able to fully duplicate the operating conditions and stack boundary conditions of high efficiency pressurized SOFC power modules projected for both IGFC plants and nearer-term natural gas fired 1 MW distributed power generation systems. An array of block test stands in Canton, Ohio, and Derby, United Kingdom, will serve to validate the durability and reliability of the IP-SOFC block technology since these tests incorporate the functional block design selected for the commercial system and utilize balance of plant ejectors, insulation, and heat exchange components representative of product. Performance targets, as measured by power output at design point operating conditions, have been achieved at the block scale, and the degradation rates have been tracking at less than 1%/1,000 hours. Subscale test articles have exceeded 16,000 hours of testing at representative system operating conditions with power degradation rates maintained at <1%/1,000 hours. Degradation mechanisms continue to be elucidated following the long term tests, and optimized anodes and cathodes are being screened for the slightly reduced degradation rate required for entry into service of 1 MW distributed generation units; current cell technology exhibits sufficient performance levels to meet the efficiency targets for the 1 MW system. LGFCS produces fuel cell modules on their prototype production line in Canton, Ohio. High volume manufacturing cost models predict system costs meeting the SECA IGFC $700/kW target and internal targets for market entry systems.

SECA Core Technology R&D—Cathodes

Oxygen Surface Exchange Behavior in Thin Film $La_{0.6}Sr_{0.4}Co_{0.2}Fe_{0.8}O_{3-\delta}$ Cathodes Studied. Using in situ synchrotron radiation techniques, the oxygen surface exchange behavior in heterostructures of $La_{0.6}Sr_{0.4}Co_{0.2}Fe_{0.8}O_{3-\delta}$/$Gd_2O_3$-doped CeO_2/Y_2O_3-stabilized ZrO_2 (LSCF/GDC/YSZ) was studied by Argonne National Laboratory (ANL). Applying electrical potentials across the heterostructure results in significant expansion or contraction of the out-of-plane LSCF lattice parameter, and those lattice parameter changes can be correlated with oxygen vacancy concentrations in the LSCF film. These results demonstrate that oxygen transport across the LSCF/atmosphere interface has a larger energy barrier than transport across the LSCF/GDC interface under both anodic and cathodic conditions. By measuring the time dependence of the heterostructure lattice response as a function of temperature and oxygen partial pressure, the exchange coefficient was determined to be ~2×10^{-5} cm/s to 1×10^{-4} cm/s in the 500°C–600ºC range with an activation energy of ~1.1 eV. The results of these measurements demonstrate that in situ X-ray techniques can be used to provide local performance data from LSCF cathodes.

Relative Importance of Surface Diffusion and Bulk Diffusion Estimated in LSCF. Patterned thin films of $La_{0.6}Sr_{0.4}Co_{0.2}Fe_{0.8}O_{3-\delta}$ (LSCF) were deposited using DC magnetron sputtering and photolithography at Boston University. Patterned thin films of various triple phase boundary lengths were fabricated, and impedance spectroscopy was performed on them. The impedance spectra modeled using a simple scaling analysis and also by a two-dimensional transport model reveal that surface incorporation followed by bulk diffusion to the two-phase boundaries is the dominant mechanism of oxygen reduction and transport to the electrolyte at low temperatures and low oxygen partial pressures. By contrast, surface adsorption, surface diffusion to the triple phase boundaries (TPBs), and incorporation at the TPBs seem to be equally important at higher temperatures and higher oxygen partial pressures. Parallel to this effort, total reflection X-ray fluorescence and hard X-ray photoelectron spectroscopy were used

to analyze the surface of calcium doped lanthanum manganite, $(La_{0.87}Ca_{0.13})_{0.95}MnO_3$ (LCM), and LSCF thin films. These measurements have revealed the LCM surfaces in our experiments to be enriched in Mn and the LSCF thin films enriched in Sr. Ancillary evidence from atomic force microscopy (AFM) reveals these Sr-enriched regions on the LSCF surface to be present in the form of islands.

Dramatic Enhancement of Oxygen Exchange Kinetics Discovered for Epitaxially-Strained $La_{0.7}Sr_{0.3}MnO_3$. Measurements of the oxygen exchange kinetics on $La_{0.7}Sr_{0.3}MnO_3$ thin films were made at Carnegie Mellon University (CMU). Films were prepared by pulsed laser deposition at CMU to have controlled surface crystallographic and microstructural features. Epitaxial (100) and (110) $La_{0.7}Sr_{0.3}MnO_3$ thin films having smooth surface morphologies were deposited on $SrTiO_3$ and $NdGaO_3$ single crystal substrates. Film thicknesses varied from 50 nm to 600 nm, and the film strain states varied from being coherently strained to the substrate to being relaxed with large dislocation contents. The chemical surface exchange coefficients, k_{chem}, a basic parameter indicative of the electrocatalytic activity of SOFC cathodes, were determined experimentally using electrical conductivity relaxation. The transient relaxation experiments were carried out from 600°C to 900°C. Two parallel surface exchange processes were observed in these films. The two k_{chem} processes had different activation energies (E_A) that were also a function of surface orientation. These two processes were assigned to (1) the defect-free surface response of individual orientations and (2) the regions of the surface having intersecting extended defects, specifically dislocations. Surprisingly, tensile strain on the (110) native surfaces led to vastly improved exchange values, being over three orders of magnitude faster than values obtained under compressive strain for the (100) surface. Even values for (110) surfaces under compressive strain were orders of magnitude greater than for (100) films under tensile strain, indicating that the nature of strain and orientation can be optimized simultaneously to improve surface exchange kinetics in SOFC electrodes.

Both Activity and Stability of LSCF Cathodes Enhanced by Surface Modification Through Infiltration. Georgia Institute of Technology has demonstrated enhancement in activity and stability of LSCF cathodes in commercial cells through infiltration of a thin catalyst. Further, Raman spectroscopy and synchrotron-based X-ray analyses have been successfully used to probe catalyst-modified LSCF cathode surface, potentially providing critical insights into the mechanism of electrode processes and a scientific basis for rational design of more efficient cathode materials and structures. Solution infiltration process was optimized for commercial cells with larger size, and the performances of the cells with catalyst-infiltration, evaluated at 750°C and 0.7 V, were directly compared with those without infiltration under the same conditions. While the commercial cells with lanthanum strontium manganite (LSM)-infiltrated LSCF demonstrated better stability and activity than the cells without surface modification, the $Pr_xSr_{1-x}MnO_{3-\delta}$ (PSM)- and $PrSrCoMnO_{5+\delta}$ (PSCM)-infiltrated cells showed even better performance than the LSM-infiltrated ones.

Promising Cathode Contact Materials Identified and Assessed. Lawrence Berkeley National Laboratory (LBNL) is focused on cathode contact material (CCM) selection and development. The primary challenge addressed during FY 2012 concerns electrical connection and bonding between the interconnect and SOFC cathode layers. Historically, cathode materials such as LSM are used as a CCM paste to bond the cell to the interconnect. High temperature is typically required to achieve good bonding, which leads to rapid oxidation of the stainless steel interconnect. If a temperature low enough to avoid oxidation of the steel (<1,000ºC) during the bonding step is employed, poor bonding and eventual delamination of the contact material occurs. The goal of the work at LBNL is to identify candidate cathode materials displaying adequate properties after bonding at <1,000ºC. To this end, novel composite mixtures of conventional cathode materials and glass or inorganic binders were developed and tested on lab-scale cells. In the developed composites, the cathode powder conducts electrons and the glass or inorganic binder serves to promote bonding within the CCM layer and at the interfaces with adjoining materials. Many glass and inorganic binders were screened and down-selected to a few promising composites. These were tested in situ for >500 hours. Encouraging stability and performance were achieved.

Spatial Variation of Surface Co Valence in LSCF Cathodes Due to Operational Conditions Measured. X-ray absorption spectroscopy (XAS) measurements of the L_{23}-edge of Co in $La_{0.6}Sr_{0.4}Co_{0.2}Fe_{0.8}O_{3-\delta}$ ($LSC_{20}F_{80}$) and $La_{0.6}Sr_{0.4}Co_{0.5}Fe_{0.5}O_{3-\delta}$ ($LSC_{50}F_{50}$) thin films deposited on a $Gd_{0.1}Ce_{0.9}O_{2-\delta}$ (GDC) layer on a YSZ electrolyte generated at Montana State University were conducted at the Advanced Light Source of Lawrence Berkeley National Laboratory to determine the spatial variation of the surface Co valence with changes in operational conditions including bias potential and humidity. A strong variation in the valence of surface elements due to non-homogenous gas flow and humidity was identified. Any study that reports surface valence values needs to demonstrate that the measured spectrum is representative of the entire surface, and not an average value across the entire surface or the spectrum associated with a single position. For degradation considerations, it is

the extremes of the elemental valence shifts that are of importance and not the average values since the extreme values represent localized positions where a degradation mechanism is active. A number of studies have shown that temperature homogeneity is an important feature of performance, so the finding that homogeneity in gas atom availability is a similarly important criterion should not be surprising. One complication is that, unlike temperature homogeneity, reactant gas atom availability changes with operation since the reactant gas is consumed, modifying its distribution and diffusion. Furthermore, the scale of local inhomogeneities is on the macroscale (100s of microns) rather than the nanoscale since rapid gas atom diffusion is sufficient to maintain a local balance at these very small scales.

Novel SOFC Cathode Infiltrate Based on EISA Technique Demonstrated. National Energy Technology Laboratory-Regional University Alliance and Carnegie Mellon University researchers demonstrated a stable mesoporous cathode infiltrate material intended for SOFCs. High surface area mesoporous $La_{0.8}Sr_{0.2}MnO_3$ (LSM) materials were generated by the evaporation induced self assembly (EISA) process and applied to the porous internal structure of the SOFC cathode in an effort to increase the overall cell efficiency. Mesoporous particle surface area and thermal stability were controlled by manipulation of the infiltrate slip chemistry, especially by alteration of the surfactant. The method was optimized to infiltrate a 10 wt% LSM charge, which possessed a surface area of >40 m^2/g and was thermally stable in cell tests at 750°C lasting more than 200 hours, in a single step. Compared to other reported infiltrate processes, the newly developed method produces the highest known single-step infiltrate loading, and the infiltrate surface area is approximately 5–10 times greater. Application of the mesoporous infiltrate reduced cell polarization resistance measured in symmetric cells by more than 20% on average, and improved full cell power density by more than 30%.

Long-Term SOFC Cathode Microstructural Evolution Examined using Phase-Field Model. A phase-field model for describing three-phase electrode microstructure, i.e., electrode-phase, electrolyte-phase, and pore-phase, in SOFCs has been formulated by National Energy Technology Laboratory-Regional University Alliance researchers. The proposed simulation framework reproduces the real electrode microstructure and describes useful material features and the effect of evolving microstructures on the material properties. Using the phase-field approach, the coupled phenomena of phase coarsening and grain growth in the three-phase electrodes (microstructural evolution) dictate the predicted bulk morphological microstructure and material features, such as porosity, interfacial area, triple-phase boundary length, etc. The model output depends significantly on the prescribed kinetic phase boundary growth parameters and three-phase volume fractions. For example, the triple-phase boundary evolution was specifically simulated and determined to be one of the principal early degradation components, though the evolution rate depends on the initial parameter values selected. The current model version will be further matured to support robust, computationally guided material design that accelerates microstructural and materials optimization in novel SOFC electrodes, and supports understanding of long-term intrinsic cell degradation using computer simulation. A letter further describing detailed results and entitled "Phase-Field Modeling of Three-Phase Electrode Microstructures in Solid Oxide Fuel Cells" was published in *Applied Physics Letters*.

Two Extended Duration In Situ XRD Tests of Cathodes on Anode Supported SOFCs Successfully Demonstrated. Two 1,000 hour in situ X-ray diffraction (XRD) tests were demonstrated on the cathodes of anode supported cells in the XRD test fixture at Pacific Northwest National Laboratory (PNNL). Both tests were conducted on cells at 750°C. One of the cells was operated under constant current conditions approximating an operating voltage of 0.8 V while the other cell was held at open circuit voltage (OCV) for the test duration. Calculations of the similarity index indicated that the rate at which changes in the XRD patterns from the operating cell occurred appeared to follow a trend similar to that of changes in the power density. Additionally, because in situ XRD experiments entail the acquisition of numerous XRD scans collected continuously throughout the extended duration test, the summation of scans over 200 hour intervals were found to accumulate count times sufficient to enable the resolution of trace phases with concentrations of less than 2 wt% in the cathode, which included $LaCoO_3$, Fe_3O_4, and Co_3O_4. In fact, using these integrated patterns, it was even possible to detect peak shifts that occurred in Fe_3O_4 and Co_3O_4 due to gradual lattice strain. Thus, the list of potential contributions of this new technique in the analysis of SOFC cathodes was further expanded.

SECA Core Technology R&D—Anodes and Coal Contaminants

WVU Researchers Further Advance Their Innovative Strategies for Operation of SOFCs on Coal Syngas. Trace impurities such as phosphine in synthesized coal gas (syngas) are harmful to conventional SOFC anode materials, which is one of the main hindrances for producing clean and efficient power from coal using SOFCs. Researchers from National Institute

for Fuel Cell Technology (NIFT) at West Virginia University (WVU) have combined multiple expertise in experimentation and modeling to address this issue. Recent experiments conducted at NIFT show that the degradation of cell performance due to PH_3 contaminant is sensitive to the fuel composition, especially the steam concentration. The secondary phases of P formed inside the SOFC anode lead to a higher rate of electrochemical degradation under wet fuel than under relatively dry fuel. Using in situ gas composition measurements, it was shown that this phenomenon was obscured in the past by air leaks in the system. On another front, the team discovered that in addition to nickel, YSZ material is also affected by the contaminant, a hitherto unknown phenomenon. To minimize the effect of contaminants, an all ceramic SOFC made of novel materials has been tested successfully. All the information gained from experiments culminated in a validated degradation model that can predict performance degradation rates over extended time using the results from accelerated tests.

SECA Core Technology R&D—Interconnects and Contact Materials

Cobalt and Nickel Improve Performance of Spinel Coatings for SOFC Interconnects. Auburn University has shown that cobalt and nickel additions are beneficial to the performance of spinel coatings used to coat ferritic stainless steel interconnects for SOFCs. These results, combined with findings related to the minimum chromium content needed in the alloy, provide a basis for designing alloy-coating systems for extending the lifetime of SOFCs. Obtaining long performance life is a critical step toward commercialization of SOFCs to take advantage of the fuel flexibility of SOFCs and provide efficient conversion using a wide variety of fuels.

Affordable Manufacturing Process for Coating Stainless Steel SOFC Interconnects Scaled Up. A cost-effective electrodeposition process to apply high-quality coatings to SOFC interconnects in a mass production scenario is being developed, optimized and validated by Faraday Technology and West Virginia University. The FARADAYIC℠ Electrodeposition Process can be used to deposit a Mn-Co alloy with a controlled composition and thickness that can subsequently be converted to a spinel by thermal exposure at high temperatures in an oxidizing environment. Faraday has scaled its process capabilities from 25 cm^2 to 100 cm^2 SOFC interconnects and demonstrated the ability to coat interconnects containing gas flow field features. Continued analysis and refinement of the economic assessment based on using batch manufacturing for the pulse reverse electrodeposition process demonstrated that the innovative coating technology can meet DOE's high volume target of 1.6 million plates per annum for 250 MW fuel cell stacks at a cost of ~$1.85 per 625 cm^2 coated interconnect.

Long-Term Evaluation of Protective Interconnect Coatings Approaches Three Years. $(Mn,Co)_3O_4$ (MC) spinel exhibits promising behavior as a protective layer on candidate SOFC interconnect steels. A Ce-modified version of the coating was developed at PNNL to improve the interfacial adhesion between the steel substrate and the oxide scale that grows beneath the spinel coating. Tests to evaluate the long-term performance of the coated steel are in progress. In one such test, AISI 441 ferritic stainless steel, coated with Ce-modified manganese cobalt (Ce-MC) spinel, has exhibited low, relatively stable area-specific resistance after 25,000 hours at 800ºC (the test is still in progress). This coating/steel combination also exhibited excellent performance in a ~6,000 hour test under realistic SOFC stack operating conditions (using the SECA Core Technology Program stack test fixture). To further improve oxide scale adhesion and spallation resistance, a series of surface treatments (performed by Allegheny Ludlum) are also under long-term investigation. Ce-MC coatings were applied to the surface treated AISI 441 and then subjected to oxidation testing at 800°C and 850ºC in air. Over 18,000 hours of testing at 800ºC, and 12,000 hours of testing at 850ºC, spinel-coated, surface-treated coupons, e.g., surface blasted or surface ground, have exhibited substantially improved spallation resistance compared to spinel-coated mill reference coupons. The long-term surface treatment oxidation tests are still in progress.

SECA Core Technology R&D—Seals

Stability of Viscous Glass Sealants During Temperature Cycling and Under Hydrogen Demonstrated. Detailed study of down-selected galliosilicate glasses at Alfred University focused on their stability under temperature cycling and under hydrogen. The GaBA series are low-alkali galliosilicate glasses for sealing at 850°C, while the GaSiB series are alkali-free galliosilicate glasses for sealing at 750°C. Three of the four glasses are partially crystalline after sealing, and the fourth remains almost completely amorphous. Therefore, this set of sealants provides a wide range of engineering options for implementation into SOFC designs; the crystalline phases act as a composite reinforcement to reduce the overall seal viscosity. In both air and dry hydrogen, the stability of the chosen glasses is excellent, with no changes in the microstructures noted for samples in contact with Al_2O_3-coated stainless steel and 8YSZ. Thermal cycling does not affect the crystallized glasses to any quantifiable extent, lending confidence in the materials for application at 750°C and 850°C.

SECA Core Technology R&D—Fuel Processing

Adsorption Capacity Performance Improved by Optimizing the Adsorbent Preparation Method. Adsorbent materials are used for upstream clean-up of alternative fuel sources, such as anaerobic digester gas (ADG), for SOFC applications. Research at Pennsylvania State University's Earth and Mineral Sciences Energy Institute has led to improvements in adsorption capacity performance. Previous work at Penn State has shown that Cu-Ti-Ce mixed metal oxide adsorbents with the molar ratio of 1:9:1 for Cu:Ti:Ce are superior to the commercial SulfaTrap R7 adsorbents. The effect of preparation method, including co-precipitation and impregnation method, on the performance of the adsorbent has recently been studied. It was found that the adsorbent prepared by co-precipitation method at the pH value of 7 has the best capacity. The prepared adsorbents have also been characterized by N_2 physisorption and H_2 temperature programmed reduction. The results suggested that the high capacity may be attributed to the highly dispersed CuO phase and relatively higher surface area. Furthermore, the regenerability of the Cu-Ti-Ce adsorbent has been investigated over numerous cycles. Although the capacity decreased with increasing number of cycles, the capacity after five cycles still reached 0.95 mmol H_2S/g Ads (or 3.2 wt%), about 30% higher than that for the fresh TDA SulfaTrap R7 adsorbent. This implies that the CuO-TiO_2-CeO_2 (1:9:1) adsorbent being developed by Penn State is promising for H_2S removal from biogas streams. The integrated SOFC system test was conducted with hydrogen, ADG, and reformed diesel fuel.

SECA Core Technology R&D—Modeling and Simulation

Multi-Physics Computer Code at LG Fuel Cell Systems Extended to Transient Calculations of Large Scale Models. LG Fuel Cell Systems, Inc. (LGFCS) (formerly Rolls-Royce Fuel Cell Systems) has developed a multi-physics computer code (MPC) for SOFC performance calculations of the LGFCS fuel cell structure to support fuel cell product design and development. The MPC is based in the CD-adapco STAR-CCM+ computational fluid dynamics software package which has been enhanced with new models that allow for coupled simulations of fluid flow, porous flow, heat transfer, chemical, electrochemical and current flow processes in SOFCs. The MPC user interface includes a set of Java macros to automate all STAR-CCM+ tasks and a Microsoft Excel spreadsheet to store model inputs and outputs. The MPC has been extended from steady-state to transient calculations, which requires the capability to analyze a range of time scales from small values (<0.1 seconds) associated with fluctuations in electrical currents to large values (>1 second) associated with changes to convective flow and thermal boundary conditions. The MPC has been enhanced with an acceleration algorithm to greatly reduce the time taken to obtain converged solutions on large scale models for both steady-state and transient calculations. The MPC executes this algorithm during run time, and an interface has been developed to enable it to communicate with STAR-CCM+. Steady-state simulations of bundle models have been successfully validated against experimental data obtained by LGFCS, and working transient calculations have been demonstrated up to the bundle model scale.

Healing Behavior of SCN-1 Glass Sealant Quantified through Mechanistic-Based Model at PNNL. The usage of self-healing glasses as hermetic seals is a recent advancement in sealing technology for planar SOFCs. Because of its capability for restoring its mechanical properties at elevated temperatures, the self-healing glass seal is expected to provide high reliability in maintaining the long-term structural integrity and functionality of SOFCs. In order to accommodate the design of and to evaluate the effectiveness of such engineering seals under various thermo-mechanical operating conditions, a mechanistic-based self-healing model was developed at Pacific Northwest National Laboratory to quantitatively capture and predict the crack healing behavior of SCN-1 glass. The model was calibrated by experimental measurements combined with the kinetic Monte Carlo model methodology.

It was found that high operating temperature shortens the healing time. For the cases being considered, crack closure is mostly dominant at extremely high temperatures (>900ºC), while the crack healing stage primarily determines the total healing time at low temperatures (<800ºC) when interfacial diffusion is considerably slower. A high external confining pressure accelerates crack healing. However, such influence becomes less effective as the temperature decreases. In addition, the healing rate is highly sensitive to the healing activation energy, which may be affected by environmental or surface chemical conditions. Higher activation energy hinders the healing process while lower activation energy shortens the healing time.

SOFC Modeling Software Benchmarked against Experimental Data. The Solid Oxide Fuel Cell Multi-Physics (SOFC-MP) software tool developed by Pacific Northwest National Laboratory to predict the temperature and current density distributions within planar multi-cell SOFC stacks was successfully benchmarked against experimentally measured data from a state-of-the-art stack. The data comprised in situ thermocouple measurements from multiple cells in a tall stack with sufficient resolution to capture the temperature

profile along the fuel flow direction during operation. Model simulations were then performed for ten cases with different fuel compositions and temperature boundary conditions. The numerical predictions matched well with the experimental data. In particular, the temperature distribution with different amounts of steam-methane reformation (SMR) occurring on the cell was well captured. The use of the endothermic SMR reaction directly on the SOFC anode is highly desirable for stack cooling and must be well understood for successful usage of coal and natural gas fuel compositions. This successful benchmarking of the numerical model against experiments ensures that the approach adequately captures the physics of interest, and stack designers can now use the tool to predict the operating temperature field of their SOFC designs with different fuel compositions.

Tool Developed to Generate Reduced Order Models for SOFC System Modeling. A modeling framework that automatically creates reduced order models (ROMs) for SOFC stacks was created by Pacific Northwest National Laboratory. Simulations for operation and control of an entire power generation system require numerical submodels for every individual component. Computationally fast thermodynamic submodels are conventionally used for SOFCs but lack any insight to distributions of temperature and other key parameters within the stack. Highly detailed SOFC stack models exist for design purposes but are much too computationally slow for use in system-level simulation. The developed tool solves this dilemma by utilizing the existing detailed model to generate a computationally efficient ROM. The framework interface guides the user through the analysis procedure, samples and interrogates the multi-parameter operating space using the detailed stack model, performs regression to generate the response surfaces, and implements the response surfaces into a ROM submodel for general use within system modeling software. The framework also contains integrated graphical tools for sensitivity and error analysis to ensure that the design space sampling and regression is sufficient for the ROM to approximate the highly nonlinear stack response. Therefore, this ROM tool provides a useful way for the modeler to leverage deep knowledge from a detailed SOFC model and package it within a fast submodel for study of power generation systems.

Innovative Concepts

Thermal Spray Manufacturing of SOFCs Successfully Demonstrated. A key barrier to the commercialization of SOFCs is the excessively high capital cost involved with developing a manufacturing infrastructure for fabricating sufficient quantities of the multilayered cells for demonstration units. In addition, to accommodate low initial rates of market adoption, low-cost manufacturing is imperative to establishing a commercially viable fuel cell technology business. Progress in thermal spray manufacturing technology at GE Global Research, through support of the DOE SECA program, has demonstrated feasibility for dramatically reducing low-volume SOFC manufacturing costs. Recently, single cell performances have been demonstrated at 0.5 W/cm^2. In addition, the thermal sprayed cells exhibited excellent hermeticity with open circuit voltage values comparable to conventional sintered cells. The thermal spray manufacturing process is scalable to a large cell area, reducing part count, and is a modular process that allows flexibility in accommodating production volume and design changes, a critical feature for producing demonstration/prototype units. In addition to significantly reducing capital costs, thermal spray manufacturing builds an integrated electrolyte-to-metal seal, eliminating the need for the traditional post-fabrication glass sealing methods. Continued development with the DOE SECA program will focus on optimizing the manufacturability of these cells to ultimately build stacks and systems.

Improved Flowfield Structures for Direct Methanol Fuel Cells Developed. A unique direct methanol fuel cell design has been developed by NuVant that enables use of highly concentrated fuel streams while mitigating, in large part, fuel crossover within the cell. Reduced methanol crossover significantly improves fuel efficiency and power generation per unit volume of fuel solution, also known as gross fuel energy density (GFED). The new configuration required design of a porous graphite barrier plate that would regulate the delivery of methanol fuel (which can be synthesized from gasified coal) to the cell electrodes, while also normalizing the fuel concentration across the surface of the electrode. The patterned plate, or integrated flowfield diffusion layer (IFDL), was evaluated and optimized using Fluent computational fluid dynamics modeling software. In order to correlate the model to experimental data, one side of the IFDL plate must be treated with a hydrophobic coating to allow for the products to readily exit the fuel cell and to optimally direct the flow of the liquid feed methanol. A Teflon® coating/impregnation method is being developed to evenly coat the single side of the IFDL plate. Fuel cell testing was performed with the non-treated IFDL plates, and GFED reached a maximum of 781 Wh/L with fuel utilizations up to 79.4% for cells that have operated up to 80 hours in duration. Mathematical modeling of the entire fuel cell is being employed to rapidly optimize the GFED and fuel utilization by varying fuel cell parameters. These results will be correlated with experiment and can help predict the appropriate configurations to improve the GFED to 1000 Wh/L or greater without significant losses in fuel

utilization. A small stack, consisting of two fuel cells connected in series, has been constructed and evaluated. Work is underway to minimize the fluctuations in cell performance. A furnace has been purchased to enable rapid prototyping of IFDL plates and to thermally flow Teflon® modified IFDL plate.

Fuel Cell Stack with Low Cost Metal Alloy as Current Collector Developed. The University of Akron designed and fabricated a fuel cell stack by integration of three and five Ni/YSZ anode-supported fuel cells in series. The series configuration was achieved with low cost metal alloy connecting the anode of each cell to the cathode of the adjacent cell. The metal alloy interconnects and current collectors were tailored by coating with a highly conductive paste to improve the durability and decrease the resistance. Low resistance of the interconnects and current collector allows the three- and five-cell stacks to produce open circuit voltages of 3.0 V and 4.6 V, respectively, which are close to the expected fuel cell Nernst potential. The result from this study provides an insight into the fabrication process and operating conditions of the coal-based fuel cell.

SBIR – Cathodes

SOFC Cathode Enhancement Accomplished through the Development of a One-Step Vacuum-Assisted Infiltration Technique. A cost-effective, one-step vacuum pressure infiltration thermal treatment (VPIT) technique was developed by Materials & Systems Research Inc. (MSRI), teaming with Argonne National Laboratory (ANL), and was implemented successfully on scalable cells with per-cell active area varying from 2 cm^2 to 100 cm^2. LSM-8YSZ-based cathode backbone microstructures were engineered for allowing an active catalyst to be loaded heavily enough to cover the cathode grains, particularly along the triple-phase boundaries. Strontium-doped samarium cobaltite ($Sm_{0.6}Sr_{0.4}CoO_3$, or SSC) was investigated as the electrocatalyst. Important parameters affecting the one-step infiltration process were tailored for an efficient infiltration of the SSC precursor solution, including the solvent physical properties (such as polarity, surface tension, and gelation rate) and infiltration conditions (SSC precursor concentrations and the SSC loading level). Extensive studies of the precursor concentration effects on the infiltration efficiency and cell performance improvement showed that a highly concentrated precursor solution (1.4 M) was much desirable. Long-term stability tests of the infiltrated cells repeatedly showed performance improvement, but also promoted a proper measure to be taken to sustain the performance enhancement longevity. A strategy to mitigate the nano-sized particle growth and coarsening issue was developed in Phase I by properly organizing the catalysts at desirable deposition locations. The resulting cells (treated cells or SSC-S3-5-s) were evaluated and showed significant improvement by demonstrating a degradation rate less than 2.5% /1,000 hours over a 2,500 hour test. Periodical voltage-current sweeps and electrochemical impedance spectroscopy measurements suggested that the mitigation solution retains the activity of the infiltrated nano-sized SSC catalysts effectively. Proof-of-concept tests of a hybrid stack comprising both a baseline cell and SSC catalyst infiltrated cells successfully demonstrated the feasibility of implementing the advanced one-step VPIT technique for practical large-scale applications.

SBIR – Seals

High-Temperature Viscous Sealing Glasses Exhibit Promising Behavior for SOFCs. The compositional range for glasses to be used as viscous seals for SOFCs explored in Phase I has been expanded, and forty-three new compositions were prepared and analyzed in the current reporting period by Mo-Sci Corporation. Three compositions with improved properties compared to the preferred glasses developed in Phase I were selected for more detailed study. Viscosity measurements indicate that 'self-healing' behavior should be possible at temperatures as low as 675°C for these new glasses. Interfacial reactions of the new sealing glasses with aluminized 441 stainless steel (SS441) and a nickel/yttria stabilized zirconia (Ni/YSZ) bilayer tested at elevated temperatures show that the new glasses are thermo-chemically compatible with the SOFC materials. Glass stability against volatilization was measured at 750°C for 2,000 hours, and the total weight loss of Glass 73 was calculated to be 4.5% under flowing wet forming gas and 1.9% under stagnant dry air after the 40,000 hour design lifetime. Hermetic seal tests were conducted using a newly constructed test manifold. A seal between SS441 and a Ni/YSZ bilayer with Glass 73 has survived 80 thermal cycles (room temperature to 750ºC) to date under dry air over the course of >2,500 hours. Another Glass 73 seal has survived 48 thermal cycles to date under wet forming gas. Self-healing of glass seals that were intentionally cracked by thermal shock was observed for SS441/ Glass 73/YSZ-bilayer samples reheated to 800°C. In summary, the new glasses possess desirable thermo-mechanical and thermo-chemical characteristics and exhibit promising hermetic sealing and self-healing behavior under SOFC operational conditions.

SBIR – Cross-Cutting Materials, Testing, and Manufacturing

Low-Cost Protective Coatings for SOFC Interconnect Components Developed. NexTech has developed a low-cost aerosol spray deposition

coating process for applying protective oxide coatings to metallic components, enabling their adoption as alternatives to traditional ceramic interconnect materials for intermediate temperature SOFCs. Comprehensive strategies have been identified for translating the pilot-scale process to high-volume production, where it is capable of providing low-cost coatings (<$2/part) at 400 MW annual stack production volumes. Refined cost and manufacturing models have been developed to encompass volumes from prototyping through pilot-scale production and high-volume production, with strategies identified to reduce volume manufacturing costs within each regime. In parallel to the cost and manufacturing analysis, performance validation of the protective coating has been performed and an integrated predictive model of coated interconnect lifetime based on likely failure mechanisms developed. Coated samples have displayed excellent electrical performance and stability in representative operating conditions at temperatures between 800°C and 900°C for greater than 1,000 hours. Further validation of the coating was achieved through application-specific stack testing. Degradation rates for cells with interconnects without the protective coating were five times higher than for cells with coated interconnects, and long-term three-cell stack testing with coated interconnects has demonstrated excellent stability for greater than 1,000 hours, running at 800°C under constant load.

SBIR – Fuel Processing

Cost-Effective Fuel Flexible Reformer Operates at Water Neutral Conditions. Precision Combustion, Inc. (PCI) has previously successfully demonstrated efficient, durable, fuel flexible autothermal reformer (ATR) operation under water neutral condition. Development of a low pressure drop nozzle was continued to demonstrate ATR operation with no evidence of inlet feed unmixedness or coking. This low pressure nozzle has been tested with an ATR fuel reformer using Tier II diesel for a total of about 300 hours in order to evaluate and demonstrate the long-term durability under water neutral condition. Test results showed relatively stable catalyst temperature profile and comparable reformate composition to PCI's high pressure nozzle. This developmental effort will lead to minimized parasitic losses for the auxiliary power unit system while providing uniform flow and reliable performance over a wide operating range. Additionally, through the Phase II Supplemental effort awarded in 2010, PCI has successfully scaled up the preparation method for an alternative, cost-effective catalyst and performed multiple tests to determine the applicability, effectiveness, and durability of this material for practical, low cost, stand-alone diesel fuel ATR operation. PCI has investigated and evaluated NETL catalysts as a path toward comparing different catalyst options to determine the optimal catalyst for fuel reformer application and commercialization. Testing of the pyrochlore catalyst at different metal catalyst loadings was completed and compared with standard PCI reforming catalyst. Tests are ongoing to develop the performance maps and to optimize the operating conditions for both NETL's Rh-pyrochlore catalyst and PCI's Rh catalyst formulation. Testing of PCI's fuel reformer using different biodiesel blends (B-50, B-73 and B-99) was successfully performed to demonstrate the fuel flexibility of the reformer system. Finally, a full balance of plant system was integrated with a 5 kWth ATR and was utilized to perform steady state reactor operation at 3–5 kWth power levels.

SBIR – Balance of Plant

Catalytic Heat Exchanger for Preheating Cathode Air in SOFC-based Systems Successfully Developed and Validated in Lab-Scale Testing. To reduce the balance of plant (BOP) costs of SOFC-based systems, FuelCell Energy has developed a catalytic heat exchanger which combines the functionalities of two pieces of equipment—the cathode air preheater and catalytic oxidizer—into a single multi-functional device. The conceptual design of a highly effective catalytic cathode air preheater, which is expected to meet all process requirements in terms of thermal performance and pressure drop, was developed for application in a 60 kWe SOFC power plant. The design has advantages over the conventional separate catalytic oxidizer and cathode air preheater design in terms of:

- More compact physical dimensions resulting in a significantly smaller BOP.
- Increased plant performance due to less heat loss and pressure drop associated with two separate pieces of equipment.
- Projected cost savings at high volume production of up to 80% compared to the conventional separate catalytic oxidizer and cathode air preheater design.

A lab-scale (3 kWe) catalytic heat exchanger was designed, fabricated, and tested to validate the design features developed for the 60 kWe unit. The 3 kWe heat exchanger exceeded the thermal performance requirements (when corrected for test facility temperature limitations) and demonstrated low pressure drop. The robustness of the design to self-regulate maximum temperature at up to twice the design fuel flow rate was demonstrated. Overall, the feasibility of a catalytic heat exchanger for SOFC systems was verified. FuelCell Energy intends to utilize the developed design on future 60 kWe SOFC system demonstrations.

SECA Adds Core Technology R&D and SBIR Projects

There were two solicitations in FY 2012. Under the Core R&D Funding Opportunity Announcement 677, four projects were selected for electrochemical performance enhancement activity, and three projects were selected for durability of cathode materials. Four new Phase I projects were selected under the SBIR/STTR solicitation. These 11 new projects are listed below.

New Projects in FY 2012

University/Company	Project Title
Electrochemical Performance Enhancement	
Leland Stanford Junior University	Surface-Modified Electrodes: Enhancing Performance Guided by In-Situ Spectroscopy and Microscopy
University of Wisconsin	Enhancement of SOFC Cathode Electrochemical Performance Using Multi-Phase Interfaces
Boston University	Unraveling the Role of Transport, Electrocatalysts, and Surface Science in the SOFC Cathode Oxygen Reduction Reaction
West Virginia University Research Corporation	Fundamental Understanding of Oxygen Reduction and Reaction Behavior and Developing High Performance and Stable Cathode with Heterostructured Surface
Durability of Cathode Materials	
University of Connecticut	Study of the Durability of Doped Lanthanum Manganite Cathode Materials "Real World" Air Exposures Atmospheres
University of Maryland	Mechanistic Enhancement of SOFC Cathode Durability
Georgia Tech Research Corporation	Fundamental Investigation and Rational Design of Durable, High-Performance SOFC Cathodes
SBIR/STTR	
SEM-COM	Stable Glass-Ceramic Nanocomposites as Compliant Seals for SOFCs
NexTech Materials	SOFC Protection Coatings Based on a Cost-Effective Aluminization Process
nGimat	Low Cost Spray-On Coatings for Protection of SOFC Interconnects and BOP Components
QuesTek Innovations	Low-Cost Alloys for High-Temperature SOFC System Components

2012 Annual SECA Workshop in Pittsburgh, Pennsylvania

The SECA program held its 13th annual workshop July 24–25, 2012, in Pittsburgh, Pennsylvania. Dan Rastler, senior manager of Strategic Initiatives & Demonstrations for Electric Power Research Institute (EPRI), and Haukur Asgeirsson, manager of Power Systems Technologies at DTE Energy, were the featured speakers. Principal investigators of projects made oral and/or poster presentations on recent findings, conclusions, and recommendations, which will be used by DOE to guide future work and to make programmatic and funding decisions for the upcoming fiscal years. The workshop proceedings can be found on the program's website at http://www.netl.doe.gov/seca.

Summary

SECA met its final power block cost goal of $400/kW (Year 2000 dollars) in 2010. Driven by Industry Team feedback and extensive systems analyses, SECA is now aggressively pursuing R&D to address remaining commercialization hurdles, with particular emphasis on SOFC stack robustness, reliability and endurance. The near- to mid-term goal is the validation of scaled, low cost entitlement stacks in a system configuration, up to and including modules suitable for use as the building blocks of multi-MW systems.

SECA will ultimately enable construction and utilization of fuel cell-based, near-zero emission coal and natural gas power plants with greatly reduced water requirements, capable of capturing 99% of carbon at costs not exceeding the typical cost of electricity available today. Achievement of this goal will have significant impact for the nation, given the size of the market, expected growth in energy demand, and the age of the existing power plant fleet. This is particularly important to the nation's energy security, given abundant domestic fossil energy resources. Federal funding support of this research is appropriate due to the game changing, transformational nature of the technology, accompanied by risks higher than the private sector initially can accept. In parallel, SECA Industry Teams will take advantage of the inherent scalability and fuel flexibility of SOFCs in seeking nearer-term, smaller-scale commercial applications for this efficient, environmentally friendly technology which have less risk than a first-of-a-kind full-scale IGFC (or NGFC) system. Success in these spin-off applications, e.g., distributed generation, military, will further SOFC technology advancement and widespread commercial deployment through the resultant manufacturing and operational experience.

2012 Fuel Cells Portfolio Projects by State

New Projects in Italics

State	Project Title	Performer Name
Alabama	Effect of SOFC Interconnect-Coating Interactions on Coating Properties and Performance	Auburn University
California	Catalyst Infiltration in Support of Anode Supported Cell Development	Lawrence Berkeley National Laboratory - LBNL
	Surface-Modified Electrodes: Enhancing Performance Guided by In-Situ Spectroscopy and Microscopy	*Leland Stanford Junior University*
Connecticut	High Performance Catalytic Heat Exchanger for SOFC Systems	FuelCell Energy Inc.
	Novel Water Neutral Diesel Fuel Processor and Sulfur Trap	Precision Combustion, Inc.
	SECA Coal-Based Systems - FuelCell Energy	FuelCell Energy Inc.
	SECA Coal-Based Systems - UTC Power	UTC Power Corporation
	Study of the Durability of Doped Lanthanum Manganite Cathode Materials "Real World" Air Exposures Atmospheres	*University of Connecticut*
Georgia	Theory, Investigation and Stability of Cathode Electro-catalytic Activity	Georgia Tech Research Corporation
	Fundamental Investigation and Rational Design of Durable, High-Performance SOFC Cathodes	*Georgia Tech Research Corporation*
	Low Cost Spray-On Coatings for Protection of SOFC Interconnects and BOP Components	*nGimat*
Illinois	Solid Oxide Fuel Cell Research and Development	Argonne National Laboratory - ANL
	Low-Cost Alloys for High-Temperature SOFC System Components	*QuesTek Innovations*
Indiana	Improved Flow Field Structures for Direct Methanol Fuel Cells	NuVant Systems Inc.
Maryland	*Mechanistic Enhancement of SOFC Cathode Durability*	*University of Maryland*
Massachusetts	Chemistry of SOFC Cathode Surfaces: Fundamental Investigation and Tailoring of Electronic Behavior	Massachusetts Institute of Technology
	Solid Oxide Fuel Cell Cathodes: Unraveling the Relationship Between Structure, Surface Chemistry and Oxygen Reduction	Boston University
	Unraveling the Role of Transport, Electrocatalysts, and Surface Science in the SOFC Cathode Oxygen Reduction Reaction	*Boston University*
Missouri	High-Temperature Viscous Sealing Glasses for Solid Oxide Fuel Cells	Mo-Sci Corporation
Montana	Synchrotron Investigations of LSCF Cathode Degradation	Montana State University
Multiple	NETL-Regional University Alliance Fuel Cells Initiative	National Energy Technology Laboratory
New York	Performance Degradation of LSCF Cathodes	GE Global Research
	Viscous Glass/Composite SOFC Sealants	Alfred University
Ohio	Manufacturing Analysis of SOFC Interconnect Coating Processes	NexTech Materials Ltd.
	Phase III Xlerator Program: Electrodeposited Mn-Co Alloy for Solid Oxide Fuel Cell Interconnects	Faraday Technology Inc.
	Rolls-Royce SOFC Model Development	LG Fuel Cell Systems
	SECA Coal-Based Systems - Rolls-Royce	LG Fuel Cell Systems
	Small Scale SOFC Demonstration Using Bio-Based and Fossil Fuels	Technology Management Inc.
	Techno-Economic Analysis of Scalable Coal-Based Fuel Cells	The University of Akron
	Stable Glass-Ceramic Nanocomposites as Compliant Seals for SOFCs	*SEM-COM*
	SOFC Protection Coatings Based on a Cost-Effective Aluminization Process	*NexTech Materials Ltd.*
Pennsylvania	Investigation of Cathode Electrocatalytic Activity using Surface Engineered Thin Film Samples and High Temperature Physical Property Measurements	Carnegie Mellon University
	Solid Oxide Fuel Cells Operating on Alternative and Renewable Fuels	Pennsylvania State University
Rhode Island	Testing and Evaluation of SOFC in Extreme Conditions	Naval Underwater Warfare Center

2012 Fuel Cells Portfolio Projects by State (Continued from page 19)

New Projects in Italics

State	Project Title	Performer Name
Tennessee	Reliability of Materials and Components for Solid Oxide Fuel Cells - ORNL	Oak Ridge National Laboratory - ORNL
Utah	SOFC Cathode Enhancement Through a Vacuum-assisted Infiltration	Materials & Systems Research Inc.
Washington	Low Cost Modular SOFC Development - PNNL	Pacific Northwest National Laboratory - PNNL
West Virginia	Direct Utilization of Coal Syngas in High Temperature Fuel Cells	West Virginia University
	Fundamental Understanding of Oxygen Reduction and Reaction Behavior and Developing High Performance and Stable Cathode with Heterostructured Surface	*West Virginia University*
Wisconsin	*Enhancement of SOFC Cathode Electrochemical Performance Using Multi-Phase Interfaces*	*University of Wisconsin*

II. SECA INDUSTRY TEAMS

A. Atmospheric Pressure Systems

II.A.1 SECA Coal-Based Systems—FuelCell Energy

Hossein Ghezel-Ayagh
FuelCell Energy, Inc.
3 Great Pasture Road
Danbury, CT 06813
Phone: (203) 825-6048; Fax: (203) 825-6273
Email: hghezel@fce.com

DOE Project Manager: Travis Shultz
Phone: (304) 285-1370
Email: Travis.Shultz @netl.doe.gov

Subcontractors:
- Versa Power Systems, Inc., Littleton, CO
- Versa Power Systems, Ltd., Calgary, Alberta, Canada

Contract Number: DE-FC26-04NT41837

Start Date: February 27, 2004
End Date: September 30, 2012

Fiscal Year (FY) 2012 Objectives

- Improve anode-supported solid oxide fuel cell (SOFC) components to enhance cell performance, lower performance degradation rate, and decrease cost. Incorporate the cell component improvements in fabrication of scaled-up cells and stacks.
- Enhance stack robustness and reliability during assembly, conditioning, transport and operation (steady-state and transient) at system representative conditions.
- Conduct a 5,000 h test of a 96-cell, scaled-up stack (15 kW) to demonstrate a steady state degradation of ≤2%/1,000 h.
- Conduct a 3,000 h test of a 30 kW stack meeting ≤1.5% loss of performance per 1,000 h of operation.
- Design, fabricate and test an assembly of 60 kW stack module hardware to demonstrate fit, finish and functionality of component design and assembly procedures.
- Develop the preliminary design of a ~60 kW proof-of-concept module (PCM) unit, including SOFC stack module and balance-of-plant (BOP) equipment, for future demonstrations.

FY 2012 Accomplishments

- Long-term endurance tests of single cells continue to show low performance degradation rates. An 81 cm^2 active area cell test, featuring third generation tape casting, screen-printing, and co-firing (TSC-3) cell design in combination with alloy coating accumulated over 18,000 h of operation at 750°C, with a performance degradation rate of 0.32%/1,000 h (at 500 mA/cm^2). Another single cell test conducted at a lower operating temperature of 650°C accumulated over 14,000 h with a degradation rate of <0.5%/1,000 h.
- Thin fuel cell anode structure with improved hydrothermal stability was developed and verified in a 16-cell (550 cm^2 cell active area) stack test. The improved anodes have been implemented in the standard cell fabrication process for 25 cm x 25 cm cell size.
- A 28-cell (121 cm^2 cell active area) stack, used for evaluating a pre-coated interconnect material, accumulated over 20,000 h of operation with degradation rate of 0.4%/1,000 h.
- Fuel cell stack manufacturing capacity of 500 kW/year was demonstrated through a three-month production run period.
- The first 96-cell (550 cm^2 active area) stack block (GT058116-0001), a representative of the manufactured building blocks for large-scale modules (>50 kW), was fabricated utilizing TSC-3 cells and tested for >5,000 hours. This stack achieved 16 kW of DC Power during the steady state operation. The second 96-cell stack (GT058116-0003) was fabricated and tested for stability of performance at system representative conditions. The stack exhibited a degradation rate of 1.4%/1,000 h during ~3,500 h of steady state testing. Tests of this stack were completed in Q2 2012.
- Two 96-cell stack blocks were integrated in a 30 kW stack tower arrangement for testing under system relevant operating conditions. Four additional 96-cell stack blocks were fabricated for a 60 kW module and factory tested using procedures developed for the final quality control and performance check-out.
- Detailed designs of a Quad Base configuration and non-repeat stack module hardware for a 60 kW PCM were completed. A 60 kW module using four mock stacks was fabricated and tested successfully, verifying the functional objectives of the non-repeat components. The 60 kW stack module was tested at temperatures of >600°C, characterizing the electrical resistance, gas flow distributions and leakage, effectiveness of the internal heat exchanger, and verifying the mechanical integrity of components subjected to thermal cycling.

- Design and fabrication of a subscale (3–5 kW) stack module, intended for rapid integration and testing of 16–32 cell stacks under various system operating conditions, were completed. The operation of the sub-scale stack module was successfully validated.
- A 60 kW system configuration was developed implementing an improved process design to increase the utilization of high temperature heat available in the SOFC plant exhaust stream. The electrical efficiency for the system at rated power is estimated to be 61.8% (lower heating value [LHV] of natural gas), with the potential for nearly 89% overall (thermal plus electrical) efficiency for combined heat and power (CHP) applications.
- SOFC stack factory cost estimate was updated to $147/kW (Year 2007 dollars), meeting the Phase III target of ≤$175/kW. The updated cost estimates resulted in a power island cost of $635/kW (Year 2007 dollars) for a ~670 MW baseline integrated gasification fuel cell (IGFC) System, meeting the U.S. Department of Energy (DOE) target of ≤$700/kW.

Introduction

FuelCell Energy, Inc. (FCE) is in Phase III of a multi-phase project to develop SOFC modules and power blocks for application in coal-based IGFC power plants. The primary objective of the project is to develop affordable and highly efficient multi-MW SOFC systems that have near-zero emissions of SOx and NOx, result in low water consumption, and capture >90% of CO_2 (carbon dioxide).

FCE utilizes the SOFC technology of its partner, Versa Power Systems, Inc. (VPS), in the development of IGFC power plants. VPS has well-established processes, quality control procedures, and equipment for the manufacturing of fuel cells. Key SOFC technology research and development activities for the project include improving cell and stack operating range, improving stack reliability and robustness, reducing cell and stack costs, and reducing cell performance degradation rate. System development activities consist of completing conceptual design and factory cost estimation for the SOFC cell stack and power island of the multi-MW baseline power plant and developing the preliminary design for a >50 kW PCM unit power plant.

Approach

Fuel cell development work has been focused on key cell issues related to cost reduction, endurance improvement, and performance enhancement. The main technical approach includes extension of the operating temperature window, reduction of average operating temperature, thermo-mechanical strength improvement, and scaled-up cell stack fabrication process development. The emphasis is placed on the development of a thin anode substrate with improved thermo-mechanical strength and hydrothermal stability. Material solutions with enhanced electrochemical properties have been evaluated. Various cell component design considerations, such as anode substrate thickness and porosity, have been evaluated to identify the optimum cell configuration for operation at high power density on coal syngas. Parameters such as performance (power, thermal management, and efficiency), design simplicity, technical risk, manufacturability, and cost have been considered in the design selection process.

Baseline power plant conceptual design (work performed during Phase I and Phase II) focused on evaluating process alternatives that increase power plant efficiency, meeting carbon capture requirements, and minimizing cost of the power plant's power island. Various process configuration analyses and parametric studies were conducted considering cell voltage, current density, fuel utilization, stream recycle levels, and process components. Conceptual design of a PCM test unit included the process configuration evaluations and operating parameter studies.

Results

The on-going endurance tests of the improved cathodes and modified anodes in single cells (81 cm^2 active area) continued to demonstrate very low performance degradation rates. A cell test at 750°C (and 500 mA/cm^2) accumulated over 18,000 h with an average performance degradation rate of <0.3%/1,000 h, as shown in Figure 1. To expand the operating temperature window

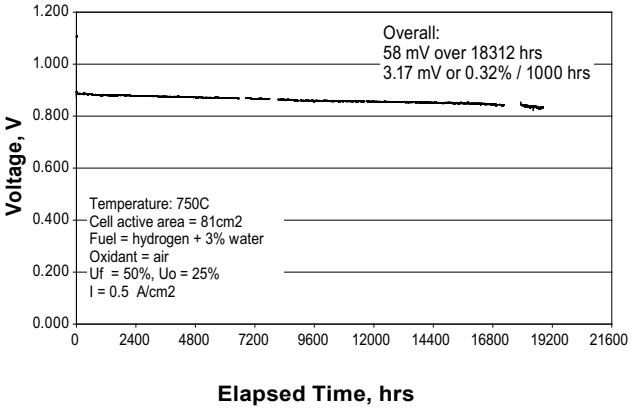

FIGURE 1. Long-term performance stability of a TSC-3 cell featuring alloy coating

(for stack implementation of the cell technology), the performance degradation rate at temperatures other than 750°C, in the range 650–800°C has been investigated. A single cell test conducted at lower operating temperature of 650°C accumulated over 14,000 h. The cell performance degradation rate was ~0.5%/1,000 h.

To improve the cell and stack robustness, a hydrothermally stable thin TSC-3 cell was developed. The design was validated in a 16-cell (550 cm^2 cell area) stack test by completing five thermal cycles while progressively increasing anode gas humidity during heat-up and cool-down. The newly developed cell met the hydrothermal stability requirements for the most stringent anode gas humidity conditions. The standard cell manufacturing process was modified based on the hydrothermally stable anode substrate material developments. The cell manufacturing process yield of >90% has been regained based on fabrication of over 1,000 cells (25 cm x 25 cm size).

The effect of cathode gas humidity level on the cell performance degradation is largely due to higher chromium (Cr) vapor pressure when moisture is present in the cathode feed gas. Both Cr oxide formation at cathode and Cr_2O_3 deposition significantly increase cathode overpotential (performance loss). The use of a coating for stainless steel components (such as an interconnect) can mitigate Cr transfer to cathode. A recent single cell test (1,900 h testing) of TSC-3 cell employing an advanced coating showed an improved cell performance degradation rate of 0.56%/1,000 h (~1,100 h period) at 3.5% cathode gas humidity level.

Long-term endurance tests of advanced pre-coated interconnects and cathode corrugations (flow media) in stacks have shown very low performance degradation rates. The 28-cell (121 cm^2 cell active area) stack test evaluating the pre-coated interconnect material accumulated over 20,000 h of operation with degradation rate of 0.4%/1,000 h.

A long-term steady state test of a 96-cell (550 cm^2 cell area) stack block, at system representative operating conditions, was conducted. Overall the stack test accumulated over 5,500 h. The test was interrupted several times by external factors resulting in multiple thermal cycling of the stack. The overall stack performance degradation rate was ~1.6%/1,000 h. Another long-term steady state test of a 96-cell stack was initiated. Figure 2 shows the test results over a 3,500-h period, indicating overall stack performance degradation rate of ~1.4%/1,000 h.

The SOFC module concept development focused on the design of a 60 kW module, based on an array of four stacks (quad), each stack containing a 96-cell block. The stacks in the quad are assembled on a single fixed-end base. The quad base design provides the support structure and facilitates the gas flow distribution to the stacks. The design of the 60 kW stack module consists of highly engineered components that require verification for functionality and performance. To test the engineered hardware components as assembled, a 60 kW stack module utilizing mock (non-working) stacks was constructed. The major components included the quad base, high temperature flanges, fuel gas (radiative) heat exchanger, conductive module gaskets, hot buss bars, stack compression springs and vessel/module enclosure. Figure 3 shows the assembled module in the test facility before installation of the module enclosure.

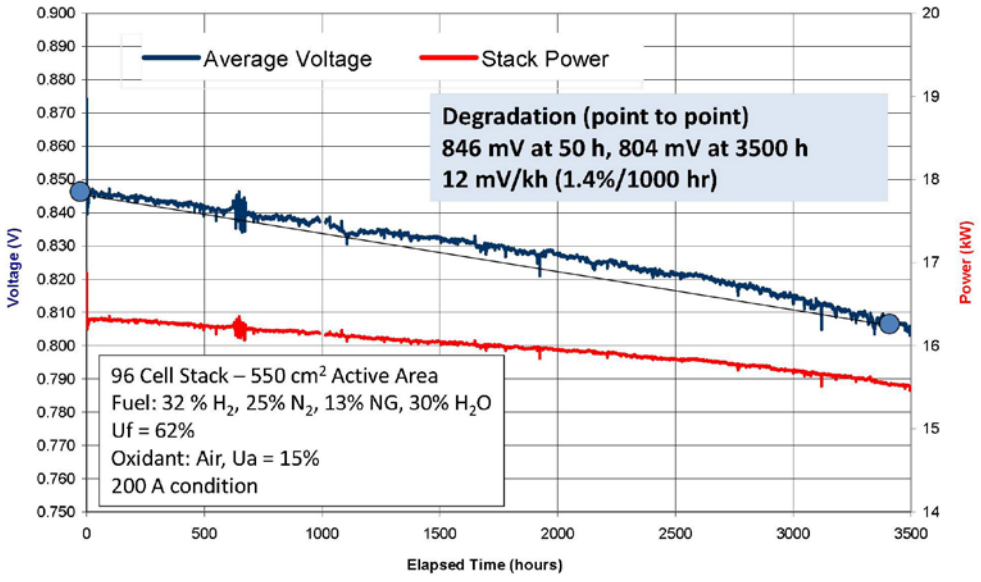

FIGURE 2. Long-term steady state test of a 96-cell (550 cm^2 cell area) stack

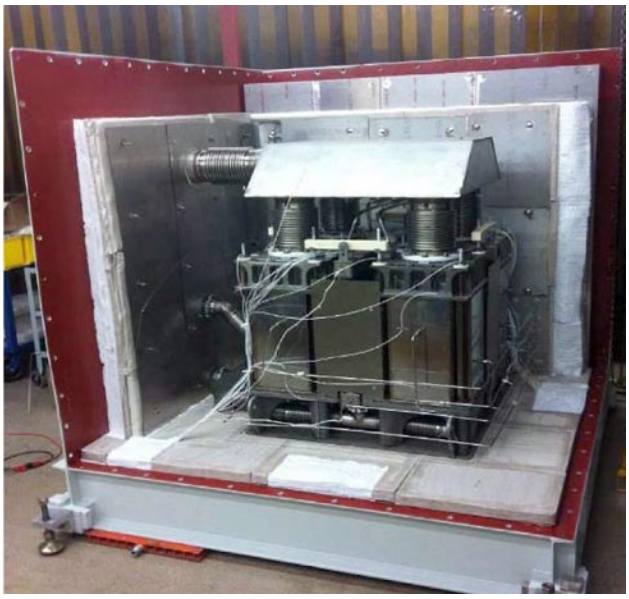

FIGURE 3. 60 kW mock stack quad assembly module prior to vessel closure

The 60 kW mock stack quad assembly was subjected to cold flow tests for measurements of gas flow uniformity among the stacks. Subsequently, the assembly underwent testing in hot environment similar to the actual system conditions. The hot test results showed that the anode gas flow variation between the four stacks was within +0.39% to -0.59% range. The cathode side gas flow variation was found to be within +0.45% to -0.35% range. The current design was proven to provide very good flow distribution. Performance of the electrical (configuration) system for the mock stack module was tested by passing 200 A current through the series-stack assembly (the four stacks within the module are electrically connected as two parallel strings) and power take-off subsystem. Based on the hot test results, power loss for the 60 kW module buss system is projected to be 307 W. Dielectric (isolation) component performance was also verified successfully at high voltage condition during the hot test. Another important accomplishment of the module hot test was monitoring/characterization of the anode gas superheater (radiative) performance. The theoretical model for the heat exchanger (HX) was refined/calibrated using stack and superheater surface temperature and the gas temperature data from the hot test. The refined model was then utilized to predict the HX effectiveness subject to the system operating conditions. Performance projection for the HX with actual operating stacks was verified to exceed the design target.

To serve as a test vehicle for stacks of 16–32 cells (550 cm^2 active area), a sub-scale (3–5 kW) stack module was designed, fabricated and integrated into the 30 kW SOFC test facility modified to operate at lower ranges

FIGURE 4. 3–5 kW module integrated into the modified 30 kW test facility

of flows. Figure 4 shows the module installed in the test facility. The small scale module is expected to facilitate quick assembly and installation turnaround needed to test stacks with minimal facility down time. It is feasible to replace a stack in less than one day. The 3–5 kW module will also act as a test bed for new design features planned for more compact and lower cost SOFC modules. The module design was successfully validated with operation of two consecutive stacks. The validation tests were utilized to verify various system operational modes including heat-up and shutdown.

A new 30 kW stack tower, for a planned >3,000 h test, was assembled using two 96-cell stack blocks. The stack blocks were satisfactorily performance tested at the factory. Cold flow tests of the stack blocks conducted to characterize both anode and cathode side flow distributions confirmed that they are within acceptable limits. Figure 5 shows the stack tower assembly.

The conceptual design for the 60 kW PCM test unit focused on preliminary engineering design documentation required to conduct the PCM system hazard and operability (HAZOP) studies. This included process flow diagram, piping and instrumentation diagrams, preliminary control philosophy, and the alarm list. A system configuration improvement implemented in the design process resulted in enhancing the CHP capabilities of the 60 kW PCM system. High temperature heat available in the SOFC plant exhaust stream is an important attribute when considering the overall system efficiency and plant economics. Process modeling and simulations of the reconfigured PCM system have been performed for the full power, rated power, and heat-up modes of operation. Table 1 summarizes performance for the full power case. The electrical efficiency for the full power case is estimated to be 61.8% (LHV natural gas),

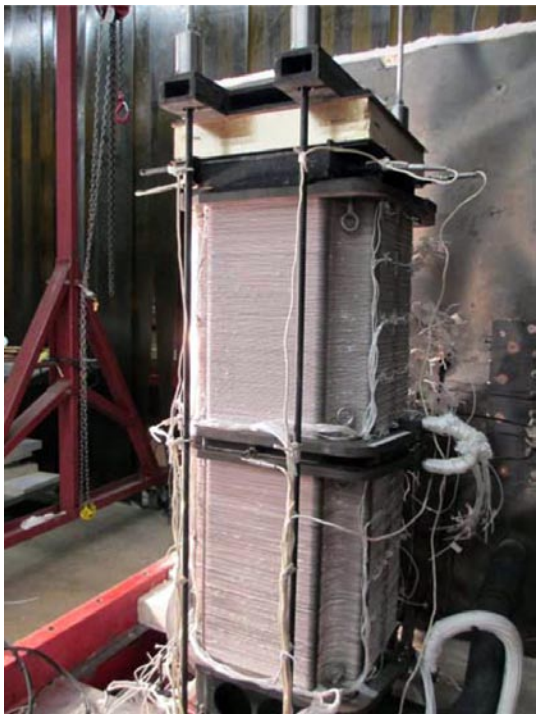

FIGURE 5. 30 kW stack tower

with the potential for nearly 89% overall (thermal plus electrical) efficiency for CHP applications.

The factory cost report for the baseline power plant system has been revised to update the SOFC stack block, stack module and balance-of-plant factory equipment costs in Year 2007 U.S. dollars. The updated stack block cost estimate is $147/kW, and the power island factory equipment cost is $635/kW. The cost numbers are based on a peak power output of 671.8 MW net AC. Both costs meet the Solid State Energy Conversion Alliance (SECA) program Phase III requirements ($175/kW and $700/kW, respectively).

Conclusions and Future Directions

Significant progress was made in addressing the key issues related to degradation and endurance of the SOFC components while focusing on the objectives of reducing the cost of manufactured cells. A hydrothermally stable thin TSC-3 cell which offers substantial cost savings has been developed. Major cell material improvements were validated. The standard cell manufacturing process was modified based on the recently developed hydrothermally stable anode substrate material. Several long-term endurance tests were continued from prior years. These long-term (>14,000 h) endurance tests have validated the longevity of the core SOFC tri-layer technology under a wide range of operating temperatures.

SOFC stack development focused on increasing stack reliability and endurance. Improved metallic interconnect plates were incorporated in Phase III stack design after validation tests. Stack tests were conducted to further define and design a standardized stack building block unit. Eight 96-cell (15 kW nominal) stacks were fabricated and successfully factory conditioned and acceptance tested. One stack was tested for >5,000 h with an average degradation of <1.6%/1,000 h. The results were almost duplicated in a second stack which showed a degradation of <1.4% after 3,500 h of operation. Two stack blocks were utilized in fabrication of a 30 kW stack tower to be tested in the last quarter of Year 2012.

A 60 kW fuel cell stack module containing an assembly of identical stacks was developed to lay the

TABLE 1. 60 kW PCM system performance estimate at full power conditions

PCM System Performance Summary

POWER GENERATION PROFILE:		
Fuel Cell DC Power	**70.2**	**kW**
Inverter Efficiency	95.0	%
Inverter Loss	3.5	kW
SOFC Gross AC Power	66.7	kW
Prime Movers	1.5	kW
Parsitic AC Power	1.3	kW
Net AC Power Consumption	2.8	kW
Net SOFC Plant AC Output	63.9	kW

Energy Input		
Fuel Flow	17.31	lb/hr
Fuel Low Heating Value	20392	BTU/lb
Fuel Energy (LHV)	103.4	kW
Fuel High Heating Value	22610	BTU/lb
Fuel Energy (HHV)	114.6	kW

SOFC EFFICIENCY (Fuel to Electricity)		
Electrical Efficiency (LHV)	**61.8**	**%**
Electrical Efficiency (HHV)	55.7	%

CHP		
Available Heat To 250 °F	77546	BTU/hr
	22.7	kW
Available Heat To 120 °F	95715	BTU/hr
	28.1	kW

CHP EFFICIENCY		
Total Efficiency (LHV) to 250°F	**83.8**	**%**
Total Efficiency (HHV) to 250°F	75.5	%
Total Efficiency (LHV) to 120°F	**88.9**	**%**
Total Efficiency (LHV) to 120°F	80.2	%

foundation for building blocks scalable for deployment in coal based power plants of the future. Testing of the non-repeat hardware for a 60 kW PCM using both cold-flow experiments as well as hot tests simulating the operating environment has been conducted successfully. The tests showed that the module and the non-repeat component designs meet the system requirements. The uniformity of cathode and anode flow distributions between the stacks, and the anode fuel heat exchanger performance were verified. The dielectric isolation of stacks from the compression assembly and flow pipes at potentials of up to 150% of the design value, as well as acceptable performance of all current collection equipment at operating temperature were checked. Overall, the operability and robustness of the 60 kW stack module design were verified.

The design of a multi-stack 60 kW PCM system, as a gateway to larger system, was modified with enhancements to waste-heat recovery and co-generation capabilities. A failure mode analysis using the industry-wide HAZOP discipline was conducted to ensure the safe operation of the multi-stack system.

An update of the cost analysis for the baseline power plant system revealed that SOFC stack and power island (utilizing coal derived syngas fuel) are amenable to meet the DOE's factory cost targets of $175/kW and $700/kW (2007 US$), respectively.

FY 2012 Publications/Presentations

1. H. Ghezel-Ayagh, R. Way, P. Huang, J. Walzak, S. Jolly, D. Patel, C. Willman, K. Davis, M. Lukas, B. Borglum, E. Tang, M. Pastula, R. Petri, and M. Richards, "Solid Oxide Fuel Cell Stack Module Development for Fuel Flexible Power Generation," *ECS Transactions*, 2011 Fuel Cell Seminar & Exposition, Orlando, Florida, October 31 – November 3, 2011, Vol. 42, Issue No. 1, pp. 233-239.

2. H. Ghezel-Ayagh, "SOFC Development for Large-Scale Integrated Gasification Fuel Cell Power Plants," International Colloquium on Environmentally Preferred Advanced Power Generation (ICEPAG), Costa Mesa, California, February 7–9, 2012.

3. H. Ghezel-Ayagh, "Progress in SECA Coal-Based Program," 12th Annual SECA workshop, Pittsburgh, Pennsylvania, July 26–28, 2011.

II.A.2 SECA Coal-Based Systems—UTC Power

Praveen Narasimhamurthy (UTC Power, Primary Contact), Eileen Bartley (UTC Power), Dan Hennessy (Delphi), Andrew Rosenblatt (Delphi), Rick Kerr (Delphi), Jonathan Schneider (Delphi)

UTC Power
195 Governors Highway
South Windsor, CT 06074
Phone: (860) 727-2667; Fax: (860) 998-9236
Email: praveen.narasimhmaurthy@utcpower.com

DOE Project Manager: Joseph Stoffa

Phone: (304) 285-0285
Email: Joseph.Stoffa@netl.doe.gov

Subcontractors:

- Delphi, West Henrietta, NY
- United Technologies Research Center (UTRC), East Hartford, CT
- Battelle/Pacific Northwest National Laboratory, Richland, WA

Contract Number: NT0003894

Start Date: October 1, 2011
End Date: September 30, 2012

Fiscal Year (FY) 2012 Objectives

- Complete accelerated test strategy for seal degradation.
- Develop concepts for interconnect interfacial control of area-specific resistance (ASR).
- Demonstrate improved anode interconnect stability at a stack level with improved adhesion process.
- Fabricate Gen 4 stack to test interfacial control concepts.
- Develop accelerated test platform for evaluating interconnect coatings and surface treatments.
- Complete interlayer Robust Engineering optimization project.
- Optimize current repeating unit seal, using accelerated test platform.
- Shortlist new concepts for seals (through accelerated thermal cycling testing) for further development and scale-up.
- Fabricate and thermal cycle test short stacks with new, low cost, high cyclability repeating unit seals.
- Complete stack cost analysis to determine conformance to Solid State Energy Conversion Alliance (SECA) requirements.
- Demonstrate improved performance stability on Gen 4 stack tested for >3,000 hours.
- Design, develop and build a 25 kW capable breadboard.
- Demonstrate thermally self-sustained operation.
- Demonstrate 3,000 hours of system level endurance operation (1,500 hours as part of Phase I).

Accomplishments

- An accelerated test strategy has been completed for the repeating unit to repeating unit glass seal using a rapid thermal cycle furnace with the addition of steam. Eight hundred thermal cycles were completed on shear test coupons with no reduction in shear strength of the glass seal. A second accelerated test strategy was developed for the cell-to-retainer braze seal using a rapid thermal cycle furnace with a dual atmosphere (H_2 and air) capability. Four tests were completed, each with 425 thermal cycles.
- A concept selection process was completed for the control of interconnect interfacial ASR.
- Improvements in anode interconnect stability were demonstrated in bench and stack testing. Process development is ongoing to reduce part-to-part variation.
- A 30-cell Gen 4 stack was built with several interfacial control concepts and was tested for 4,700 hours at normal operating conditions. The best treatment combinations degraded an average of 0.64% per 500 hours.
- An accelerated test platform was developed for evaluating interconnect coating and surface treatments. Samples were soaked at 850°C for 1,000 hours prior to analysis of ASR, surface condition, coating thickness, bend testing, and chrome migration.
- The interlayer Robust Engineering project was completed, resulting in the optimization of solids loading, firing parameters, and print screen mesh. An increase in power of greater than 50% was realized on button cell testing with the optimized treatment levels.
- Completed 1,240 load hours on a stack module as part of Phase I endurance testing. The 1,240 hours was inclusive of 1,000 continuous load hours. This was made possible by making substantial

improvements to the test stand reliability compared to previous years. The endurance test was stopped at 1,240 hours, in consultation with U.S. Department of Energy (DOE), to facilitate modifications to the test stand for Phase II.

- Performed conceptual trade-studies of 18 different system concepts for the SECA Phase II breadboard and selected the Duo P concept as the final configuration based on high scores for system efficiency, system reliability, controllability, development cost and cost of future product.
- Completed the conception and design of a 25 kW breadboard. Ordered all critical balance of plant (BOP) for the breadboard, comprising of, but not limited to, heat exchangers, a catalytic burner, hydro-desulfurizer, fuel reformer, anode heater and anode recycle blower.
- Completed conception and design of the control strategy for the breadboard.
- Started ex situ performance verification and endurance testing of the low-cost anode recycle blower at operating temperatures.
- Successfully completed all the critical design reviews for the breadboard design and started fabrication of the Phase II breadboard.

Introduction

In addition to its high power density, a key advantage of the solid oxide fuel cell (SOFC) system is its high system efficiency, particularly when its high temperature co-product heat can be used in combination with its electrical output. The other advantage of SOFC is that the system could potentially be very simple with minimal requirement for external fuel processing. SOFC is also tolerant to some fuel contaminants that are known to cause degradation in stacks of other technologies such as proton exchange membrane (PEM).

Delphi has been developing SOFC systems since 1999. After demonstrating its first generation SOFC power system in 2001, Delphi teamed with Battelle under the SECA program to improve the basic cell and stack technology, while Delphi developed the system integration, system packaging, and assembly.

Current and prior generation Delphi stacks have demonstrated performance that shows good potential to meet SECA durability goals. The focus in Phase 1 of this SECA program has been on further improving the overall durability of the stack while lowering cost and improving manufacturability. In addition to large stationary applications, the same SOFC stacks can be used in other applications which are good fits for the technology, including transportation. In transportation, SOFC stacks will initially be used in auxiliary power units (APUs) to provide hotel load power to heavy duty trucks during periods of rest and idle.

United Technologies Corporation (UTC) Power is a world leader in developing and producing fuel cells that generate energy for buildings and for transportation, space and defense applications. UTC Power has successfully completed multiple installations of its newest generation fuel cell system, the 400 kW phosphoric acid PureCell®, for the commercial combined heat and power (CHP) market. UTC Power and United Technologies Research Center developed conceptual process designs for a wide range of SOFC power systems ranging from 250 kW up to 100+ MW with a focus on meeting the system efficiency and carbon separation targets specified in the SECA minimum requirements. As part of SECA Phase I, UTC Power has designed, built and commissioned a test stand capable of testing a stack up to 50 kW and subsequently tested a Delphi stack module for 1,240 hours on simulated coal syngas. In support of the design of a 250–1,000 kW SOFC Power Module, UTC Power is designing and building a 25 kW breadboard that shall demonstrate thermally self-sustained operation and 3,000 hours of system level endurance operation (1,500 hours as part of Phase I).

Approach

Delphi utilized a staged approach to develop a modular SOFC system for a range of fuels and applications. Major subsystems and individual components were developed and tested as building blocks for applications in targeted markets. These were then integrated into a “close-coupled” architecture for integrated bench testing, as well as a stationary power unit (SPU) and an APU for the stationary and transportation markets, respectively.

UTC Power utilized a gated product development approach to designing and developing 250–1,000 kW SOFC power modules that could eventually be combined and configured to 100+ MW units. The first step in this development process was to demonstrate endurance of a stack module on simulated coal syngas. Following successful endurance demonstration, the stack module would be integrated into a lab-scale system or breadboard that consists of an on-board fuel processing system (FPS), air processing system (APS), and exhaust management system (EMS). The intent of this phase of the development process is to demonstrate thermally self-sustaining operation combined with system level endurance in a lab environment. Post successful breadboard demonstration, the experience gained could

be utilized to design larger power plants that would be fabricated and tested in subsequent project phases.

Results

The SECA coal-based systems (CBS) project is a continuation of the core hardware development activities begun in SECA cost reduction project. The efforts in SECA CBS are more application-driven as Delphi and UTC move this technology closer to pilot and production releases. The SECA CBS program will support and address the development of fuel cells for central generation applications. This market has unique demands, and development tasks must address specific issues that are economic drivers of the design and application.

Delphi continues to make progress with improved cell fabrication techniques by focusing on material and process improvements. A key element is Delphi's partnership with commercial suppliers of production materials to develop a consistent supply of production grade material and optimize the material properties to provide robust performance in the solid oxide fuel cell stack and ultimately the fuel cell system. The principles of the Delphi manufacturing system design (MSD) are continuously applied to develop control and quality standards for each step of the manufacturing process. By focusing efforts in these areas early in the development process, Delphi has been able to scale up the fabrication process to mass quantities while maintaining high quality standards.

Scale-up of the Gen 4 stack was a major focus for FY 2012. Several failure modes that were discovered with the Gen 3 stacks have been eliminated, resulting in low, linear power degradation during durability testing. A 38-cell Gen 4 stack demonstrated a maximum initial power of 7.2 kW at an average power density of 470 mW/cm^2 and average cell voltage of 0.79 volts, when tested on 48.5%H_2/48.5%N_2/3%H_2O fuel.

Several concepts for interconnect interfacial ASR control were incorporated into a 30-cell Gen 4 stack, that has completed 4,700 hours of continuous durability testing. The best treatment combinations degraded an average of 0.64% per 500 hours. The Gen 4 stack has successfully completed 72 deep thermal cycles from 750ºC operating temperature to <100ºC with a total power degradation of approximately 8%. The successful stack test results provide confidence that the stacks have the potential to meet SECA durability goals and will survive periods of maintenance and shutdowns in larger power plants.

As part of SECA Phase I, UTC Power designed, built and commissioned a test stand capable of testing a stack up to 50 kW to support validation testing of stack modules to meet performance, reliability, cost, and endurance metrics (Figure 1). Phase I endurance testing of the 25 kW test article was delayed due to multiple test stand anode inlet inert gas heater failures. Testing was also impacted due to some performance anomalies observed in the stacks. The heater issue was resolved in early 2012, and several other improvements to the test stand reliability were implemented. DOE and UTC/Delphi discussed and decided that the 1,500 hour durability portion of the testing was to consist of a single stack operated until integration of Phase II. The intent was to use the testing to identify and mitigate issues pertaining to stand and cell stack reliability. The stack module completed 1,240 load hours, inclusive of 1,000 continuous load hours after which the endurance test was stopped to facilitate modifications to the test stand for Phase II.

FIGURE 1. Stack module at UTC Power test stand

In support of the design of a 250–1,000 kW SOFC Power Module, UTC Power is designing and building a 25 kW breadboard (Figure 2) that shall demonstrate thermally self-sustained operation and 3,000 hours of system level endurance operation (1,500 hours as part of Phase I). UTC Power performed conceptual trade-studies of 18 different system concepts for the SECA Phase II breadboard and selected the Duo P concept as the final configuration based on high scores for system efficiency, system reliability, controllability, development cost and cost of future product. The team has completed the conception and preliminary design of a 25 kW breadboard based on the Duo P concept. A critical part of the design was related to identifying and/or designing all critical BOP for the breadboard, comprising of, but not limited to heat exchangers, a catalytic burner, hydro-desulfurizer, fuel reformer, anode heater and anode recycle blower. Some of the components such as the desulfurizer, fuel reformer, anode heater and anode recycle blower were designed in-house by leveraging UTC Power's expertise/prior experience in these areas.

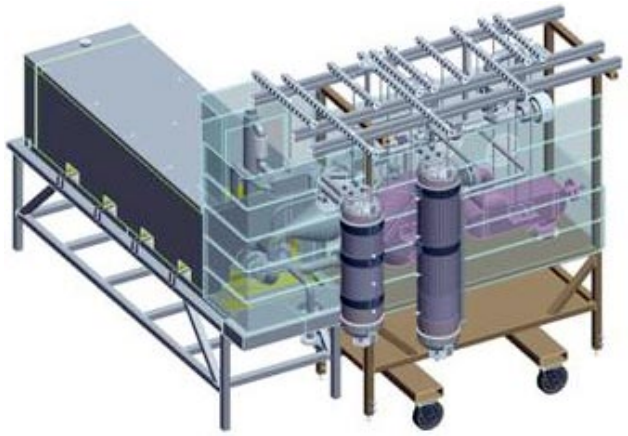

FIGURE 2. 25 kW SOFC breadboard

Other components were sourced from qualified UTC suppliers. All component and system level critical safety analyses such as the Functional Analysis (FA), the Hazard Analysis (HA) and the Failure Mode and Effects Analysis (FMEA) were completed. As part of the stage-gate process that UTC Power uses for its new product development, the team has successfully completed the conceptual and preliminary design reviews for the breadboard design and has started fabrication of the unit.

UTC Power completed the design and development of the control strategy for the breadboard. In an effort to improve system reliability, extensive lab testing of the control software has been initiated. In addition, performance verification and endurance testing of the low-cost anode recycle blower at operating temperatures has been initiated to gather ex situ endurance hours on the blower and improve blower reliability.

Conclusions and Future Directions

SECA CBS is focused on the stationary markets, with Delphi leading stack development for a coal syngas based MW-scale power module. Development will continue to improve the electrochemical performance stability, durability, and reliability of the Gen 4 stack while continuing cost reduction activities through manufacturing enhancements, cell and stack design and materials development.

UTC is leading the systems development work. Current and future work efforts are directed at developing a packaged system design with improved reliability and cost. The scaled stacks developed and tested during Phase I shall be integrated into a thermally self-sustaining 15–25 kW demonstration breadboard power plant. The breadboard shall be tested in accordance with guidance provided in the DOE-approved test plan and the SECA Minimum Requirements, and the performance and cost evaluated with respect to the metrics specified therein. This power plant shall form the basis for larger power plants to be fabricated and tested in subsequent project phases.

FY 2012 Publications/Presentations

1. Praveen Narasimhamurthy (UTC Power) and Rick Kerr (Delphi), "Coal-Based IGFC Project Phase I FC26-08NT0003894," 12th Annual SECA Workshop, July 26, 2011, Pittsburgh, Pennsylvania.

2. Dan Hennessy, "Solid Oxide Fuel Cell Development at Delphi," Fuel Cell Expo Technical Conference, Tokyo, Japan, March 2, 2012.

3. Dan Hennessy, "Solid Oxide Fuel Cell Diesel Auxiliary Power Unit Demonstration," DOE ARRA Program Peer Review, Washington, DC, May 16, 2012.

4. Dan Hennessy, "Solid Oxide Fuel Cell Development at Delphi," Fuel Cell Conference, Orlando, Florida, November 2, 2012.

II. SECA INDUSTRY TEAMS

B. Pressurized Systems

II.B.1 SECA Coal-Based Systems—LG Fuel Cell Systems

Richard Goettler (Primary Contact), Greg Rush, Ted Ohrn, Mark Scotto
LG Fuel Cell Systems Inc. (formerly Rolls-Royce Fuel Cell Systems (US) Inc.)
6065 Strip Avenue NW
North Canton, OH 44720
Phone: (330) 491-4821; Fax: (330) 491-4808
Email: richard.goettler@lgfcs.com

DOE Project Manager: Patcharin Burke
Phone: (412) 386-7378
Email: Patcharin.Burke@netl.doe.gov

Subcontractors:
- Rolls-Royce Fuel Cell Systems Limited, Loughborough and Derby, UK
- Case Western Reserve University, Cleveland, OH
- University of Connecticut, Storrs, CT
- University of South Carolina, Columbia, SC
- Matrix Innovations, Lynchburg, VA
- Oak Ridge National Laboratory, Oak Ridge, TN
- Pacific Northwest National Laboratory, Richland, WA

Contract Number: FE0000303

Start Date: September 1, 2009
End Date: September 30, 2012

Fiscal Year (FY) 2012 Objectives

- Achieve extended durability testing of subscale test articles to further define the degradation trends of the current cell technology.
- Finalize stack component designs for uniform flow distribution and simplified stack manufacturing.
- Continue the Phase 1 metric stack test and submit a Phase 1 factory cost report.
- Commence the Phase 2 metric stack test in a thermally self-sustaining test rig and submit a Phase 2 factory cost report.
- Improve substrate characteristics and qualify a next generation substrate.

FY 2012 Accomplishments

- Subscale test articles have exceeded 16,000 hours of testing under system relevant conditions. Degradation mechanisms have continued to be mapped for these longer duration tests.
- Similar area specific resistance values for strips as subscale articles confirms pressure drop design features for manifold components achieve requisite fuel flow uniformity at strip scale. A design more suitable to high volume manufacturing has been selected.
- A two-strip (7.6 kW) Phase 1 metric test has started, and the degradation rate through 1,600 hours is tracking at <1%/1,000 hours.
- Five strips were prepared for the Phase 2 metric test. The test is planned to start during the final quarter of government FY 2012.
- LG Fuel Cell Systems', Inc., (LGFCS') substrate supplier has resolved quality issues experienced during 2011, and a Gen2 substrate that incorporates raw material and processing changes for lower cost at high volume manufacturing is meeting mechanical property specifications. An extensive mechanical property database is being generated including evidence for acceptable slow crack growth behavior as necessary for long-term reliability.

Introduction

The LGFCS Solid State Energy Conversion Alliance (SECA) program is aimed at demonstrating the viability of the LGFCS integrated-planar solid oxide fuel cell (IP-SOFC) technology, which is being developed for the distributed energy market, for eventual scale-up to a megawatt scale system suitable for incorporation into centralized power generation facilities employing coal gasification and carbon sequestration. The integrated gasification fuel cell (IGFC) systems offer efficiencies of >50% (higher heating value), inclusive of CO_2 capture. The LGFCS stack concept is based on thin planar cells which are series-connected on a fuel-carrying porous ceramic support substrate [1-3]. These active substrates are the elemental building block of the fuel cell stack and are grouped together to form a megawatt scale IP-SOFC system as shown schematically in Figure 1. These cells are applied onto the substrates using well established thick film screen printing techniques. Contrary to other SOFC developers who seek ever larger single cell active areas, LGFCS desires smaller cells to reduce current levels and achieve lower ohmic (I^2R) losses. LGFCS currently prints 60 cells of ~1.3 cm^2 on each side of the substrate. This represents a switch in design philosophy from a low voltage, high current fuel cell to a high voltage, low current approach. Substrates having the

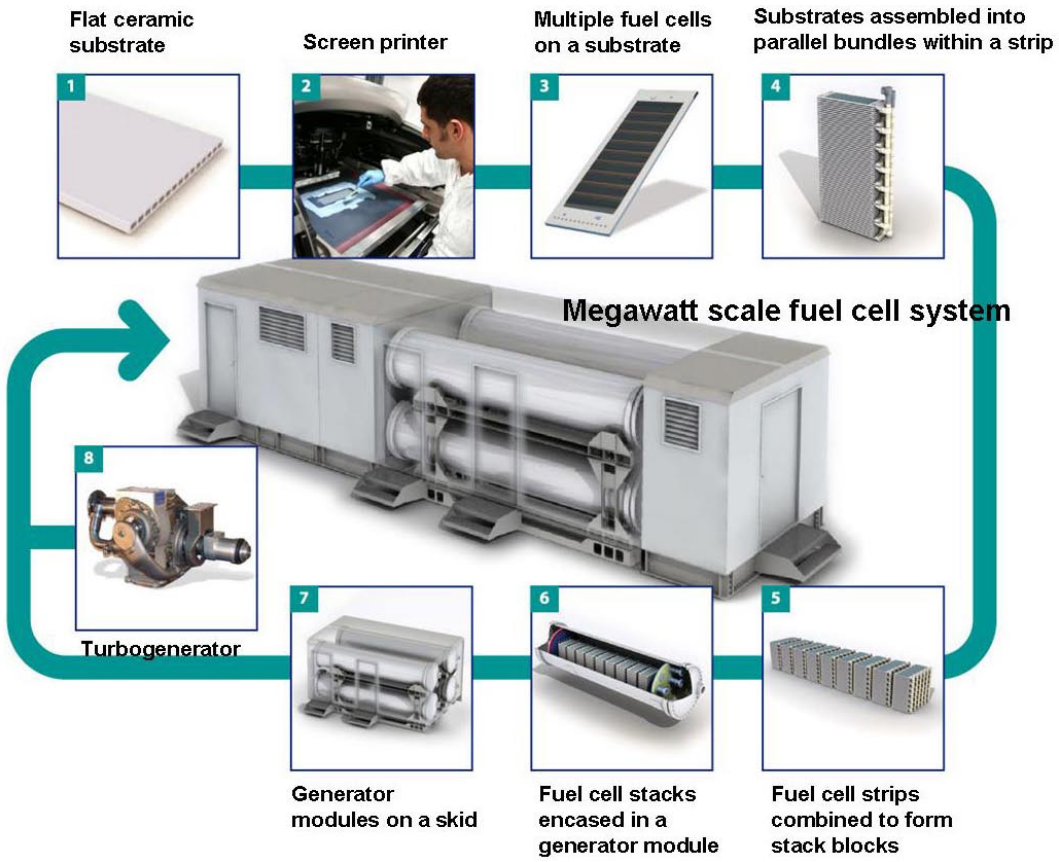

FIGURE 1. Schematic of the planned LGFCS 1 MW distributed power generation system

narrow 60-cell design (adopted pre-SECA) allow the use of lower conductivity and lower cost-basis materials to meet in-plane conductance requirements which has been an important materials substitution for achieving the U.S. Department of Energy (DOE) costs target of <$700/kWe (in 2007 dollars). FY 2012 activities were focused on continued subscale durability testing of the selected lower cost and optimized active cell layers (extending past 16,000 hours for some conditions), block-scale metric testing to demonstrate meeting the SECA Phase 1 degradation targets of <2%/1,000 hours, and the extension of the mechanical property database of stack components to develop life prediction reliability methodologies.

Approach

The LGFCS SOFC system operates at pressures up to seven bar. Benefits of pressurized operation are improved IGFC system efficiency (DOE system models predicting 57% efficiencies inclusive of CO_2 capture) [4] with higher volumetric power densities allowing smaller footprints. LGFCS has developed in-house designed pressurized test stands ranging from subscale substrates for testing single and 5-cell articles, bundle rigs (~350 W) which tests the fundamental stack assembly unit, stack block rigs (~20 kW) and tier rigs (~125–250 kW). All scales of test rigs can duplicate the operating conditions planned for the commercial power systems and thus serve as the source of initial pre-commercialization verification of the long-term durability of the cell and stack technology. Subscale test units are highly instrumented to allow detailed breakdown of area specific resistance (ASR) between ohmic versus polarization contributions and to identify degradation sources between that of the anode, cathode and interconnect cell layers. These subscale tests are run at the extremes and mid-points of block temperature and fuel utilization to bracket degradation trends and provide estimates of the degradation trends for larger scale tests. Cell technologies meeting target degradation rates in subscale test are then tested at bundle then block level. Electrochemical models are used to analyze the performance results at all scales.

The stack block is the heart of the LGFCS SOFC power system. It contains the fuel cell stack and components of the fuel and air sub-systems that establish the thermal, flow and compositional boundary conditions for the stacks. The stack block is the basic repeat unit which will be packaged into the generator module illustrated in Figure 1. Testing at the block-scale provides

representative durability and reliability testing of future product, and such tests will provide the foundational database validating the commercial readiness of the LGFCS SOFC cell and stack technology. Product representative balance of plant (BOP) components and features such as the insulation system, ejectors, off-gas burners, reformers and heat exchangers are included in the block test rigs to provide crucial system-level qualification as necessary to shorten the path to commercialization. The block rigs achieve product level heat balancing including representative fuel and air recycle loops and provide for thermal self-sustaining block tests. The University of Connecticut is performing assessments of the alloys selected by LGFCS for the BOP components, with particular emphasis on chromium release rates and alternate alloys and/or coatings for mitigating chromium volatility to minimize long-term degradation associated with chromium poisoning of the cathode.

Manufacturing of the fuel cell stacks are performed on the process verification line (PVL), located in Canton, Ohio, and includes a screen printing line representative of that required for a high volume factory. Current substrate/cell sizes and stack architecture are that planned for market entry product. The experience on the PVL along with the current stack assembly operations have guided the inputs for the activity based cost model that was developed for estimating the high volume manufacturing costs for the SOFC power module. Projected power module costs meet the <$700/kW SECA target.

Not only must the fuel cell stack meet electrochemical performance and durability targets, it must demonstrate structural integrity to meet reliability/mean time to failure necessary for commercial launch. Stack mechanical reliability is being investigated in collaboration with Oak Ridge National Laboratory (ORNL) where detailed mechanical characterization of the substrate is being performed. Substrates with the permeability characteristics for low diffusive losses are being supplied to LGFCS, and the as-received substrate and fully processed active substrates meet the specified strength requirements supported by finite element analysis. Further validation of the stack reliability will be obtained by thorough residual property measurements of stack components following long-term block-scale testing. Time-dependent reliability prediction methodologies are being explored based on slow crack growth behavior of the ceramic components comprising the all-ceramic LGFCS stack. The slow crack growth characteristics of the porous substrate are being measured by ORNL. The substrate material exhibits moderate tolerance to slow crack growth at the roughly 800°C–900°C use temperatures for measurements made thus far in air and simulated fuel environment of 3.5% H_2/3.5% H_2O/93% N_2. Future testing will be at H_2O levels representative of stack outlet fuels as well as testing in stack representative reformate fuels.

Results

The 1 MW product system cycle is shown in Figure 2. The block test rigs mimic the product cycle to various extents, but each rig achieves representative

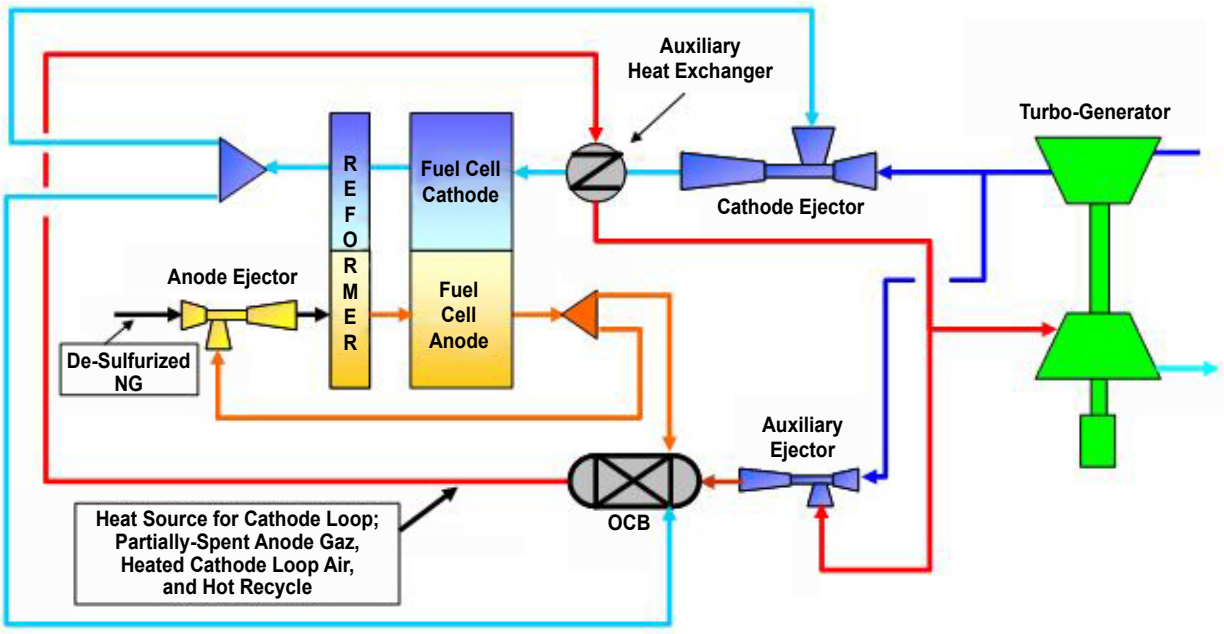

FIGURE 2. Diagram of the cycle configuration for the LGFCS 1 MW distributed power generation system

operating conditions for the stacks. The Phase 1 metric stack test is being performed in the block test rig located in Canton, Ohio. This rig incorporates a single pass anode loop of representative reformate fuel as would exist in a natural gas distributed power generation system. It therefore differs from the system 1 MW product design that utilizes anode loop recycle for chemical recuperation in an internal steam reformer; the spent fuel provides the moisture content necessary for the reforming reaction with the incoming natural gas. The Canton rig achieves the representative ambient cathode air moisture levels and includes a system representative cathode recycle loop. Since the endothermic steam reforming is not present, the off-gas burning of the unspent fuel is performed external to the test rig to maintain the appropriate heat balance, and therefore the Canton rig does not include the auxillary loop feature of the 1 MW product cycle. The three block scale test rigs located in Derby, United Kingdom, fully duplicate the product cycle (shown in Figure 2) except that the rigs use compressed air rather than the air being supplied by a turbo-generator. The incoming air to the rig is heated by electrical heaters to duplicate the heat input of the turbine compressed air and to maintain a close match in overall heat balancing as what is designed for actual product.

The Phase 1 metric test incorporates two strips (stacks) that, combined, generate approximately 7.6 kW at normal design conditions. The durability data on the time of this report (Figure 3) is out to 1,600 hours with the power degradation trending at ~0.8%/1,000: under the SECA Phase 1 requirement of <2%/1,000 hours. This test will run a total of 5,000 hours. The Phase 2 metric test is scheduled to begin in the final quarter of government FY 2012. The Phase 2 test will be run in one of the United Kingdom test rigs. That test will consist of five strips generating approximately 19.2 kW at normal operating conditions, is scheduled to run for 3,000 hours, and must meet the Phase 2 power degradation target of <1.5%/1,000 hours. The five strips are fabricated and have passed quality control checks for per-bundle open circuit voltages following a strip reduction sequence prior to build-up into the block. The general configuration of the block tests is shown in Figure 4. The strips are located within the block box, and the metallic components shown include reformer/heat exchangers, ejectors and general pipework, and hardware for fuel feed and for directing air flow uniformly within the block. The ceramic fuel manifold components within the strips have been optimized to achieve adequate fuel flow uniformity throughout the strip to allow operation at high (greater than 80%) fuel utilization while avoiding regions of local fuel starvation that could adversely impact long-term degradation rates.

The SECA metric tests are required to extend 5,000 hours (Phase 1) and 3,000 hours (Phase 2), but the overall program goal is to demonstrate cell technology able to achieve a 40,000-hour/5-year service life. Towards that goal, LGFCS is testing subscale test articles to longer times than the metric test requirements to ascertain the long-term durability of its current fuel cell technology. The results of these longer term tests are shown in Figure 5. The test conditions bracket the 810°C–910°C

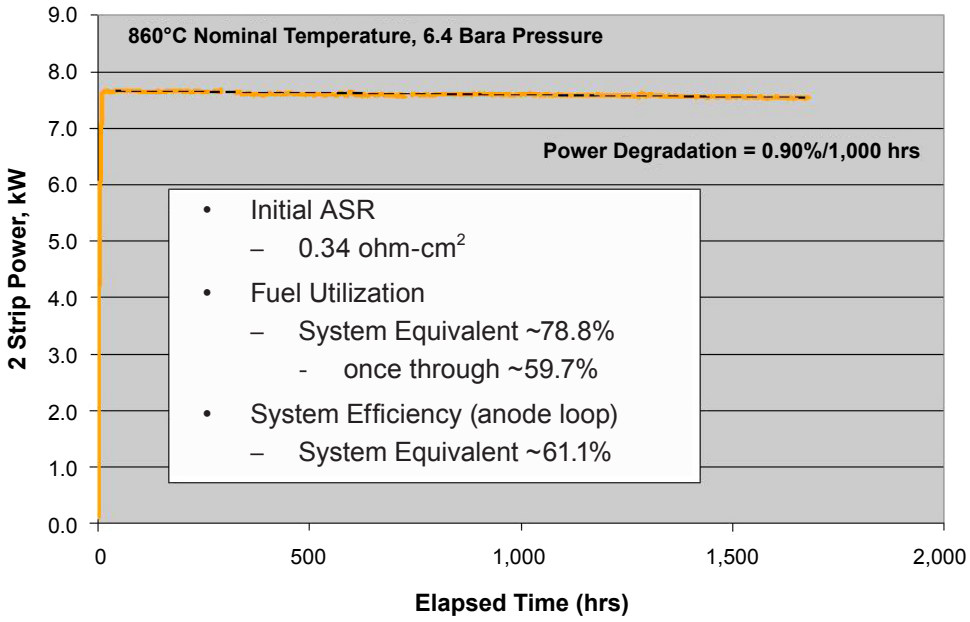

FIGURE 3. Phase 1 metric test durability results

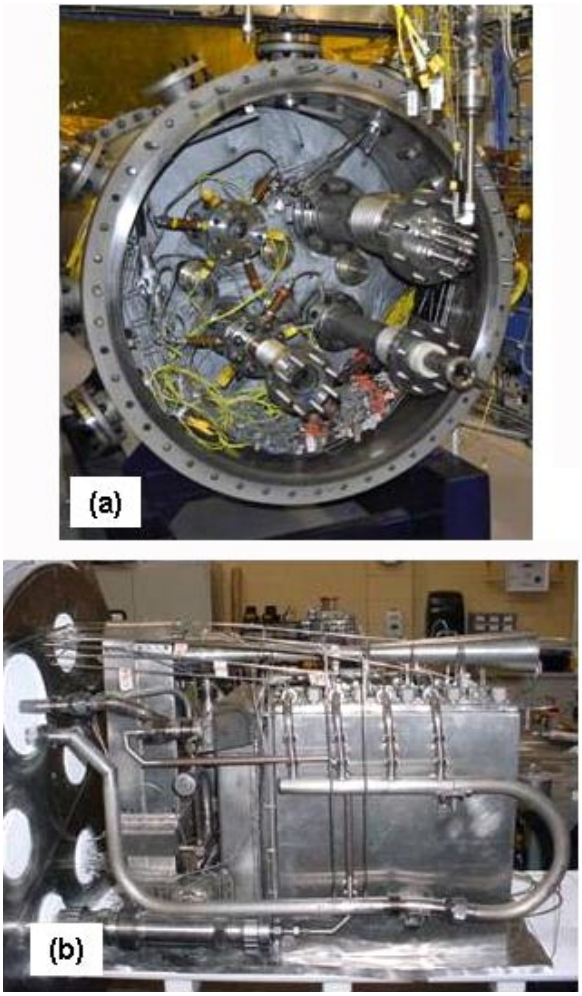

FIGURE 4. Block-scale, system representative test rigs for SECA metric testing: (a) pressure vessel with inserted block chamber and (b) block arrangement

temperature range for strips within a block, and the tests are run at inlet, stack mid-point and peak fuel utilization conditions. Average degradation rates all trend at <1%/1,000 hour, and the degradations rates have been reasonably similar at scales ranging from 5-cell articles, to bundles and now strip-level in the metric block tests. These degradation rates provide for ~2-year service life, sufficient for full-scale technology demonstrations, and development efforts continue to progress the durability to 3–5 year service life.

Electrochemical impedance spectroscopy (EIS) is routinely performed on the subscale test, and the results of that analysis show that the dominant degradation mechanism at block inlet and average temperature is associated with the cathode. Detailed transmission electron microscopy and electron energy loss spectroscopy reveals some cathode phase segregation. Cathode densification is beginning to show

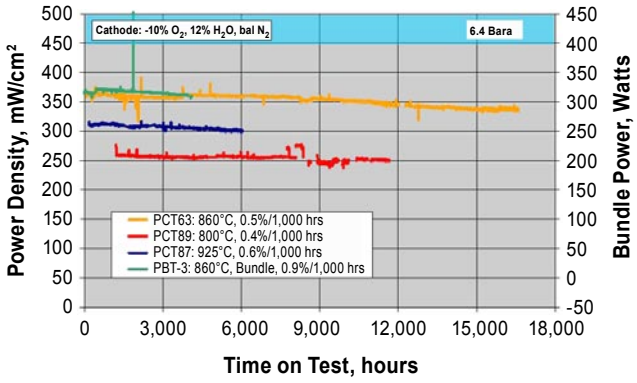

FIGURE 5. Subscale test article degradation rate for the cell technology selected for Phase 1 and Phase 2 metric stack-block tests

at 16,000 hours; this was relatively absent at 8,000 hours. Optimized lanthanum strontium manganite -based cathode compositions are currently being screened to further lower the cell degradation to the levels required by DOE SECA and LGFCS for SOFC products exhibiting service life of 40,000 hours. Anode contributions to degradation are most prevalent at the peak block temperatures (>900°C). Optimized and alternate anode technologies are being screened to limit microstructure coarsening and nickel volatility, but the most important driver for extending block service life is the lowering of the peak block operating temperatures. New cell technology that includes changes to multiple active layer materials has demonstrated a significant lowering of area specific resistance (by ~33% at 860°C, 1 bar pressure) and activation energy that affords the opportunity to reduce peak operating temperatures. These lower ASR cell technologies are entering long-term durability assessments.

Conclusions and Future Direction

During government FY 2012 LGFCS has continued to expand its durability database to assess the lifetimes of its current technology. The Phase 1 metric test of two strips (7.6 kW) is showing degradation rates <1%/1,000 hours and aligns closely with the degradation rates of the subscale test articles, some of which have now exceeded 16,000 hours of test time. The similar durability across scales can allow the subscale articles to be relied on to provide the initial, more cost effective screening of the various active layer technologies that are being investigated to extend the service life. LGFCS has acquired a detailed understanding of the sources of ASR degradation, and EIS plus post-test analysis results have guided the selection of optimized cathode and anode layers that are now being tested for their ability to deliver longer service lives. The LGFCS stack is

comprised entirely of ceramic substrates and manifolds with glass-ceramic based seals and joints. Validating the long-term structural reliability of the stack is a top priority. Residual property measurements from long-term block tests will provide the volume of test data required for Weibull-based CARES analysis and will support validation of time-dependent life predictions based on slow crack growth mechanisms. LGFCS has made significant investments in system relevant pressurized test rigs. The block-scale test rigs match completely the systems conditions, components, environment and stack boundary conditions of the planned initial 1 MW distributed energy product and therefore will serve as the proving ground for the commercial readiness (durability, reliability and cost) of the LGFCS stack technology.

FY 2012 Publications/Presentations

1. S. Lee, T. Ohrn, Z. Liu, Z. Xing, and R. Goettler, "Parametric Electrochemical Impedance Spectroscopy Analysis on High Pressure In-Plane SOFC," Proc. 221st ECS Meeting, Seattle, Washington, May 6–10, 2012.

2. Presentation at 2012 SECA Workshop, Pittsburgh, Pennsylvania, July 26–28, 2012.

References

1. US Patent 7,422,820.

2. G. Agnew, M. Bozzolo, R.R. Moritz, and S. Berenyi, *Proc. ASME Turbo Expo*., **2**, 801 (2005).

3. G. Agnew, R. Collins, M. Jorger, S. Pyke, and R. Travis, *ECS Trans*. **7**(1), 105 (2007).

4. National Energy Technology Laboratory Report DOE/NETL 40/080609, August 6, 2009.

III. SECA CORE TECHNOLOGY R&D

A. Cathodes

III.A.1 Synchrotron X-Ray Studies of SOFC Cathodes

P.H. Fuoss (Primary Contact), K.-C. Chang, J.A. Eastman, B.J. Ingram, E. Perret, H. You
Argonne National Laboratory
9700 S. Cass Ave.
Argonne, IL 60439
Phone: (630) 252-3289; Fax: (630) 252-7777
Email: fuoss@anl.gov

DOE Project Manager: Briggs White
Phone: (304) 285-5437
Email: Briggs.White@netl.doe.gov

Contract Number: FWP49071

Start Date: June 1, 2007
End Date: May 31, 2013

Fiscal Year (FY) 2012 Objectives

- Develop a model for interpretation of $La_{1-x}Sr_xCo_{1-y}Fe_yO_{3-\delta}$ (LSCF) lattice expansion and contraction under electrochemical potential.
- Analyze X-ray diffraction results to determine cation profiles at the yttria stabilized zirconia (YSZ)/LSCF or gadolinium doped ceria (GDC)/LSCF interface of epitaxial LSCF films.
- Examine structural and chemical changes at the surface of low index single crystal surfaces during atomic layer deposition of surface modifiers on LSCF thin films.
- Prepare reports summarizing the science of solid oxide fuel cell (SOFC) cathodes with particular emphasis on in situ X-ray analysis.

FY 2012 Accomplishments

- Activation energies for oxygen surface exchange on LSCF were determined from lattice parameter measurements to be approximately 1.1 eV with a small dependence on applied electrochemical potential and little dependence on oxygen partial pressure.
- Developed a screen printing technology to reproducibly deposit fine (feature sizes down to 100 μm) Au and Pt electrodes onto SOFC cathodes.
- Found that 40 cycles of atomic layer deposition using $Mn(EtCp)_2$ and H_2O resulted in the deposition of 4.9 nm thick MnO films with 17% porosity when using LSCF as a substrate.

Introduction

The performance of SOFCs is strongly influenced by the nanoscale structure and chemistry of electrode materials under operating conditions. However, because SOFCs are operated at elevated temperatures and at near-atmospheric pressure, the utilization of traditional surface science techniques, which typically involve vacuum conditions near room temperature, requires validation. The studies being performed in this program provide the needed understanding of in situ/ex situ correlations. The results also enable the development of molecular-level models for stimulating the rational design and development of high-performance cathode materials.

Approach

We employ in situ x-ray scattering and spectroscopy technologies developed at Argonne National Laboratory to measure equilibrium structures of SOFC cathode materials at elevated temperatures and under controlled oxygen partial pressures. We examine the dynamic structural and chemical changes that occur at the cathode side of a fuel cell under conditions that simulate actual operating conditions. This work, particularly sample preparation and theoretical studies, is performed in collaboration with investigators at several universities including Carnegie Mellon and Stanford.

Results

LSCF is a promising mixed-conducting cathode for SOFCs due to its catalytic activity. Previous studies have shown that the oxygen reduction process at the cathode surface is a rate-limiting step in the performance of SOFCs [1]. Since the oxygen surface exchange coefficient, k, is a measure of the oxygen flux crossing the cathode surface at equilibrium, its determination as a function of temperature and oxygen partial pressure is important for the development of high performance cathode materials. We have developed a novel approach that uses changes in LSCF lattice parameter to determine oxygen vacancy concentrations and oxygen exchange rates.

Using in situ X-ray diffraction, we have investigated the oxygen exchange reaction mechanisms under applied electrochemical potential using pseudo half-cells. The cells consisted of an epitaxial LSCF thin film (60 nm) grown on an YSZ substrate with a GDC interlayer

(inset, Figure 1). The dependence of the oxygen vacancy concentration on electrochemical potential was indirectly measured by analyzing c-lattice parameter changes as a function of applied cathodic and anodic overpotential at different oxygen partial pressures (1.5, 15, and 150 Torr) and in a temperature range from 350°C–600°C with 50°C steps (Figure 2). We exposed the sample to the voltage profile (±0.3V, ±0.6V. ±0.9V, ±1.2V, ±1.5V) at all temperatures. Typically, the out-of-plane c-lattice parameter, i.e., the lattice parameter normal to the film surface, of LSCF increases with increasing oxygen vacancy concentration and temperature. We were able to measure both the absolute change as well as the time dependence of the change in lattice parameters and currents upon application of an electric potential mined from measured shifts in the cathode Bragg peak position with a time resolution of a tenth of a second.

The transition from an initial state to steady state upon potential application is described in terms of a characteristic time constant τ (Figure 1). Characteristic time constants were extracted by fitting lattice parameter shifts as well as measured current changes to a time dependent exponential function [2-6].

$$(y(t)-y_0)/(y_\infty-y_0)=1-\exp(-t/\tau)=1-\exp(-kt/d)$$

Here, y(t) stands for the time-dependent evolution of the current or lattice parameter shift after the potential step, y_0 is the initial current or lattice parameter shift at time t=0, and y_∞ is the steady-state current or lattice parameter shift at t=∞. Note that the same equation as for electrical conductivity relaxation (ECR) measurements is used since the underlying re-equilibrium process is thought to be the same [7]. The resulting exchange coefficients depend, however, on the applied voltage, which is not the case for ECR measurements.

From a series of measurements, the characteristic time constants τ of the c-lattice shifts were found to depend more strongly on the magnitude of the applied potential than time constants derived from the time-dependence of ionic current. This effect can be explained by the strong decrease in electrochemical potential with increasing distance from the wire electrode. The current measurements average over the whole film (due to the mesh on the bottom of the cell) and thus sample a range of effective applied potentials. The c-lattice shifts, however, are extracted from the Bragg peak shifts with the X-ray beam located 0.2 mm away from the top wire electrode and are only dependent on a single potential.

Exchange coefficients (k=d/τ) are directly calculated from the characteristic time constants τ and film thickness d. Activation energies are extracted from the slopes of lines fitted to Arrhenius plots (Figure 3). The activation energies extracted from Arrhenius plots of exchange coefficients deduced from time constants of current and c-lattice changes are all about 1.1 eV. Exchange coefficients derived from current and c-shifts have the same order of magnitude for all

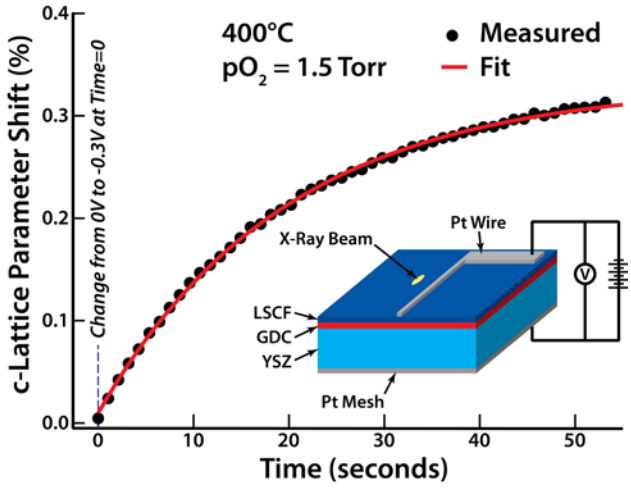

FIGURE 1. The time evolution of c-lattice parameter shift of LSCF at 400°C at 1.5 Torr upon applied cathodic potential -0.3 V at time equal to zero. Also shown is the experimental geometry using a pseudo half-cell consisting of LSCF/GDC/YSZ and the configuration for electrochemical measurements.

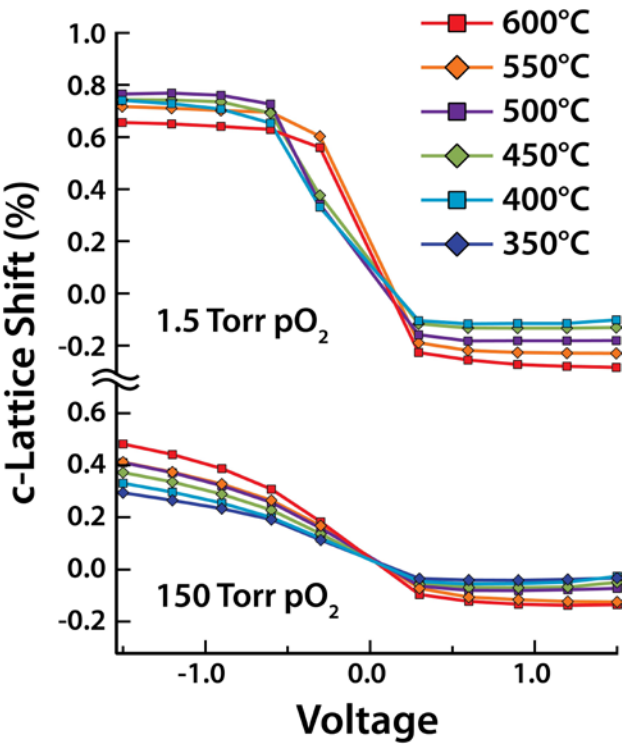

FIGURE 2. The equilibrium c-lattice parameter shift as a function of applied voltage, oxygen partial pressure and temperature for an LSCF/GDC/YSZ heterostructure.

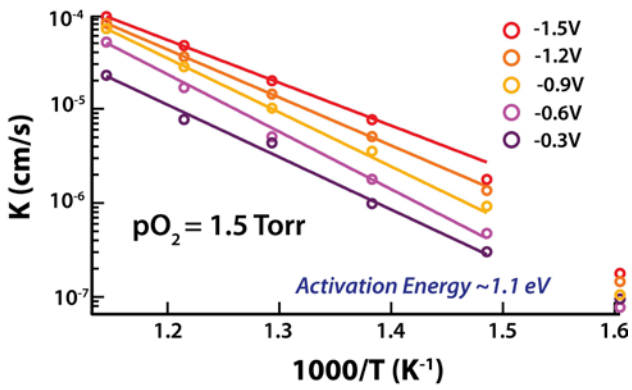

FIGURE 3. Arrhenius plot showing the surface exchange coefficient as a function of inverse temperature determined from lattice parameter changes. The activation energy for all of the partial pressures is approximately 1.1 eV.

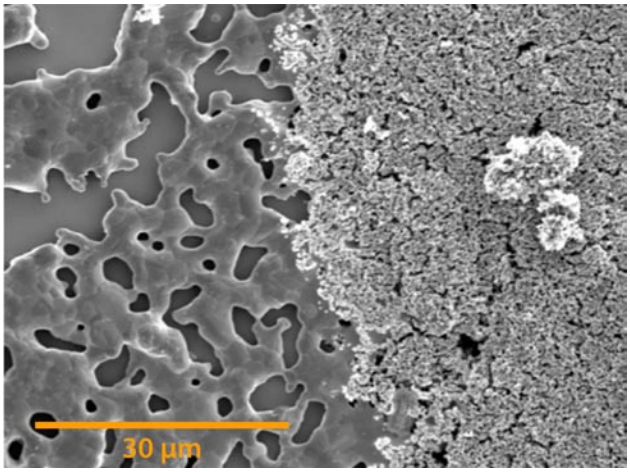

FIGURE 4. A scanning electron microscopy (SEM) image showing a layer of screen printed LSCF (right), partially sintered at 400°C for one hour, deposited on top of a screen-printed Pt layer (visible on left), which had been sintered at 1,000°C for one hour. The substrate was polished MgO.

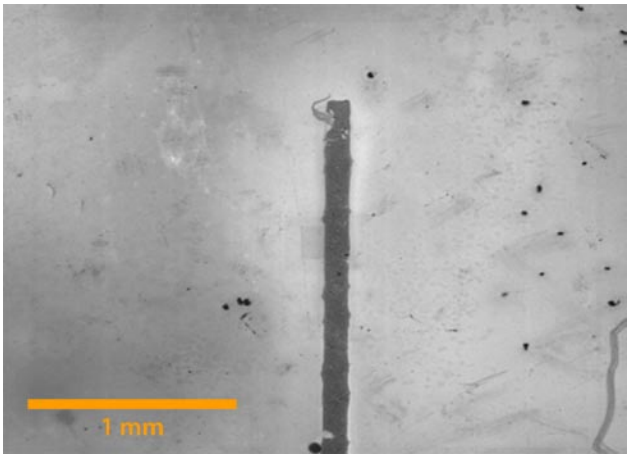

FIGURE 5. A SEM image of a screen-printed Pt strip, approximately 100 µm wide, deposited on a thin film of LSCF (using a polished YSZ substrate).

oxygen partial pressures. Previous published surface exchange coefficients of pulsed laser deposited (PLD) LSCF thin films are in the order of 2-6 × 10^{-6} cm/s in the temperature regime from 500–650°C [2], which is lower than the exchange coefficient determined in this study ~2 × 10^{-5} to 1 × 10^{-4} cm/s. However, the current work examines transport through the thin film while ECR experiments have determined conduction parallel to the surface.

We have developed a better technique to deposit electrodes onto the samples in order to improve the reproducibility of electrochemical measurements. The new technique uses screen printing to deposit electrodes on top of substrates with a controllable and reproducible shape and size. This method involves pressing a paste of the desired material through a fine mesh that can be masked to provide the desired geometry. The method has been used to produce feature sizes down to 100 µm; this capability is particularly attractive for synchrotron measurements where a straight substrate-electrode interface is required to prevent interference of the electrode with the X-ray beam footprint. To date, this technique has been used to deposit films of platinum, gold, lanthanum strontium manganite (LSM), lanthanum strontium ferrite (LSF), and lanthanum strontium cobalt ferrite (LSCF). Other materials are possible, as long as inks can be made. As the micrographs in Figure 4 and Figure 5 demonstrate, this deposition method results in continuous, porous films. The microstructure depends on the sintering history of the film, and the required sintering temperature depends on the material deposited. The first micrograph in Figure 4 shows a screen printed LSCF film, sintered at 400°C for one hour, deposited on top of a Pt film, which had previously been sintered at 1,000°C for one hour. The second micrograph in Figure 5 is an image of a 100-µm-wide Pt line deposited on a PLD deposited LSCF film, demonstrating the controllable nature of this screen-printing technique. Upcoming investigations will involve measuring the thickness of films deposited using this technique, as well as determining the long-term high temperature stability of Pt and Au electrodes.

Conclusions and Future Directions

In situ X-ray observations have demonstrated that oxygen transport across the LSCF/atmosphere interface has a larger energy barrier than transport across the LSCF/GDC interface under both anodic and cathodic conditions, and have provided insight

into the partial pressure of oxygen (pO_2) dependence of the behavior. Future investigations will focus on providing a quantitative understanding of the time- and depth-dependences of the lattice parameter (and thus oxygen vacancy concentration) responses to applied potentials, which will enable detailed understanding of the oxygen exchange kinetics as functions of T and pO_2. Depth profiling of the oxygen vacancy concentration ($V_O^{\bullet\bullet}$) will probe the ionic charge distribution near the electrochemical active surface. The results of these studies are providing needed insight into the behavior of electrochemical devices for energy storage and energy transfer applications. The time constants of the lattice parameter change and the conductivity change are similar for all oxygen partial pressures. However, the time constants of the c-lattice parameter shifts depend more strongly on the applied voltage than do time constants of ionic current changes. We attribute this effect to the fact that X-ray results are sensitive to local variations while the current reflects the average behavior of the sample. This local variation provides an important opportunity to understand the working of SOFC cathodes. Using standard synchrotron X-ray techniques, it is straightforward to measure lattice parameters in thick structures with a resolution of 1 μm in position and 10^{-4} μm in strain [8]. Thus, the results described here provide an avenue to probing the local performance of operating SOFC cathodes that have been treated with performance enhancing infiltrants.

FY 2012 Publications/Presentations

1. B.J. Ingram, J.A. Eastman, K.-C. Chang, S.K. Kim, T.T. Fister, E. Perret, H. You, P.M. Baldo and P.H. Fuoss, "In Situ X-Ray Studies of Oxygen Surface Exchange Behavior in Thin Film $La_{0.6}Sr_{0.4}Co_{0.2}Fe_{0.8}O_{3-\delta,}$" submitted to *Applied Physics Letters*, 2012.

2. E. Perret, C. Park, D.D. Fong, K.-C. Chang, B.J. Ingram, J.A. Eastman , P.M. Baldo and P.H. Fuoss, "Resonant X-Ray Scattering Studies of Epitaxial Complex Oxide Thin Films," submitted to *Journal of Applied Crystallography*, 2012.

3. E. Perret, B.J. Ingram, H. Zhou, T.T. Fister, P.M. Baldo, J.A. Eastman, and P.H. Fuoss, "The Compositino and Structure of $La_{0.6}Sr_{0.4}Co_{0.2}Fe_{0.8}O_{3-\delta}$ Thin Film Surfaces," X-Ray Sciences Gordon Research Conference, Waterville, Maine, August 7–12, 2011.

4. P.H. Fuoss, M.J. Highland, D.L. Proffit, T.T. Fister, S.O. Hruszkewycz, D.D. Fong, P.M. Baldo, G.-R. Bai, J.A. Eastman, S.K. Streiffer, G.B. Stephenson, M.-I. Richard, Carol Thompson and T.O. Mason, "Exploring the What, When, Where and Why of Materials Synthesis," 21st International Congress on X-Ray Optics and Microanalysis, Campinas, Brazil, September 5–8, 2011.

5. P.H. Fuoss, E. Perret, T.T. Fister, Hoydoo You, Kee-Chul Chang, D.D. Fong, P.M. Baldo, J.A. Eastman, M.J. Highland and Brian Ingram, "Synchrotron X-Ray Studies of SOFC Cathodes," 12th Annual SECA Workshop, Pittsburgh, Pennsylvania, July 26–28, 2011.

6. J.A. Eastman, P.H. Fuoss, E. Perret, K.-C. Chang, P. Baldo, B. Ingram, T.T. Fister, P. Salvador, "In-Situ Synchrotron X-Ray Studies of the Structure and Electrical Behavior of $La_{0.6}Sr_{0.4}Co_{0.2}Fe_{0.8}O_{3-d}$ Epitaxial Thin Films," Workshop on Oxide Electronics 18, Napa, California, September 26–28, 2011.

7. B.J. Ingram, T.T. Fister, S.-K. Kim, J.A. Eastman, M.J. Highland, P.H. Fuoss, "The Role of Temperature, Partial Oxygen Pressure and Electrochemical Polarization on Charge Transport in Thin Film Solid Oxide Fuel Cell Cathodes," MS&T'11, Columbus, Ohio, October 16–20, 2011.

8. P.H. Fuoss, B.J. Ingram, E. Perret, K.-C. Chang, T.T. Fister, P.H. Baldo, J.A. Eastman and P.A. Salvador, "Time-Resolved Correlations between the Structure and Electrical Behavior of $La_{0.6}Sr_{0.4}Co_{0.2}Fe_{0.8}O_{3-\delta}$ Epitaxial Thin Films," MRS Fall Meeting, Boston, Massachusetts, November 28– December 2, 2011.

9. E. Perret, T.T. Fister, H. Zhou, J.A. Eastman, P.A. Baldo, B.J. Ingram and P.H. Fuoss, "In Situ Synchrotron X-Ray Studies of the Surface Structure and Composition of $La_{0.6}Sr_{0.4}Co_{0.2}Fe_{0.8}O_{3-\delta}$ Thin Films," MRS Fall Meeting, Boston, Massachusetts, November 28–December 2, 2011.

10. K.-C. Chang, B.J. Ingram, Lu Yan, P.A. Salvador, and H. You, "Potential Dependent Cation Segregation and B-Site Surface Oxidation State in Model Thin Film Perovskite Cathodes," MRS Fall Meeting, Boston, Massachusetts, November 28–December 2, 2011.

References

1. S.B. Adler, *Chemical Reviews*, **104**, 4791(2004).

2. A. Zomorrodian et al., *International Journal of Hydrogen Energy*, **35**, 12443(2010).

3. A. Karthikeyan and S Ramanathan, *APL*, **92**, 243109(2008).

4. J.A. Lane et al., *Solid State Ionics*, **121**, 201(1999).

5. E.N. Armstrong et al., *Journal of the Electrochemical Society*, **158**, B492(2011).

6. J.A. Lane and J.A. Kilner, *Solid State Ionics*, **136-137**, 997(2000).

7. I. Yasuda and T. Hikita, *Journal of the Electrochemical Society*, **141**, 1268(1994).

8. J.D. Budai, W. Liu, J.Z. Tischler, Z.W. Pan, D.P. Norton, B.C. Larson, W. Wang and G.E. Ice, *Thin Solid Films*, **516**, 8013(2008).

III.A.2 Unraveling Oxygen Reduction Kinetics on SOFC Cathodes Using Patterned Electrodes and X-Ray Techniques

Srikanth Gopalan (Primary Contact), Lincoln Miara, Jacob N. Davis, Soumendra N. Basu, Karl F. Ludwig, and Uday B. Pal

Boston University
15 St. Mary's St.
Boston, MA 02215
Phone: (617) 358-2297; Fax: (617) 353-5548
Email: sgopalan@bu.edu

DOE Project Manager: Patcharin Burke
Phone: (412) 386-7378
Email: Patcharin.Burke@netl.doe.gov

Contract Number: NT0004104

Start Date: October 1, 2008
End Date: March 31, 2013

Fiscal Year (FY) 2012 Objectives

- Quantify the relative role of surfaces versus triple phase boundaries (TPB) in the oxygen reduction process in strontium doped lanthanum cobalt ferrite (LSCF).
- Probe the surface composition and the surface electronic structure using total reflection X-ray fluorescence (TXRF) and hard X-ray photoelectron spectroscopy (HAXPES).
- Develop correlations between surface composition and electronic structure with the bulk and surface defect chemistry of cathodes.

FY 2012 Accomplishments

- Patterned electrodes have been used to deconvolute the relative importance of surface diffusion pathways and bulk diffusion pathways in LSCF.
- TXRF and HAXPES measurements were performed on calcium doped lanthanum manganite (LCM) and LSCF thin films and show the LCM films to be enriched in Mn and the LSCF films to be enriched in Sr.

Introduction

In solid oxide fuel cells (SOFCs), two types of electrodes are held up as paradigms for the oxygen reduction reaction. At one end, doped lanthanum manganite, a predominantly electronic conductor, is thought to function through the surface adsorption, surface diffusion, and incorporation at the TPBs. At the other end lies LSCF which is thought to function predominantly through the bulk diffusion pathway. In the work presented here we have systematically analyzed the two different pathways in LSCF through a set of impedance spectroscopy measurements on patterned cathodes. The goal of these experiments is to quantify the contribution of the surface pathways and the bulk pathways in the oxygen reduction process.

In parallel experiments, we have used X-ray spectroscopic techniques such as TXRF and HAXPES to probe the surface chemistry and structure of thin film cathodes. The goal of these experiments is to understand the surface compositional and electronic structure changes occurring at the surface and to correlate them with the known defect chemistry of the bulk. Eventually, this understanding is expected to lead to the origins of the oxygen reduction mechanisms being investigated using patterned electrodes.

Approach

Patterned Electrode Experiments on LSCF

By systematically varying the TPB length of the thin film patterned cathodes, performing impedance spectroscopy on them as a function of temperature and oxygen partial pressure, and modeling the results using a simple scaling model as well as a detailed transport phenomena model, we have been able to separate and describe the importance of the two different oxygen pathways in LSCF.

X-Ray Spectroscopy

TXRF is a tool in which X-rays are directed on the surface of the sample and electrons ejected from the core levels. When the electrons from the higher levels fill the core holes left behind, X-rays are emitted. Analysis of the resulting X-ray spectra provides information that can be used to obtain compositional information from

the samples. By changing the angle of incidence, lower angles probing more of the surface and higher incidence angles probing more of the bulk, we can obtain surface specific compositional information. Traditionally, X-ray photoelectron spectroscopy (XPS) is a well-known technique in which material surfaces are irradiated with X-rays and the electron-emitted electronic spectra are analyzed for their binding energies. Thus XPS has been used as an excellent electronic structure measurement technique. HAXPES, which adds to the capabilities of XPS, is quickly emerging as a tool to obtain depth of information to the already known surface sensitivity of XPS and to differentiate the surface electronic structure from that of the bulk. We have used HAXPES to differentiate the surface electronic structure of LSCF from that of the bulk.

Results

Patterned Electrode Experiments on LSCF

In our experiments we have found clear evidence of both bulk transport pathways and surface diffusion pathways active in LSCF.

While at lower operating temperatures and lower oxygen partial pressures, the bulk diffusion pathways dominate the transport of oxygen; at higher temperatures and higher oxygen partial pressures, surface transport pathways emerge as just as important. Figure 1 shows the inverse polarization resistance measured as a function of temperature and oxygen partial pressure and TPB length for both LCM and LSCF. It is clear from this simple scaling plot that the dependence of the polarization resistance on TPB line length is much stronger for LCM than for the LSCF at all temperatures and oxygen partial pressures, indicating the greater importance of the surface path in LCM than in LSCF.

Further, we have used a two dimensional (2D) transport phenomena model that takes into account oxygen surface exchange, surface diffusion and bulk diffusion and deconvoluted the relative importance of these various processes in the oxygen reduction in SOFC cathodes. This model is built on the one developed for porous electrodes by Lu, et al [1]. The geometry of the model is shown in Figure 2.

The salient parameters in the model are:

(1) Diffusion resistance

$$R_D = \frac{RT}{8F^2}\frac{(W+H)}{c_o x_v^o D_v}$$

In the above equation for the diffusion resistance, R and T have their usual meanings; W and H are geometrical dimensions as shown in Figure 2; c_o is the bulk oxygen ion concentration; x_v^o is the equilibrium oxygen vacancy concentration; and D_v is the oxygen vacancy diffusivity.

(2) Ratio of oxygen surface exchange to bulk diffusion

$$\kappa = \frac{4R_o W}{c_o x_v^o D_v} \equiv \frac{\text{surface oxygen exchange}}{\text{bulk oxygen diffusion}}$$

In the above R_O is the oxygen surface exchange rate in units of mol/(cm^2.s) and the other terms have their previous meanings.

(3) Ratio of surface diffusion to bulk diffusion

$$\nu = \frac{\Gamma_o \theta_{O_s}^o D_{O_s}}{W c_o x_v^o D_v} \equiv \frac{\text{surface oxygen diffusion}}{\text{bulk oxygen diffusion}}$$

In the above equation, Γ_o is an apparent storage capacity per unit area and θ_{Os} is the fractional surface occupancy (the 0 subscript refers to the equilibrium value), and D_{Os}

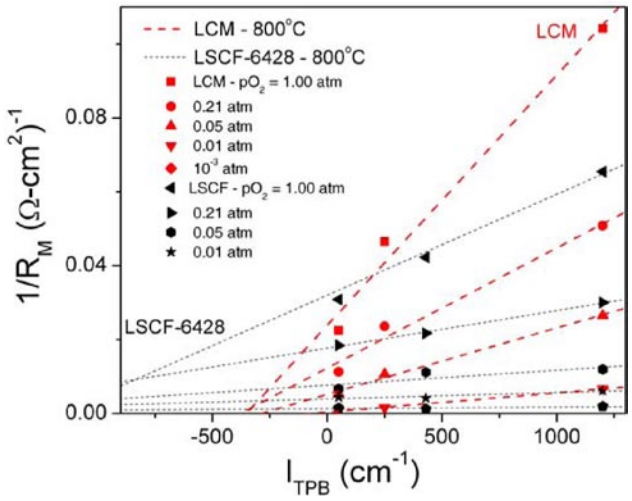

FIGURE 1. Scaling behavior of LCM and LSCF with the triple phase boundary length

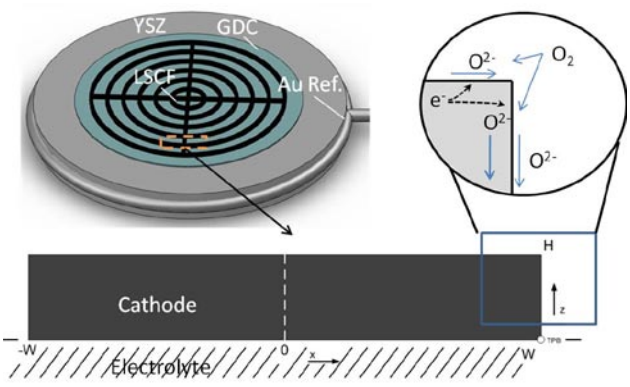

FIGURE 2. Model geometry for LSCF patterned cathodes

is the surface diffusivity of oxygen and the other terms have their previous meanings.

Figure 3 shows κ as a function of oxygen partial pressure and temperature and Figure 4 shows the R_O extracted from it. Figure 5 shows the ν as a function of oxygen partial pressure and temperature.

From these parameter estimations, it is clear that the surface exchange rate R_O stays roughly independent of oxygen partial pressure, but increases as a function of temperature with an activation energy of 115 kJ/mol. The surface diffusion on the other hand is a strong function of oxygen partial pressure and temperature, increasing as a function of increasing oxygen partial pressure and temperature. At a given temperature, the oxygen vacancy concentration decreases as a function of oxygen pressure. Thus at low oxygen partial pressures, bulk diffusion is favored over surface diffusion (ν < 1). At higher temperatures at a fixed oxygen partial pressure, the vacancy concentration presumably increases and thus the bulk diffusion rates; however the increase in ν with increasing temperature and fixed oxygen partial pressure would seem to imply that the surface diffusivity increases at a rate faster than the oxygen vacancy concentration and thus the bulk diffusivity. However, more experimentation and modeling particularly employing computational methods is required to further verify these observations.

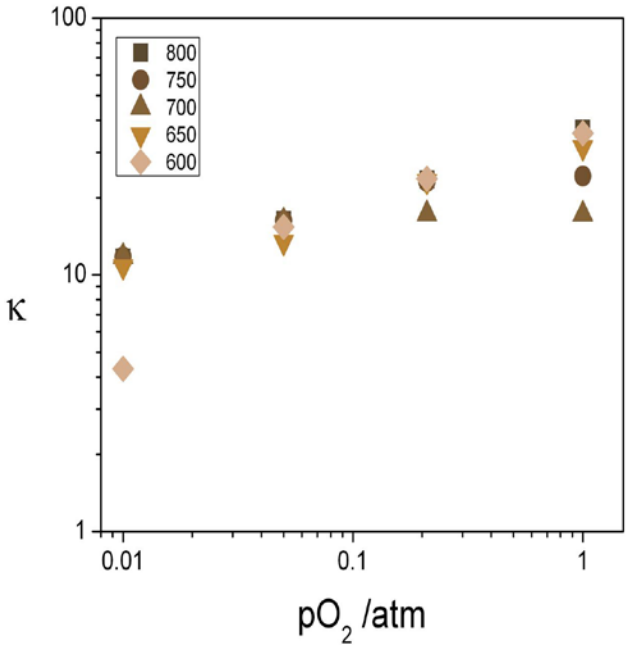

FIGURE 3. Behavior of the ratio of surface exchange to bulk diffusion in LSCF

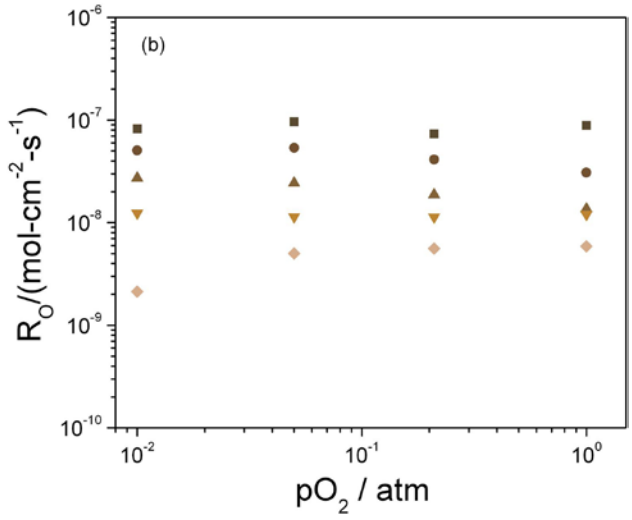

FIGURE 4. Oxygen surface exchange flux in LSCF

X-Ray Spectroscopy

We have performed TXRF measurements on thin films of lanthanum strontium managanite (LSM) and LSCF. Using a chamber designed for this project, in situ high temperature measurements were taken in air. We are able to verify that compositional changes present at high temperatures are preserved upon annealing and quenching; this knowledge allows us the opportunity to measure quenched samples from a wider range of oxygen partial pressure and temperatures.

Figure 6 shows for LSCF the strontium to A-site ratio as measured at high temperature continuously measured upon reaching 800°C for eight hours. Figure 7 reveals that for LSM quenching preservers the high temperature state, and that there is no further evolution after high temperature is reached.

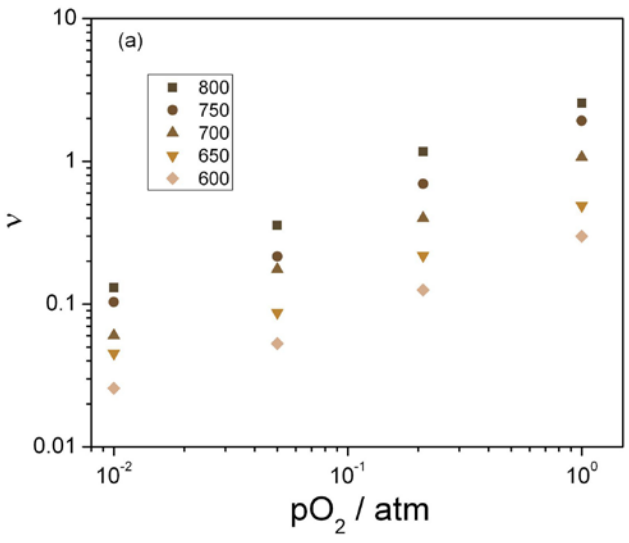

FIGURE 5. Ratio of surface diffusion to bulk diffusion in LSCF

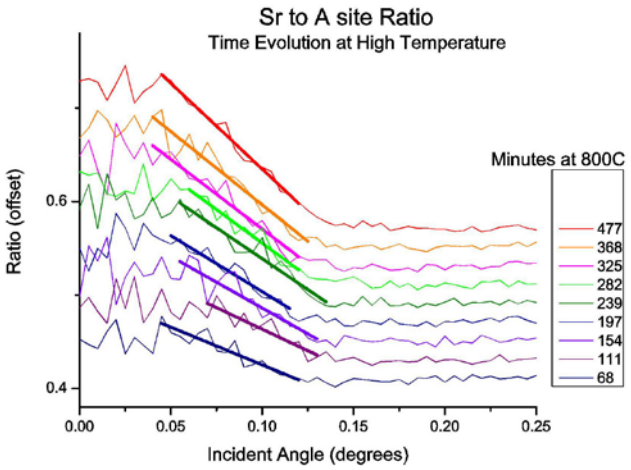

FIGURE 6. In-situ strontium to A-site ratio for LSCF measured by TXRF. Below the critical angle the slope indicates a higher concentration that is present in the bulk. The slope magnitude increases over 500 minutes, indicating further strontium enhancement over this time scale.

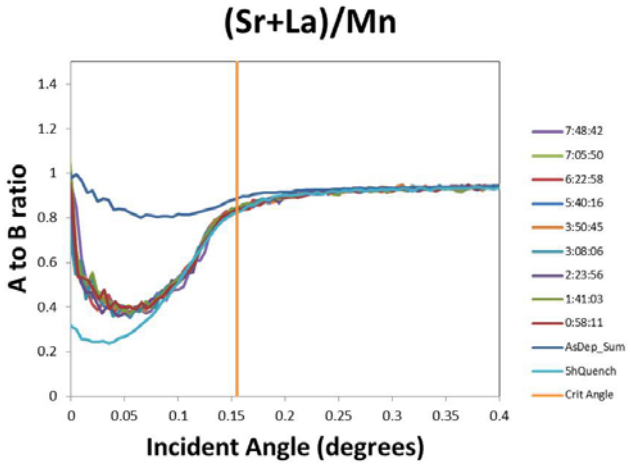

FIGURE 7. In-situ A/B ratio for LSM measured by TXRF. At high temperature the manganese concentration is higher than that of an as-deposited sample. Quenching from temperature preserves the high temperature condition.

HAXPES offers some advantages over lower energy XPS techniques. Higher incident photon energies overcome surface contamination and result in improved signals without the need to heat in vacuum. Also, HAXPES allows for a tunable penetration depth, so correlations can be made between the depth dependence seen in composition by TXRF and oxidation states of cations. Figure 8 shows HAXPES spectra for strontium 3p of LSCF.

These results clearly show the power of X-ray methods to probe the surface chemistry and electronic structure of cathode thin films. The next steps are to finish analysis of the HAXPES results and to use the combined TXRF and HAXPES results to derive a model for the surface defect chemistry of the cathodes.

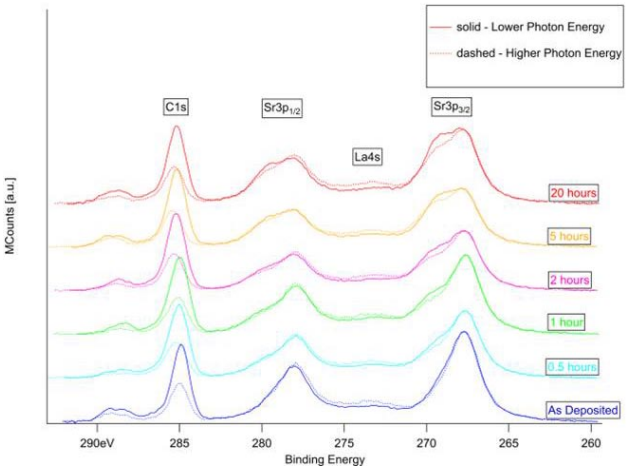

FIGURE 8. LSCF HAXPES spectra for carbon 1s, lanthanum 4s, and strontium 3p. Offset are data from an as-deposited sample as well as samples quenched from 800°C after various annealing times. Data was taken with incident photon energies of 2,140 eV and 3,000 eV.

Conclusions and Future Directions

Conclusions

Surface diffusion is equally important as bulk diffusion at higher oxygen partial pressures and temperatures in LSCF. A-site deficient LCM surfaces with 13% A-site doped with Ca are enriched in Mn compared to the bulk. LSCF thin films of composition $La_{0.6}Sr_{0.4}Co_{0.2}Fe_{0.8}O_{3-\delta}$ are enriched on the surface with Sr.

Future Directions

The TXRF and HAXPES measurements will be combined with the bulk defect chemistry model to derive a model for the surface. Further, the effect of surface electrocatalysts will be explored using patterned electrode measurements. Finally, the surface composition and structure will be correlated with the emerging understanding of oxygen reduction in cathodes.

Awards

2012 outstanding PhD award of the Boston University MSE Division awarded to Lincoln Miara whose work was funded by this cooperative agreement. His thesis title was "Kinetics of Oxygen Reduction in Perovskite Cathodes for Solid Oxide Fuel Cells: A Combined Modeling and Experimental Approach."

FY 2012 Publications/Presentations

1. L. Miara, U. Pal, and S. Gopalan, "Mechanistic Interpretation of the Oxygen Reduction Kinetics of $La_{0.85}Ca_{0.15}MnO_3$ Cathode," *ECS Trans*., 35 (1), 2119 (2011).

2. J.N. Davis, L. Miara , L. Saraf, T.C. Kaspar, S. Gopalan, U.B. Pal, J.C. Woicik, K.F. Ludwig, and S.N. Basu, "Hard X-Ray Fluorescence Measurements of Heteroepitaxial Solid Oxide Fuel Cell Cathode Material," accepted for publication in *ECS Transactions* (2011).

3. L.J .Miara, S.N. Basu, U.B. Pal, and S. Gopalan, "2D Numerical Model for Identification of Oxygen Reduction Reaction Mechanisms in Patterned Cathodes of $La_{0.6}Sr_{0.4}Co_{0.2}Fe_{0.8}O_{3-\delta}$," *J.Electrochem. Soc.,* **159** (8) F419-F425 (2012).

References

1. Lu, Y.X., Kreller, C., Adler, S.B., "Measurement and Modeling of the Impedance Characteristics of Porous $La_{1-x}Sr_xCoO_{3-\delta}$ Electrodes," *Journal of the Electrochemical Society*, 2009, 156(4), pp. B513-B525.

III.A.3 SOFC Cathode Surface Chemistry and Optimization Studies

Paul A. Salvador (Primary Contact), Lu Yan, Mioalei Yan
Carnegie Mellon University
Department of Materials Science and Engineering
5000 Forbes Avenue
Pittsburgh, PA 15206
Phone: (412) 268-2703; Fax: (412) 268-3113
Email: paul7@andrew.cmu.edu

DOE Project Manager: Patcharin Burke
Phone: (412) 386-7378
Email: Patcharin.Burke@netl.doe.gov

Contract Number: NT0004105

Start Date: September 30, 2008
End Date: March 29, 2013

Fiscal Year (FY) 2012 Objectives

- To develop samples of cathode materials having specific surface structures and chemistries using thin film preparation methods, as requested by collaborators.
- To provide lanthanum strontium manganese oxide (LSM), lanthanum strontium cobalt oxide (LSC), and lanthanum strontium cobalt iron oxide (LSCF) samples for surface characterization to collaborators at Argonne National Laboratory-Advanced Photon Source, Massachusetts Institute of Technology, and University of Nevada, Las Vegas.
- To determine the value and activation energy of k_{chem} for strained LSM (100) and (110) at different thicknesses and on different substrates.
- To substantiate further the correlation between extended defect populations and activity of textured yttria stabilized zirconia (YSZ) samples on YSZ and MgO.
- To further explore surface engineering by fabricating other coatings and alternate geometries of coatings, especially investigating mesoporous materials as electrocatalysts in collaboration with National Energy Technology Laboratory (NETL).

FY 2012 Accomplishments

- Further developed single-crystal, epitaxial, textured, and polycrystalline thin films of LSM, LSC, and LSCF with low roughness values on both insulating and electrolytic substrates of various geometries that were used in both in-house and collaborators' experimental facilities to understand the nature of the surface chemistry/reactivity of cathode materials.
- Thin film samples were characterized at Carnegie Mellon University (CMU) with X-ray diffraction (XRD), X-ray reflectivity (XRR), and atomic force microscopy (AFM) and further characterized by collaborators (separate reports) and by electrical conductivity relaxation (ECR) at CMU.
- Demonstrated that the activation energy of k_{chem} for 50 nm thick LSM films were between 1.5 eV/atom, for (100) films, and 1.9 eV/atoms, for (110) films.
- Demonstrated that the k_{chem} values for strained 50 nm thick films on $SrTiO_3$ (STO) were ≈25x greater than those on $NdGaO_3$ (NGO).
- Demonstrated that the strained (110) films had the highest exchange rate of all measured films, indicating strain can be an important enhancing factor in Solid Oxide Fuel Cells (SOFCs).
- Strained (110) films had significantly different and greater activation energies than relaxed films.
- Demonstrated that the highest activation energy process dominated at SOFC temperatures.
- Demonstrated that the extended defect process for (110) and (100) textured films decreased with grain size, while the native surface increased.
- Demonstrated that ECR could be carried out on mesoporous coatings on thin film electrocatalysts, though the response is complicated and requires further understanding.
- Demonstrated that mesoporous LSM coatings in LSM-based half-cells remove surface-related polarizations from the cathode overpotentials.

Introduction

The cathode in SOFCs is responsible for the reduction of O_2 gas and its incorporation into the electrolyte. When SOFCs are operated at specific current densities/voltages, the oxygen incorporation (or uptake) process can contribute significantly to the losses of the cell, thereby limiting the performance of the SOFC system. Two major options exist for improving the cathode performance by specifically targeting the oxygen incorporation process: changing the component solid materials or adding yet another material (a catalyst) to the existing frameworks [1,2]. In general, both of these are tantamount to improving the overall surface

reactivity while maintaining the bulk properties of existing cathodes. We have been pursuing the goal of isolating the enabling characteristics that lead to highly active surfaces, which will lead to improved cathode performance in SOFCs and an acceleration of introduction of new materials into SOFCs to allow for the U.S. Department of Energy Solid (DOE) Solid State Energy Conversion Alliance (SECA) program to meet performance metrics.

Generally speaking, the limitations in designing highly active cathodes for oxygen incorporation arise from the general lack of direct correlations between surface/interface chemistry/structure and performance of SOFC cathode materials over the appropriate ranges of SOFC operational conditions [3]. In this work, we aim to fill this need by (1) developing experimental protocols that will provide a sensitive measure of activity/stability in operational conditions and by (2) determining key correlations between structure (solid state atomic, electronic, crystallographic, and chemical) and electrochemical performance (mass and charge transfer) parameters in surface engineered samples. We have participated in an experimental program that allows us to probe the nature of atomic scale surface chemistry and microstructure and their roles in oxygen incorporation in cathode materials [4–19]. At CMU, we have provided samples to collaborators [4–8, 11, 14–19] (separate reports) and explored systematically the role of microstructure on oxygen exchange LSM [9–11,15]. Furthermore, we have applied the approach to understanding infiltration by over-coating LSCF thin films with nanoscale mesoporous coatings. Finally, we used infiltrated LSM-based half-cells with mesoporous LSM and demonstrated that surface polarizations are decreased to near zero when mesoporous coatings are included. In this report, we describe the progress at CMU on these topics.

Approach

Thin film samples are prepared using pulsed laser deposition (PLD) [6–7, 10–11, 15–17]. By calibrating the growth rate using XRR, films of specific thicknesses are fabricated. Using XRD, the orientation relationship between the film and substrate can be determined. Using AFM, the film surface topography can be determined. By correlating the results of XRR, XRD, and AFM to growth parameters, we fabricate high quality films with controlled microstructural and surface features. Specifically, the following films were fabricated; (1) epitaxial (100) and (110) films of LSM were prepared on STO and NGO substrates with thicknesses varying from 50 nm to 600 nm, which allowed for the isolation of strain and dislocation effects; (2) textured films—(110) LSM on (111) YSZ and (100) LSM on (100) MgO—were prepared to control the extended boundary populations; and (3) (621) LSM films were prepared on (621) STO. (100) LSCF films were prepared on (100)- gadolinia doped ceria (GDC) coated YSZ, on which mesoporous LSM coatings [20–21] were prepared and characterized.

ECR measurements [9–11, 15] were made on a variety of films. The oxygen pressure (PO_2) was changed between 50 mTorr and 500 mTorr, using the mass flow controller. All ECR data was modeled on the basis of a surface exchange model [15, 22–26], using one or two surface exchange coefficients [10–11, 15]. k_{chem} was obtained based on fitting the data of the relaxation curves and corrected by taking account of the chamber flush time [15]. The mathematical relationships are given as follows:

$$g(t)=\frac{\sigma_t-\sigma_{final}}{\sigma_{final}-\sigma_{initial}}=1-A\exp(-\frac{k_{1,chem}t}{L})-(1-A)\exp(-\frac{k_{2,chem}t}{L})$$

where $g(t)$ is the normalized conductivity, σ_t is the conductivity at time t, σ_{final} is the conductivity at re-equilibrium and $\sigma_{initial}$ is the conductivity at the initial equilibrium state, A is a constant, and L is the sample thickness.

Results

As indicated in past publications [4–5, 8–11, 13, 15, 18–19] and reports [6–7, 12, 16–17] and in forthcoming publications, we have been providing high quality surface engineered thin films to collaborators who are working on identifying surface chemistries and properties that lead to improved electrocatalytic performance. It is essential to characterize the details of the thin film structure to interpret properly experimental observations. At CMU, we carry out the necessary processing and characterization to ensure samples have the characteristics requested from collaborators. Reports from collaborators are given elsewhere. Figure 1 gives an example of such characterization for the 600 nm thick LSM film on (621) STO, (110) YSZ and (100) MgO. A composite theta—two theta XRD pattern (each pair taken at different out-of-plane angles [27–28]) is shown in Figure 1a, indicating the film is highly crystalline and epitaxial with the substrate. AFM images of the surface showed atomic steps (slightly bunched and nano-faceted) whose ledges run along the (012) direction, as expected [27–28]. For textured films on (111) YSZ and (100) MgO, surfaces were generally slightly rougher (root-mean-square roughness of 3 nm) than the epitaxial films, as shown in Figures 1b and 1c, but they were comparable to each other. The films on YSZ had circular surface features that correlated to the grains, while the films on MgO had step-like surface features that could not be correlated to variant boundaries. All films were well characterized for quality control before measurement.

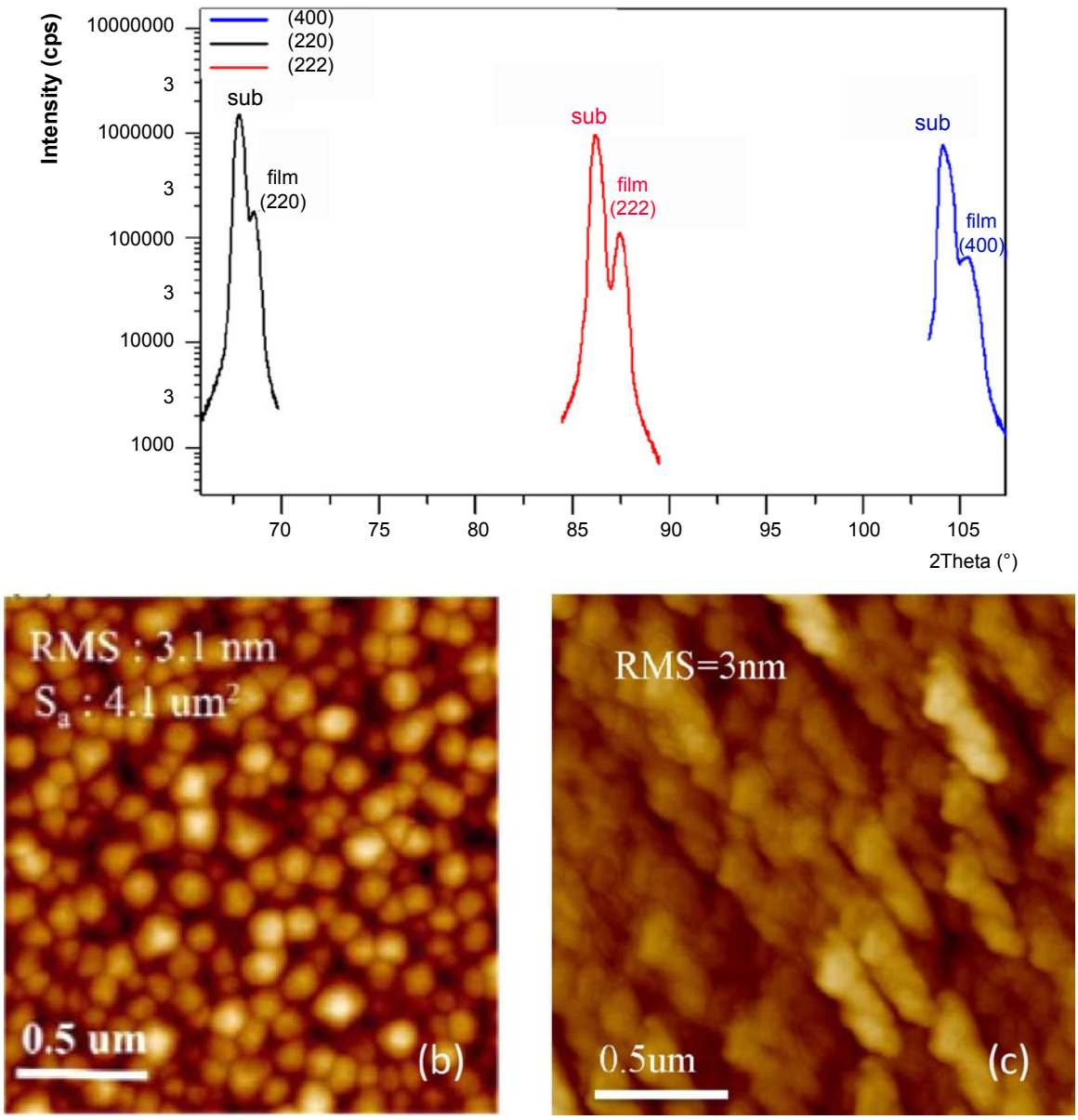

FIGURE 1. Examples of film characterization. (a) X-ray diffraction characterization of $La_{0.7}Sr_{0.3}MnO_3$ (621) deposited on $SrTiO_3$ (621), (b) AFM image of 600 nm thick textured film of (110) LSM on (111) YSZ, and (c) (100) LSM on MgO (100).

The LSM films exhibited bulk-like steady-state electrical properties and exhibited surface dominated responses in ECR [10,15]. Only one time constant (or A = 1) was needed for all ECR data registered for the epitaxial LSM on STO or NGO substrates [9–10, 15]. Two time constants (A < 1) were needed for fitting the textured films [9–10, 12, 15], both for YSZ and MgO substrates.

Previously we reported on the exchange properties for relaxed 600 nm thick low-index surfaces for LSM. However, we know that all surfaces exist within the SOFC cathode [29]. Therefore we measured the exchange properties of the (621) surface. Generally speaking, the (621) can be described as a nano-faceted surface made up of (100) terraces with (110) and (111) nanofacets as step edges and kink sites representing the intersection of the three nanofacets [27–28]. Figure 2 shows the k_{chem} values measured for the LSM (621) film deposited on STO (621). Both oxidation and reduction are similar to one another, as for the low index films. The (621) has an activation energy of ≈0.95 eV, intermediate between the values of the low-index surfaces. The (110) surface had an activation energy of ≈1.1–1.2 eV, while the (100) and (111) had activation energies of ≈0.8 eV [10]. As for the

(a)

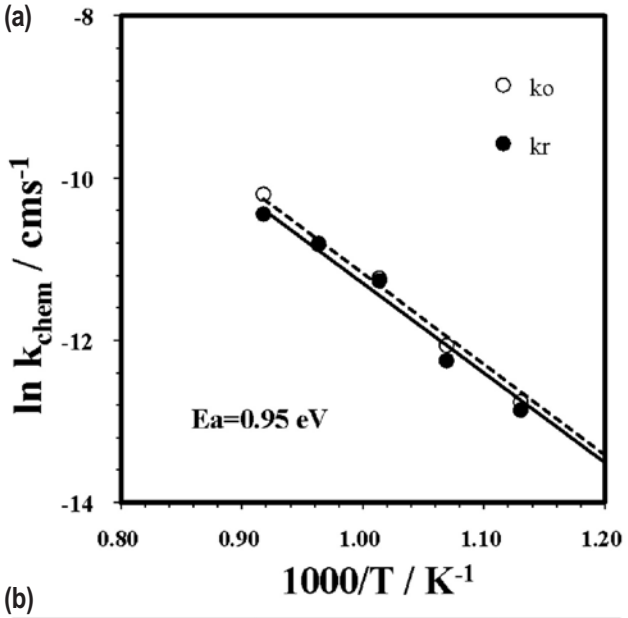

(b)

	k_{chem}	$\times 10^{-6}$	cm/s	
Temp/°C	ko (100)	ko (110)	ko (111)	ko (621)
611	1.30	2.18	2.83	2.88
714	3.74	17.20	6.40	13.22
816	10.10	64.30	16.93	37.27

FIGURE 2. (a) k_{chem} values measured for 600 nm thick (621) $La_{0.7}Sr_{0.3}MnO_3$ film plotted as ln k_{chem} vs 1/T, for both oxidation (o) and reduction (r); (b) a comparison of the values with those of the (100), (110), and (111) LSM films [10].

low-index surfaces, both the activation energy and the high temperature intercept ($1/T \approx 0$) are different on the (621) surface than the low-index surfaces. The chemical surface exchange coefficients (k_{chem}) for the four different films are shown in Figure 2b. The high index surface appears to be reasonably approximated at a complicated average of the low-index values (possibly including ledge/kink interactions as second order effects). For SOFCs, this indicates that the local activity of relaxed surfaces may range by a factor of five.

Relaxed epitaxial films have large quantities of dislocations, much larger than typically observed in ceramic microstructures. As such, one interpretation of the prior observations is that dislocations on different surfaces behave differently, if the surface exchange is dominated by the behavior around dislocations. This year we completed a model that describes how dislocations and strain play a role in surface exchange. k_{chem} values depend on substrate and thickness, but the activation energies only depend strongly on thickness [9]. We explored this further using (110) films fabricated on STO and NGO. The surface exchange coefficients for the (100) and (110) strained films are shown in Figure 3, where the activation energy clearly depends on substrate and orientation. Remembering that the (110) relaxed films had the highest activation energy [10], it is not surprising that the (110) strained films also have a higher activation energy than the (100) films. On the other hand, the dramatic enhancement in the high-temperature intercept was not foreseen. As such, strain (both compressive and tensile) leads to a great enhancement in the properties of 110-oriented films. The extrapolated differences in the strained films indicate that nearly four order of magnitude difference exists when combining strain and orientation. These epitaxial layers prepared as infiltrates are therefore expected to vastly deviate from their bulk properties and should be controlled by extrinsic factors. Interestingly, these extrinsic factors are vastly improved under strained conditions.

To explore further the role of extended boundaries, we prepared textured (110) films on YSZ (111) having two different grain sizes and (100) LSM on MgO. We reported previously that two parallel processes occurred for 600 nm thick (110) LSM films on YSZ [11,12]. An identical observation was made for films on MgO, but the value of A and its temperature dependence differed from the (110) films. The (100) surface itself and its extended defect region were less active at all temperatures as compared to (110) films, similar to that observed for epitaxial films. The percentage contributed by extended boundaries was much higher at low temperatures for the (100) films, which requires further investigation to the number of defects. On the other hand, we annealed to the (110) films and increased their grain sizes and saw a direct correlation to the increase (decrease) in the native surface (grain boundary) contribution to the surface exchange value. All of these results indicate that the true nature of surface exchange in nano-scale LSM electrocatalysts are related to both intrinsic surface features, extrinsic microstructural factors such as extended defects and strain, and the geometrical dimensions/arrangement of the particles.

To demonstrate this further in collaboration with NETL, we used mesoporous nanoscale coatings to modify both thin epitaxial films, characterized them with ECR and LSM-based half-cells, and characterized them with electrochemical impedance spectroscopy (EIS). Here we focus on demonstrating the importance of the geometrical (microstructural) features of the electrocatalysts in controlling properties in real cathodes. We used an evaporation induced self assembly (EISA) process [20, 21] to infiltrate the baseline cells, as well as a standard Pechini method to produce nanoparticle infiltrates (based on NETL's recipes [30, 31]). Both infiltrated cells had 10 wt% LSM in a microporous LSM cathode, but the EISA process produces interconnected

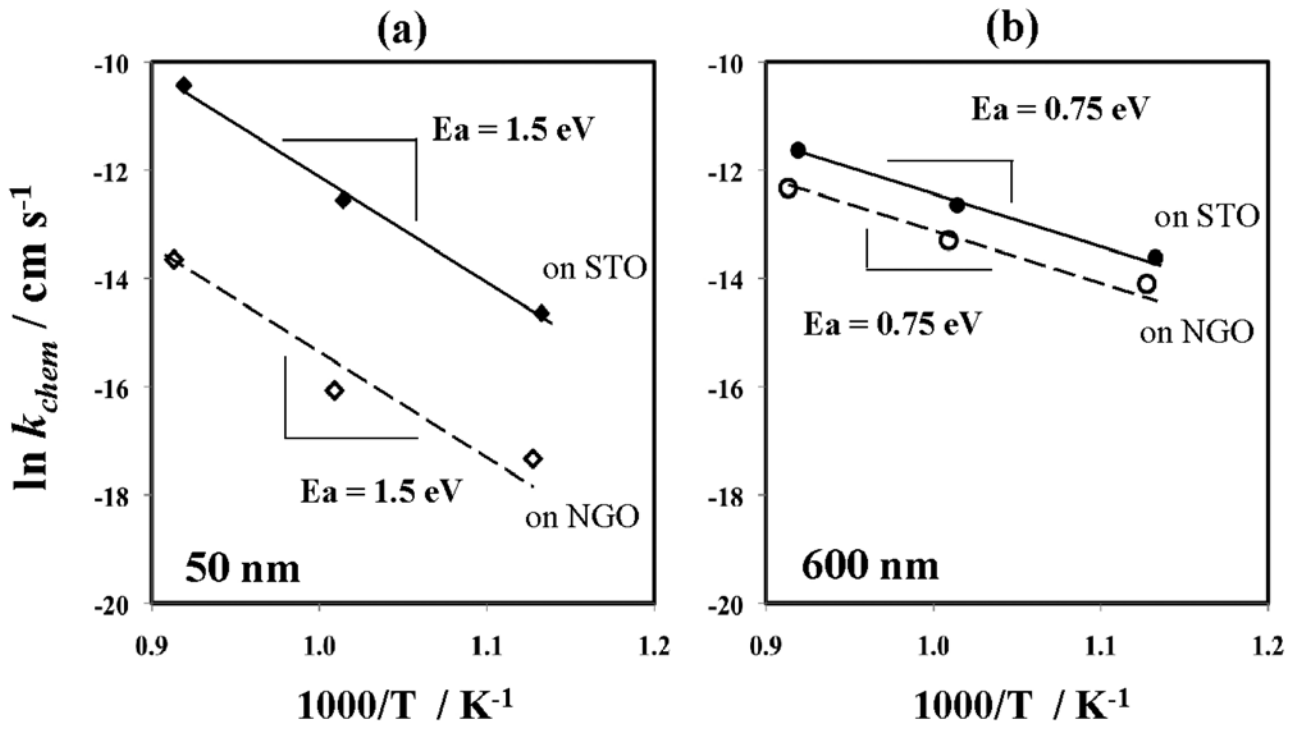

FIGURE 3. k_{chem} values of LSM films versus inverse temperature for 50 nm films on STO and NGO for (left) LSM (100) [9] and (right) LSM (110)

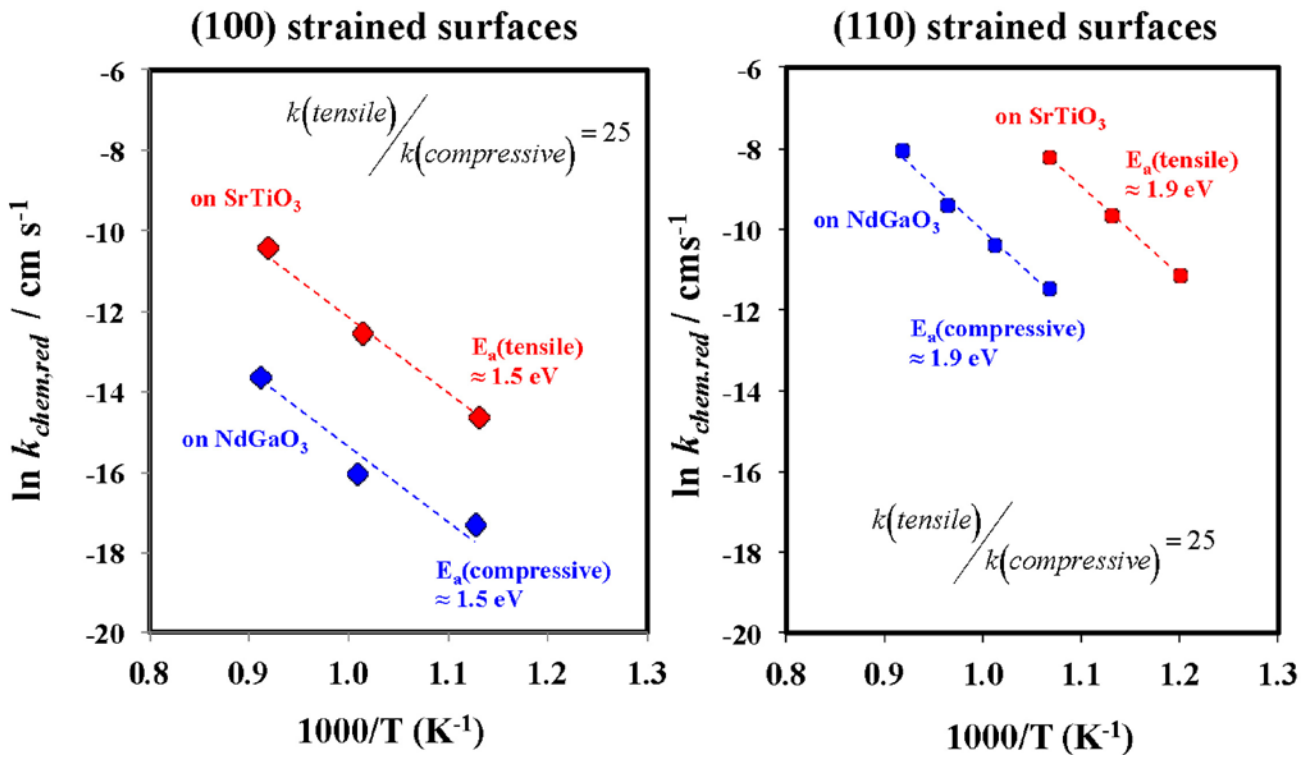

FIGURE 4. EIS data for LSM half cells that were uninfiltrated (baseline), nanoparticle infiltrated (LSM-CA), and mesoporous infiltrated (LSM-EISA), measured at 750°C

mesoporous coatings and the Pechini process produces largely isolate nanoscale particulate coatings. The EIS data registered at 750°C are shown in Figure 4. Three arcs (R_1, R_2, and R_3) fit the data [32–36] and were correlated to (1) cathode-electrolyte interface resistance at high-frequency, (2) surface-to-adsorbate charge transfer at intermediate frequency, and (3) adsorption on the surface at low-frequency [32–34]. While both infiltrates led to reductions in the R_2 and R_3 arcs (with the R_1 arc remaining nearly constant), the values of R_2 and R_3 are essentially zero for the mesoporous (EISA) coatings. This result was verified in operational SOFCs too, indicating that the extrinsic factors play an important role in electrocatalytic activity of LSM. By combining nanoscale thin film research with nanoscale infiltration research, the role of various intrinsic and extrinsic factors can be separated and understood from a basic science perspective while performance can be enhanced from a technical perspective.

Conclusions and Future Directions

The project demonstrated that surface engineered films of cathode materials can be produced and characterized in detail for structural and chemical properties. Crystallographic anisotropies were observed for epitaxial LSM single crystal films in their oxygen uptake kinetics, where high index orientation appears to be a complex average of low-index surface, with overall variations of a factor of four for heavily dislocated surfaces. It was also shown that the activation energy and pre-exponential factors are strong functions of the thickness of the films, indicating that strains and dislocations compete in importance for surface exchange. Importantly, we showed that strained 50 nm thick coatings vary in surface exchange by over three orders of magnitude. On textured (110) films, we showed that two processes are correlated to the native surface and to the extended defects (variant boundaries) in a way that positively correlates grain size with relative contribution of the processes. Similar results were shown to exist on (100) surfaces, again with strong orientation dependences. At low temperatures, the extended boundaries dominate the response at more than three orders of magnitude greater than the native surfaces. Finally, we worked with coating technologies appropriate for SOFC cathode infiltration, whose thicknesses are intermediate to our dense thin film values, to demonstrate directly that extrinsic factors (such as connectivity and surface area) play a quantifiable role in performance of LSM. Importantly, surface related polarization was reduced to zero by using mesoporous LSM instead of nanoparticle LSM. Making these direct correlations between model thin film systems and real SOFC cathodes is essential in the future to determine what the primary factors—chemistry/electronic structure/microstructure—are in determining functionality of surfaces and how many degrees of freedom can be used to optimize performance. The basic input of how surface chemistry/microstructure control surface exchange should be useful to the DOE SECA program to improve cathode activity by design, especially using future computational methods. In the next year, we aim to provide a comprehensive report of the state of surface science on SOFC cathodes.

FY 2012 Publications/Presentations

1. L. Yan and P.A. Salvador, "Substrate and Thickness Effects on the Oxygen Surface Exchange of $La_{0.7}Sr_{0.3}MnO_3$ Thin Films," *ACS Applied Materials and Interfaces,* **4**, 2541-2550 (2012) doi: 10.1021/am300194n.

2. "Surface Exchange (La,Sr)MnO_3 Films: Effects of Strain, Orientaion, and Microstructure on Oxygen Reduction," presented at European Materials Research Society Meeting Spring 2012, Strasbourg, France, May 2012.

3. P.H. Fuoss, B.J. Ingram, E. Perret, K.-C. Chang, T.T. Fister, P.H. Baldo, J.A. Eastman, and P.A. Salvador, "Time-Resolved Correlations between the Structure and Electrical Behavior of $La_{0.6}Sr_{0.4}Co_{0.2}Fe_{0.8}O_{3-\delta}$ Epitaxial Thin Films," Materials Research Society Meeting Fall 2011, Boston, Massachusetts, December 2011.

4. P.A. Salvador, L. Yan, P. Tsang, S. Akhade, T.T. Fister, J. Eastman, P. Fuoss, and J. Kitchin, "Surface Chemistry and Activity of SOFC Cathode Materials as Thin Films," MS&T 2011, Columbus, Ohio, October 2011.

5. P.A. Salvador, L. Yan, P. Tsang, "SOFC Cathode Surface Chemistry and Optimization Studies," FY 2012 Office of Fossil Energy Fuel Cell Program Annual Report, US Department of Energy, III.A.3 1-7 (2011).

6. "Oxygen Exchange in Thin Layers of SOFC Cathode Materials," presented by Paul Salvador (CMU) at 12th Annual SECA Workshop, Pittsburgh, Pennsylvania, July 2011.

7. "Microstructural Effects on the Oxygen Exchange Kinetics of $La_{0.7}Sr_{0.3}MnO_3$ Thin Films," poster presented by Lu Yan (CMU) at 12th Annual SECA Workshop, Pittsburgh, Pennsylvania, July 2011.

References

1. E. Maguire, B. Gharbage, and F.M.B. Marques, "Cathode Materials for Intermediate Temperature SOFCs," *Solid State Ionics*, (2000).

2. N.Q. Minh and T.Takahashi, Science and Technology of Ceramic Fuel Cells, Elsevier Science (1995).

3. J. Fleig, H. Kim, J. Jamnik, and J. Maier (2008), "Oxygen Reduction Kinetics of Lanthanum Manganite (LSM) Model Cathodes: Partial Pressure Dependence and Rate-Limiting Steps," *Fuel CellS,* **8:** 330-337.

4. K.-C. Chang, B. Ingram, K.R. Balasubramaniam, B. Yildiz, D. Hennessy, P.A. Salvador, N. Leyarovska, and H. You, "In Situ Synchrotron X-ray Studies of Dense Thin-Film Strontium-Doped Lanthanum Manganite Solid Oxide Fuel Cell Cathodes," *Mat. Res. Soc. Symp. Proc.,* **1126**, 1126-S08-10 (2009).

5. T.T. Fister, D.D. Fong, J.A. Eastman, P.M. Baldo, M.J. Highland, P.H. Fuoss, K.R. Balasubramaniam, J.C. Meador, and P.A. Salvador, "In Situ Characterization of Strontium Surface Segregation in Epitaxial $La_{0.7}Sr_{0.3}MnO_3$ Thin Films as a Function of oxygen partial pressure," *Applied Physics Letters,* **93**, 151904 (2008). doi: 10.1063/1.2987731.

6. P.A. Salvador, J. Meador, K.R. Balasubramaniam, P. Fuoss, J. Eastman, D. Fong, and P. Baldo, "SOFC Cathode Surface Chemistry and Optimization Studies," *FY 2007 Office of Fossil Energy Fuel Cell Program Annual Report, US Department of Energy*, Paper IV.A.4, 1-5 (2007).

7. P.A. Salvador, L. Yan, S. Wang, K.R. Balasubramaniam, P. Fuoss, J. Eastman, D. Fong, T. Fister, P. Baldo, H. You, K.-C. Chang, B. Yildiz, and I.B. Misirlioglu, "SOFC Cathode Chemistry and Optimization Studies," *FY 2008 Office of Fossil Energy Fuel Cell Program Annual Report, US Department of Energy*, III.A.2, 1-5 (2008).

8. K. Katsiev, B. Yildiz, K.R. Balasubramaniam, and P.A. Salvador, "Electron Tunneling Characteristics on La0.7Sr0.3MnO3 Thin-Film Surfaces at High Temperature," *Applied Physics Letters,* **95**, 092106 (2009). doi: 10.1063/1.3204022.

9. L. Yan and P.A. Salvador, "Substrate and Thickness Effects on the Oxygen Surface Exchange of $La_{0.7}Sr_{0.3}MnO_3$ Thin Films," *ACS Applied Materials and Interfaces,* **4**, 2541-2550 (2012). doi: 10.1021/am300194n.

10. L. Yan, K.R. Balasubramaniam, S. Wang, H. Du, and P.A. Salvador, "Effects of Crystallographic Orientation on the Oxygen Exchange Rate of $La_{0.7}Sr_{0.3}MnO_3$ thin films," *Solid State Ionics,* **194**, 9-16 (2011). doi: 10.1016/j.ssi.2011.05.004.

11. L. Yan, K.R. Balasubramaniam, K.-C. Chang, H. You, and P.A. Salvador, "Microstructural Effects on the Oxygen Exchange Kinetics of $La_{0.7}Sr_{0.3}MnO_3$ Thin Films," *Electrochemical Society Transactions,* **35**, (2011). doi: 10.1149/1.3570197.

12. P.A. Salvador, L. Yan, P. Tsang, P. Fuoss, J. Eastman, B. Ingram, H. You, K.-C. Chang, B. Yildiz, and C. Heske. "SOFC Cathode Surface Chemistry and Optimization Studies," *FY 2011 Office of Fossil Energy Fuel Cell Program Annual Report, US Department of Energy*, III.A.3 1-7 (2011).

13. H. Jalili, J.W. Han, Y. Kuru, Z. Cai, and B. Yildiz, "New Insights into the Strain Coupling to Surface Chemistry, Electronic Structure, and Reactivity of $La_{0.7}Sr_{0.3}MnO_3$," *J. Phys. Chem. Lett.,* **2**, 801–807 (2011).

14. T.T. Fister, D.D. Fong, J.A. Eastman, H. Iddir, P. Zapol, P. Fuoss, M. Balasubramanian, R.A. Gordon, K.R. Balasubramaniam, and P.A. Salvador, "Total Reflection Inelastic X-ray Scattering from a 10 nm Thick $La_{0.6}Sr_{0.4}CoO_3$ Thin Film," *Physical Review Letters,* **106**, 037401 (2011). doi: 10.1103/PhysRevLett.106.037401.

15. L. Yan, B. Kavaipatti, S. Wang, H. Du, and P. Salvador, "Electrical Conductivity Relaxation Study of Solid Oxide Fuel Cell Cathodes Using Epitaxial (001)-Oriented Strontium-Doped Lanthanum Manganite Thin Films," *Mat. Res. Soc. Symp. Proc.,* **1255**, 1255-M02-02 (2010). doi: 10.1557/PROC-1255-M02-02.

16. P.A. Salvador, L. Yan, S. Wang, K.R. Balasubramaniam, P. Fuoss, J. Eastman, D. Fong, T. Fister, P. Baldo, H. You, K.-C. Chang, B. Yildiz, K. Katsiev, C. Heske, and S. Krause, "SOFC Cathode Surface Chemistry and Optimization Studies," *FY 2010 Office of Fossil Energy Fuel Cell Program Annual Report, US Department of Energy*, III.A.3 1-6 (2010).

17. P.A. Salvador, L. Yan, S. Wang, K.R. Balasubramaniam, P. Fuoss, J. Eastman, D. Fong, T. Fister, P. Baldo, H. You, K.-C. Chang, B. Yildiz, K. Katsiev, C. Heske, and S. Krause, "SOFC Cathode Surface Chemistry and Optimization Studies," *FY 2009 Office of Fossil Energy Fuel Cell Program Annual Report, US Department of Energy*, III.A.3, 1-6 (2009).

18. K. Katsiev, B. Yildiz, K. Balasubramaniam, and P.A. Salvador, "Correlations of Electronic and Chemical State on $La_{0.7}Sr_{0.3}MnO_3$ Dense Thin-Film Cathode Surface," *Electrochemical Society Transactions,* **25**, 2309-2318 (2009).

19. B.J. Ingram, J.A. Eastman, K.-C. Chang, S.K. Kim, T.T. Fister, E. Perret, H. You, P.M. Baldo, and P.H. Fuoss, "In Situ X-ray Studies of Oxygen Surface Exchange Behavior in Thin Film $La_{0.6}Sr_{0.4}Co_{0.2}Fe_{0.8}O_{3-\delta}$," *Applied Physics Letters,* **101**, 051603 (2012).

20. R. Chao, R. Munprom, R. Petrova, K. Gerdes, J. Kitchin, and P. Salvador, "Structure and Thermal Stability of Mesoporous (La,Sr)MnO_3 Powders Prepared Using Evaporation-Induced Self-Assembly Methods," *Journal of the American Ceramic Society,* **in review**, (2012).

21. R. Chao, J.R. Kitchin, K. Gerdes, and P.A. Salvador, "Preparation of Mesoporous $La_{0.8}Sr_{0.2}MnO_3$ Infiltrated Coatings in Porous Cathodes Using Evaporation-Induced Self-Assembly Methods," *Electrochemical Society Transactions,* **35**, 2387-2399 (2011). doi: 10.1149/1.3570235.

22. M. Burriel, G. Garcia, J. Santiso, J.A. Kilner, J.C.C. Richard, and S.J. Skinner, "Anisotropic Oxygen Diffusion Properties in Epitaxial Thin Films of La2NiO4+delta," *J. Mater. Chem.,* **18**, 416-422 (2008). doi: 10.1039/b711341b.

23. G. Kim, S. Wang, A.J. Jacobson, and C.L. Chen, "Measurement of Oxygen Transport Kinetics in Epitaxial $LaNiO_{4+delta}$ Thin Films by Electrical Conductivity Relaxation," *Solid State Ionics,* **177**, 1461-1467 (2006).

24. L. Chen, C.L. Chen, and A.J. Jacobson, "Electrical Conductivity Relaxation Studies of Oxygen Transport in Epitaxial YBa2Cu3O7-d Thin Films," *IEEE Transactions on Applied Superconductivity,* **13**, 2882-2885 (2003).

25. X. Chen, S. Wang, Y.L. Yang, L. Smith, N.J. Wu, B.-I. Kim, S.S.P.A.J. Jacobson, and A. Ignatiev, "Electrical Conductivity Relaxation Studies of an Epitaxial $La_{0.5}Sr_{0.5}CoO_{3-d}$ Thin Film," *Solid Sates Ionics,* **146**, 405 (2002).

26. A. Rivera, J. Santamarı, and C. Leo. "Electrical Conductivity Relaxation in Thin-Film Yttria-Stabilized Zirconia," *Applied Physics Letters,* **78**, 610 (2001).

27. A.J. Francis, A.J. Koritnik, A. Gellman, and P.A. Salvador, "Chiral Surfaces and Metal/Ceramic Heteroepitaxy in the Pt/$SrTiO_3$(621) System," *Surface Science,* **601**, 1930-1936 (2007). doi: 10.1016/J.Susc.2007.02.026.

28. A.J. Francis and P.A. Salvador, "Chirally Oriented Heteroepitaxial Thin Films Grown by Gulsed Laser Deposition: Pt(621) on $SrTiO_3$(621)," *Journal of Applied Physics,* **96**, 2482-2493 (2004). doi: Doi 10.1063/1.1768609.

29. S. Dillon, L. Helmick, H. Miller, L. Wilson, R. Gemman, R. Petrova, K. Barmak, G.S. Rohrer, and P.A. Salvador, "The Orientation Distributions of Lines, Surfaces, and Interfaces Around Three-Phase Boundaries in Solid Oxide Fuel Cell Cathodes," *Journal of the American Ceramic Society,* **94**, 4045-4051 (2011). doi: 10.1111/j.1551-2916.2011.04673.x.

30. S. Lee, N. Miller, M. Staruch, K. Gerdes, M. Jain, and A. Manivannan, "$Pr_{0.6}Sr_{0.4}CoO_3$, Electrocatalyst for Solid Oxide Fuel Cell Cathode Introduced via Infiltration," *Electrochimica Acta*, (2011).

31. S. Lee, N. Miller, H. Abernathy, K. Gerdes, and A. Manivannan, "Effect of Sr-Doped $LaCoO_3$ and $LaZrO_3$ Infiltration on the Performance of SDC-LSCF Cathode," *Journal of the Electrochemical Society,* **158**, B735 (2011).

32. S. Adler, "Factors Governing Oxygen Reduction in Solid Oxide Fuel Cell Cathodes," *Chem. Rev,* **104**, 4791-4844 (2004).

33. P. Hjalmarsson, M. Søgaard, and M. Mogensen, "Electrochemical Performance and Degradation of $(La_{0.6}Sr_{0.4})_{0.99}CoO_{3-\Delta}$ as Porous SOFC-Cathode," *Solid State Ionics,* **179**, 1422-1426 (2008).

34. F. Baumann, J. Fleig, H. Habermeier, and J. Maier, "Impedance Spectroscopic Study on Well-Defined (La, Sr)(Co, Fe) $O_{3-\Delta}$ Model Electrodes," *Solid State Ionics,* **177**, 1071-1081 (2006).

35. Y. Huang, J. Vohs, and R. Gorte, "SOFC Cathodes Prepared by Infiltration with Various LSM Precursors," *Electrochemical and Solid-State Letters,* **9**, A237 (2006).

36. B. Kenney and K. Karan, "Estimation of Chemical and Transport Processes in Porous, Stoichiometric LSM Cathodes Using Steady-State Polarization and Impedance Modeling," *Journal of the Electrochemical Society,* **157**, B1126-B1137 (2010).

III.A.4 Theory, Investigation and Stability of Cathode Electro-Catalytic Activity

Meilin Liu (Primary Contact), Dong Ding, Xiaxi Li, Samson Lai, Mingfei Liu
Georgia Institute of Technology
School of Materials Science and Engineering
771 Ferst Drive, Atlanta, GA 30332-0245
Phone: (404) 894-6114; Fax: (404) 894-9140
Email: meilin.liu@mse.gatech.edu

DOE Project Manager: Briggs White
Phone: (304) 285-5437
Email: Briggs.White@netl.doe.gov

Contract Number: NT0006557

Start Date: September 1, 2008
End Date: August 31, 2012

Fiscal Year (FY) 2012 Objectives

- Characterize the surface composition, morphology, and electro-catalytic properties of a catalyst infiltrated $La_{0.6}Sr_{0.4}Co_{0.2}Fe_{0.8}O_{3-\delta}$ (LSCF) cathode.
- Establish the scientific basis for rational design of high-performance cathodes by combining a porous backbone (such as LSCF) with a thin catalyst coating.
- Demonstrate enhancement in activity and stability of LSCF cathodes by $La_xSr_{1-x}MnO_{3-\delta}$ (LSM) infiltration using commercially available cells.

FY 2012 Accomplishments

- Developed surface enhanced Raman spectroscopy (SERS) for studying the signal enhancement for the LSM and LSCF film.
- Characterized the atomistic and electronic structure of Co, Mn, and Sr in LSCF cathode with/without LSM coating at 850°C annealed for 400 hours using synchrotron-based X-ray absorption spectroscopy (XAS).
- Raman spectroscopy, e.g., SERS, and synchrotron-based X-ray analyses, e.g., XAS, are powerful techniques for probing electrode surfaces under various conditions. Together with the modeling and simulation tools developed earlier under this project, these characterization techniques may help us to unravel the mechanism of catalyst-infiltrated electrodes, thus providing scientific basis for rational design of more efficient cathode materials and structures.
- Demonstrated that infiltration of a thin-film coating of $La_{0.4875}Ca_{0.0125}Ce_{0.5}O_{2-\delta}$ (LCC) can significantly enhance the activity and stability of LSCF cathode.
- Optimized the LSM infiltration process for commercially available cells with LSCF cathodes and demonstrated enhanced activity and stability.
- Developed a unique microstructure for dense continuum catalyst film in porous LSCF cathodes.
- Developed new Mn-based catalysts for infiltration into porous LSCF cathodes, and demonstrated that infiltration of a thin-film coating of $PrSrCoMnO_{5+\delta}$ (PSCM) offered even higher activity than the LSM- or $Pr_{1-x}Sr_xMnO_{3-\delta}$ (PSM)- infiltrated cells using both symmetrical and full cell configurations.

Introduction

One of the reasons that LSCF based cathodes show much better performance than those based on LSM is that LSCF has much higher ionic and electronic conductivity than LSM, significantly extending the active sites beyond the triple-phase boundaries (TPBs) [1]. One obvious downfall for LSCF is that it reacts adversely with yttria-stabilized zirconia (YSZ), which can be mitigated by the use of a buffer layer of doped-CeO_2 between LSCF and YSZ [2]. However, the catalytic activity of stand-alone LSCF cathodes is likely to be limited by the surface catalytic properties. Furthermore, the long-term stability of LSCF cathodes is a concern. Thus, it is hypothesized that the *performance* and *stability* of a porous LSCF cathode may be improved by the application of a catalytically active coating through infiltration. The selection of the catalytic materials, as well as the detailed microstructures of the porous LSCF and the catalyst layer, may critically impact the performance of the proposed cathodes. The objective of this project is to optimize the composition and morphology of the catalyst layer and the microstructure of the LSCF backbone for better performance.

Approach

A surface enhanced Raman technique was developed for achieving the signal enhancement for LSM and LSCF film on underlying YSZ substrate. Also, XAS

is employed to investigate the electronic state of the cathode's cation and the structural changes under the influence of external stimuli. The solution infiltration process of LSM coating is further optimized for the LSCF cathode with large size. In addition to PSM, a novel catalyst material of PSCM is developed. The effects of PSCM, PSM, and LSM infiltration on the performance of LSCF cathodes were investigated using symmetrical and anode-supported button cells. Commercial cells with and without LSM infiltration were tested at 750°C under a constant voltage of 0.7 V.

Results

Application of surface enhanced Raman spectroscopy (SERS) to the study of LSM coated LSCF cathode in solid oxide fuel cell (SOFC)

The LSM coated LSCF cathode achieves enhancements in activity and stability, which are possibly associated with effective modification agents and degradation-resistance species. They may be present in trace amounts that become difficult to detect using conventional characterization tools because of lack of chemical sensitivity, lack of surface specificity, or limited applicability under in situ conditions. Under the right conditions, Raman spectroscopy is able to inspect the phase evolution and reaction intermediates at the electrode surface [3,4]. However, the inherently low chemical sensitivity of Raman precludes probing species present in trace amounts on the SOFC surface that are connected to cell performance. The project team successfully developed a direct current magnetron sputtering method to load silver nanoparticles as the SERS agent and obtained the enhanced Raman signal for LSM and LSCF films on a YSZ substrate [5]. As shown in Figures 1a and 1b, the Raman spectra collected from both LSCF pellets and LSM thin film were significantly enhanced after SERS conditioning while normal Raman signals of both materials were very weak because near-cubic perovskite phases have little Raman activity. Since the two materials share a similar phase, their Raman bands are in similar positions. The LSCF signal was enhanced by a rough factor of ~11, and the LSM signal was enhanced by a factor of ~6. Moreover, the Ag treatment granted some level of surface specificity to the Raman analysis since only the signal from chemical species near the Ag nanoparticles is enhanced. This feature can provide the capability to detect phase evolution on the cathode surface with superior surface sensitivity, potentially contributing to studies on the degradation mechanisms of LSCF cathodes in SOFCs.

The enhancement in sensitivity of Raman spectroscopy to cathode materials has important implications. To date, the development of new electrode

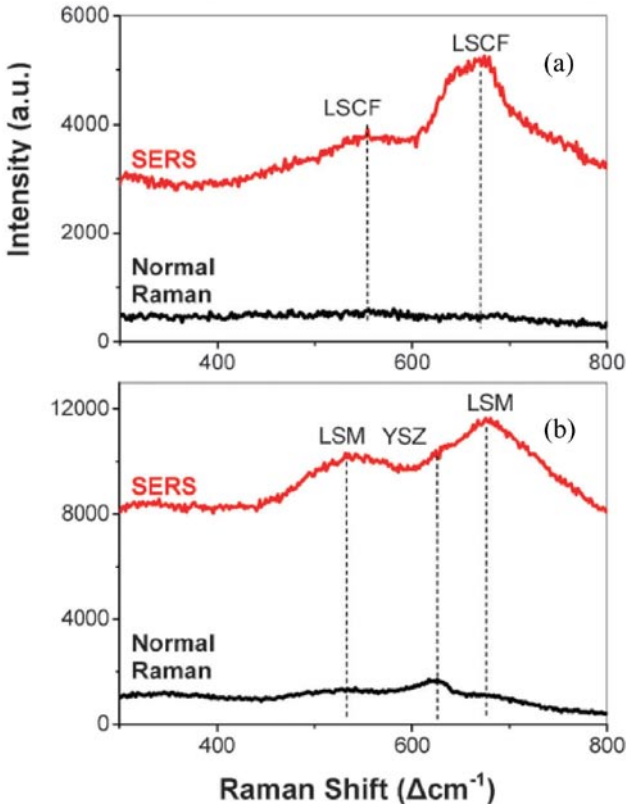

FIGURE 1. The normal Raman and SERS spectra collected from (a) an LSCF pellet, and (b) LSM film sputtered on a YSZ pellet. They were excited with green laser (514 nm).

materials for SOFC is still largely based on experience and intuition rather than scientific models, largely due to the lack of a fundamental understanding of the electrode processes, which are determined by the chemistry and structure of electrode surfaces. We believe that SERS with high sensitivity to electrode materials may be a powerful probe for surface composition and electrode structure, providing critical information for unraveling the mechanism of catalyst-coated LSCF cathode processes.

The utility of Raman spectroscopy is also illustrated in the study of a LCC infiltrated LSCF cathode. Shown in Figure 2 are typical Raman spectra collected from LSCF cathodes with or without LCC modification before and after 550 hours of operation. A typical Raman spectrum from the LSCF cathode before operation consisted mainly of two broad peaks centered at 546 cm^{-1} and 632 cm^{-1}, which correspond to E_g modes characteristic to the structure of R3c [6], which is the space group of LSCF [7]. When Raman analysis was performed on the LSCF cathode following long-term operation, the intensities of the two E_g peaks decreased considerably while two new sharp peaks appeared at 675 cm^{-1} and 995 cm^{-1}. These changes were indicative of the

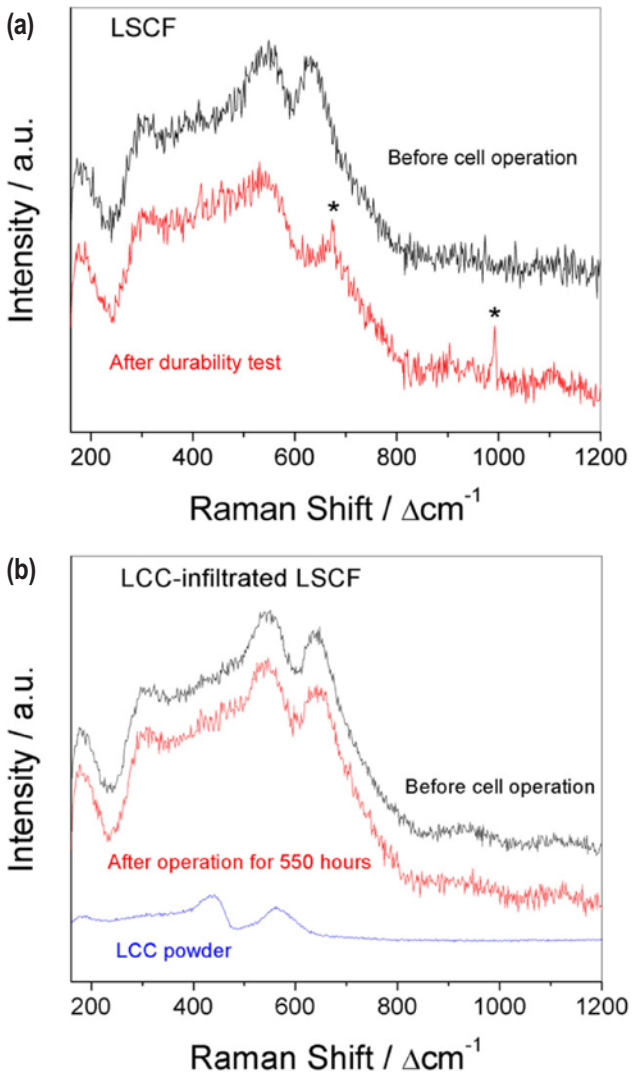

FIGURE 2. Typical Raman spectra collected from (a) LSCF and (b) LCC-infiltrated LSCF cathodes before/after durability tests, along with a spectrum collected from LCC powder.

degradation of the LSCF phase and the emergence of a new Raman active phase out of the original LSCF. These changes to the cathode material's phase composition are likely a major component of the performance degradation observed for the unmodified LSCF. On the other hand, as displayed in Figure 2(b), spectra obtained from the LCC-infiltrated LSCF cathode both before and after long-term operation were largely similar; no new peaks or notable changes in the peaks were observed after operation. As for evidence of the presence of LCC itself, one may note that the low loading amount of the nanoparticles likely approaches the lower sensitivity limits of Raman spectroscopy. However, evidence could be seen in a small, sloped shoulder centered at 435 cm^{-1} in the spectra for the LCC-infiltrated sample corresponding with a broad peak in the spectrum collected from LCC powder, which is also shown in Figure 2b. The spectra for the un-infiltrated LSCF are slightly less sloped in the same spot. In addition, relatively higher peak intensity for 546 cm^{-1} versus the un-infiltrated LSCF spectra can be observed, corresponding with the other peak in the LCC powder spectrum. Although these spectral differences are subtle, the stabilizing effect of the LCC on the cathode is quite clear when comparing the sets of spectra in Figures 2a and 2b.

Comparative study of LSM-infiltrated LSCF and blank LSCF cathode using XAS

We employed XAS to probe the atomistic and electronic structure of "critical ions" in electrode materials under in situ conditions so that the structural changes under the influence of external stimuli on a particular cation or anion can be directly correlated with the electrochemical response of the electrode under the same conditions. The soft X-ray absorption near-edge spectroscopy (XANES) data reveal that both Mn and Co cations are reduced by the charge imbalance caused by oxygen vacancy formation in the as-prepared LSM infiltrated LSCF at 750°C under reducing conditions. However, after annealing, only the Co cation is reduced while the Mn cation remains unchanged. The hard X-ray K-edge XANES indicate that the Mn cation in as-prepared LSM infiltrated LSCF reduces at 750°C, whether it is heated in oxidizing or reducing condition, while the Co cation is unaffected. However, when the LSM infiltrated LSCF is annealed long-term, the in situ spectroscopy shows that the Mn cation is unaffected by oxidizing or reducing conditions while the Co cation undergoes a charge-compensating oxidation state change for the electrochemical change in oxygen stoichiometry. Thus, when the Co cation is located in the subsurface LSCF backbone, it does not participate in electrochemical reactions except under strongly reducing conditions. However, once the annealing process enables Co diffusion into the LSM thin film on the surface, the Co displaces Mn as the charge-compensating cation for changes in oxygen stoichiometry, an important change in the fundamental electrochemical reactions taking place.

Further investigation in the Mn and Co K-edge Fourier-transformed (FT) extended X-ray absorption fine structure (EXAFS) showed that the local structures of both cations showed significant peak growth after brief thermal treatments and annealing, which indicates ordering of coordination shells. The Fe, Co, and Sr K-edge FT EXAFS data indicated that the annealed LSM-infiltrated LSCF has local structures similar to as-prepared LSCF. In contrast, slight contractions were observed in the Fe-O, Co-O, and Sr-O coordination shells in the annealed LSCF. Although these observations were not significant enough to be used as direct evidence of

phase segregation or Sr enrichment, they are not present in the annealed LSM infiltrated LSCF cathode material, further indicating the enhancement in stability under operating conditions. The oxidation state changes, the ordering phenomenon, and local structure contractions are observations uniquely obtained through the XAS technique and provide useful insight into the effects of thermal treatments and oxidizing and reducing atmospheres on structure and electronic state.

Exploration of new catalysts for LSCF cathode surface modification

We have demonstrated that dense, continuous LSM films can be successfully fabricated with the desired structure, composition, morphology, and thickness on LSCF substrate using an infiltration process (non-aqueous and water-based solution). Since degradation of LSCF cathodes is likely related to SrO segregation or enrichment on the surface [8], a continuous thin film coating of LSM on LSCF may suppress surface segregation or enrichment of SrO under operating conditions. Thus, we explored several catalysts that have similar structure to that of LSCF and LSM, as to be discussed in the next two sections.

Electrochemical properties of catalyst coated LSCF cathode

Since the LSM continuous thin film coating successfully demonstrated enhanced activity and stability for the LSCF cathode, we attempted to synthesize new catalysts based on the knowledge we obtained from the LSM coating. Since Mn in the B-site has been demonstrated to play a key role in the activation process under operation and the suppression of SrO segregation from LSCF, Mn should be retained in the catalytic layer. Mn-containing materials are usually more stable under SOFC operation conditions than Co- and/or Fe-containing materials. More active Mn-containing catalyst coatings were also examined to further enhance performance. Moreover, a perovskite-based catalyst may form a continuous and dense film on the LSCF cathode due to the structural similarity. Thus, a series of Mn-containing active catalysts for infiltration were developed, especially perovskite PSM and double perovskite PSCM. Shown in Figure 3a is typical impedance spectrum for an LSCF cathode with and without catalyst infiltration at 750°C under open circuit condition (OCV). Clearly, the PSM infiltration significantly reduces the interfacial polarization resistance (R_p) of LSCF cathode even under OCV condition, in contrast to the LSM infiltration. The PSCM infiltration further decreases R_p at the same concentration of infiltration. Figure 3b shows the temperature

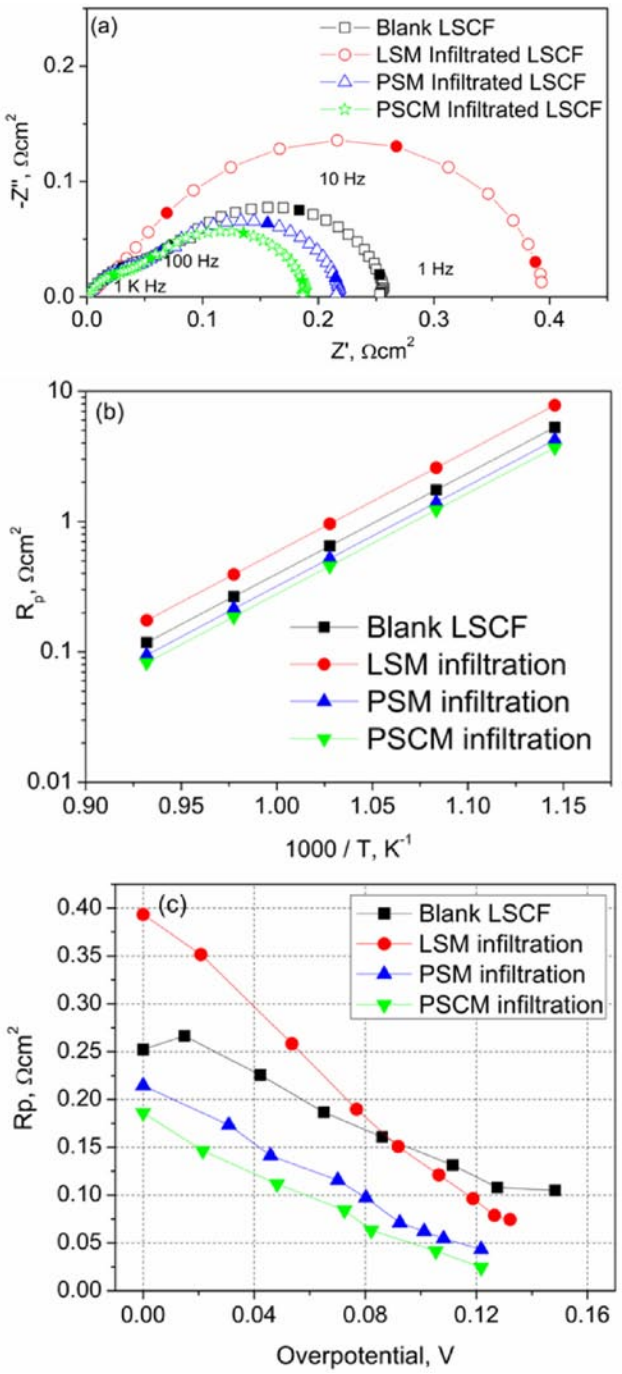

FIGURE 3. (a) Typical impedance spectrum of various catalysts infiltrated LSCF cathodes measured at 750°C under open circuit conditions; (b) temperature dependence of interfacial polarization resistance (R_p) of various catalysts infiltrated LSCF cathodes under open circuit conditions (OCV); and (c) interfacial R_p versus overpotential (η) for various catalysts infiltrated LSCF cathodes measured at 750°C.

dependence of R_p for these catalyst-infiltrated LSCF cathodes. At an intermediate temperature range, the PSCM infiltration presents the minimum R_p among these Mn-containing catalysts. All curves appear to

have similar slopes, indicating that the oxygen reduction reaction mechanism of the LSCF cathodes with infiltration remains the same. An important phenomenon for the Mn-containing catalyst infiltration is its activation behavior which presents the electrochemical properties of the cathode with a cathodic current passage. We employed symmetrical cells with a three-electrode configuration and used steady-state polarization to evaluate these behaviors. Unlike LSM infiltration, the PSM and PSCM infiltrated LSCF cathodes initially show lower R_p compared to blank LSCF cathodes, followed by the fast reduction in R_p at a given cathodic overpotential. This suggests that the PSM and PSCM infiltration are able to result in more improvement in performance during operation.

Cathode performance and stability improvements by different catalysts infiltration into LSCF cathode

Figure 4a shows the typical performance of homemade button cells infiltrated with different catalytic coatings and operated at 750°C under constant voltage of 0.7 V. Within 600 hours, the cells with PSCM-infiltrated LSCF cathodes showed the best performance with significant activation behavior. Compared to cells with LSM and PSM infiltration, the PSCM infiltrated cells showed a gradual increase in performance, implying a continuous activation during operation. The long-term activation phenomenon could counter some other degradation mechanism to offer constant performance, which has attracted our attention for further study. Also, we demonstrated the enhancement in activity and stability of commercial cells provided by Materials System and Research Incorporation (MSRI) (tested for a few hundred hours thus far). Shown in Figure 4b are typical performance data for a MSRI cell infiltrated with 0.1 M LSM solution, as measured at 750°C and 0.7 V. For a direct comparison, the performance of a blank MSRI cell is shown under the same conditions. The initial output power density was over 0.6 Wcm^{-2}. A gradual degradation over time is visible. As expected, the LSM infiltrated MSRI cell showed a significant activation behavior. Although its initial output power density was slightly lower than that of the blank cell, the output power increased quickly with time in the first two hours and then showed a gradual increase with time. This tendency is similar to our finding using symmetrical cells as well as our modeling prediction.

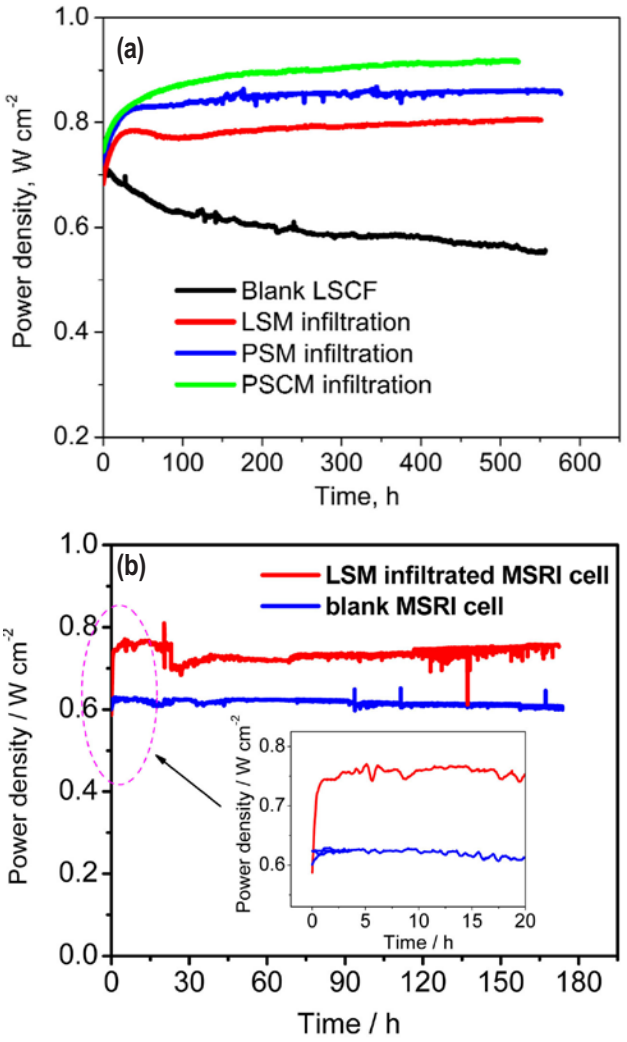

FIGURE 4. (a) Power density over time of the anode-supported cells with various catalysts infiltrated LSCF cathodes at 750°C with a constant voltage of 0.7 V. (b) Power density over time of the commercial cells with or without LSM infiltration.

Conclusions

A surface enhanced Raman technique was developed and the signal enhancements were obtained for LSM and LSCF films on underlying YSZ substrate. X-ray absorption spectroscopy was employed to investigate the electronic state of the cathode's cations and the structural changes under the influence of external stimuli, and the results are in agreement with our previous finding. These powerful characterization techniques, together with multi-scale modeling and simulation tools developed under this project, may help us to unravel the mechanism of catalyst-infiltrated electrodes, thus providing the scientific basis for rational design of more efficient cathode materials and structures. The solution infiltration process of LSM coating was further optimized for commercial cells with larger LSCF cathodes. Enhancement in activity and stability was demonstrated in a relatively short time. In addition to PSM, novel infiltration catalyst PSCM was developed. The PSCM infiltration was demonstrated to possess a lower R_p under OCV condition and further performance

improvement with operation in symmetrical and full cell configurations. These catalyst infiltrations led to unique microstructures in porous LSCF cathodes, which may be associated with improvements in performance.

FY 2012 Publications/Presentations

1. X. Li, K. Blinn, Y. Fang, M. Liu, M.A. Mahmoud, S. Cheng, L.A. Bottomley, M. El-Sayed, and M. Liu, "Raman Spectroscopy Study of SOFC Electrode Surfaces," invited talk presented to the Symposium on In Situ Characterization of Fuel Cell Electrodes, MRS fall meeting, Boston, Massachusetts, November 28–30, 2011.

2. M.F. Liu, D. Ding, K. Blinn, X.X. Li, L.F. Nie, and M.L. Liu, "Enhanced Performance of LSCF Cathode Through Surface Modification," *International Journal Of Hydrogen Energy*, 2012, 37(10): p. 8613-8620.

3. Y. Bai, M. Liu, D. Ding, K. Blinn, W. Qin, J. Liu, and M. Liu, "Electrical and Electrocatalytic Properties of a $La_{0.8}Sr_{0.2}Co_{0.17}Mn_{0.83}O_3$-delta Cathode for Intermediate-Temperature Solid Oxide Fuel Cells," *Journal Of Power Sources,* 2012, 205: p. 80-85.

4. J.J. Choi, W.T. Qin, M.L. Liu, "Preparation and Caracterization of $(La_{0.8}Sr_{0.2})_{0.95}MnO_{3-\delta}$ Thin Films and LSM/LSCF Interface for SOFCs," *Journal of the American Ceramic Society*, 2011, 94: p.3340–3345.

5. S. Lai, M.F. Liu, R.E. Rettew, M.L. Liu, F.M. Alamgir, "In-situ Characterization of SOFC Cathodes Using Synchrotron-Based X-ray Absorption Spectroscopy", *Catalysis Today*, Submitted.

6. M. Liu, "In Situ Characterization and Modeling of Surface and Interfaces in Fuel Cells," invited lecture, Lehigh University, September 14, 2011.

7. M. Liu, "Surfaces and Interfaces in Heterogeneous Electrodes for Chemical and Energy Transformations," invited talk to Symposium on Fuel Cells/Energy Conversion, MS&T 2011, Columbus, Ohio, October 18, 2011.

8. M. Liu, "Rational Design of Materials for SOFCs," Plenary lecture presented to Annual Meeting of Korean Ceramic Society, Gwangju, South Korea, October 24–25, 2011.

9. M.E. Lynch, D. Ding, W.H. Harris, J.C. Andrews, Y. Liu, P. Pianetta, W.K.S. Chiu, and M. Liu, "Flexible Multiphysics Simulation of Porous Electrodes: Conformal to 3D Reconstructed Microstructures," Nano Energy (2012), http://dx.doi.org/10.1016/j.nanoen.2012.08.002.

References

1. S.P. Jiang, "A Comparison of O_2 Reduction Reactions on Porous $(La,Sr)MnO_3$ and $(La,Sr)(Co,Fe)O_3$ Electrodes," *Solid State Ionics*, 2002. 146(1-2): p. 1-22.

2. D. Stover, H.P. Buchkremer, and S. Uhlenbruck, "Processing and Properties of the Ceramic Conductive Multilayer Device Solid Oxide Fuel Cell (SOFC)," *Ceramics International*, 2004, 30(7): p. 1107-1113.

3. Y.M. Choi, H. Abernathy, H.T. Chen, M.C. Lin, and M.L. Liu, "Characterization of O-2-CeO_2 Interactions Using In Situ Raman Spectroscopy and First-Principle Calculations," *Chemphyschem*, 2006, 7(9): p. 1957-1963.

4. L. Yang, S.Z. Wang, K. Blinn, M.F. Liu, Z. Liu, Z. Cheng, and M.L. Liu, "Enhanced Sulfur and Coking Tolerance of a Mixed Ion Conductor for SOFCs: $BaZr_{0.1}Ce_{0.7}Y_{0.2-x}Yb_xO_{3-delta}$," *Science*, 2009, 326(5949): p. 126-129.

5. X. Li, K. Blinn, Y. Fang, M. Liu, M.A. Mahmoud, S. Cheng, L.A. Bottomley, M. El-Sayed, and M. Liu, "Application of Surface Enhanced Raman Spectroscopy to the Study of SOFC Electrode Surfaces," *Physical Chemistry Chemical Physics*, 2012.

6. D. Varshney, A. Kumar, and K. Verma, "Effect of A Site and B Site Doping on Structural, Thermal, and Dielectric Properties of BiFeO(3) Ceramics," *Journal of Alloys and Compounds*, 2011, 509(33): p. 8421-8426.

7. L.W. Tai, M.M. Nasrallah, H.U. Anderson, D.M. Sparlin, and S.R. Sehlin, "Structure and Electrical-Properties of $La_{1-X}Sr_xCo_{1-Y}Fe_yO_{3-2}$. The System $La_{1-X}Sr_xCo_{0.2}Fe_{0.8}O_3$," *Solid State Ionics*, 1995. 76(3-4): p. 273-283.

8. S.P. Simner, M.D. Anderson, M.H. Engelhard, and J.W. Stevenson, "Degradation Mechanisms of La-Sr-Co-Fe-O_3 SOFC Cathodes," *Electrochemical And Solid State Letters*, 2006, 9(10): p. A478-A481.

III.A.5 Cathode Contact Materials for Anode-Support Cell Development

Michael C. Tucker (Primary Contact),
Lutgard DeJonghe
Lawrence Berkeley National Laboratory
MS 62-203
1 Cyclotron Rd.
Berkeley, CA 94720
Phone: (510) 486-5304
E-mail: mctucker@lbl.gov

DOE Project Manager: Joseph Stoffa
Phone: (304) 285-0285
Email: Joseph.Stoffa@netl.doe.gov

Contract Number: MSD-NETL-01

Start Date: October 1, 2011
End Date: September 30, 2012

Fiscal Year (FY) 2012 Objectives

- Identify and develop candidate materials, architectures, and concepts to solve issues related to delamination and degradation of cathode contact material.
- Initiate in situ testing using commercially-available lab-scale fuel cells.
- Target high-risk/high-benefit strategies and novel technical approaches.

FY 2012 Accomplishments

- Determined effect of production method on conductivity and bonding of composite cathode contact material (CCM) pastes.
- Determined in situ performance and stability for novel composite CCM candidates in contact with Pt current collectors, using commercially-available anode-supported cells.
- Determined in situ performance and stability for novel composite CCM candidates in contact with MCO-coated 441 steel current collectors, using commercially-available anode-supported cells.
- Conducted post-mortem analysis of in situ tested cells to determine extent of reaction between layers.

Introduction

The main focus of the Lawrence Berkeley National Laboratory (LBNL) project is to support industrial Solid State Energy Conversion Alliance (SECA) teams in their effort to commercialize solid oxide fuel cell (SOFC) technology that meets the SECA performance and cost targets. In order to achieve this goal, it is necessary to improve the performance of SOFC components through selection of appropriate materials and development of novel yet inexpensive alternative materials, architectures, and concepts. The primary challenge addressed by LBNL during FY 2012 concerns electrical connection and bonding between the interconnect and cathode layers, shown in Figure 1. Historically, cathode materials such as $La_xSr_{1-x}MnO_{3-\delta}$ (LSM) are used as a CCM paste to bond the cell to the interconnect. High temperature is typically required to achieve good bonding, however, leading to rapid oxidation of the stainless steel interconnect. If a temperature low enough to avoid oxidation of the steel (<1,000ºC) during the bonding step is employed, poor bonding and eventual delamination of the contact material occurs. The goals of the work at LBNL are to (a) screen known candidate cathode materials to ascertain whether they can be used as CCMs displaying adequate properties after bonding at <1,000ºC; and (b) identify and develop novel materials, architectures, and approaches to solving this issue.

Approach

Accordingly, in FY 2012 the LBNL core effort has been focused on the following issues:

- Identification of promising novel composite candidates, consisting of conventional cathode

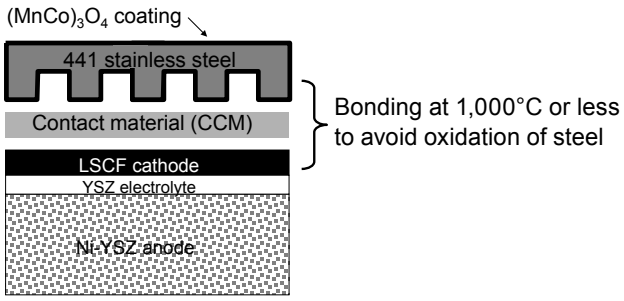

FIGURE 1. Schematic of CCM placement in cell stack

material powder and glass or inorganic binder added to improve bonding.

- Synthesis and characterization of candidate composites, including determination of sintering behavior, conductivity, bonding, coefficient of thermal expansion (CTE), and reaction with neighbor materials.
- Down-selection of the most promising candidates, and determination of the long-term stability of their area-specific resistance (ASR) in relevant test geometries using model cathode and interconnect layers.
- Demonstration of the best materials in lab-scale cells operating under realistic conditions.

Results

Screening of candidate CCM composites

A long list of glass and inorganic binder additives were identified as candidates for application in CCM materials. The compositions were purchased from Schott, SEM-COM, Aremco, Cotronics, and Spruce Pine. The properties of primary relevance, including conductivity, sintering behavior, CTE, and reactivity with $Mn_{1.5}Co_{1.5}O_4$ (MCO) and $La_{0.6}Sr_{0.4}Co_{0.2}Fe_{0.8}O_{3-\delta}$ (LSCF) were then determined. The summary of this screening effort suggested a short list of the most promising composite CCM candidates. The best glasses were SCZ-8 and Schott E (GM31107). The best inorganic binders were Aremco 830, 542, 503T and 644A.

Testing of most promising candidates

These candidate additives were then incorporated into ASR specimens in which electrical resistances of the individual 441-MCO/CCM interfaces were monitored over time. Figure 2 shows a schematic of the sample geometry and ASR results. LSM with 830, 644A, SCZ-8, and Schott E were the most promising composites. They provided low, and stable ASR for ~200 h at 800ºC.

These down-selected candidates were then subjected to in situ testing using commercially available anode-supported button cells (MSRI). The CCM candidates are used to bond MCO-coated 441 interconnect meshes to the LSCF cathode of the cells. The cells were then operated at 800ºC with hydrogen fuel for >500 h. Figure 3 shows the results for the best performing composites. They all provided good initial performance, and LSM/SCZ-8 provided the best stability.

Conclusions and Future Directions

- Many candidate CCM composites were synthesized and screened for relevant physical properties.

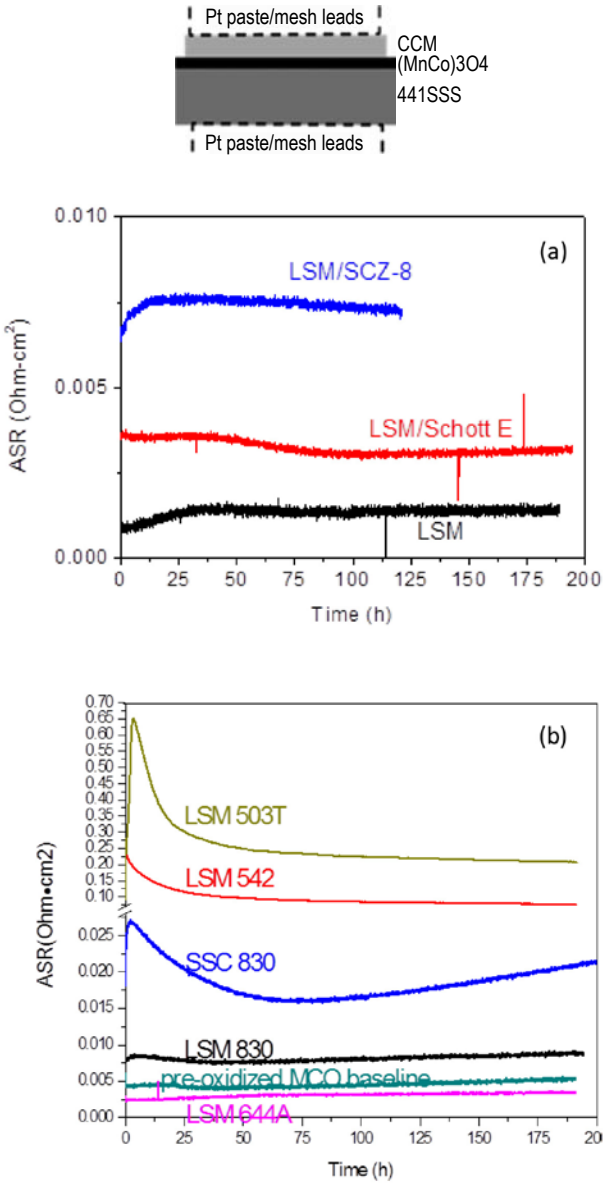

FIGURE 2. ASR for various CCM compositions at 800°C

- LSM with SCZ-8 and Schott E (GM31107) glass or Aremco 830, 542, 503T and 644A inorganic binders were chosen as the most promising candidates, and ASR testing was conducted with these compositions. Initial results indicated that the glasses, 644A, and 830 provide low, stable ASR.
- These best candidates were subjected to in situ testing using MCO-coated 441 steel current collectors and anode-supported cells.
- Novel solutions to the CCM issue were assessed and developed, and shown to be quite promising.

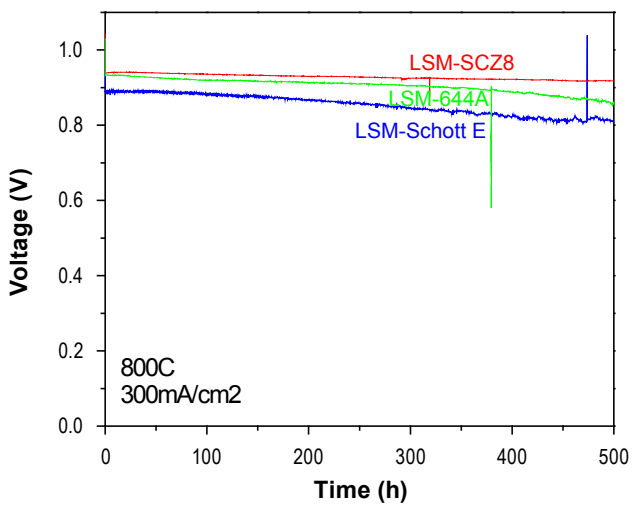

FIGURE 3. Cell performance for in situ testing of CCM compositions at 800°C

Special Recognitions & Awards/Patents Issued

1. U.S. patent application: Improved electrical contact material

FY 2012 Publications/Presentations

1. M. Tucker, L. Cheng, "Integrated Thermal Management Strategy and Materials for Solid Oxide Fuel Cells." *J. Power Sources*, 196 (2011) 10074–10078.

2. M. Tucker, L. Cheng, L. DeJonghe, "Glass-Containing Composite Cathode Contact Materials for Solid Oxide Fuel Cells." *J. Power Sources*, 196 (2011) 8435– 8443.

3. M. Tucker, L. Cheng, L. DeJonghe. "Selection of Cathode Contact Materials for Solid Oxide Fuel Cells." *J. Power Sources* 196 (2011) 8313– 8322.

4. M. Tucker, L. Cheng, "Cathode Contact Materials for SOFCs." Presented at the Electrochemical Society meeting, Boston, MA.

III.A.6 Source of Chemical Heterogeneities on Doped $LaMnO_3$ Dense Thin-Film Cathode Surfaces

Bilge Yildiz (Primary Contact), Wonyoung Lee
Massachusetts Institute of Technology
Department of Nuclear Science and Engineering
77 Massachusetts Avenue, 24-210
Cambridge, MA 02139
Phone: (617) 324-4009; Fax: (617) 258-8863
Email: byildiz@mit.edu

DOE Project Manager: Briggs White
Phone: (304) 285-5437
Email: Briggs.White@netl.doe.gov

Subcontractor:
Clemens Heske
University of Nevada, Las Vegas (UNLV)
Las Vegas, NV

Contract Number: NT0004117

Phase I Start Date: October 1, 2008
Phase I End Date: March 31, 2010

Phase II Start Date: April 1, 2010
Phase II End Date: September 30, 2011

Phase III Start Date: October 1, 2011
Phase III End Date: September 30, 2012

Fiscal Year (FY) 2012 Objectives

- Observation of local electronic structure, electron tunneling properties, and chemical characteristics on $La_{0.7}Sr_{0.3}MnO_3$ (LSM) dense thin-film model cathodes at elevated temperatures and reactive gas environment with oxygen.
- Identify mechanisms of the cation surface segregation and secondary phase formation on perovskite thin films by consideration of elastic and electrostatic interactions.

FY 2012 Accomplishments

We demonstrated the effects of temperature and oxygen pressure on the surface cation chemistry and the surface electronic structure of LSM as a model system. LSM film surfaces exhibit an electronic transition from a semiconducting state to metallic-like state at elevated temperatures, with the lower transition temperature with the lower oxygen pressure.

We systematically assessed the mechanism of the cation segregation and secondary phase formation on perovskite films by consideration of elastic and electrostatic interactions. Stoichiometric deficiency in A-site and smaller size mismatch between the dopant and the host cation suppressed the cation segregation on the film surface. Oxygen chemical potential was shown to control the cation segregation on the surface by changing the charge distribution near the film surface.

Introduction

The slow rate of oxygen reduction reaction (ORR) at the cathode is one of the main barriers for implementation of high-performance solid oxide fuel cells (SOFCs) at intermediate temperatures (500°C–700°C). It is generally agreed that the ORR kinetics is limited by the surface exchange reactions on the surface of mixed ionic electronic oxide cathodes. The structural, chemical and electrochemical properties of the cathode surface are of importance to improve the ORR reactivity. However, the dynamic nature of surface structure and chemistry, driven by the harsh conditions of high temperatures and oxygen partial pressure in SOFCs, has resulted in difficulties to probe and fundamentally understand the origin of the activation and deactivation of ORR kinetics on the surfaces. Although cation segregation and phase separation on the surface of perovskite oxides have been commonly observed, the driving forces to cation segregation and its impact on the surface electrochemical activity remain yet unclear.

In this report, we show changes in the surface chemical and electronic state of LSM as a model system. We assessed two key parameters for reactivity with oxygen: (1) chemical environment on the LSM surface, in particular, the segregation of Sr cations and oxygen vacancy formation, probed with angle-resolved X-ray photoelectron spectroscopy and (2) surface electronic structure, probed using scanning tunneling microscopy and spectroscopy (both at ambient and in situ at elevated temperatures). Furthermore, we report the driving forces of cation rearrangements in perovskite thin films by consideration of elastic and electrostatic interactions. The effects of the elastic energy on the cation segregation were investigated with two control parameters: A-site stoichiometry and dopant size in the perovskite thin films. The higher chemical stability was observed

from A-site deficient LSM thin films and smaller size mismatch between the dopant (Ba, Sr, Ca) and the host cation (La). Excess available cation sub-lattice space accommodates the dopant cations in the bulk. The effects of the electrostatic energy on the cation segregation were investigated with control of oxygen chemical potential during annealing. Distribution of charged defects, especially oxygen vacancies, influenced the level of cation segregation and phase separation on the surface. Observed difference in extent of surface segregation and phase separation suggests the different electronic and electrochemical properties on the surface. Electronic and electrochemical investigations of these samples are under progress. On the basis of our experimental results, we discuss the possible mechanisms for segregation and secondary phase formation at the perovskite thin film surfaces. These results contribute to understanding the role of elastic and electrostatic energy contributions to cation segregation on the surface of perovskite cathodes, and to elucidating the role of surface chemical heterogeneities to the ORR kinetics.

Approach

X-ray diffraction (XRD) measurements were performed employing a PANalytical Expert Pro MPD diffractometer to determine the phase purity and the strain states. Scanning tunneling microscopy/spectroscopy (STM/STS) at room temperature as well as at elevated temperatures was used to investigate the surface morphology and electronic structure of the strained films. The measurements were performed in a modified ultra high vacuum (UHV) system designed by Omicron Nanotechnology, with a variable temperature scanning tunneling microscope. The chemical state of the surfaces was probed using angle-resolved X-ray photoelectron spectroscopy (XPS) using a five-channel hemispherical electron analyzer, equipped in the same chamber with the STM. CasaXPS 2.3.15 software was used to assess the spectra and calculate the relative intensity of each constituent by employing the Shirley background. The total intensity of each constituent was normalized by their corresponding cross section values from Scofield's table. We removed carbon contamination from the surfaces of the air-exposed perovskite thin films by heating them in oxygen pressure of 5×10^{-5} mbar at 500ºC for at least 30 min in the UHV chamber. All STM, STS, and XPS results reported here were obtained after the cleaning process. A pyrolytic boron nitride (PBN) heater was used to evenly heat the perovskite thin films during the cleaning process as well as during the STM experiments at high temperatures. STM measurements were performed in the constant-current mode using Pt/Ir tips, with a bias voltage of 1–2 V applied to the tip and a tunneling current of 100–500 pA.

Results

Part I: Effects of temperature and oxygen pressure on surface electronic structures of LSM thin films

We have investigated the effect of surface oxygen vacancy formation on the surface electronic structure of tensile-strained LSM thin films. In particular, the energy gap of the LSM thin films was explored as a function of temperature and oxygen pressure. Epitaxial 10–15 nm thick LSM films were grown by pulsed laser deposition [2] on (001) $SrTiO_3$ (STO) as the model systems. Thin films were deposited with a KrF excimer laser at a wavelength of 248 nm and laser beam energy of 550 mJ/pulse at 10 Hz. The deposition was performed at 815ºC with oxygen pressure of 10 mTorr and with the target-to-substrate distance of 6 cm. After deposition, the sample was cooled at 10°C/min to room temperature in an oxygen pressure of 10 Torr. XRD results indicated that films were fully strained with the (001) out of plane orientation with 0.8% in-plane tensile strain at room temperature. The energy gaps of LSM/STO films were measured and analyzed as a function of temperature and oxygen pressure. The sample was cleaned by Ar sputtering (2.0 keV, 20 mA for 2 min) in $\sim 2 \times 10^{-6}$ mbar of argon and annealing at 500°C–550°C for 1 hr in $\sim 3 \times 10^{-3}$ mbar of oxygen. The sample was then cooled down to room temperature slowly in the same oxygen pressure. All measurement was performed after stabilizing the temperature more than 1 hr at each temperature.

Figure 1 shows the measured energy gap of the LSM/STO thin films as a function of temperature and the oxygen pressure. First, the transition from a semiconducting state with an energy gap to a metallic-like state with no-gap occurred at elevated temperatures. Black squares represent the measured energy gap in the oxygen pressure of $\sim 3 \times 10^{-3}$ mbar. At room temperature, the LSM/STO thin films showed a semiconducting state with an energy gap of 1.86 ± 0.15 eV. As the temperature increased in the oxygen pressure of $\sim 3 \times 10^{-3}$ mbar, the energy gap decreased and completely disappeared at 450°C–500°C. This transition to a metallic-like state at elevated temperatures was observed in all oxygen pressures tested. However, the oxygen pressure affected the transition temperature. With lower oxygen pressure, the transition occurred at the lower temperature. The transition to a metallic-like state took place at 300°C–350°C and 100°C–150°C in the oxygen pressures of $\sim 3 \times 10^{-5}$ and $\sim 4 \times 10^{-10}$ mbar, respectively. After cooling to room temperature and maintaining each oxygen pressure, the samples recovered their semiconducting states with the slightly lower values. It should be noted that Figure 1 contains data from two sets of LSM thin films from different sample batches but with

the same configuration (LSM films on STO substrates). All samples showed quantitatively similar behavior, substantiating that this electronic transition is not limited to a specific sample but is a general characteristic of LSM thin films. The possible mechanism for this partial recovery will be discussed later in this report. We will carry out more STM/STS experiments in even higher oxygen pressure (~10^2 mbar) to verify the effect of the oxygen pressure on the energy gap. This series of supporting experiments will provide better understanding of the oxygen pressure effects on the electronic structures on the LSM/STO thin film surfaces.

The transition from a semiconducting state to a metallic-like state can be attributed to several mechanisms including surface reconstruction, chemical change, and defect formation. First, Fuchigami et al. [3] reported that a surface structure can be reversibly converted through adsorption and desorption of oxygen on the surface, resulting in the transition between an insulating and a metallic-like state. Figures 2a and 2b show the surface morphologies from one set of LSM thin films measured at room temperature and 500ºC in an oxygen pressure of ~3 × 10^{-5} mbar, respectively. The surface of LSM/STO films showed well-resolved and atomically smooth terraces with the height difference between each layer at 4.0 ± 0.3 Å, in good agreement with the lattice parameter of the LSM (3.88 Å). The step height within the temperature range tested showed no distinguishable change as shown in Figure 2c. We found no clear evidence that a major structural change occurs at elevated temperatures, resulting in the observed changes in the electronic structure shown in Figure 1.

Secondly, changes in surface chemistry can be considered to induce electronic transition. Cation segregation at elevated temperature can cause the formation of hole-rich regions on the surface, as cation dynamics can take place at high temperature on oxide surface [2]. However, the temperature at which we observed the disappearance of the energy gap is too low to enable significant cation mobility that may alter the surface cation compositions. Figure 3 shows the concentration ratios of cations by X-ray photoelectron spectroscopy (XPS) for surface action chemistries as a function of temperature in the base pressure of 2 × 10^{-9} mbar or lower. The surface composition of this second sample set used for STM/STS analysis in this quarter was measured after the cleaning processes. From the result with an emission angle of 0º, there was no noticeable change in cation concentration ratios, Sr/(La+Sr), Sr/Mn, and La/Mn, from room temperature up to 500ºC. In contrast, the result with an emission angle of 70º showed increase of Sr/Mn and La/Mn as temperature increased, while the Sr/(La+Sr) ratio remained constant up to 500ºC. In other words, either A-site cation (La and Sr) segregation or B-site cation (Mn) depletion was occurring at the surface. Given the fact that the emission angle of 70º is more surface sensitive, this chemical changes at elevated temperature might imply the possibility of surface reconstruction at the very top surface, while the rest of the film remains perovskite structures. After cooling to room temperature, both Sr/Mn and La/Mn decreased, but they were still higher than the initial ratios at room temperature. This partially reversible behavior is consistent with the observed energy gap evolution with temperatures, indicating these two observations might be closely related. However, the fact that the measured energy gap had similar values from two different surface structures

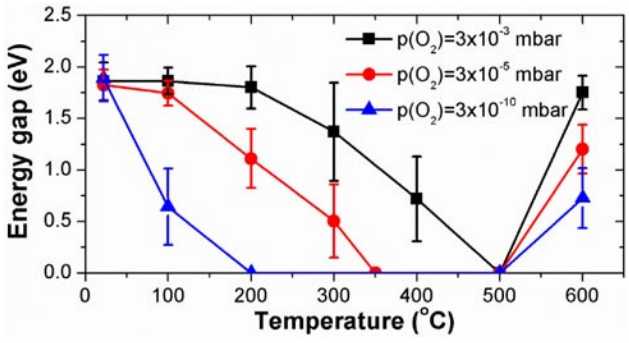

FIGURE 1. The energy gap of LSM/STO thin films as a function of temperature and oxygen pressure. Black squares, red circles, and blue triangles were measured energy gaps in oxygen pressures of ~3 × 10^{-3}, ~3 × 10^{-5}, and ~4 × 10^{-10} mbar, respectively.

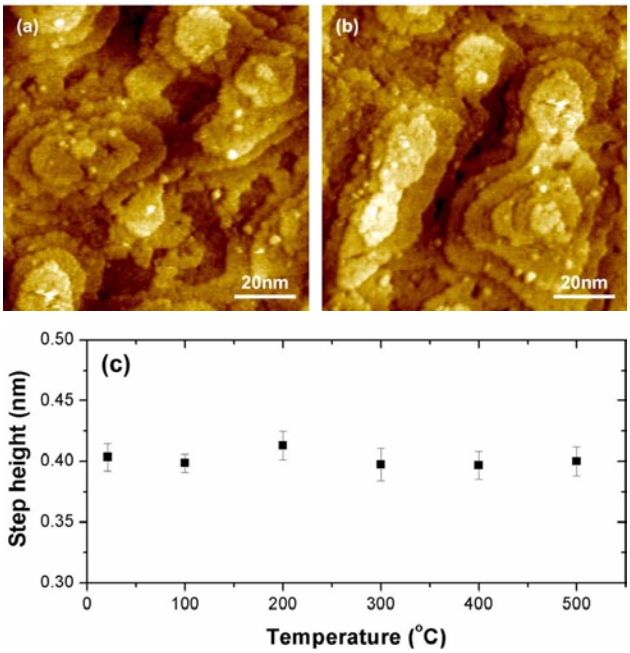

FIGURE 2. Surface morphologies of LSM/STO thin films in an oxygen pressure of ~3 × 10^{-3} mbar (a) at room temperature, (b) at 500ºC. (c) The step height evolution with temperatures.

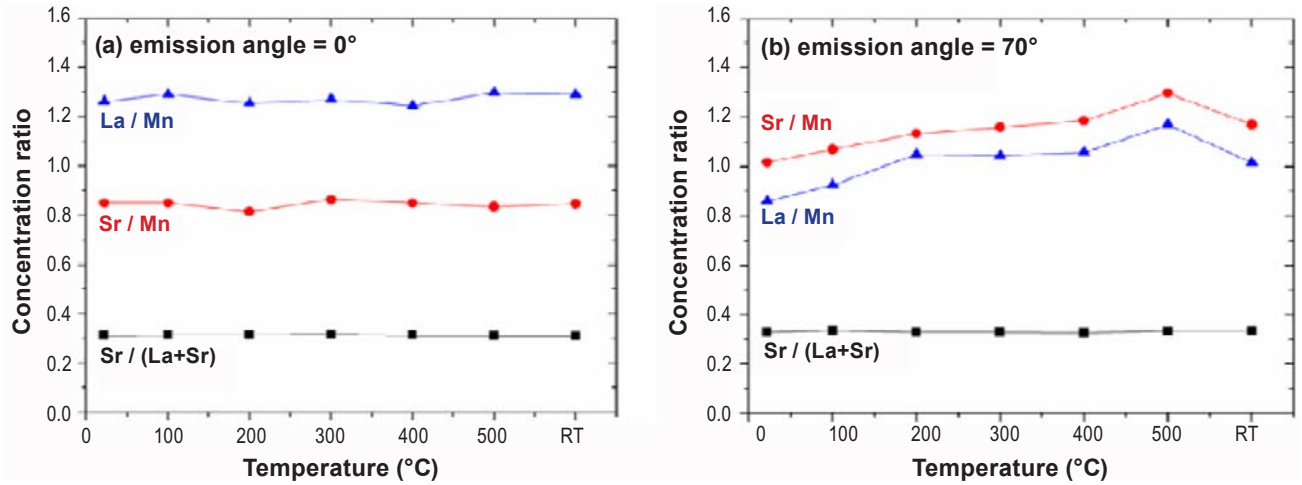

FIGURE 3. Concentration ratios of cations (La, Sr, and Mn)

suggests the effect from the chemistry-induced structural changes may also not be a dominating factor for this electronic transition. Further systematic investigation will be performed by Massachusetts Institute of Technology for structural analysis and by University of Nevada, Las Vegas (UNLV) for chemical analysis.

We are pursuing the hypothesis that the electronic transition from a semiconducting to a metallic-like state originates mainly from oxygen vacancy formation at the surface. Formation of oxygen vacancies at the surface can induce additional defect states in the energy gap, resulting in the delocalization of the charge carriers at elevated temperatures [4,5]. The vacancy formation energy at 0 K on the LSM surface is 1.26 eV lower than that in the bulk, resulting in several orders of magnitude higher concentration of oxygen vacancy on the surface [6]. This high concentration of oxygen vacancy in transition metal oxide can modify the *d* band structure of the neighboring transition metals and induce defect states in the energy gap. The exponential increase of vacancy formation with temperature can explain the rapid transition from a semiconducting state to a metallic-like state. This defect induced transition is partially reversible within this range of temperature and oxygen pressure. The energy gaps were recovered to their initial values after cooling to room temperature, but slightly smaller than the initial ones. After cooling process, the excess vacancies on the surface would be filled by the oxygen to reach an equilibrium state at room temperature. However, not all vacancies will be filled because the available oxygen in the chamber is limited, and the temperature is low for fast re-oxidation, resulting in partial recovery in the low oxygen pressure. Note that the energy gap values were similar for all samples after annealing at 500°C–550°C in the oxygen pressure of ~3 × 10^{-3} mbar. This indicates that the complete recovery of the oxygen stoichiometry at the surface was achieved by filling up the excess vacancies on the surface. This strong dependency on temperature and oxygen pressure suggests that this transition originates mainly from the defect formation on the surface, especially oxygen vacancies.

More systematic investigation of the cation oxidation states is required as a measure in quantifying the relative presence of surface oxygen vacancies on the LSM films. The formal oxidation state of Mn ions is known to be related to oxygen vacancy formation [7,8]. The removal of originally negatively charged oxygen ions as neutral species leads to the reduction of the nearest-neighbor transition metal ions, Mn, by the following chemical reactions.

$$2Mn_{Mn}^{\bullet} + O_O^{\times} \leftrightarrow 2Mn_{Mn}^{\times} + V_O^{\bullet\bullet} + \frac{1}{2}O_2$$

Reduction of Mn ions, a decrease in the positive charge of the transition metal ions, is accompanied by the decrease in the binding energy of the core level (chemical shift) in Mn 2p emission. Moreover, the 3s core levels of the 3d transition metals are known to exhibit exchange splitting due to the interaction between the 3s hole and 3d electrons [9]. This exchange splitting energy of Mn 3s emission shows a linear relation with the Mn valence [10]. The expected splitting of the 3s level is ~6.5 for Mn^{2+}, ~5.5 for Mn^{3+} and ~4.5 for Mn^{4+}. Co-work with the UNLV team is in progress for this high resolution XPS study at elevated temperatures with angle-resolved measurements.

Part II: Driving forces for cation segregation on the surface in perovskite-structured thin film cathodes

We have investigated the mechanisms of the cation segregation and phase separation on perovskite thin

films by consideration of the elastic and electrostatic interactions. It has been recognized that the major driving forces are the elastic and the electrostatic energy, which lead to the equilibrium segregation to the surface and interface [7]. Systematic investigation of the perovskite thin films with varying elastic and electrostatic energy in the system can allow us to understand the mechanisms of cation rearrangements and therefore to control and optimize the dopant segregation in the perovskite cathode materials. The effects of the elastic energy on the cation segregation were investigated with two control parameters, A-site stoichiometry and the lattice mismatch between the dopant (Ca, Sr, Ba) and the host cation (La) in doped lanthanum manganite as model systems. The effects of the electrostatic energy were investigated by controlling the oxygen chemical potential during annealing, which influences the distribution of charged oxygen defects in the films.

Conclusions and Future Directions

Part I of the project investigated the effect of temperature and oxygen pressure on the surface electronic structure of LSM thin films. The transition from a semiconducting state with an energy gap to a metallic-like state with no-gap was observed at elevated temperature. Oxygen pressure also influences this observed transition; with lower oxygen pressure, the transition occurred at the lower temperature. The semiconducting states were recovered by re-annealing in oxygen. This strong dependency on temperature and oxygen pressure suggests the observed electronic transition originates mainly from oxygen vacancy formation at the surface, which can modify the d band structure of the neighboring transition metals and induce defect states in the energy gap. The surface cation chemistry is further analyzed with UNLV team, and the result will be discussed in the next report.

Part II of the project investigated the mechanism of cation segregation and secondary phase formation in perovskite materials by consideration of elastic and electrostatic interactions. The effects of the elastic energy on the cation segregation were investigated with two control parameters, A-site stoichiometry and the lattice mismatch between the dopant and the host cation in doped lanthanum manganite as model system. The higher chemical stability upon annealing was observed on A-site deficient LSM and on the lanthanum manganite films with smaller size mismatch between the dopant and the host cation. The relatively higher stability is considered to be due to the excess space available to dopant in the A-site sub-lattice in the bulk. The effects of the electrostatic energy were investigated by controlling the oxygen chemical potential during annealing, which influences the distribution of charged oxygen defects in the films. The suppressed cation segregation was observed with lower pressure during annealing because of the electrostatic interactions between the dopants and the oxide ion vacancies near the surface. Observed difference in extent of surface segregation and phase separation with the control of the elastic and electrostatic interactions suggests the different electronic and electrochemical properties on the surface. Electronic and electrochemical investigations of the film surface will be discussed to elucidate the impact of cation segregation and phase separation on the ORR kinetics at the cathode surface. Figure 4 shows preliminary results of electronic properties of surface structures. Secondary phases on the film surface showed similar lateral dimensions, but the contrast of vertical dimensions were opposite. They appeared as protrusions with AFM scanning, i.e., higher compared to the film surface, while appearing as depressions with STM scanning, i.e., lower compared to

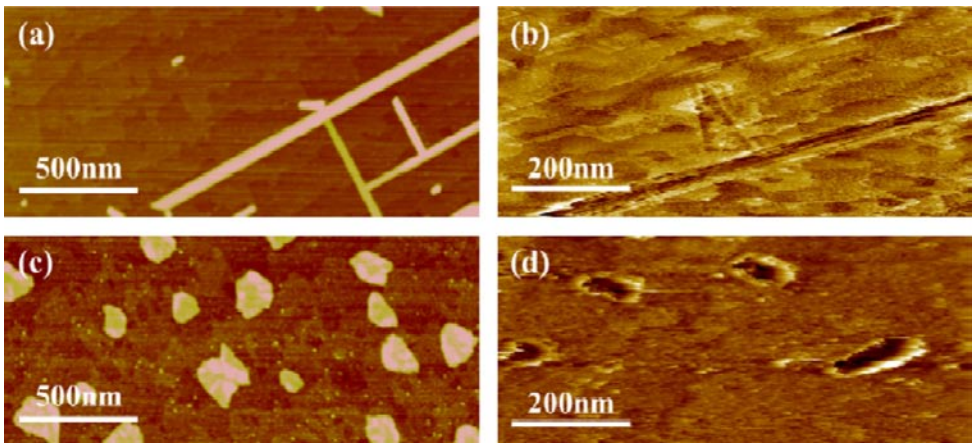

FIGURE 4. Surface morphologies after annealing at 830°C for 1 hr in air (a) on LBM by AFM, (b) on LBM by STM, (c) on LSM by AFM, and (d) on LSM by STM

the film surface. This discrepancy originates the source for vertical information from both techniques. The height in AFM scanning provides the geometrical information; in contrast the height in STM scanning provides the density of states at given bias voltage. Even if the feature is geometrically protruding from the surface, it will appear as a depression if the feature is less conducting or insulating. Therefore, this comparison provides direct evidence that this secondary phase formed upon annealing is electronically insulating.

FY 2012 Publications/Presentations

1. Conference presentation, May 2012, "The Role of Chemical Heterogeneities on Oxygen Reduction Kinetics on the Surface of Thin Film Cathodes," 221th Meeting of Electrochemical Society, Seattle, Washington, USA.

2. Wonyoung Lee, Zhuhua Cai, and Bilge Yildiz, Conference Proceeding, "Role of Chemical Heterogeneities on Oxygen Reduction Kinetics on the Surface of Thin Film Cathodes," *Electrochemical Society Transaction*, 2012, **45**, 405-412.

References

1. M. Sase, K. Yashiro, K. Sato, J. Mizusaki, T. Kawada, N. Sakai, K. Yamaji, T. Horita, H. Yokokawa, *Solid State Ion.* **2008**, 178, 1843.

2. K.R. Balasubramaniam, S. Havelia, P.A. Salvador, H. Zheng, J.F. Mitchell, *Appl. Phys. Lett.* **2007**, 91, 232901.

3. K. Fuchigami, Z. Gai, T.Z. Ward, L.F. Yin, P.C. Snijders, E.W. Plummer, J. Shen, *Phys. Rev. Lett.* **2009**, 102, 066104.

4. H. Dulli, P.A. Dowben, S.H. Liou, E.W. Plummer, *Phys. Rev. B* **2000**, 62, R14629.

5. R. Bertacco, J.P. Contour, A. Barthelemy, J. Olivier, *Surf. Sci.* **2002**, 511, 366.

6. G. Vovk, X. Chen, C.A. Mims, *J. Phys. Chem. B* **2005**, 109, 2445.

7. Q.-H. Wu, M. Liu, W. Jaegermann, *Mater. Lett.* **2005**, 59, 1480.

8. V.R. Galakhov, M. Demeter, S. Bartkowski, M. Neumann, N.A. Ovechkina, E.Z. Kurmaev, N.I. Lobachevskaya, Y.M. Mukovskii, J. Mitchell, D.L Ederer, *Phys. Rev. B* **2002**, 65, 113102.

9. E. Beyreuther, S. Grafström, L.M. Eng, C. Thiele, K. Dörr, *Phys. Rev. B* **2006**, 73, 155425.

10. V.A.M. Brabers, F.M. Van Setten, P.S.A. Knapen, *J. Solid State Chem.* **1983**, 49, 93.

11. M.F. Yan, R.M. Cannon, H.K. Bowen, *J. Appl. Phys.* **1983**, 54, 764.

III.A.7 Synchrotron Studies of SOFC Cathode Degradation

Y.U. Idzerda
Dept. of Physics
Montana State University
Bozeman, MT 59717
Phone: (406) 994-7838; Fax: (406) 994-7838
Email: Idzerda@physics.montana.edu

DOE Project Manager: Patcharin Burke
Phone: (412) 386-7378
Email: Patcharin.Burke@netl.doe.gov

Contract Number: NT0004115

Start Date: March 3, 2010
End Date: September 2, 2012

Fiscal Year (FY) 2012 Objectives

- Characterize electron valence variations and modifications occurring at a variety of length scales from millimeters to the nanometer range at the cathode surface and in the cathode/electrolyte interface region of solid oxide fuel cell (SOFC) related materials.
- Correlate valence variations with effects of bias potential, gaseous environment including PO_2 and humidity, and possible synergistic effects between them.
- Identify methods to mitigate or prevent degradation from valence variation to develop improved $La_{1-x}Sr_xCo_yFe_{1-y}O_{3-\delta}$ (LSCF) cathodes.

FY 2012 Accomplishments

- Demonstrated elemental surface valence determination with a field of view of 10 mm x 10 mm and a spatial resolution of 200 μm x 200 μm.
- Identified large surface Co valence variation between Co^{3+} and Co^{2+} across an LSCF cathode operated over 100 hours at 850°C and +450 mV bias potential at 75% humidity.
- Developed a method to significantly reduce spatial valence variation with the inclusion of laminar flow across the cathode surface.

Introduction

Although the structural and chemical properties of cathodes play an important role in SOFC operation, it is the properties of the surface and interface that determine the overall performance and are most sensitive to degradation. Maintaining the electron and oxygen ion transport properties of a surface or interfacial region relies on the chemical and structural characteristics of the surface and buried interface. A poor-quality surface may inhibit the creation of the mobile species necessary for SOFC operation. A poor-quality interface may degrade the ion transport performance, e.g., it may be the major hindrance to ion transport and reduce the overall performance. The properties of the surface may be very different from the bulk due to reduced co-ordination, roughness, or surface segregation, creating barriers to ion formation and mobility. Moreover, surfaces and interfaces represent regions where electrochemical and mechanical stresses can be relieved in wholly unanticipated manners with important ramifications on the overall properties [1]. Finally, as SOFC architectures move toward more nanostructured materials and tailored interface properties, the oxygen ion transport is exclusively surface/interface transport.

To meet U.S. Department of Energy technical targets, methods to characterize and mitigate cathode degradation need to be developed and demonstrated. In particular, methods to investigate surfaces before and after operation as a component of an SOFC are necessary for degradation studies. The spatial resolution is an important aspect of the characterization tool because characterizing the spatially averaged behavior will fail to identify the extremes of the variation, which are precisely the regions that are expected to initiate degradation. Correlations between surface chemistry and electronic structure and operational conditions can then be used to identify methods to prevent or mitigate cathode degradation.

Approach

Synchrotron-based soft X-ray absorption (XAS) is an element-specific, non-destructive probe with the sensitivity to address each element in the cathode of an SOFC to determine the cathode chemical and electronic properties with good spatial resolution. These techniques can be well adapted for determining surface chemistry, including segregation and surface species

electron valence as a function of operational conditions. Improvements made at the advanced light source (ALS) allow for acquisition of complete XAS spectra in as little as 15 seconds (instead of 5-10 minutes), allowing for the spatially resolved surface electron valence mapping over a 1 cm^2 area with 200 μm resolution (representing 2,500 separate XAS scans) in a reasonable time frame (a day).

In the experimental setup, four-probe conductivity measurements of symmetric half-cells [2,3] grown by pulsed-laser deposition (PLD), consisting of a $Gd_{0.1}Ce_{0.9}O_{2-\Delta}$ (GDC) thin film deposited on an yttrium-stabilized zirconia (YSZ) electrolyte substrate with $La_{0.6}Sr_{0.4}Co_{0.2}Fe_{0.8}O_{3-\delta}$ (LSC20F80) or $La_{0.6}Sr_{0.4}Co_{0.5}Fe_{0.5}O_{3-\delta}$ (LSC50F50) dense electrodes were performed on *both* sides. The symmetrical nature of the samples allows the study of how oxygen dissociation and recombination affect performance at either the cathode or anode using easily controlled electrical potentials rather than chemical potentials. Gold mesh contacts are pressed on each side of the sample with ceramic disks and held together with alumina fasteners. The discs are perforated to allow access of the humidified air. After 48-100 hours of operation, the anode and cathode are characterized using various soft-X-ray probes, including valence mapping.

Results

The major conclusion from valence mapping studies is that strong variation in the valence of surface elements occurs due to non-homogenous gas flow. Any study that reports surface valence values under normal operational conditions should demonstrate that the measured spectrum is representative of the entire surface and not an average value across the entire surface or the spectrum associated with a single position. For degradation considerations, it is the extremes of the elemental valence shifts that are of importance and not the average values since the extreme values may represent localized positions where a degradation mechanism is active. A number of studies have shown that temperature homogeneity is an important feature of performance, so finding homogeneity in gas atom availability similarly important should not be surprising. One complication is that unlike temperature homogeneity, reactant gas atom availability changes with operation since the reactant gas is consumed, modifying its distribution and diffusion. The scale of local inhomogeneities should be on the macroscale (100s of microns) rather than the nanoscale where rapid gas atom diffusion is sufficient to maintain a local balance at these very small scales. This required a major improvement in the rapidity with which spectra could be acquired and the automation of batch data analysis with high-level data representation, i.e., reducing the 2,500 scans to a limited number of important values to display the valence variation across the sample surface.

The study has shown that the spatial mapping of the Co valence at the surface of the LSCF cathode allowed for the identification of large variations in Co valence (going from Co^{2+} to predominantly Co^{4+}, depending on the operational conditions). The study has also shown that the distinct variation in the Co valence at a given bias potential can be mapped to the air inlets present in the cathode or anode air inlet configuration. Figure 1 reproduces the Co valence surface mappings with an overlay of the air inlets for both sides of the symmetric cell.

A major difficulty that was overcome was separating contributions from different Co valence in the individual XAS spectra. Reference Co and Fe valence spectra were measured and can be reproduced with molecular orbital theory. These reference spectra are now used for the valence decomposition in the individual spectra. This automated process means that the data analysis can be rapidly performed.

The study has also shown that the distinct variation in the Co valence depends strongly on the availability of water vapor (humidity). Although local probes of humidity at the 100 μm scale are not available, the observable effect of the humidity variation is easily quantifiable at that scale. In Figure 2 is shown the L_{23}-edge Co XAS spectra used for valence identification at different points radially outward from a LSCF cathode.

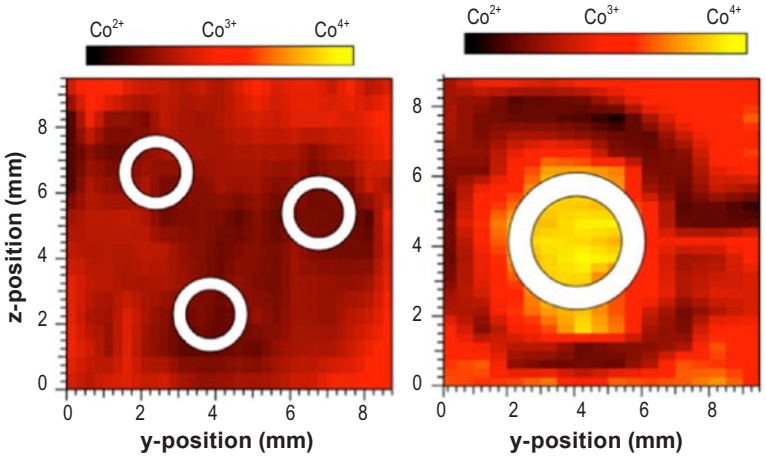

FIGURE 1. Co valence mappings of both sides of a symmetric cell overlayed with representations of the two sets of air inlets for bias potential of -500 Mv (left) and +500 Mv (right)

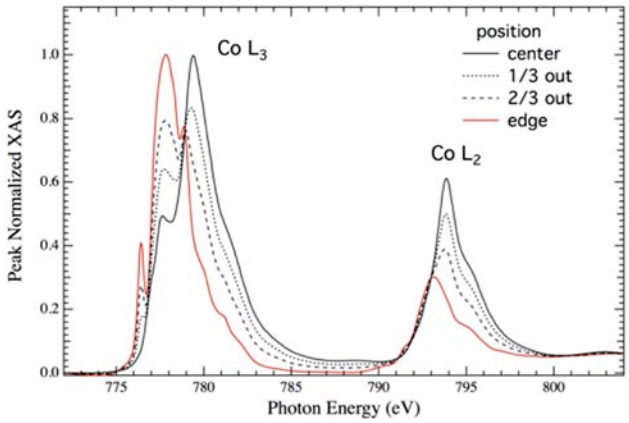

FIGURE 2. Co L_{23} XAS spectra for valence extraction at selected positions (center to edge) of a LSCF cathode after operation for 100 hours at 850°C, 450 Mv bias and 75% humidity

The variation is larger than has been observed for dry air flow, indicating that water vapor availability plays an even more important role than PO_2 availability. Such an area mapping is shown in Figure 3 for both positive and negative electrodes of a cell operated at 800°C for 40 hours at a potential bias of 500 mV and 75% humidity. The black to red color bar spans a variation of 35% to 60% (30% to 100%) in the Co valence composition ratio for the negative (positive) electrode. The spatial resolution is 200 µm by 200 µm for an 8 mm by 8 mm square sample, but higher resolution is achievable. The mapping shows a non-uniform distribution, demonstrating the role of the humidity from non-uniform air flow across the sample.

Finally, success was demonstrated for one mitigation strategy: modifying the Co valence to maintain charge neutrality (in addition to introducing laminar flow in the air flow inlets). By using a higher than normal Co concentration (a 50:50 LSCF film), oxygen vacancy concentrations in the electrodes can be maintained by reducing the initial imbalance of oxygen vacancies in the electrolyte in comparison to the electrode, e.g., higher doping in the electrolyte or lower doping in the electrodes. This increase in Co concentration need not be through the entire cathode, but can be an enhanced doping at the surface region only to retain the preferred bulk properties of the 20:80 LSCF cathode. Matching the catalytic activity of the electrode to the ion transport rate of the electrolyte will also lead to a more stable concentration of oxygen vacancies in the electrode. Strontium stabilization can be accomplished by co-doping (A-site and B-site dopants) in the near surface region of the LSCF. In either case, overall cell performance need not be sacrificed for improved lifetime.

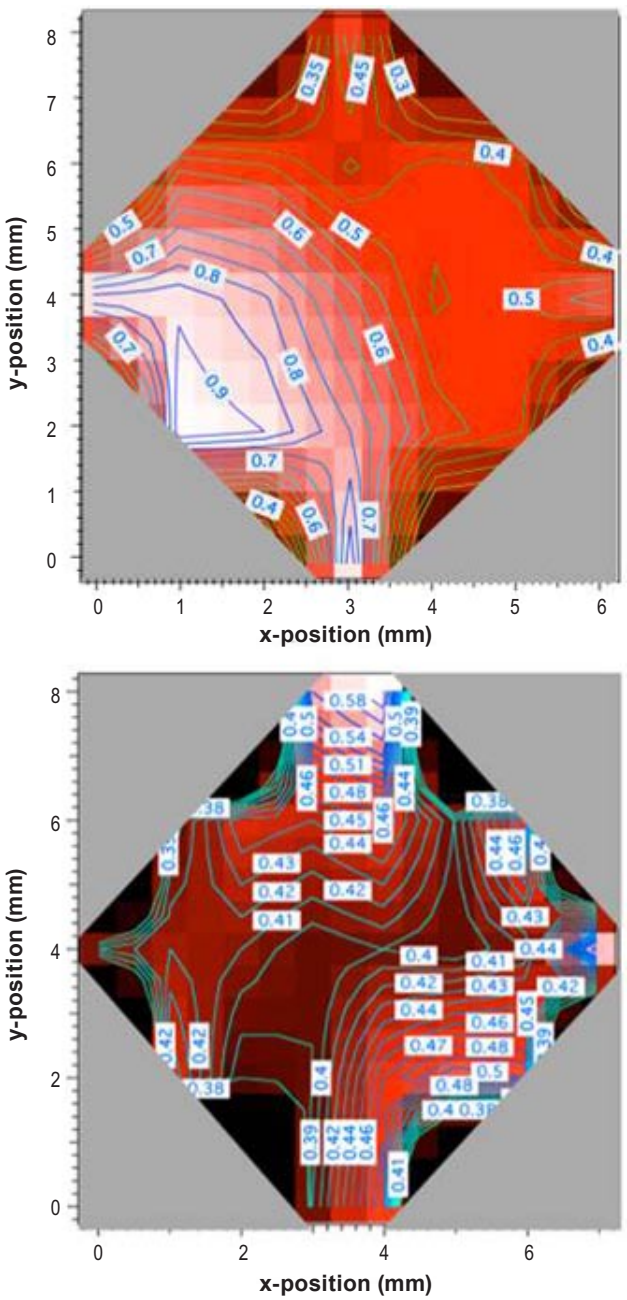

FIGURE 3. Area map of the Co^{3+} to Co^{2+} ratio for positive (top) and negative (bottom) electrode

Conclusions and Future Directions

A strong variation in the valence of surface elements due to non-homogenous gas flow and humidity has been demonstrated. Any study that reports surface valence values needs to demonstrate that the measured spectrum is representative of the entire surface and not an average value across the entire surface or the spectrum associated with a single position. For degradation considerations, it is the extremes of the elemental valence shifts that

are of importance and not the average values since the extreme values represent localized positions where a degradation mechanism is active. One complication is that unlike temperature homogeneity, reactant gas atom availability changes with operation since the reactant gas is consumed, modifying its distribution and diffusion. Furthermore, the scale of local inhomogeneities is on the macroscale (100s of microns) rather than the nanoscale since rapid gas atom diffusion is sufficient to maintain a local balance at these very small scales.

Further insight into the mechanism of Co valence modification can be obtained by determining the variation of crystallite size and crystallite orientation as the bias potential is modified. These measurements are planned for the next quarter.

Special Recognitions & Awards/Patents Issued

1. Martin Finsterbusch, "Degradation Mechanisms of Solid Oxide Fuel Cell Cathodes," Thesis dissertation (2012).

FY 2012 Publications/Presentations

1. M. Finsterbusch, J.A. Schaefer, and Y.U. Idzerda, "Oxygen Vacancy Induced Sr Segregation in $La_{0.6}Sr_{0.4}Co_{0.2}Fe_{0.8}O_{3-\delta}$," *Solid State Ionics* 212, 70 (2012).

2. B.C. Eigenbrodt, M. Finterbusch, Y.U. Idzerda, and R.A. Walker, "High Temperature In-situ Vibrational and Ex-situ Absorption Analysis of Reduced and Oxidized Yttria Stabilized Zirconia," *Solid State Ionics* (submitted), 2012.

3. Y.U. Idzerda, "Sr Out-Diffusion and Spatially Mapped Co Valence for Operational LSCF Cathodes," 12th Annual SECA Workshop, Pittsburgh, Pennsylvania, July 26–28, 2011.

4. Y.U. Idzerda, "Implementing the ALS Strategic Vision," Condensed Matter Seminar, Advanced Light Source, Berkeley, California, 2012.

References

1. A. Lussier, J. Dvorak, S. Stadler, J. Holroyd, M. Liberati, E. Arenholz, S.B. Ogale, T. Wu, T. Venkatesan, and Y.U. Idzerda, *Thin Solid Films* 516, 880 (2008).

2. M. Becker, A. Mai, E. Ivers-Tiffee, and F. Tietz, "Solid Oxide Fuel Cells (SOFC IX)," The Electrochemical Society Proceedings Series, Pennington, New Jersey, 514 (2005).

3. C. Collins, J. Lucas, T.L. Buchanan, M. Kopczyk, A. Kayani, P.E. Gannon, M.C. Deibert, R.J. Smith, D.-S. Choi, and V.I. Gorokhovsky, *Surface & Coatings Technology* 201, 4467 (2006).

III.A.8 NETL RUA Cathode Engineering R&D

Kirk Gerdes
U.S. Dept of Energy
National Energy Technology Laboratory
3610 Collins Ferry Rd.
Morgantown, WV 26507
Phone: (304) 285-4342; Fax: (304) 285-4469
Email: Kirk.Gerdes@netl.doe.gov

DOE Project Manager: Kirk Gerdes
Phone: (304) 285-4342
Email: Kirk.Gerdes@netl.doe.gov

Contract Number: FWP-2012.03.04

Start Date: March 15, 2012
End Date: September 30, 2012

Fiscal Year (FY) 2012 Objectives

- Rigorously examine stability of infiltrate material through direct electrochemical testing and post-operational microscopy.
- Demonstrate infiltrated Solid State Energy Conversion Alliance (SECA) scale cell's stable performance of 20% improvement in power density for 500 hours at 0.8 V compared to a baseline cell.
- Complete the examination of mesoporous infiltrate performance, and report comprehensive results.
- Demonstrate (at least five attempts) the toughened, doped lanthanum ferrite oxides (LFO) porous cathode architecture formed through in situ pore forming strategies in multi-cell array testing.
- Generate public report on the key conclusions from the work.

FY 2012 Accomplishments

- Demonstrated stability of infiltrate material $(LaSr)CoO_3$ (LSC) and completed detailed evaluation of infiltrate material wetting of cathode backbone. Demonstrated significant durability, and even improved baseline cell degradation performance.
- Generated mesoporous infiltrate materials and infiltrated commercial cathodes in single step up to 15 wt%. Demonstrated the importance of backbone/infiltrate combination in explaining performance improvement.
- Demonstrated infiltration benefit using a state-of-the-art cell supplied by SECA industrial team. Statistically significant power density improvement of greater than 35% was demonstrated.
- Reported the detailed technical results of cathode materials development in three published reports, two presentations, and one PhD dissertation.

Introduction

A solid oxide fuel cell (SOFC) is a device which generates electrical energy by exchanging oxygen ions between an oxygen-containing process stream such as air and a process stream containing an oxidizeable material such as hydrogen. The SOFC cathode facilitates the reduction of oxygen to an ionic form in preparation for transport across the impermeable electrolyte membrane. This electrochemical oxygen reduction process is sensitive to the material composition and physical structure of the cathode, and the oxygen reduction reaction (ORR) efficiency can be impacted by chemical or structural alterations.

Methods to improve the efficiency of the ORR typically focus on addition of electrocatalytic material into the porous cathode or focus on control of the cathode microstructure to increase the abundance of beneficial structural features. Proposed changes to cathode materials and microstructure must be carefully evaluated according to four principal criteria: (1) the magnitude of achievable performance enhancement under relevant SOFC operating conditions, (2) the chemical compatibility of materials with unaltered components in the fuel cell, (3) long term stability of new materials and engineered structures, and (4) the cost associated with implementation of the new methods.

Although a SOFC cathode is typically composed of a 60 μm thick porous ceramic, the cathode is particularly active at the locations within 1–10 μm of the interface between cathode and electrolyte, and material deposition is therefore preferred at the solid interface. Cathode infiltration attempts to deposit highly active material at specific locations inside the cathode, including difficult-to-reach interfaces. The primary challenges of cathode infiltration are (1) ensuring that the desired infiltrate material phase is deposited; (2) achieving proper distribution of infiltrate into the active regions of the cathode; and (3) ensuring that the material is stable as evaluated by electrochemical, thermochemical, and thermomechanical performance metrics.

Another approach to enhancement of cathode performance is exercise of control over the cathode microstructure using techniques of ceramics engineering. Control of microstructure allows a ceramicist to tailor the cathode for enhancement of desirable features such as increasing cathode porosity, improvement of mechanical strength, or to increase the total number of active boundaries within the cathode. The challenges to microstructural engineering are (1) engineering the cathode microstructure using a practical and inexpensive process, (2) ensuring that the engineered structures remain thermally stable at relevant operating conditions, and (3) verifying that the resulting cathode demonstrates a sufficient performance enhancement to justify cost. The target of the present research effort is to demonstrate a practical method for engineering microstructure that results in improved and stable cathode performance.

Approach

In the infiltration portions of the project, a porous ceramic SOFC cathode of standard composition ($La_{1-x}Sr_xMnO_3$ or $La_{1-x}Sr_xFe_{1-y}Co_yO_3$) is infiltrated with materials intended to enhance the chemical activity of the cathode and enhance the oxygen reduction reaction. Materials suitable for infiltration into the cathode are identified, the materials are generated and infiltrated, and the impact on cathode performance is electrochemically evaluated. Materials demonstrating improved cathode performance are also screened through extended testing to ensure that long-term stability will be adequate to meet lifetime performance metrics. After performance screening using a cost-effective, small-scale (button cell) test system, the infiltration techniques and methods are scaled up to begin approaching more relevant commercial scales.

The FY 2012 effort begins the transition of the technology to larger cell scales, from approximately 2 cm^2 to 16 cm^2.

Infiltrate materials are developed using two principal methods. Method 1 produces widely dispersed, dense nanoparticles of diameters approximately 20–50 nm and surface areas of approximately 2–5 m^2/g. Method 2, known as evaporation induced self assembly (EISA), produces widely dispersed particles possessing inherent mesoporosity. The mesoporous materials feature increased particle size at 50–100 nm, but also 10 times enhanced the surface area at 20–50 m^2/g. Method 1 is used to screen constituent materials for performance, wettability, and chemical stability. Several novel infiltrate materials are generated by Method 1 and include $(LaSr)CoO_3$, $(LaSr)(CoPt)O_3$, and $(LaSr)FeO_3$. Method 2 is restricted to more conventional materials, in order to concentrate research on the EISA process and evaluation of material stability. Materials include LSM and LSC.

In the cathode microstructural engineering efforts, the objective is to develop engineered SOFC cathode microstructures that are tailored to provide a high triple-phase boundary (TPB) concentration, low resistance to gas diffusion, and optimal architecture for nano-catalyst impregnation. Structural engineering may focus on specific phases within the cathode, or on the overall cell architecture; efforts to engineer the phases are intended to enhance the ionic and electronic conductivity of the cells. Architectural engineering is intended to enhance gas flow, mechanical strength, and connectivity of phases.

Through prior years' efforts, different cathode engineering methods were compared for efficacy in control of the cathode microstructure. The leading method emerging from comparative evaluation produces a foam-like cathode structure with engineered porosity from the electrolyte surface to the interconnect. This method engineers submicron pores (nanopores) within the open foam structure to enhance the TPB concentration while retaining porosity for optimal gas flow and infiltration of the cathode active area.

Cells possessing the novel foamed microstructure or infiltrated with electrocatalytically active materials are then operated electrochemically for at least 200 hours at 750-800°C using hydrogen as the fuel source. Long duration tests lasting 1500+ hours have also been completed to assess the stability of infiltrated specimen. Cells under test are also periodically probed with electrochemical impedance spectroscopy, and results are used to examine changes in the electrode polarization and cell ohmic resistance. The quality of structure and infiltration is evaluated visually and spectroscopically on the basis of structural features, particle size, and uniformity of infiltrate coverage. The battery of results are used to evaluate the performance of all candidate materials in order to identify the infiltrate materials and structures demonstrating the greatest performance improvement and/or greatest stability.

Results

Throughout FY 2011, substantial success was achieved in both infiltration and microstructural engineering efforts. $La_{0.6}Sr_{0.4}CoO_{3-\delta}$ (LSCo) nanoparticle material infiltration produced average performance improvements greater than 40% in average power density and appeared to stabilize the base cell, and suppresses degradation. Mesoporous infiltration demonstrated similar performance improvements and polarization tests indicated an increase in relative power density of up to 40% after 200 hours of operation, and impedance tests indicated a decrease in polarization resistance of up to 28%. Cathodes generated using the in situ foaming

process were shown to be well controlled and highly porous. In FY 2012, the cathode materials research focus has pivoted towards final provenance of cathode engineering methods (especially pertaining to long-term stability) and scale-up of the techniques to sizes and materials that begin to approach commercially relevant scales and cell chemistries.

The electrocatalyst infiltration techniques were used to examine changes in cell performance with operation time for commercial cells possessing a composite cathode modified by nanostructured LSC. Figure 1 shows data indicating that the polarization resistance (R_p) of both a baseline cell and an infiltrated cell increased as the operation progressed for 1,500 h, but the degradation rate of the infiltrated cell was statistically indistinguishable from that of the baseline cell. This result implies that there is no measurable negative effect of infiltrated electrocatalysts on the cells' time-dependent performance for these systems. The stable performance of the infiltrated cells is attributable to characteristics of the unique composite cathode microstructure, which requires a relatively smaller mass of infiltrate to achieve cathode activation and accordingly minimizes agglomeration and loss of electrocatalyst surface area.

The infiltration technique was applied to state-of-the-art SECA industrial team button cells, and the performance and stability were evaluated. Figure 2 shows the improvement in performance and the decrease in resistance that were observed for manufacturer cells Type 1 and Type 2. The result shows that the infiltration

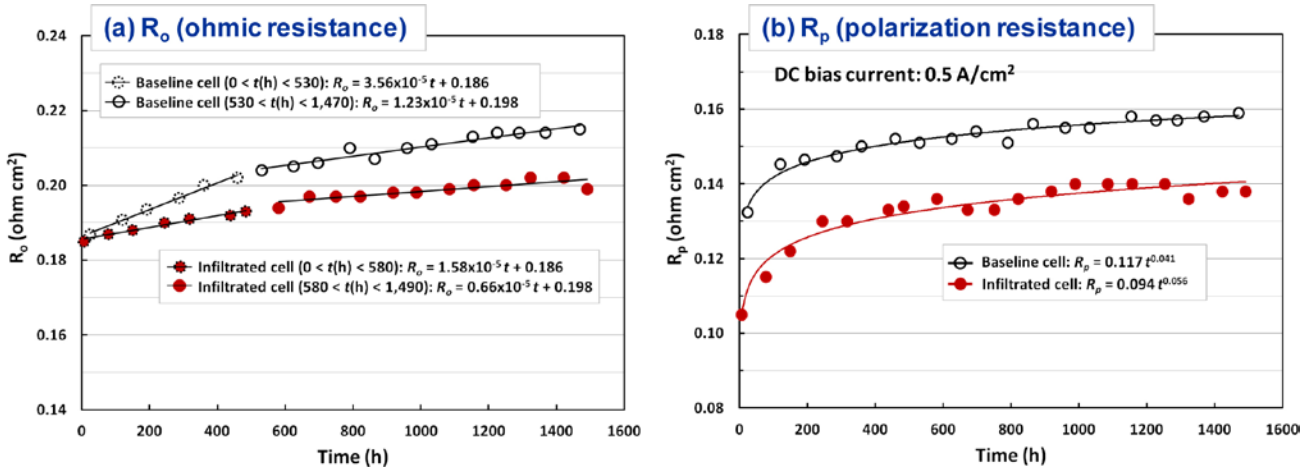

FIGURE 1. Long-duration (1,500 hour) cell stability test comparing the changes in ohmic resistance and polarization resistance between standard and infiltrated cells

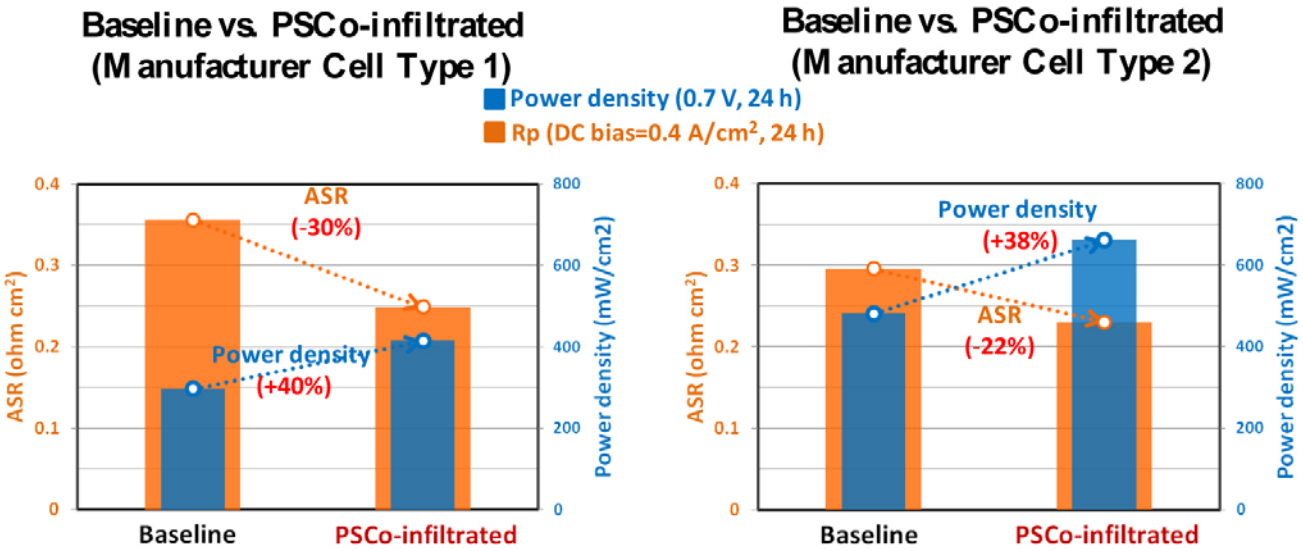

FIGURE 2. Performance results obtained through infiltration of button cells using state-of-the-art cells obtained from SECA industrial partner

methods developed through FY 2011 on a standard (commercial) cell are transferable to an industry team's unique cell microstructure and chemistry, and that a significant improvement in performance is realizable even though the base cell is optimized for performance in the industry team's SOFC system. Through the end of FY 2012, the project will proceed with scale-up from cells possessing a 2 cm^2 active cathode to cells with a 16 cm^2 active cathode. The planar cells also feature more realistic flow geometries, and the cell test system utilizes standard thermal management techniques.

The mesoporous infiltration technique resulted in significant improvements in FY 2012, especially in efficiency of infiltration and final provenance through impedance tests and full electrochemical operation tests. In particular, the EISA infiltration process was improved to allow infiltration with concentrated precursor solutions to both reduce the number of required infiltration steps and to promote the generation of the mesoporosity of the coating. The improved EISA process generates 10 wt% LSM in a commercial LSCF cathode in a single infiltration step. Figure 3 depicts the resultant microstructure of the infiltrate. The perovskites infiltrated with EISA were examined under transmission electron microscopy and appeared to be continuous coatings with mesoporous microstructure, which is distinctively different from the isolated or segregated nanoparticles reported in conventional infiltration methods.

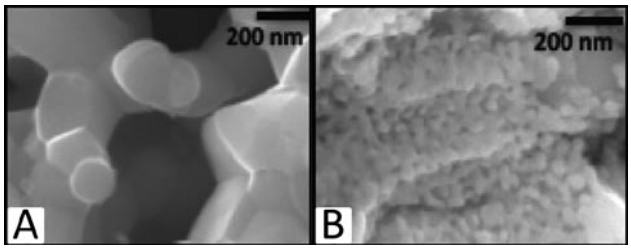

FIGURE 3. (a) Scanning electron microscopy image of LSCF cathodes on an SOFC button cell, and (b) infiltrated by EISA process

The infiltration using the EISA process was also tested under electrochemical conditions and compared to the conventional infiltration methods. Electrochemical impedance spectra suggested that the most significant enhancement of mesoporous coatings comes from medium (1 kHz) and low (1 Hz) frequency range, which is commonly referred to as the resistances arising from oxygen diffusion and dissociative adsorption on the surface. A similar trend was also seen in the button cells tested under the real SOFC operating conditions. As shown in Figure 4, the mesoporous coating was responsible for a 30% reduction of the total polarization resistance of the button cells, which is about 13% more than the reduction caused by LSM infiltrated with Pechini method. Infiltrate morphology must be considered to maximize the effect of cathode infiltration in a particular catalyst/backbone system.

Further efforts using in situ foaming techniques were completed to understand the effect of processing parameters on the microstructure of in situ foamed cathodes. Studies focused on varying polymer precursor compositions in the ceramic-polymer precursor suspension while retaining the solids loading constant with vehicle as solvent. As shown in Figure 5, the sample with 8:4:1 precursor composition displayed the highest porosity and most elongated pore shape (circular pores = 3.14; elliptical pores >3.14). Microscopic analysis indicates that the pores at the top of the cathode (the region farther from substrate) appear to have higher mean pore area than those nearer to the substrate under similar porosity levels. This is a desirable feature in SOFC applications as the similar porosity level implies

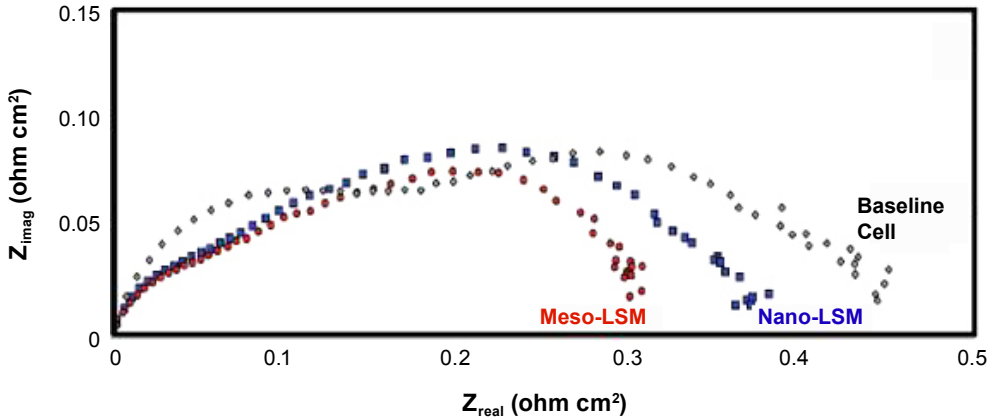

FIGURE 4. Electrochemical impedance spectra of the baseline MSRI button cell with LSCF cathode infiltrated with LSM; data include the button cell without infiltration (grey), with LSM infiltration using EISA (red) and Citric method (blue)

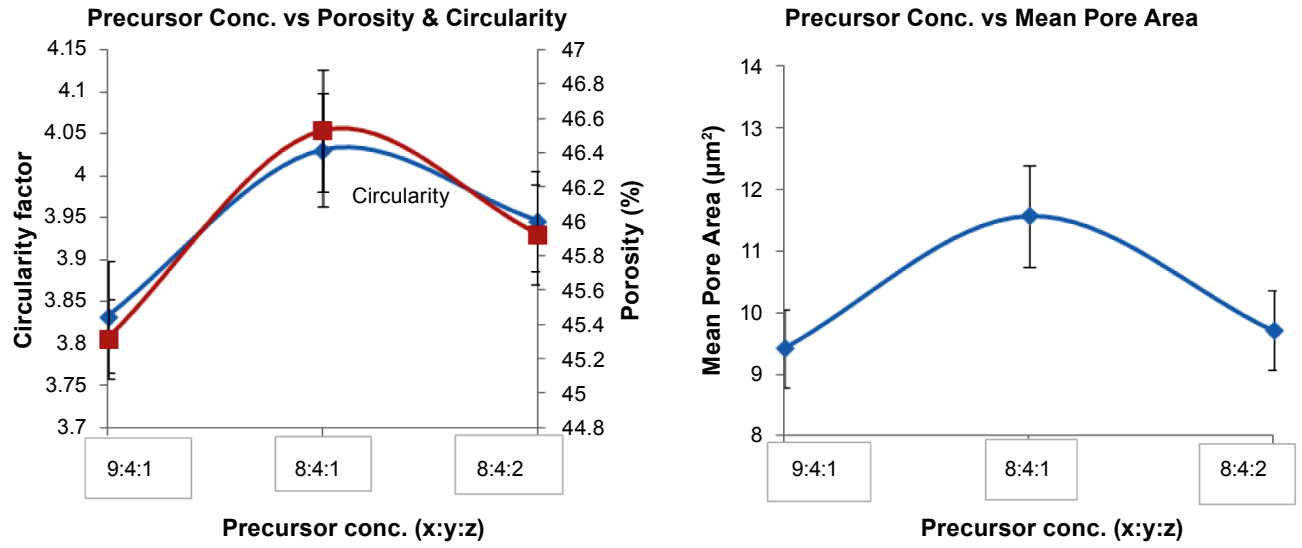

FIGURE 5. Correlation between precursor composition and resultant microstructures

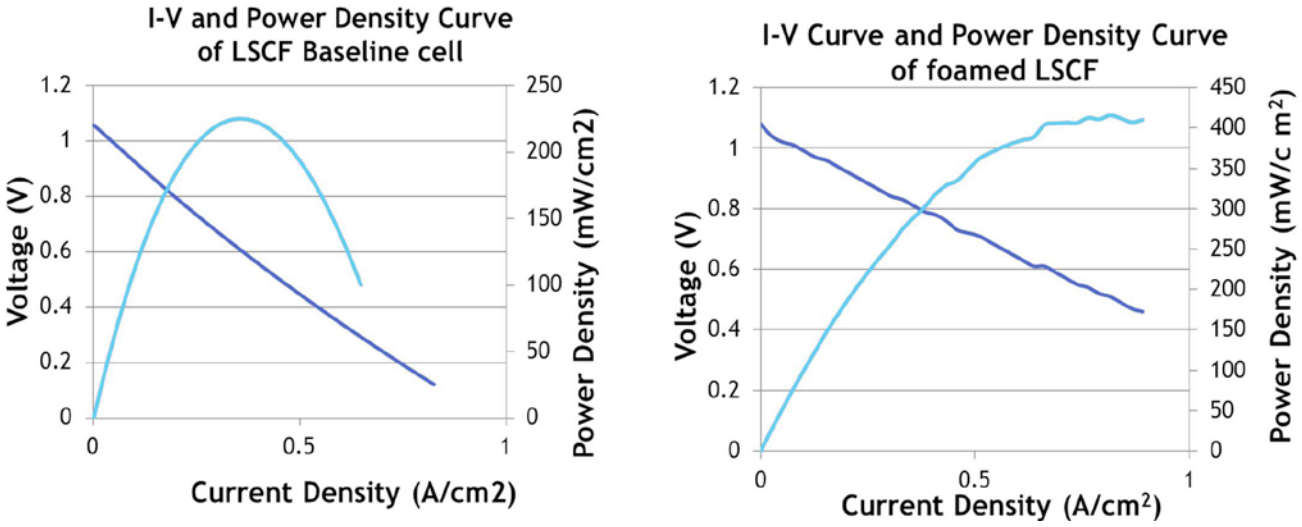

FIGURE 6. Current-voltage and power density curves for baseline and in situ foamed cathodes. Peak power density of the in situ foamed cathode is shown to be nearly 2x improved.

that there are bigger pores in the cathode away from the electrolyte, which supports better gas diffusion and improved accessibility for infiltration.

The cathode processed using the 8:4:1 precursor composition and an identical cell fabricated with a standard cathode (baseline cell) were tested under moist hydrogen on the anode and ambient air flow on cathode at 800ºC. The performance of the SOFC with the in situ foamed cathode showed a significant improvement over the baseline cell, exhibiting a nearly 70% increase in maximum power density over the baseline cell as shown in Figure 6. Efforts continue to engineer the cathode structure and scale testing to a 16 cm^2 platform.

Conclusions and Future Directions

The FY 2012 cathode engineering effort has continued to provide valuable data confirming the potential of specific cathode microstructural engineering and infiltration techniques to substantially improve the cathode performance. In particular, the present effort has used commercially applicable infiltrate materials and mesoporous structures demonstrating substantial performance increases, verified long-duration stability, and improved the quality of application methods to reduce the number of processing steps. The dense $(LaSr)CoO_3$ infiltrate and the mesoporous LSM

infiltrate generated by EISA in particular demonstrated significantly positive impacts and have been tested in cooperation with industrial partners with the anticipation of scale-up.

Efforts to engineer microstructures were shown to be effective in enhancing the cell power performance. The highly porous foam cathode specifically demonstrates promising increases in peak power output, and the methods for engineering the cathode solution to achieve specific microstructural character are rigorously understood. The foamed cathode technique was demonstrated with materials typical of current cathodes, and the method could be transferred directly to industrial partners.

Future efforts principally include scale-up of final infiltrate testing demonstrations to full stacks and development of industrial scale processes for generating and applying engineered cathode materials. In particular, infiltration tests with industrial partners must be completed in a battery of long-duration tests executed using actual operating conditions to ensure that the materials will demonstrate acceptable performance over the lifetime of the cell service to justify the additional cost of adding the infiltrate. The foamed microstructural engineering technique will be finalized on button cells and scaled up to the more commercially relevant 16 cm^2 cell system. Foamed structures will also be produced for infiltration with the advanced infiltrate materials developed here.

FY 2012 Publications/Presentations

1. Shiwoo Lee, Nicholas Miller, and Kirk Gerdes, "Long-Term Stability of SOFC Composite Cathode Activated by Electrocatalyst Infiltration," *v159, 7, J Electrochemical Society,* 2012, pF801-F808.

2. Shiwoo Lee, Paul Ohodnicki, and Kirk Gerdes, "Control of Activity and Stability by Tailoring Microstructure of Electrocatalyst-Modified Composite Cathode of SOFC," 220th Meeting Electrochemical Society, Honolulu, Hawaii, October 7–12, 2012.

3. Robin Chao, "Improving Solid Oxide Fuel Cell Cathode Performance by Infiltrating Mesoporous Perovskite Coatings," Doctoral Thesis, Carnegie Mellon University, March 2012.

4. Sodith Gandavarapu, "Micro Structural Engineering of Cathode Material in Solid Oxide Fuel Cell Applications," Masters Thesis, West Virginia University, August 2012.

5. Robin Chao, et al, "Structure and Relative Thermal Stability of Mesoporous (La,Sr)MnO_3 Powders Prepared Using Evaporation-Induced Self-Assembly Methods," *Journal of the American Ceramic Society*, (online, 2012) DOI: 10.1111/j.1551-2916.2012.05236.x.

6. Kirk Gerdes, Shiwoo Lee, "Performance Enhancement of SOFC Cathodes by Infiltration of Electrocatalytic Agent," ORD Merit Review, May 17, 2012.

7. Mingjia Zhi, Shiwoo Lee, Nicholas Miller, Norbert H. Menzler, and Nianqiang Wu, "An Intermediate-Temperature Solid Oxide Fuel Cell with Electrospun Nanofiber Cathode," *Energy Environ. Sci.*, 2012, 5, 7066–7071.

III.A.9 NETL RUA Cathode Modeling R&D

Kirk Gerdes
U.S. Dept of Energy
National Energy Technology Laboratory
3610 Collins Ferry Rd.
Morgantown, WV 26507
Phone: (304) 285-4342; Fax: (304) 285-4469
Email: Kirk.Gerdes@netl.doe.gov

DOE Project Manager: Kirk Gerdes
Phone: (304) 285-4342
Email: Kirk.Gerdes@netl.doe.gov

Contract Number: FWP-2012.03.04

Start Date: March 1, 2012
End Date: September 30, 2012

Fiscal Year (FY) 2012 Objectives

- Validate the cathode oxygen reduction reaction model by using independently published experimental data. Transfer improved oxygen reduction reaction (ORR) model to parallel three dimensional (3D) multi-physics model.
- Complete 3D multi-physics model to include revised ORR model and real cathode microstructure obtained by focused ion beam (FIB)-scanning electron microscope (SEM).
- Complete full geometrical and topological examinations of solid oxide fuel cell (SOFC) cathodes.
- Refine a microstructural evolution model describing grain growth over thousands of hours of simulated operation time.
- Continue examination of electrode degradation processes including cation migration, intergranular phase formation, and breakdown of crystalline structures.
- Generate public report on the key conclusions from the work.

FY 2012 Accomplishments

- Completed and validated ORR model describing parallel competitive pathway (two phase boundary [2PB] vs. triple phase boundary [3PB]) in $(LaSr)MnO_3$ (LSM), and began re-constitution of the model for $(LaSr)(CoFe)O_3$ (LSCF).
- Completed the first version of the 3D multi-physics model incorporating the revised ORR model and real cathode microstructure obtained from FIB-SEM experiments.
- Completed FIB-SEM reconstructions and full geometrical and topological examinations of SOFC cathodes including a LSM baseline cathode, a LSCF cathode operated for 1,500 hours, a cathode formed by in situ foaming techniques, and a LSM cell operated for 1,500 hours.
- Completed a microstructural evolution model for an LSM/LSCF cathode describing the growth of constitutive grains over thousands of hours of operation time and tuned models using actual microstructures.
- Continued examination of electrode degradation processes associated with cation migration, formation of intergranular phases (including between infiltrate and backbone), and breakdown of constitutive crystal structures.

Introduction

An SOFC is a device which generates electrical energy by exchanging oxygen ions between an oxygen containing process stream such as air and a process stream containing an oxidizeable material such as hydrogen. The general principles of operation and associated global electrochemistry are describable in basic terms, but the fundamental correlations between discrete reaction and transport processes are complex. Still more complex are the degradation processes, which are influenced by both the contemporaneous operating condition and by the cumulative history of degradation.

Cathode materials in particular are subjected to intrinsic and extrinsic degradation processes, and both primary (direct) and secondary (multi-step or indirect) modes exist. The SOFC cathode facilitates the reduction of oxygen to an ionic form in preparation for transport across the impermeable electrolyte membrane. The electrochemical oxygen reduction process is sensitive to the material composition and physical structure of the cathode, and the oxygen reduction reaction (ORR) efficiency can be impacted by changes in chemistry and structure.

In order to understand electrode degradation, mathematical descriptions of the fundamental transport processes and real 3D microstructure are required to inform more comprehensive models investigating the

multi-scale physics of operation and describing the long-term evolution of the cathode microstructure. In addition, discrete modes of electrode degradation must be examined to determine the conditions under which the mode is active, and also to predict degradation rates under common operating conditions. The individual modeling efforts must be coupled to generate the ultimate product, a comprehensive mathematical tool assisting selection of cathode materials and microstructures by predicting performance and long-term microstructural evolution.

The projects described here each focus on maturation of component models generated in support of a comprehensive anode/electrolyte/cathode degradation model. Individual projects investigate fundamental cathode structure and reaction processes, develop higher-order models describing cathode operation and microstructural evolution, and begin to examine detailed degradation processes occurring in the electrolyte and anode. In one fundamental research effort, the details of the ORR on the LSM-based cathode system are described and an advanced one dimensional (1D) reaction model is generated. The models are informed with data obtained from an advanced microscopic technique to produce detailed 3D geometric and topological maps of the microstructure of real SOFC cathodes and anodes. Results from the fundamental modeling efforts are passed to a 3D multi-physics model predicting chemical, thermal, and electrical potential distributions throughout the cathode. The results are used to predict dynamic and steady state performance, and model results are validated through comparisons to data reported in the literature by independent research groups. The fundamental data are also passed to a cathode evolution model based on phase field principals, which can predict finite changes in microstructure that occur over thousands of hours of operation. Fundamental degradation processes that include phase disruption and crystallographic breakdown of the anode/electrolyte/cathode are also considered. In particular, cathode aging due to cation diffusion, degradation arising from secondary phase formation, and crystal phase breakdown are examined.

Approach

At the conclusion of FY 2011, substantial advancements in each of the component reaction and degradation models was completed. The ORR model for LSM was modified and tested to show performance differences between competing reaction pathways. Detailed 3D microstructural reconstructions of an LSM cathode were generated by FIB-SEM and application of advanced visualization software. Information from these sub-models was incorporated into the multi-physics continuum model, and both steady and dynamic simulations were completed. A phase field model describing cathode microstructural evolution was constituted and basic simulations of three-phase structures were completed. Substantial efforts were also completed to describe various critical degradation modes in cell components including formation of secondary phases, breakdown of crystal structure at phase interfaces, and phenomena postulated to relate to cation migration within the cathode.

The independent efforts completed in FY 2011 served as the foundation for pursuit of matured models and improved probative techniques through FY 2012. In particular, substantial efforts are made to validate the constitutive models using independently collected experimental data and to combine the validated models to create higher order performance modeling tools. Further research focuses on fundamentally characterizing and quantifying detailed modes of degradation that cannot be captured from the present understanding of solid state ionic transport, microstructural evolution, and other thermodynamically responsive processes.

To complete the FY 2012 goals, the basic ORR model was modified to include a description of adsorbed surface charge and a subsequently induced dipole near the LSM surface, and equations were re-constituted for the common cathode material known as LSCF. Results obtained from the fundamental ORR model were applied to the 3D multi-physics model and the full model validated for performance using independently collected experimental data. The dynamic multi-physics model predicted distributions of local thermodynamic values, over-potentials, Faradaic currents, and parameters relevant to cathode performance. These model predictions were experimentally tested through research collaborations with Solid State Energy Conversion Alliance (SECA) program partners.

In parallel to the multi-physics model development, the phase field model must be tuned to accurately reflect microstructural evolution in LSM cathodes, and must incorporate experimental data collected by FIB-SEM from as-received and operated cell specimen. The phase-field model was enhanced to track the temporal changes in geometrical and topological structure, and to provide dynamic structural updates to the 3D multi-physics model. The predictive accuracy of the model must be further improved by tuning with experimental data collected from aged specimen, using FIB-SEM techniques.

The core predictive models described above will elucidate the principal processes of transport and evolution for the bulk material. However, it is not clear that all physical sources of critical degradation processes are identified, and even if identified the processes typically remain undefined in a fundamental sense. It is

necessary therefore to examine fundamental processes of degradation within the cathode and anode including cation migration, crystallographic phase separation, and secondary phase formations, to name a few prominent modes. In particular, one phenomenon of degradation manifests as temporally changing polarization resistance occurring over tens of hours in an unpolarized cell in response to thermal perturbation. The phenomenon is probed via electrochemical and microanalytical techniques to discover its true physical source, which is postulated to be associated with reversible cation migration or thermally induced elastic structural reconfiguration.

Other important fundamental examinations include those of nanoscale structures at critical cathode interfaces, as the character of these locations is suspected to strongly influence the cell performance. In particular, interfaces between cathode infiltrates and the cathode backbone are examined both for degradation (through cation exchange) and functionality. Interfaces between electrode backbone and electrolyte particles are examined to search for the presence of unwanted secondary phases that may negatively impact the ionic or electronic transport within the electrode. Examples include examination of phosphine-induced breakdown of yttrium stabilized zirconium (YSZ) in the anode.

Results

During FY 2012, the ORR model was validated for LSM cathodes operating in both forward and reverse modes. The model was directly validated through comparison to peer-reviewed published literature generated by independent research efforts and also through incorporation into a 3D multi-physics model that ensured proper phenomenological performance. An example of the predictive capability of the cathode model is given in Figure 1, which depicts the crossover of total current density from dominance by the 3PB process to dominance by the 2PB process. Knowledge of the relative contribution of each microstructural region, whether 3PB or 2PB, to the total current density, provides insight into possible locations for degradation and regions that should be engineered for performance.

Incorporation of electrode microstructural and compositional features continued to improve agreement between 3D multi-physics model representations and the actual electrode activity. Figure 2 depicts the oxygen vacancy distribution within the cathode near the interface with the current collector as simulated using the 3D multi-physics model. The dynamic model includes long-range multi-physics and is informed with details of the true cathode microstructure that have been obtained through careful FIB-SEM experiments. Initial model

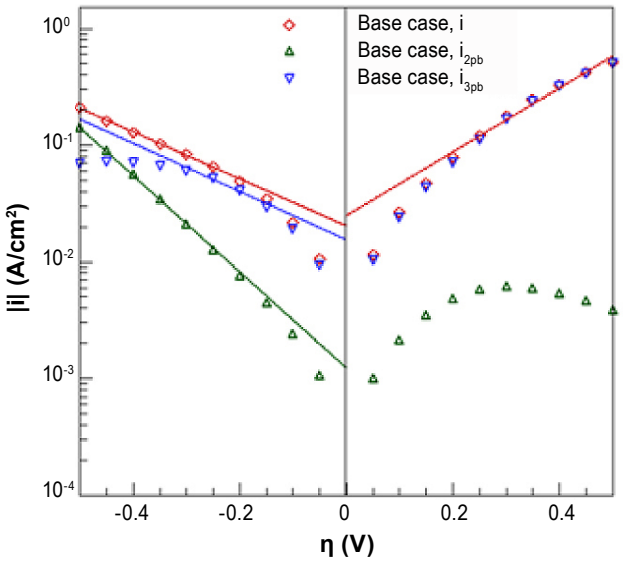

FIGURE 1. Predicted polarization curve with 2PB and 3PB contributions for the base case

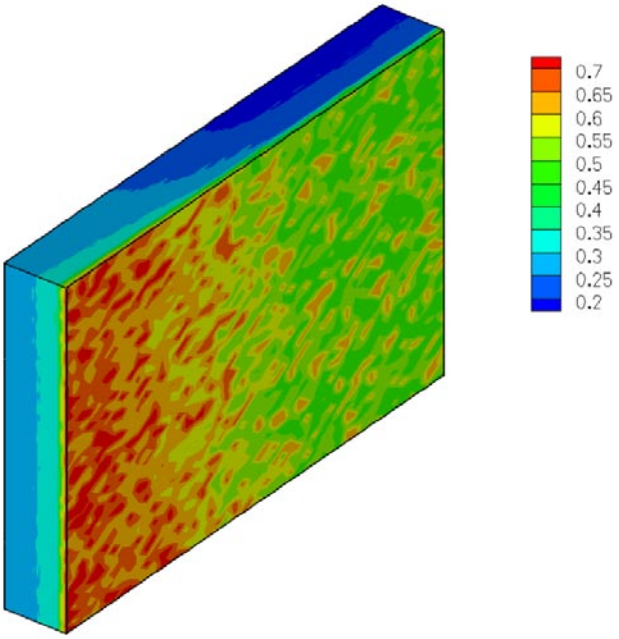

FIGURE 2. LSM vacancy (mol/m^3) distribution in a cathode area under a current collector/air channel corner

validation efforts have been completed by applying specialized tools and advanced analytical techniques to actual cathodes and cathode simulacra, and models have been further refined on the basis of that data.

The geometrical data obtained by FIB-SEM were also used to derive values for transport related parameters relevant to the 3D multi-physics model. Figure 3 shows a reconstructed cathode with a fluid flow

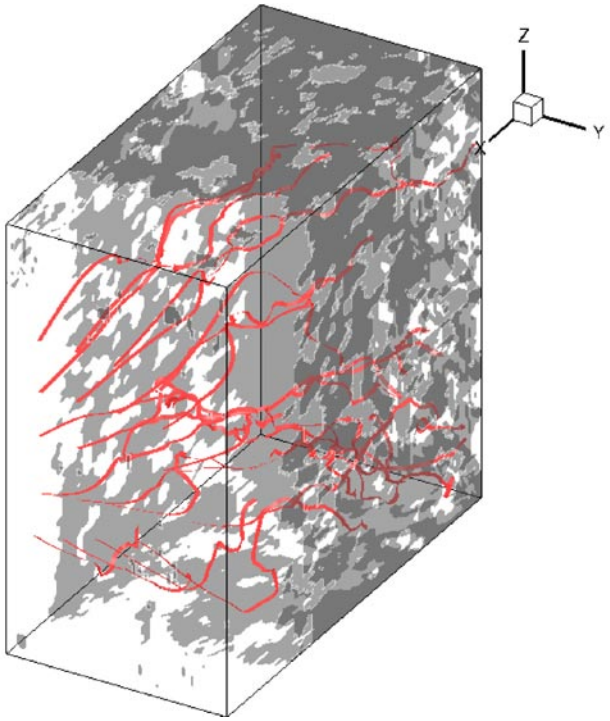

FIGURE 3. FIB-SEM reconstruction of cathode depicting flow lines used to calculate pore tortuosity

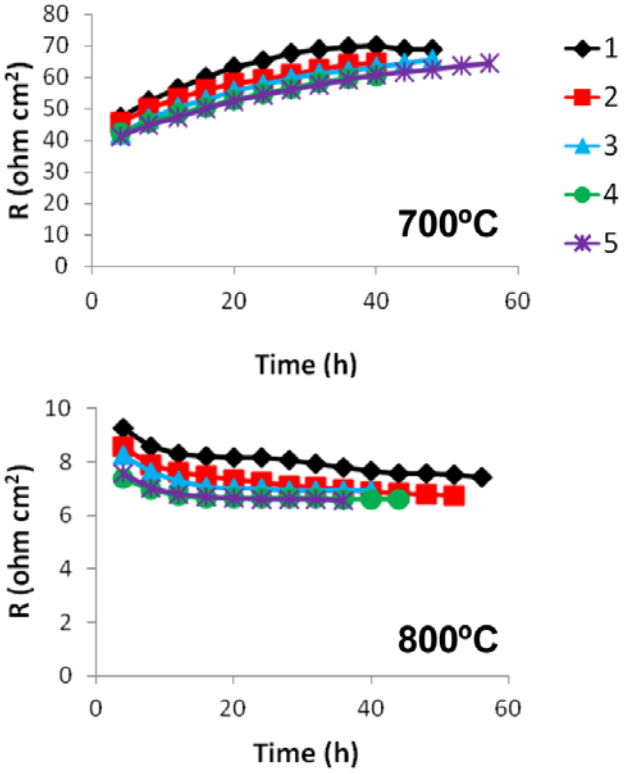

FIGURE 4. Temporal polarization measured for a LSM/YSZ symmetric cell during a series of thermal cycles between 700ºC and 800ºC. The polarization indicates reversible transition between steady thermodynamic states at these temperatures.

model overlay to calculate the tortuosity of the cathode. The microstructural evolution model for an LSM/LSCF cathode was developed in parallel to describe the growth of cathode constitutive grains over thousands of hours, and geometrical and topological features within the cathode were examined, including pore tortuosity and grain contact angles. The expanded microstructural evolution model permits tracking of such geometric features over long time scales, and the resulting microstructures can be passed to the 3D multi-physics model to update its performance predictions.

Finally, electrode degradation processes were examined that were associated with cation migration, formation of intergranular phases (including between infiltrate and backbone), and breakdown of constitutive crystal structures. Specific examinations included a cathode aging effect postulated to be linked to a reversible cation migration, observation of a possible nucleation point for LSCo infiltrated cathodes, identification of an yttrium-phosphorus-oxygen (Y-P-O) phase in anodes exposed to PH_3, and breakdown of the c-YSZ structure within the anode.

Cathode aging is examined by exposing symmetric cells to thermal cycles and monitoring the polarization resistance obtained through electrochemical impedance spectroscopy. The cathode polarization measurement indicates that a thermally activated reversible transition occurs between thermodynamic steady states at 700ºC and 800ºC. Figure 4 depicts the measured polarization for a series of thermal cycles between 700ºC and 800ºC with data indicating that the reversible steady states are achievable after sufficient thermal exposure. Analytical techniques are currently being applied to discern the physical process(es) creating the observed impedance effect, with an emphasis on investigation of cation segregation.

Nanoscale cathode structures created in the anode and cathode during cell operation are also inspected using the analytical technique of tunneling electron microscope (TEM). Anodes most often demonstrate the growth of intergranular phases, typically as a result of exposure to contaminate materials. TEM analysis is used to identify the specific location of microstructural attack, whether within the constituent particles themselves, or in the grain boundaries or at critical interfaces. An example of an unwanted intergranular phase growth is depicted in Figure 5, which shows that upon exposure of the anode to syngas containing trace levels of phosphine, a Y-P-O phase develops that attacks the YSZ. Such attack degrades the structure of the ionic conductor, which leads to lower ionic transport (increased cell resistance)

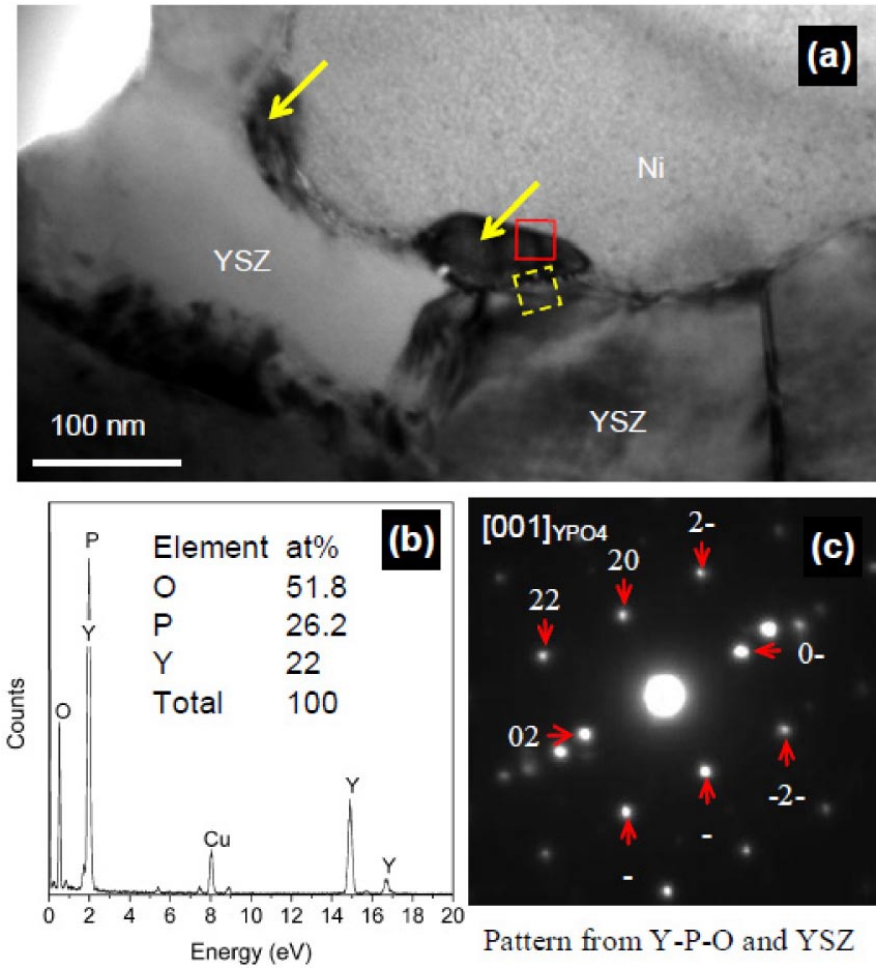

FIGURE 5. (a) Precipitates growth at YSZ/YSZ/Ni triple grain junctions (indicated by yellow arrows); (b) precipitate spectrum and chemical composition; and (c) the selected area diffraction pattern taken from the area with Y-P-O phase and YSZ phase

or mechanical fatigue. Quantifying the degradation rate from discrete processes such as this will allow incorporation into the global degradation model and make such a model more accurately predictive.

Conclusions and Future Directions

The cathode modeling effort has provided a critical framework to research prediction of long term performance and microstructural evolution in the SOFC cathode. The research combines information from fundamental performance modeling and investigation of the cathode microstructure with higher-order multi-physics models to produce a consistent, informed evaluation of the cathode performance. In particular, the ORR mechanism investigation has quantified the extent of competition between reaction pathways within the cathode. Such information is useful to efforts to mitigate cathode degradation as well as investigation of methods for enhancing cathode performance. The 3D microstructural reconstructions have produced compelling images which can be probed with advanced visualization software to observe previously unattainable microstructural details. This information supports higher order models with directly measured parameters instead of theoretically determined parameters, which ultimately enhances the predictive accuracy of the models.

The multi-physics models describing performance and microstructural evolution of the cathode system are rapidly maturing and have generated important predictions of cathode operation. In particular, the 3D dynamic continuum model has shown distributions of performance properties and evaluations of the local states throughout the cathode. Validation of the models using independently collected experimental data has demonstrated model fidelity and ensured that core predictive capabilities are accurate. The model has incorporated basic parameter evaluations from complimentary efforts and provided information on the

topological and geometric evolution of real cathodes. Future efforts will focus on continued integration of the models and generation of an overarching model allowing generation of comprehensive long-term forecasts for full stack performance.

FY 2012 Publications/Presentations

1. Mingyang Gong, Randall Gemmen, Xingbo Liu, "Modeling of Oxygen Reduction Mechanism for 3PB and 2PB Pathways at Solid Oxide Fuel Cell Cathode from Multi-Step Charge Transfer," *Journal of Power Sources* 201 (2012) 204– 218.

2. Harry Abernathy, Harry Finklea, David Mebane, Xiaoke Chen, Kirk Gerdes, Maria Salazar-Villalpando, "Reversible Aging Behavior of LSM Electrodes at Open Circuit," *Journal of Power Sources*, Volume 216, 15 October 2012, Pages 11-14.

3. Gregory A. Hackett, Kirk Gerdes, Xueyan Song, Yun Chen, Vaithiyalingam Shutthanandan, Mark Engelhard, Zihua Zhu, Suntharampillai Thevuthasan, Randall Gemmen, "Performance of Solid Oxide Fuel Cells Operated with Coal Syngas Provided Ddirectly from a Gasification Process," *Journal of Power Sources* 214 (2012) 142-52.

4. H.O. Finklea, X. Chen, I. Celik, S.R. Pakalapati, K. Gerdes, and Y. Chen, "1D and 2D Simulation of Impedances in an Anode-Supported SOFC," 221st Meeting of the Electrochemical Society, Seattle, Washington, May 9, 2012.

5. X. Liu, Y. Li, M. Gong, K. Gerdes, R. Gemmen, R. Pakalapati, I. Celik, and T. Horita "Characterization and Modeling of Infiltrated SOFC Cathode," 220th Meeting Electrochemical Society, Honolulu, Hawaii, October 7–12, 2012.

6. Qun Li, Linyun Liang, LongQing Chen, et al., "Phase-Field Modeling of Three-Phase SOFC Electrode Microstructures," submitted, *Applied Physics Letters*.

7. Yun Chen, Song Chen, Gregory Hackett, Harry Finklea, John Zondlo, Ismail Celik, Xueyan Song, Kirk Gerdes, "Microstructure Origin of Electrochemical Degradation of SOFC Anodes Operated in Phosphine-Containing Fuels," submitted, *Solid State Ionics*.

8. YA Mantz, "Density-Functional Study of the $La_2Zr_2O_7$ (001) and (011) Surfaces and Bulk," (TPR-3334), submitted to *Phys. Rev. B*.

III.A.10 Development of SOFC Cathodes

J.S. Hardy (Primary Contact), J.W. Templeton, J.W. Stevenson (Primary Contact)
Pacific Northwest National Laboratory
P.O. Box 999, MS K2-44
Richland, WA 99352
Phone: (509) 375-2627; Fax: (509) 375-2186
Email: john.hardy@pnnl.gov

DOE Project Manager: Briggs White
Phone: (304) 285-5437
Email: Briggs.White@netl.doe.gov

Contract Number: FWP40552

Start Date: October 1, 2011
End Date: September 30, 2012

Fiscal Year (FY) 2012 Objectives

- Perform 1,000 hour in situ X-ray diffraction (XRD) scans of working lanthanum strontium cobalt ferrite (LSCF) cathodes on anode-supported solid oxide fuel cells (SOFCs) under varying operating conditions.
- Investigate the effects of 3% humidity in air on the performance of anode-supported SOFC cathodes at varying temperatures.

FY 2012 Accomplishments

- Demonstrated 1,000 hours of continuous XRD scans of the cathode on an anode-supported SOFC that detected secondary phases present in concentrations of less than 2 wt%.
- Measured increases of up to nearly 20% in the area specific resistance (ASR) of cells with lanthanum strontium manganite/yttria stabilized zirconia (LSM/YSZ) cathodes after 3% humidity was introduced into the cathode air stream.

Introduction

It is generally accepted that the cathode is a major contributor to internal losses in the SOFC. Therefore, improvements in the cathode can lead to higher SOFC power density and efficiency, which will help SOFC manufacturers achieve the long-term Solid State Energy Conversion Alliance (SECA) goals relating to cost and power stability. LSCF is currently a leading candidate amongst cathode materials due to its ability to conduct both electrons and oxygen ions, both of which are beneficial to cathodic performance in the SOFC. Meanwhile, LSM/YSZ is also a well-established cathode material due to the stability in performance that it offers. The focus of this task in FY 2012 was on demonstrating the feasibility of performing in situ XRD of operating cathodes for extended durations, e.g., 1,000 hours and on determining the extent to which humidity in the cathode air is an important parameter to consider in achieving increased SOFC performance and stability. Extending the duration of in situ XRD testing enhances the potential to use this newly developed research capability to investigate the underlying causes of degradation in operating cathodes during fuel cell operation.

Approach

XRD analysis of operating LSCF cathodes was performed using a Bruker D8 Advance XRD fitted with an Anton Paar HTK 1200 heating chamber. A small scale button cell test fixture that is compatible with the heating chamber was developed to operate 13 mm diameter anode-supported button cells. XRD patterns were measured continuously for 1,000 h while electrochemical performance data was simultaneously being collected. One cell was operated at ~0.8 V over the duration of the test, while a subsequent cell was held at open-circuit voltage (OCV) during testing for comparison. Upon completion of the tests, the Cluster Analysis add-on module for Jade [v9.3; Materials Data, Inc., Livermore, California] XRD analysis software was used to calculate the similarity index (SI) of each XRD pattern relative to the first pattern measured. To improve statistics, patterns taken within sequential intervals of time, e.g., 20-hour or 200-hour periods, were integrated together and similarity indices for those intervals were also compared to the first in the resulting series. Once it was established that the XRD patterns were generally becoming less similar to the original pattern as a function of time, the patterns were plotted together for visual inspection to evaluate what specific changes were occurring in the spectra to cause the observed decrease in SI.

Humidity tests were conducted by operating button cells with LSM/YSZ cathodes at 800°C, 850°C, 900°C, and 950°C while collecting electrical voltage and current data. Six cells were tested under constant current conditions at each temperature, with three of them approximating an operating voltage of 700 mV while the other three approximated 800 mV. The air that was supplied to the cathode was alternated between dry and

moist, spending approximately 100 h at one humidity level before switching to the other. The dry air had a dew point of -40°C and the moist air contained ~3% water, as achieved by directing the flow of dry air through a water bubbler at room temperature. In addition to current-voltage data, electrochemical impedance spectroscopy (EIS) data was also recorded periodically throughout the tests.

Results

Two 1,000 hour in situ XRD tests were performed on the cathodes of anode-supported cells operating at 750°C in the XRD test fixture. The power density and SI of the XRD patterns from the cell operated at a constant current approximating 0.8 V are plotted as a function of time in the chart in Figure 1. It was found that an exponential decay equation provided a good fit to the SI data and highlighted a decreasing rate of decline such as was also exhibited by the power density. This curve fit is shown with a black line that overlays the red one hour SI data. The SI data for the longer time frames was fit by a simple linear equation to further emphasize the general decrease in similarity of the XRD patterns to the initial pattern as time progressed. While the change in the XRD patterns reflected by the general decrease in SI suggests a correlation to the decrease in power density over time, a visual inspection of XRD patterns integrated over 20 h intervals during the first 80 hours of testing and over 250 h intervals covering 1,000 hours of testing found that the specific changes responsible for the change in SI were too subtle for visual identification.

On the other hand, although not shown, the trend in SI for the cell that was held at OCV during in situ XRD was found to be dominated by changes in the intensity

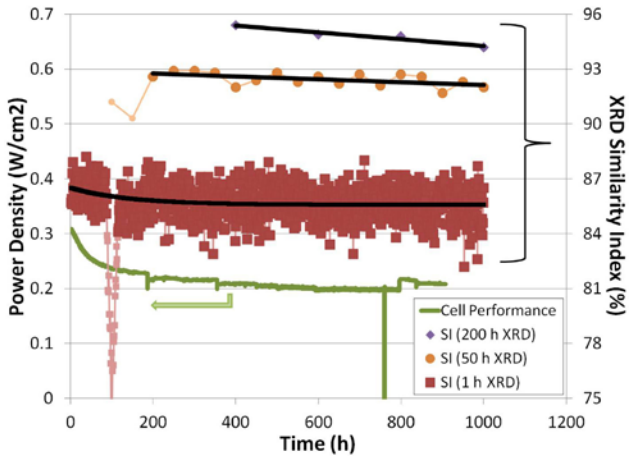

FIGURE 1. The power density and SI of the XRD patterns for the cell operated in the XRD test fixture at a constant current approximating 0.8 V are plotted as a function of time

of the peaks arising from the gold current collector. Although efforts were made to avoid interactions of the incident x-rays with the current collector, in the SI, the changes in the gold peaks overshadowed shifts in peaks from phases related to the cathode that were pinpointed through visual comparison of the XRD patterns. Although no significant changes were found in the LSCF pattern itself, changes were detected in Fe_3O_4 and Co_3O_4 which were present as minor secondary phases. Because XRD scans were taken continuously throughout the extended duration test, a summation of scans collected during 200 h intervals comprised count times that were high enough to make possible the resolution of minor phases with concentrations less than 2 wt%. The phases detected in the cathodes examined in both of the 1,000 h tests are listed in Table 1. Figures 2 and 3 illustrate the shifts that occurred in the major peaks of Fe_3O_4 and Co_3O_4, respectively, by overlaying the 200 h integrated patterns on one another. These shifts are representative of what was observed for the other peaks detected for these two phases. It was interesting to note that the larger Fe_3O_4 lattice expanded while the smaller Co_3O_4 lattice contracted over time. If these phases had been inter-diffusing to form a solid solution, the peaks would have been converging over time. However, the XRD measurements show them to be diverging.

TABLE 1. Phases detected in the LSCF cathode during in situ XRD of a cell at OCV and operating at ~0.8 V

	OCV	Operating
LSCF	97 wt%	91 wt%
$LaCoO_3$	<2 wt%	<2 wt%
Fe_3O_4	<2 wt%	<7 wt%
Co_3O_4	<2 wt%	—

The humidity tests found that ~3% water in the cathode air caused an increase in the ASR. This effect was more pronounced at lower temperatures, did not appear to be dependent on operating voltage, and was at least partially reversible upon reintroduction of dry air. This effect is demonstrated in the chart in Figure 4 in which the relative ASRs of the cells operated at 850°C are expressed as a percentage of their average ASRs over the initial five hours. Green lines represent cells tested at ~700 mV while red lines represent cells tested at ~800 mV. The periods during which moisture was present in the cathode air are shaded in blue. With every change between moist and dry air, there was an abrupt change in the ASR with the subsequent trend resembling an exponential decay toward a maximum or a minimum when the air was changed to moist or dry, respectively. This effect was also exhibited in cells tested at other temperatures, except it was more pronounced at 800°C and progressively less pronounced

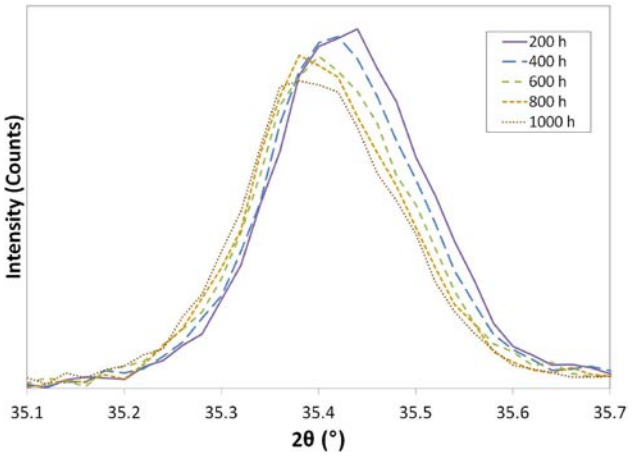

FIGURE 2. The major XRD peak of Fe_3O_4 is shown to shift to lower angles over time when 200 h integrated patterns are plotted together

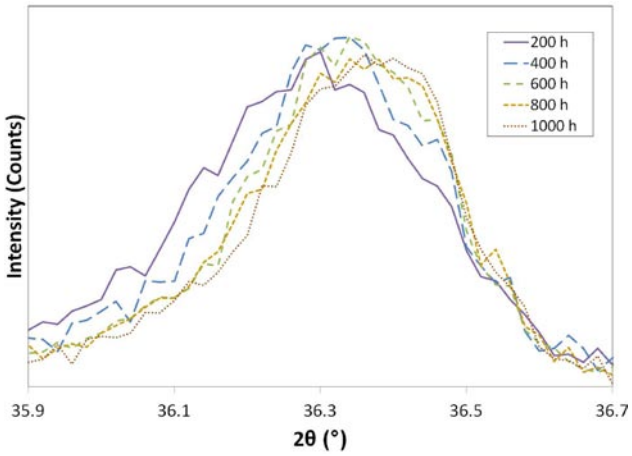

FIGURE 3. The major XRD peak of Co_3O_4 is shown to shift to higher angles over time when 200 h integrated patterns are plotted together

as temperature increased to 900°C and 950°C. The mechanisms contributing to this effect are currently under investigation using the analysis of difference in impedance spectra (ADIS) method [1].

Conclusions and Future Directions

- Demonstrated 1,000 h extended duration SOFC testing with in situ XRD.
- Detected trace phases that were present in concentrations of less than 2 wt% in the LSCF cathode through integration of 200 hours of in situ XRD scans.
- Determined that Fe_3O_4 detected in the cathode exhibited lattice expansion while Co_3O_4 exhibited lattice contraction during 1,000 h at 750°C and OCV.

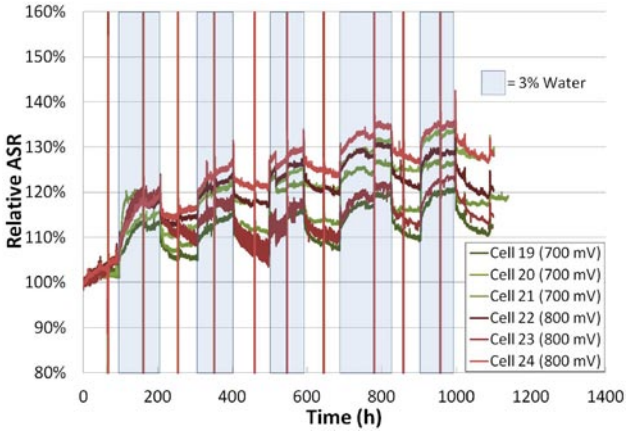

FIGURE 4. The relative ASRs of the cells operated at 850°C are expressed as a percentage of their average ASRs over the initial five hours of the test

- Will perform in situ XRD of LSCF cathodes at 700°C and 800°C during 1,000 h cell operation at ~0.8 V to determine the effect of temperature on the cathode composition and structure.
- Measured the following effects of introducing 3% humidity into the cathode air on cells with LSM/YSZ cathodes:
  - The ASR increased following what appeared to be an exponentially decaying rise to a maximum.
  - The increase in ASR was increasingly pronounced as temperature was decreased.
  - The effect of humidity on ASR did not appear to be dependent on operating voltage in the range of 0.7 to 0.8 V.
  - The increase in ASR appeared to be at least partially reversible upon reverting back to dry air.
- Will investigate the mechanism behind the humidity effect described above using ADIS.
- Will perform similar humidity tests on cells with LSCF cathodes.

FY 2012 Publications/Presentations

1. Z. Lu, J.S. Hardy, J.W. Templeton, and J.W. Stevenson, "Extended Reaction Zone of $La_{0.6}Sr_{0.4}Co_{0.2}Fe_{0.8}O_3$ Cathode for Solid Oxide Fuel Cell," *Journal of Power Sources* 198, 90-94 (2012).

2. J.S. Hardy, J.W. Templeton, D.J. Edwards, Z. Lu, and J.W. Stevenson, "Lattice Expansion of LSCF-6428 Cathodes Measured by In Situ XRD During SOFC Operation," *Journal of Power Sources* 198, 76-82 (2012).

3. Z. Lu, J.S. Hardy, J.W. Templeton, J.W. Stevenson, D. Fisher, N. Wu, and A. Ignatiev, "Performance of Anode-Supported Solid Oxide Fuel Cell with Thin Bi-Layer Electrolyte by Pulsed Laser Deposition," *Journal of Power Sources* 210, 292-296.

4. J.S. Hardy, Z. Lu, J.W. Templeton, and J.W. Stevenson, "Improvement of Cell Performance Through Reduction of Ohmic and Polarization Resistance," 2011 Fuel Cell Seminar & Exposition, Orlando, Florida, November 2011.

5. J.S. Hardy, J.W. Templeton, D.J. Edwards, Z. Lu, and J.W. Stevenson, "In Situ XRD Measurement of LSCF Lattice Expansion in Operating SOFC Cathodes," 2011 Fuel Cell Seminar & Exposition, Orlando, Florida, November 2011.

6. J.S. Hardy, J.W. Templeton, D.J. Edwards, and J.W. Stevenson, "In Situ XRD of Operating LSCF Cathodes Suggests Gradual Compositional Change," International Conference and Exposition on Advanced Ceramics and Composites, Daytona Beach, Florida, January 2012.

References

1. S.H. Jensen, A. Hauch, P.V. Hendriksen, M. Mogensen, N. Bonanos, and T. Jacobsen, "A method to separate process contributions in impedance spectra by variation of test conditions," *Journal of the Electrochemical Society,* 154[12] B1325-B30 (2007).

III. SECA CORE TECHNOLOGY R&D

B. Anodes and Coal Contaminants

III.B.1 Evaluation of Ni-based SOFC Anodes

O.A. Marina (Primary Contact), C.A. Coyle, D.J. Edwards, J.W. Stevenson
Pacific Northwest National Laboratory
PO Box 999
Richland, WA 99352
Phone: (509) 375-2337; Fax: (509) 375-2186
Email: olga.marina@pnnl.gov

DOE Project Manager: Briggs White
Phone: (304) 285-5437
Email: Briggs.White@netl.doe.gov

Contract Number: FWP40552

Start Date: October 1, 2011
End Date: September 30, 2012

Fiscal Year (FY) 2012 Objective

Determine effects of high water content in fuel on the performance of nickel-based solid oxide fuel cell (SOFC) anodes.

FY 2012 Accomplishments

- Tested nickel/yttria-stabilized zirconia (YSZ) anode-supported cells for up to 2,300 hours in synthetic reformate containing variable water levels (corresponding to a range of fuel utilizations) at 700ºC, 800ºC, and 900ºC.
- Performed direct current (DC) electroctrochemical characterization, alternating current (AC) electroctrochemical characterization, and post-test microstructural characterization.

Introduction

To achieve the expected lifetime target of 40,000 h for stationary applications, SOFCs are required to show long-term stability. Understanding of the degradation mechanisms in SOFCs is critical to improve the SOFC stack durability. Nickel agglomeration is a well known degradation phenomena in Ni-based catalysts and is accelerated by high water vapor content [1]. However, the Ni particles in the sintered SOFC composite anodes are typically much larger than those in the reforming catalysts. Additionally, the rigid YSZ matrix in Ni/YSZ cermet substantially slows down Ni agglomeration. Nevertheless, it had been reported that high water vapor caused significant Ni coarsening in the SOFC anodes as well [2,3], and as a result, substantial microstructural and electrochemical degradations have been observed. The electrochemical performance of the anode is directly associated with the triple-phase boundary length, which is reduced by the grain growth of nickel. The Ni transport mechanism is still being debated [4]. At least two different mechanisms, surface/grain boundary diffusion or gas phase transport of volatile $Ni(OH)_2$ species, may be responsible for nickel grain growth. The kinetics of both mechanisms is accelerated by the high steam concentration in the gas phase. The main objective of this project is to determine if the high steam content in fuel gas produced at high fuel utilizations accelerates SOFC degradation.

Approach

Tests were performed at three temperatures, 700°C, 800°C, and 900°C, using Ni/YSZ anode-supported button cells. Cells were comprised of the Ni/YSZ bulk layer (a 40/60 volume percent solids ratio), a 7 μm active Ni/YSZ electrode (50/50 solids volume percent), an 8 mole percent YSZ electrolyte, and $(La_{0.8}Sr_{0.2})_{0.95}MnO_3$ (LSM)-YSZ composite cathode. The anode current collector was Ni mesh embedded in Ni paste. The cathode current collector was Ag mesh/Ag paste for tests at 700°C and 800°C and Au foil/LSM paste for tests at 900°C. Several cells with Au foil/LSM paste were tested at 800°C as well. The fuel gas consisted of synthetic reformate created by pre-equilibrating hydrogen and carbon dioxide over a separate Ni/YSZ catalyst bed at the test temperature to yield a nominal composition of H_2-CO-CO_2-H_2O = 33-21-24-22% at 700°C, 31-24-21-24% at 800°C, or 29-26-19-26% at 900°C assuming that methane is not produced. Variable humidity levels corresponding to various (45-80%) fuel gas utilizations were created by adding oxygen to the fuel gas upstream of the cell. Thus, in the discussion below, a reference to 45% fuel utilization (for example) means that that particular cell was supplied with fuel which was 45% oxidized. The cathode was supplied with oxygen. Cells were pre-conditioned in reformate at 0.8 V for 100-250 hours to obtain a stable baseline.

Multiple (up to eight) cells were tested simultaneously in one furnace at each temperature for 1,000-2,300 hours at a constant current corresponding to either 0.8 V or 0.7 V, while monitoring the cell voltage. Each condition was duplicated at least once to confirm reproducibility. This approach allowed elimination of occasional “bad” cells exhibiting a degradation pattern

substantially different from others. Each furnace also included two control cells operated on reformate without increased humidity level. Electrochemical impedance spectra were obtained at regular time intervals to separate ohmic and electrodic losses of cells. Post-test anode characterization was performed using scanning electron microscopy (SEM) with energy dispersive spectroscopy (EDS) to establish whether Ni particles had coarsened. The microstructures were quantified subsequently by image analysis method using Image J. From Ni/YSZ anodes tested at 900°C eight nickel elemental maps were obtained by SEM using the L line from nickel, so that the Ni appeared red and the remainder of the anode (pores and YSZ) was black. The Analyze Particles tool was used to calculate the intersected area of the Ni grains.

Results

Some performance loss (voltage decrease) was always observed during long-term tests of button cells. In general, voltage loss at 700°C was minimal, while the rate of degradation increased with increasing temperature. During the 2,300 hour test at 700°C, the cell voltage was nearly constant for the first 1,000 hours, then decreased slightly, 0.6% per 1,000 hours. Both control and 45% fuel utilization cells exhibited similar behavior, as shown in Figure 1. The cell area specific resistance (ASR) increased 3-15% in total during the 2,300 hour test. Within experimental scatter, no significant difference in the performance of control cells and cells with higher humidity corresponding to 70% fuel utilization was observed. The open-circuit voltage (OCV) remained steady and stable in time. As determined from the impedance spectroscopy data, none of the cells tested at 700°C showed changes in the ohmic resistance, while the electrodic resistance slightly increased. This increase came from a process observed in impedance spectra in the high frequency range (~0.5-1 kHz); this range is typically reported to be affected by electrochemical cathodic reactions. This degradation was independent of the humidity level and was therefore attributed to cathode degradation. No electrochemical degradation in the Ni/YSZ anodes at 700°C was identified.

Following the termination of the tests, the cells were analyzed by SEM. No evidence of microstructural changes in the Ni/YSZ anodes was found. However, extensive Ag deposits were clearly distinguished at the YSZ electrolyte-LSM/YSZ cathode interface. It is apparent that Ag migrated from the Ag paste used as a cathode current collector, probably via electromigration, because Ag was found at the active interface only. The "spiky" appearance of those deposits suggested a vapor transport mechanism.

Higher performance losses were observed during long-term tests at 800°C and especially at 900°C. While a clear dependence between the overall cell degradation and the humidity level was observed, no direct indication of the anode degradation at elevated humidity levels was established. Cells tested at 45% fuel utilization exhibited ~5-12% increase in the ASR over 1,000 hours at 800°C (Figure 2) and ~20-30% increase in the ASR at 900°C. At higher humidity levels corresponding to 70-80% fuel utilization cells failed within 1,500-2,000 hours of testing at 900°C mostly because of massive ohmic losses. No cell failure was observed at 800°C under otherwise identical conditions. The open circuit voltage (OCV) remained stable for cells tested at 45% fuel utilization at 800°C but decreased constantly in time when the humidity was elevated to match 70-80% fuel utilization. At 900°C the OCV decreased on most cells, including controls. It was believed that the barium aluminosilicate glass seals used in the laboratory test alumina test fixtures aged rapidly

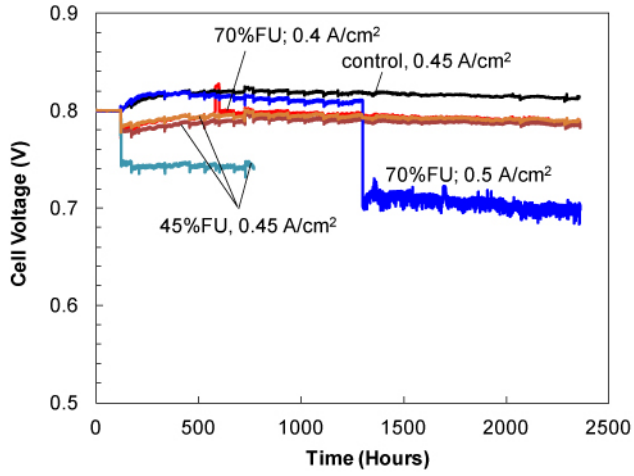

FIGURE 1. Cell voltage of anode-supported cells at 700°C during tests at low (control), 45%, and 70% fuel utilizations

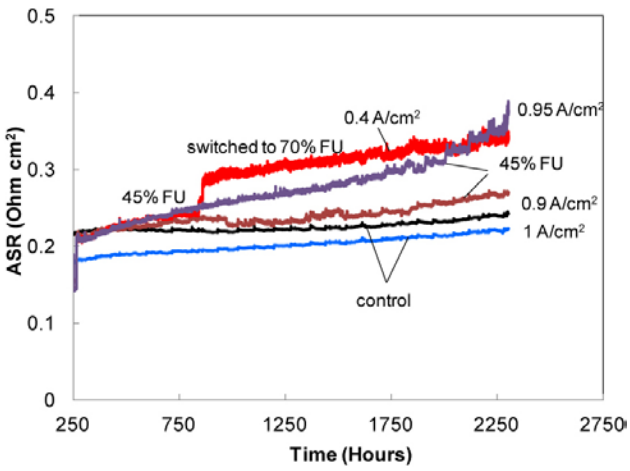

FIGURE 2. Area specific resistance of anode-supported cells tested at 800°C at low (control), 45%, and 70% fuel utilizations

at 900°C at steam concentrations above 30% in the fuel gas. Such aging is likely due to glass degradation via hydrolysis followed by loss of a hermetic seal that led to a diminished open-circuit voltage, and an apparent cell voltage decrease. The process was slower at 800°C and was not noticed at 700°C.

All cells with the Ag cathode current collector also showed an increase in electrodic resistance with time at 800-900°C. Cells with a Au cathode current collector did not exhibit an increase in the electrodic resistance (but ohmic losses were increased in time). Figure 3 illustrates impedance spectra of the anode-supported cell obtained at a high humidity level corresponding to 80% fuel utilization during a 1,500 hour test at 900°C. The cell had a Au cathode current collector. The electrodic resistance is seen to remain constant with testing time. Therefore, progressive electrodic losses at 800-900°C in all other cells cannot be attributed to the anode degradation, as the anode was identical in all cells. As at lower temperatures, no direct evidence of microstructural changes in the Ni/YSZ anode was found after the tests. Figures 4 and 5 show representative microstructures for a control cell and a 45% fuel utilization cell, respectively; both cells were tested at 900°C. While modest nickel grain growth could be completely ruled out, the detailed image analysis performed on the anodes tested at 900°C at low (control) and 45% fuel utilization gave almost identical values of the average intersected area of the Ni grains: 0.89±0.13 μm^2 for the control cell and 0.90 ± 0.09 μm^2 for the 45% utilization cell.

In extended tests lasting over 1,000 hours, an additional increase in the electrodic resistance in the mid-to-low frequency range was detected in impedance spectra obtained from the cells with the Ag cathode current collector at 800°C and 900°C. A substantial amount of Ag was always observed at the active cathode/electrolyte interface in the post-test SEM analyses because of Ag migration. Thus, cathode degradation and seal degradation dominated performance degradation observed during the 800-900°C tests.

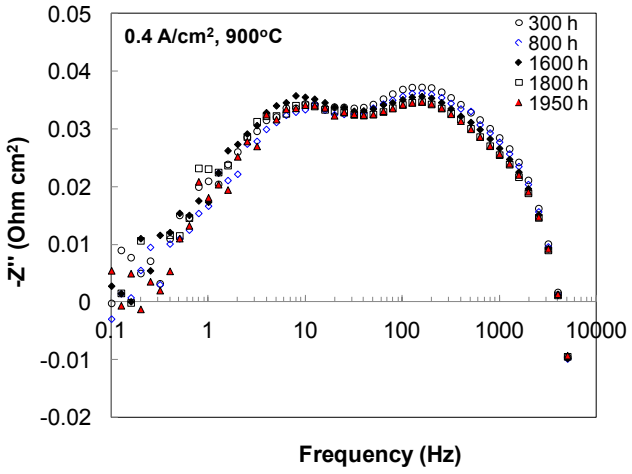

FIGURE 3. Bode plot of impedance spectra of an anode-supported cell operated at 900°C in reformate with a humidity level corresponding to 70% fuel utilization. Spectra were obtained after 300, 800, 1,600, 1,800, and 1,950 hours of operation at a current of 0.4 A/cm^2.

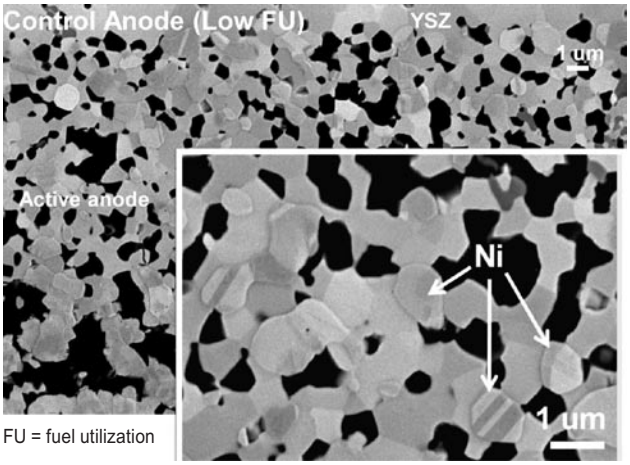

FU = fuel utilization

FIGURE 4. Microstructure of an active anode after a 1,000 hour test at 900°C at low fuel utilization

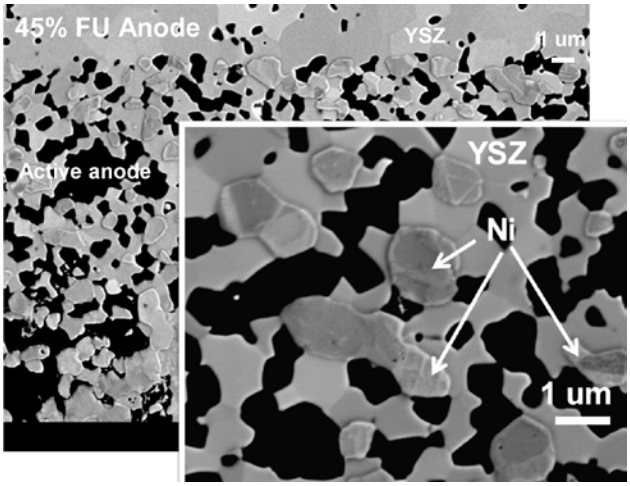

FIGURE 5. Microstructure of an active anode after a 1,000 hour test at 900°C at 45% fuel utilization

Conclusions and Future Directions

- Multiple Ni/YSZ anode-supported button cells were tested simultaneously at three different temperatures (700°C, 800°C, and 900°C) under increased humidity levels to determine whether high fuel utilization would lead to accelerated performance losses for SOFCs. A reliable reproducible data set was obtained from which odd cell behaviors were eliminated.

- During long-term tests up to 2,300 hours, a low degradation rate of <1% /1,000 hours was measured in reformate at high humidity corresponding to 45-70% fuel utilization. This was comparable to that on control cells operated at lower humidity (less than 5% fuel utilization).
- A higher rate of degradation (a 5-30% increase in ASR per 1,000 hours) was observed at 800°C and 900°C both for control cells and those tested at higher humidity.
- While accelerated losses in SOFC performance were indeed observed when tested at 800°C and 900°C in synthetic reformate at humidity levels corresponding to 45-70% fuel utilization, those losses could not be attributed to the Ni/YSZ anode degradation. No apparent Ni particle growth was observed after 1,000 hour tests at 900°C with steam content up to 50% in the fuel gas.
- The main degradation at high temperatures came from glass seal aging at increased humidity levels and also from Ag migration from the cathode current collector to the cathode/YSZ interface.
- Post-test analysis will be performed on the remaining tested cells to evaluate stability of anode microstructure. Future work will be focused primarily on improving sulfur tolerance of Ni-based anodes.

FY 2012 Publications/Presentations

1. O.A. Marina, C.A. Coyle, D.J. Edwards, and J.W. Stevenson, "Effect of Fuel Utilization on the Performance of Nickel/Zirconia Anode-Supported SOFCs," Submitted to 222nd meeting of the Electrochemical Society, October 2012.

References

1. J. Sehested, Catal. *Today*, 2006, 111, 103-110.

2. A. Ioselevich, A.A. Kornyshev, W. Lehnert, *Solid State Ionics*, 1997, 124, 221–237.

3. L. Holzer, B. Iwanschitz, T. Hocker, B. Münch, M. Prestat, D. Wiedenmann, U. Vogt, P. Holtappels, J. Sfeir, A. Mai, T. Graule, *J. Power Sources*, 2011, 196, 1279–1294.

4. H. Yokokawa, H. Tu, B. Iwanschitz, A. Mai, *J. Power Sources*, 2008, 182, 400–412.

III.B.2 Utilization of Coal Syngas in High Temperature Fuel Cells: Degradation Mechanisms and Lifetime Prediction

Ismail Celik
West Virginia University (WVU)
P.O. 6106
Morgantown, WV 26506
Phone: (304) 293-3209; Fax: (304) 293-6689
Email: ismail.celik@mail.wvu.edu

DOE Project Manager: Briggs White
Phone: (304) 285-5437
Email: Briggs.White@netl.doe.gov

Contract Number: ER46299

Start Date: August 1, 2009
End Date: July 31, 2013

Fiscal Year (FY) 2012 Objectives

- Implement new characterization methods.
- Develop remedies for impurity effects.
- Identify the tolerance limits of solid oxide fuel cell (SOFC) anode for specific impurities.
- Predict the lifetime of the anode for a given impurity level.

FY 2012 Accomplishments

- Experimentally verified that Ni migration in Ni-yttrium stabilized zirconia (YSZ) is induced by electrostatic force and chemical potential gradient of phosphorous and the rate of migration is much less when the cell is not loaded with current.
- Investigation of the nanostructure of the anode using high resolution transmission electron microscopy (HRTEM) revealed that, in addition to Ni, YSZ crystalline structure is also affected by phosphine (PH_3).
- It was found that the rate of cell performance degradation is strongly dependent on the steam concentration present in the fuel.
- Monitored the in situ concentrations of trace impurities using a mass spectrometer and found no evidence that PH_3 and hydrogen sulfide (H_2S) impurities convert to oxidized forms, e.g., HPO and SO_2, under the operating conditions of button cells. The in situ gas concentration experiments also revealed significant air leaks in the test stands.
- Extended the degradation model to simulate the experimentally observed sensitivity of PH_3 induced degradation to steam concentration and a decent agreement was achieved between predictions and experiments.
- Developed new modeling tools to simulate polarization and impedance responses of the cells at different times after impurity exposure.
- Synthesized Ni free SOFCs using $La_{1-x}Sr_xV_{1-y}M_yO_3$ (Vanadates) and samaria doped ceria (SDC) anode, lanthanum strontium gallate magnesite (LSGM) electrolyte and lanthanum strontium cobalt ferrite (LSCF) cathode. With maximum power densities reaching 401 mW/cm^2 and 288 mW/cm^2 in wet H_2 and coal syngas respectively at 800°C, these in-house cells showed order of magnitude higher performance than similar anodes in literature.
- Synthesized $Y_{0.8}Ca_{0.2}Cr_{0.8}Co_{0.2}O_3$ (YCCC) materials to be tested as alternative anodes and demonstrated that electric conductivity for the in-house YCCC anodes was redox stable and was higher than that for similar anodes reported in literature.
- Synthesized an all ceramics SOFC using $Sr_2MgMoO_{6-\delta}$ (SMM) and $Ce_{0.9}Gd_{0.1}O_2$ (GDC) anode. The maximum power density for the cell at 800°C was found to be 290 mW cm^{-2} and 180 mW cm^{-2} in wet H_2 and in clean syngas, respectively, and the new anode is shown to be more resistant to PH_3 poisoning.
- Extended the lifetime of cells exposed to PH_3 using a pre-filter which captures the impurity before it enters the SOFC. It is estimated that one such filter could last upwards of 10,000 hrs in 2 ppm PH_3.
- Tested Ni-GDC anodes with Ni-GDC barrier layer under H_2S attack. It was shown that these anodes are resistant to H_2S poisoning event at concentrations as high as 1,000 ppm.

Introduction

This project is supported under the U.S. Department of Energy (DOE) Experimental Program to Stimulate Competitive Research (EPSCoR), a program designed to enhance the capabilities of EPSCoR states in energy research and economic development through the support of advanced research at academic institutions. The long-term goal is to establish an internationally recognized,

sustainable fuel cell research center for coal-based clean power generation which serves as a technology resource for the emerging fuel cell industry in West Virginia. Towards this goal, a multidisciplinary team of research professionals who have worked together for several years and have attained strong credentials in their respective areas of expertise was formed. Our strengths are in (1) applying nanotechnology to develop and fabricate materials for advanced coal-based fuel cells, (2) state-of-the-art material characterization and fuel cell testing facilities involving both ex situ and in situ measurement techniques, and (3) multi-dimensional modeling of fuel cells at various scales using high-performance computing. During the first phase of the project, a laboratory infrastructure was developed, interactive working relationships were solidified, and national recognition for the work conducted by the center in the area of coal-based clean power generation via fuel cells was attained. The research cluster has proven itself to be sustainable with team members working together on other related projects. Based on the progress made, we obtained a three-year continuation of funding from DOE EPSCoR with cost share from the National Energy Technology Laboratory, West Virginia State, and West Virginia University (WVU). The goal under this project is to further expand the infrastructure for fuel cell research at WVU and to increase our reputation as a centre of excellence and thus ensure continued funding. The technical objectives of the current project are to determine underlying mechanism for contaminant degradation, formulate remedies to reduce degradation rates, establish the tolerance limits of contaminant levels in the coal syngas for SOFCs, and to predict the lifetime of the cells for a given contaminant level.

Approach

The research cluster is based on a multi-scale, multi-disciplinary approach conducted by eight faculty members in four departments at WVU. The work is organized under three integrated projects, (1) characterization of contaminant effects, (2) multi-scale continuum modeling, and (3) anode material development. The knowledge base gained from experiments (Projects 1 and 3) is used in multi-scale computational models (Project 2) to establish the tolerance limits for the impurities and to predict the lifetime of SOFCs operating on coal syngas with the impurities.

Results

Characterization of Contaminant Effects

The effects of the electric current and the moisture concentration on the degradation of Ni/YSZ anode upon exposure to PH_3 were studied using half cell tests. In situ electrochemical testing was combined with the ex situ material characterization methods to analyze the degradation of the SOFC anode. Specifically, the Ni migration behavior at the Ni/YSZ anode was quantitatively investigated. Nickel migration was induced by the electrostatic force and the chemical potential difference of phosphorous. In addition, the presence of moisture accelerated the cell degradation in the PH_3-containing fuel as shown in Figure 1. Figure 2a shows clearly the segregation of Ni towards the cell surface which is quantified in Figure 2b. It is observed that this process occurs even without current albeit at a relatively slower rate. Other fuel cell tests have also shown (Figure 3) the negative effect of the steam concentration on the fuel cell performance.

Commercially available anode-supported button cells featuring a conventional Ni/YSZ interlayer and dense YSZ electrolyte were electrochemically operated at 800°C with the fuel containing PH_3 and subsequently examined by scanning electron microscopy (SEM) and transmission electron microscopy (TEM). The key findings are (1) degradation of SOFC is indeed fuel dependent; (2) significant microstructure degradation was found in the anode of the SOFC, and the microstructure degradation is observed both for Ni and YSZ; and (3) the microstructure degradation of YSZ appears to be fuel dependent as well.

In situ measurements with the Cirrus MKS mass spectrometer focused on finding leaks in the test stands to ensure that any results concerning the reactions of PH_3 or H_2S inside the furnace or on the anode were not compromised by air leaks. Also, an isotope of O_2,

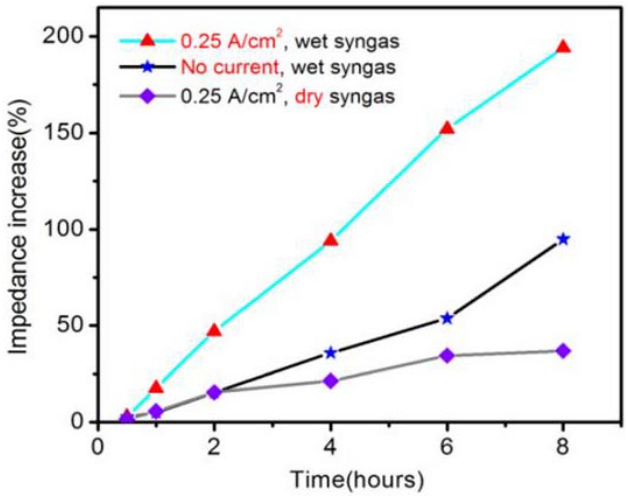

FIGURE 1. Polarization impedance as a function of operation time (5 ppm PH_3 at 800°C) at a current density of 0.25 A/cm^2, without current load, and in dry coal-syngas, respectively

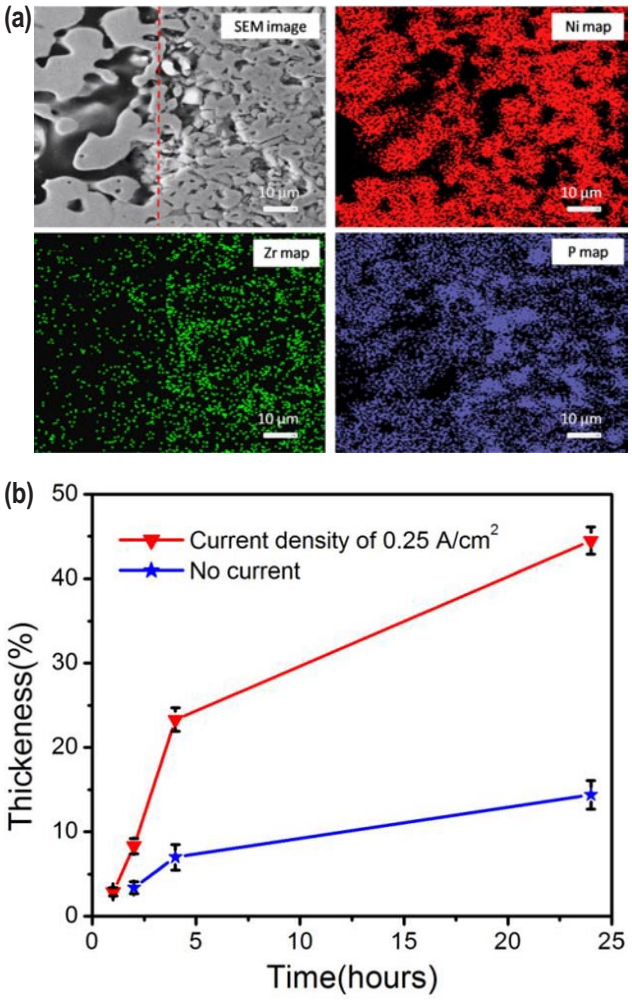

FIGURE 2. (a) Elemental maps collected from the cross-sections of the fuel cells. Ni converted to Ni-P secondary phases in the anode exposed to 5 ppm PH_3-containing coal-syngas at 800°C for 24 hours at the current density of 0.25 A/cm^2. The top surface of the anode is shown along the boundary line. (b) Ratio of the top Ni-P compound layer thickness to the whole anode thickness as a function of time of exposure to 5 ppm PH_3-containing coal-syngas at 800°C.

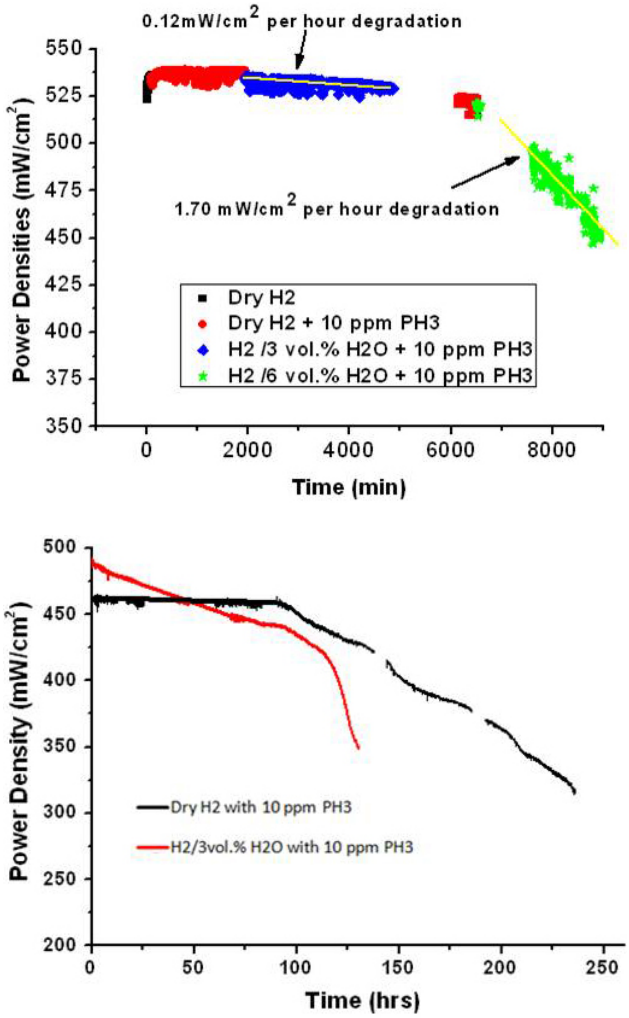

FIGURE 3. Variation of SOFC power density under different testing conditions

$^{18}O^{16}O$, has an identical mass (34) to that of H_2S or PH_3. The concentration of $^{34}O_2$ in air is 855 ppm, enough to interfere with measurements of H_2S or PH_3 at the ppm level. The test stand that uses mica gaskets to form the seal was particularly leaky. In the experiments with dry H_2 fuel, although water was not added to the gas stream, the partial pressure of water was on the order of 1 torr. When O_2 partial pressures are sufficiently low, H_2S and PH_3 partial pressures can be monitored down to the 10 ppm level. H_2S and PH_3 mass 34 signals at the exhaust show very slow rises (ca. hours) to steady state signals after adding these gases to the fuel stream, indicating considerable adsorption of these gases within the fuel stream surfaces inside and outside the furnace. Mass 64 was monitored in order to detect a potential reaction product (HPO_2) of PH_3 with H_2O at 800ºC; the signal remained at the noise level (~10^{-3} torr) with 50 ppm PH_3 and 1–2 torr of H_2O in hydrogen. In an experiment with an operating cell exposed to 100 ppm H_2S, there were transients in the mass 34 signal when the cell current was turned on and off. These transients are attributed to desorption of H_2S as the cell heats up, and re-adsorption of H_2S when the cell cools down. No significant changes in the mass 64 signals (SO_2) were observed in the presence of an operating cell.

Continuum Level Modeling

A previously developed impurity degradation model is used to simulate the effects of steam (Figure 3) on degradation of SOFC anodes due to PH_3. The model parameters were recalibrated for anode supported geometry using the new experiments (Figure 3). Simulations were performed for button cells with

1,025 µm thick anode, operating under 10 ppm of PH_3 contamination, at a constant current density of 0.6 A/cm^2 and fuel concentrations of 97% H_2, 3% H_2O and 100% H_2, 0% H_2O for wet and dry cases, respectively. With the new modifications to the model, reasonable agreement was achieved between the simulations (Figure 4) and the experimental results (Figure 3) that show the effect of steam on degradation due to PH_3. To assess the overall performance of the cell at different stages during the gradual degradation, the voltage-current (V-I) behavior and impedance response of the cell were calculated at different times using the condition of the anode at that instant. The V-I curves obtained at different points on the degradation curve (Figures 4b and 4d) show that after exposure to PH_3, the limiting current for the cell decreases gradually and the activation losses increase. In accordance with experiments, the simulated impedance curves also show that series resistance increased gradually with the time of exposure whereas the activation losses increase abruptly after remaining more or less constant for over 100 hours.

Anode Materials Development and Cell-Testing

The $La_{1-x}Sr_xV_{1-y}M_yO_3$ vanadates are synthesized in house by solid-state sintering of precursor metal oxides and salts in reducing atmosphere. Mg and Mn are introduced as the B-site dopants into the baseline lanthanum strontium vanadate (LSV) perovskite system to make new perovskite phases of magnesium-doped lanthanum strontium vanadate (LSMV) and manganese-doped lanthanum strontium vanadate (LSM'V) (Mn-doped). Figure 5 shows the direct current conductivities for commercial and different lab-made vanadates measured in wet H_2 with four-probe van der Pauw method. The results indicate addition of more Sr as A-site dopant changes the system conductivity behavior from semi-conductor to metallic conductor.

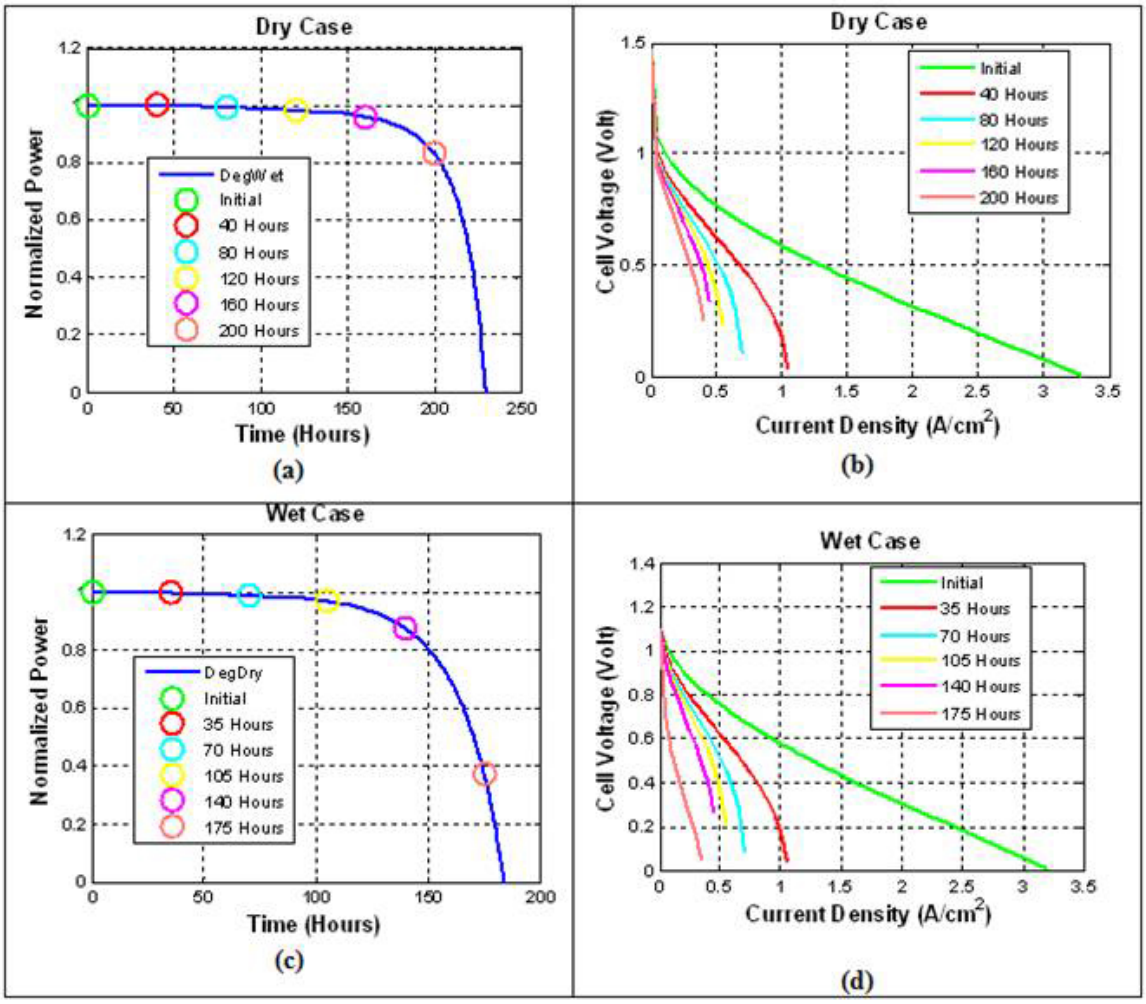

FIGURE 4. Predicted degradation curve and V-I curves at different times of phosphine exposure for dry hydrogen (top) and wet hydrogen (bottom) fuel cases

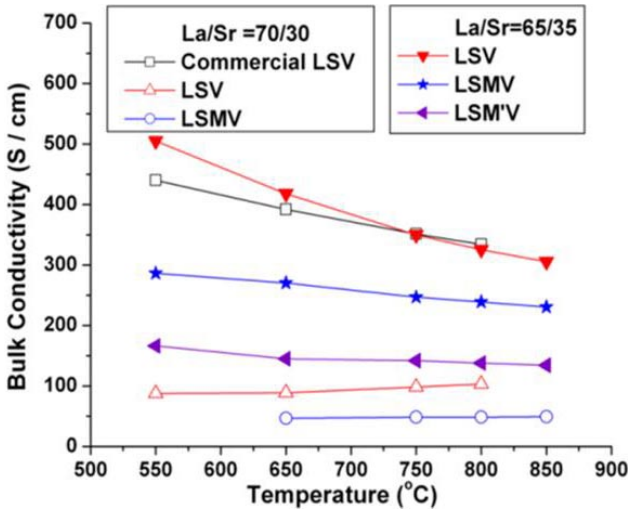

FIGURE 5. DC conductivities measured in wet H_2 for lab-made and commercial lanthanum vanadates with different dopant concentration and types

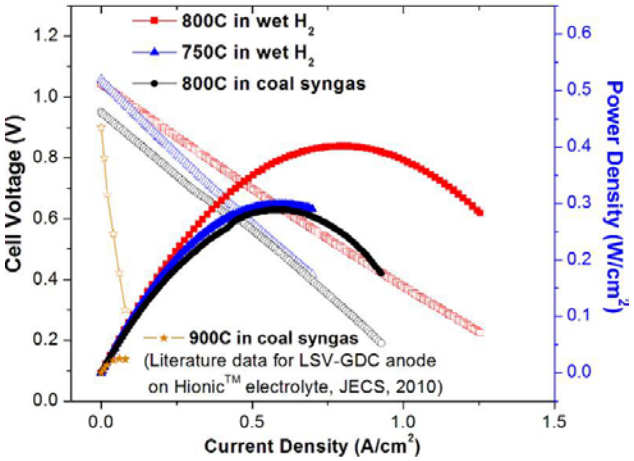

FIGURE 6. Performances of LSGM-supported Ni-free SOFC with LSV-SDC anode at IT in different fuels, in comparison to literature reported data

Introduction of Mg and Mn reduces the electrical conductivity for LSV, but the new LSMV and LSM'V phases still have much higher conductivity than typically required for alternative SOFC anode material (>10 S/cm).

The as-synthesized LSV and LSMV powders are combined with SDC ($Sm_{0.2}Ce_{0.8}O_2$) oxides to make LSV-SDC and LSMV-SDC composite anodes, and deposited onto (La,Sr)(Ga,Mg)O_3 (LSGM) electrolyte with $La_{0.6}Sr_{0.4}Co_{0.2}Fe_{0.8}O_3$(LSCF) cathode to form Ni-free electrolyte-supported SOFC. It can be seen from Figure 6 that the in-house made SOFC with LSGM electrolyte and LSV-SDC anode showed an order of magnitude higher performance than similar LSV-GDC anode in literature, with maximum power densities reaching 401 mW/cm^2 and 288 mW/cm^2 in wet H_2 and coal syngas respectively at 800°C. This can be attributed to the reduced anode/electrolyte contact resistance, superior conductivity of LSGM and change of catalytic activity for LSV due to Sr doping. Further investigation is under way to understand the high performances for LSV-SDC and LSMV-SDC anodes and evaluate their stability with current load against sulfur contaminant in coal syngas.

YCCC materials have been recently developed as redox-stable ceramic anode which can withstand the thermal cycling for an SOFC stack. This study contributes to optimize the synthesis route and explore the rate-limiting factors for a YCCC material system. The YCCC oxides with the listed formula ($Y_{0.8}Ca_{0.2}Cr_{0.8}Co_{0.2}O_3$) are manufactured by sol-gel method. Comparing to vanadate anode, the whole synthesis process for YCCC can be readily carried out in ambient air, and suitable for larger-scale production. After high temperature annealing, secondary phases

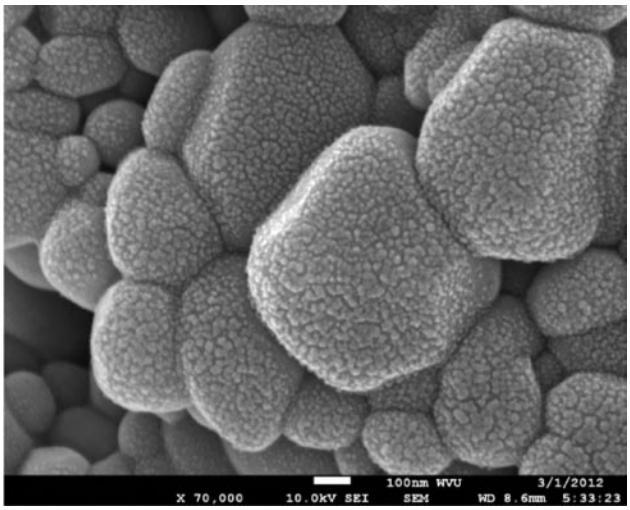

FIGURE 7. Sol-gel derived YCCC oxide particles after sintering at 1,200°C

are reduced and the synthesized YCCC powders still maintain relatively large surface area as result of the sol-gel process (Figure 7).

An all-ceramic SOFC anode composed of a mixture of SMM and GDC on a YSZ) electrolyte was synthesized and tested in clean and PH_3-contaminated hydrogen and coal syngas. The initial electrochemical performance of the cell at 800°C was 290 mW cm^{-2} and 180 mW cm^{-2} in wet H_2 and in clean syngas. In wet H_2 with 10 ppm PH_3 under 0.15 A-cm^{-2} load, the cell displayed stable performance over the first 40 h, but then slowly degraded over the next 80 h leading to a 47% decrease in power output (0.59 h^{-1}%). The anode performance was much improved compared to typical Ni/YSZ cermet anodes. X-ray photoelectron spectroscopy results did not detect P at the anode/electrolyte interface nor throughout the

bulk of the anode in either a phosphide or phosphate form which makes this composition one worthy of further investigation.

Another area of focus for the group has been on developing a testing stand for planar fuel cells (16 cm^2 active area). The initial test fixture consists of two Haynes 242 blocks with channeling to accommodate a co-flow pattern. The connecting pipes are Inconel 601 and the furnace providing the high temperature environment is a kiln purchased from Paragon Industries Inc. Additional insulation was used around the loading portion of the stand in the front of the furnace to ensure a reasonably uniform temperature profile. The cells tested to date are YSZ electrolyte supported (200-300 µm in thickness) with traditional SOFC electrodes.

Two studies were conducted aiming at mitigating the degradation of the SOFC anode fueled by syngas containing PH_3 and H_2S impurities. All tests were performed at 800°C with a syngas composition of 32% H_2, 18% H_2O, 31% CO and 19% CO_2. The total fuel flow rate to the anode was kept constant at 200 sccm and the air flow to the cathode was constant at 300 sccm.

A thin Ni-based prefilter installed upstream of the SOFC anode has been designed and tested as a means of removing the PH_3 from the syngas before the fuel enters the SOFC anode. After an initial break-in period at 800°C for 60 hr in pure syngas, the anode-supported cell was subjected to a constant flow of 10 ppm PH_3. After that the cell performance showed a slight decrease in voltage (at constant current) of about 10 mV, then it remained stable for the next 150 hr. It is observed that the PH_3 reacts instantaneously with Ni and moves through the filter as a coherent reaction front. The same SOFC without the filter was reloaded in the test stand and operated at steady-state for the next 50 hr in pure syngas with no sign of deteriorating performance. In other tests, similar positive results were found with a Fe-based filter and with a combination Ni/Fe-based filter proving that the prefilter is an economical and effective method for preventing the SOFC anode against PH_3 attack. Finally, a back-of-the-envelope calculation revealed that such a filter would have a lifetime of over 10,000 hours when exposed to syngas with 2 ppm PH_3.

In another study, a Ni-GDC hybrid anodes were fabricated in an anode-supported cell design and exposed to wet hydrogen and syngas with various concentrations of H_2S at 800°C under constant current conditions. Some of the prototype anodes contained a 5 µm-thick GDC barrier layer between the Ni-GDC anode and the YSZ electrolyte. The results of these tests verify that the composite Ni-GDC anode was in fact resistant to H_2S at concentrations up to 1,000 ppm H_2S in wet hydrogen at 800°C. The ohmic resistance is seen to be nearly constant over the entire course of the test, while the polarization resistance increases upon initial exposure to 100 ppm H_2S but then levels off thereafter. A similar cell operated stably for nearly 300 hours at 100 ppm H_2S in syngas. Cells without the GDC barrier layer had a significantly lower tolerance for the H_2S impurity over the same time span. The team hypothesizes that the GDC barrier layer assists in the prevention of Ni oxidation at the anode/electrolyte interface by acting as an oxidation catalyst for the H_2S, thereby preventing the H_2S from attacking the Ni and reducing its electrochemical activity.

Conclusions and Future Directions

The future goals for the group include the following.

- Completion of the SMM/GDC composite anode supported cell and subsequent full cell testing in fuels containing the trace impurities of interest including, full densification of the electrolyte given the processing issues outlined above.
- Re-initiation of the large cell testing with the goal of optimizing seal configuration.
- A new pre-filter for PH_3 removal will be designed and fabricated in order to remove trace PH_3 more efficiently before the syngas is fed into SOFCs.

Electrochemical tests will be combined with materials characterization technique to evaluate the PH_3 pre-filter performance. Based on our results that showed most structural and chemical changes are at the scale of nanometers, work will continue to use the TEM to analyze the anodes from various cells. To further understand the effect of various fuels on the degradation of the anode, the nanostructure and chemistry of an anode operated for different durations of time and different fuels including bio-gas will be investigated. In order to understand the effect of contaminants on various electrolytes currently being used in SOFCs, work will continue on studying the nanostructure and chemistry evolution of GDC and SDC electrolytes exposed to PH_3 contamination. Measurements of gas phase chemistry and electrochemistry will be carried out to study the chemical reactions between PH_3 and hydrogen/syngas. In terms of measurement accuracy, leak testing will be incorporated into the plan. A series of degradation experiments are also planned at different steam concentrations, such as 1%, 3%, and 6%, and current densities to provide data for modeling effort. Mass spectrometry measurements will be carried out for in situ investigation of the PH_3 status during the cell operation.

The degradation model will be validated against the newly designed experiments that will be conducted

shortly. The degradation model will be included in an in-house SOFC three dimensional simulation code, DREAM SOFC, and initially the flow by anode experiments conducted at Pacific Northwest National Laboratory will be simulated for model validation purpose. Long-term degradation simulations will be performed at low contaminant concentrations, and the results will be compared to those found in the literature. The validated model will be used to predict tolerance limits over 10,000 hours of operation.

Furthermore, research work will look into the following issues based upon recent findings:

- Evaluation of electrochemical performance and sulfur tolerance for LSV and LSMV alternative anodes through long-term stability test in coal syngas.
- Optimization of YCCC material chemistry from fundamental understanding of electrode kinetics, and eventually develop high performance SOFC from YCCC material system.
- In-depth investigation on degradation mechanism for SMM composite anodes, and further optimization of SMM SOFC performance and stability via development of anode-supported configuration.

Special Recognitions & Awards/Patents Issued

1. Dr. Xingbo Liu and his co-workers won the prestigious R&D 100 award for Year 2011 for their work on "Electroplated Coating for Solid Oxide Fuel Cell Interconnects."

2. A poster titled "Sulfur Tolerant Anode for Solid Oxide Fuel Cell Using Coal Syngas," by Sean Belardo, an undergraduate researcher in Dr. Xingbo Liu's team was selected for presentation at 2012 Posters on the Hill event conducted by Council on Undergraduate Research at Capitol Hill, Washington, D.C., on April 24, 2012.

FY 2012 Publications/Presentations

1. Phil Gansor, Chunchuan Xu, Katarzyna Sabolsky, John Zondlo, Edward M. Sabolsky, "Phosphine Impurity Tolerance of $Sr_2MgMoO_{6-\delta}$ Composite SOFC Anodes," Journal of Power Sources, 198, 7-13, 2012.

2. Song Chen, Yun Chen, Harry Finklea, Gregory Hackett, Xueyan Song, "Crystal Defects of Yittria-Stabilized Zirconia in the Solid Oxide of Fuel Cells and Their Evolution upon Cell Operation," Solid State Ionics, 206, 104-111, 2012.

3. Fatma Cayan, Suryanarayana R. Pakalapati, Ismail Celik, Chunchuan Xu, John Zondlo, "A Degradation Model for Solid Oxide Fuel Cell Anodes Due to Impurities in Coal Syngas: Part I Theory and Validation," Fuel Cells, DOI: 10.1002/fuce.201100027, 2012.

4. Yun Chen, Song Chen, Harry Finklea, Xueyan Song, Gregory Hackett, Kirk Gerdes, "Microstructure and Chemistry Evolution of Triple Phase Boundaries in the Anode of Solid Oxide Fuel Cells," Solid State Ionics, 204-205, 87-90, 2011.

5. Chunchuan Xu, John W. Zondlo, Mingyang Gong, XingBo Liu, "Effect of PH_3 Poisoning on a Ni-YSZ Anode-Supported SOFC Under Various Operating Conditions," Journal of Power Sources, 196,116-125, 2011.

6. Chunchuan Xu, John W. Zondlo, Edward M. Sabolsky, "A Prefilter for Mitigating PH_3 Contamination of a Ni-YSZ Anode," Journal of Power Sources, 196 (2011) 7665-7672.

7. Chunchuan Xu, Phillip Gansor, John W. Zondlo, Katarzyna Sabolsky, Edward Sabolsky, "An H_2S-Tolerant Ni-GDC Anode with a GDC Barrier Layer ," Journal of the Electrochemical Society, 158 (11) B1-B12 (2011).

8. Chunchuan Xu, John Zondlo, Edward Sabolsky, "Exploring Remedies for PH_3 Poisoning of a Ni-YSZ Anode SOFC in Coal-Syngas Fuel," ASME 2011 Energy Sustainability Conference & Fuel Cell Conference.

9. Fatma N. Cayan, Suryanarayana R. Pakalapati and Ismail Celik, "A Degradation Model for Solid Oxide Fuel Cell Anodes Due to Impurities in Coal Syngas," 9th Fuel Cell Science, Engineering and Technology Conference, Washington, D.C., August 7–10, 2011.

10. Suryanarayana R. Pakalapati, Yasemin Vural, Chunchuan Xu, John Zondlo, Ismail Celik, "Three-Dimensional Modeling of a SOFC Operating on Biogas," in the proceeding of ASME 9th International Fuel Cell Science Technology and Engineering Conference, Washington D.C., August 7–10, 2011.

11. Mingjia Zhi, Jinlong Yan, A. Manivannan, and Nianqiang Wu, "Degradation Mechanism of Nickel-Yttria Stabilized Zirconia Anode Materials in PH_3 Containing Coal Syngas," 219th ECS Meeting, Montreal, Canada, May 2011.

12. Yasemin Vural, Suryanarayana Pakalapati, Ismail Celik, "A Continuity Outlet Boundary Conditiion for the Lattice Boltzmann Method," Proceedings of the ASME 2012 Fluids Engineering Division Summer Meeting, Rio Grande, Puerto Rico, July 8–12, 2012.

13. S. Pakalapati, I. Celik, H. Finklea, M. Gong, and X. Liu, "A Micro-Scale Model for Oxygen Reduction on LSM-YSZ Cathode," ECS Transactions, 35(1):963-976, 2011.

14. Jinlong Yan, Mingjia Zhi, Nianqiang Wu, "PH_3 Poisoning Effect on Ni/YSZ Cermet Solid Oxide Fuel Cell Anode," 87th Annual Meeting of the West Virginia Academy of Science and the 4th Biennial STaR Symposium, Charleston, West Virginia, April 21, 2012.

15. Mingjia Zhi, Jinlong Yan, Ayyakkannu Manivannan, Nianqiang Wu, "Degradation Mechanism of Nickel-Yttria Stabilized Zirconia SOFC Anode Materials in PH_3 Containing Coal Syngas," 219th ECS Meeting, Electrochemical Society. Montreal, QC, Canada, 2011.

16. Xueyan Song, Yun Chen, Song Chen, Harry Finklea, Ismail Celik, Gregory Hackett, Kirk Gerdes, "Microstructure and Chemistry of Ni/YSZ Anode for Cells Operated in H_2, Syngas and Syngas Containing PH_3," 12th Annual SECA Workshop, Pittsburgh, Pennsylvania, July 26–28, 2011.

17. Xueyan Song, Song Chen, Yun Chen, Gregory Hackett, Harry Finklea, and Kirk Gerdes, "Crystal Defects of YSZ in Solid Oxide Fuel Cells and Their Microstructure Evolution Upon Cell Operation," 220th Meeting of the Electrochemical Society, B12 Solid State Electrochemical Cells: Materials and Techniques for Measurements, Abstract#1581, Boston, Massachusetts, October 14, 2011.

18. Harry Finklea, Chunchuan Xu, John Zondlo, Mingyang Gong, XingBo Liu, "Phosphine Poisoning of the Ni-YSZ Anode in SOFCs Using Syngas Fuel," 219th Meeting of the Electrochemical Society, Symposium on Electrochemistry and Climate Change, Abs. #127, Montreal, Canada, May 2, 2011.

19. Xueyan Song, Song Chen, Yun Chen, Harry Finklea, Chunchuan Xu, John Zondlo, Ismail Celik, Gregory Hackett, Kirk Gerdes, "Evolution of Yttria Stabilized Zirconia in SOFC Operated Using Fuel of H_2, Syngas, and Syngas Containing PH_3," poster, 12th Annual SECA Workshop, Pittsburgh, Pennsylvania, July 26–28, 2011.

20. Ismail Celik, Harry Finklea, Bruce Kang, Xingbo Liu, Edward Sabolsky, Xueyan Song, Nick Wu, John Zondlo, Fatma Cayan, Yun Chen, Chunchuan Xu, Raju Pakalapati, Y. Vural, "Progress on SOFC Contaminant Study at West Virginia University," 12th Annual SECA Workshop, Pittsburgh, Pennsylvania, July 26–28, 2011.

21. Sean Belardo, Mingyang Gong, Xingbo Liu. Poster presentation "Research on Impurity-Tolerant SOFC Anode for Coal Syngas Operation," 9th WV Annual Undergraduate Research Day at the Capitol, Charleston, West Virginia, January 2012.

22. Sean Belardo, Mingyang Gong, Xingbo Liu. Poster presentation "Study of Alternative Solid Oxide Fuel Cell Anodes for Coal Syngas Operation," Council for Undergraduate Research 2012 Posters on the Hill Conference, U.S. Capitol Hill, Washington, D.C., April 2012.

23. S.R. Pakalapati, I. Celik, H. Finkea, and J. Escobar-Vargas, "A Computational Study of Anomalous Cathode-Reference Voltages on Anode Supported Button SOFCs," 221st ECS Meeting, Seattle, Washington, May 6–10, 2012.

24. H.O. Finklea, X. Chen, I. Celik, S.R. Pakalapati, K. Gerdes, "1D and 2D Simulation of Impedances in an Anode-Supported SOFC," 221st ECS Meeting, Seattle, Washington, May 6–10, 2012.

III. SECA CORE TECHNOLOGY R&D

C. Interconnects and Contact Materials

III.C.1 Effect of SOFC Interconnect-Coating Interactions on Coating Properties and Performance

Jeffrey W. Fergus
Auburn University
Materials Research and Education Center
275 Wilmore Laboratories
Auburn, AL 36849
Phone: (334) 844-3405; Fax: (334) 844-3400
Email: jwfergus@eng.auburn.edu

DOE BES Project Manager: Timothy Fitzsimmons
Phone: (301) 903-9830
Email: Tim.Fitzsimmons@science.doe.gov

DOE NETL Project Manager: Briggs White
Phone: (304) 285-5437
Email: Briggs.White@netl.doe.gov

Contract Number: ER46497

Start Date: June 15, 2008
End Date: June 14, 2012

Fiscal Year (FY) 2012 Objectives

- Identify the effects of Co/Mn ratio and Ni doping on amount of reaction with chromia and the properties of the reaction layer formed at the alloy-coating interface.
- Evaluate the effect of reducing the chromium content in the ferritic stainless steels used for solid oxide fuel cell (SOFC) interconnects.
- Evaluate site occupancy in the spinel structure.

FY 2012 Accomplishments

- The electrical resistance of the chromium containing spinel phase decreases with increasing cobalt content.
- Nickel additions can lead to a decrease in the amount of reaction between the spinel phase and chromia. In contrast to iron and titanium, nickel can be incorporated into the high-chromium spinel layer.
- Reduced chromium content in the alloy leads to high iron contents in the oxidation scale for uncoated alloys and in the coating for coated samples.
- Neutron diffraction results confirm the preference of Cr and Mn for the octahedral site and Co for the tetrahedral site in the spinel structure.

Introduction

The high operating temperature of SOFCs, which provides their excellent fuel flexibility, can lead to degradation of individual fuel cell components. One form of degradation is chromium poisoning of the cathode, which results from volatilization of chromium from the chromia scale formed on alloys used for the interconnect. The amount of chromium volatilization, and thus the associated cell poisoning, can be minimized by applying a ceramic coating to the alloy surface. One promising coating material is the spinel $(Mn,Co)_3O_4$ [1-4], which has been shown to reduce chromium volatilization [5-6].

Although chromium can form a spinel phase with other transition metals, chromium has not been observed in the coating during use in an SOFC [7-8]. However, with time, interaction of the coating with the chromia scale or with other SOFC components can lead to changes in the coating composition, which can affect properties and thus performance. The purpose of this work is to study the interaction between chromia and potential interconnect coating materials to provide information needed to design effective coatings for long-time SOFC operation.

Approach

The project addresses three aspects of coating properties and performance, (i) thermodynamics, (ii) transport properties, and (iii) physical properties. The thermodynamic aspects include phase equilibria, crystal structure stability, and chemical activity. The transport properties to be evaluated include conductivity and diffusion rates. The physical properties are those that are important for coating performance, such as the coefficient of thermal expansion. These aspects will be evaluated for the original coating composition and for compositions resulting from interaction of the coating with other fuel cell components by preparing bulk analogues of the compositions expected after the interaction occurs. Characterization of these bulk analogues will provide valuable information for evaluating any changes in the performance after interaction with other components. Finally, the results will be used to identify compositions with potentially improved performance, and these promising compositions will be similarly evaluated. This knowledge and understanding will allow coatings to be designed so that the expected compositional changes during operation increase the conductivity in an amount

that offsets the increase in resistance due to growth of the chromia scale. In this case, the coating electrical resistance, and thus the associated overpotential, would be constant with time, so fuel cell performance would not degrade during operation.

Results

As noted in previous reports, the addition of chromium to $(Mn,Co)_3O_4$ decreases the electrical resistance. Since the area-specific resistance will be dominated by the lowest resistance phase, the electrical conductivity of chromium-containing spinel phases is important for fuel cell performance. Figure 1 shows that the electrical conductivities of $(Mn,Co)_2CrO_4$ and $(Mn,Co)_{1.5}Cr_{1.5}O_4$ increase with increasing cobalt composition. Although cobalt may be beneficial to the coating performance, it is relatively expensive, so lower cost replacements for cobalt are desirable.

One potential dopant is nickel, which has been evaluated in this project. The replacement of cobalt with nickel in $Mn_{1.5}Co_{1.5}O_4$ leads to a small decrease in conductivity. However, as shown in Figure 2, the conductivity is still in the same range as $(Mn,Co)_3O_4$ and is higher than chromium-containing composition. The reactivity of nickel-doped composition $Mn_{1.5}CoNi_{0.5}O_4$ was evaluated with a diffusion couple with Cr_2O_3. Figure 3 shows the chromium concentration gradient for undoped and nickel-doped spinel samples and indicates that the thickness of the high-chromium spinel is less in the nickel-doped sample. This is similar to results for iron and titanium additions shown in previous reports. One difference between the behavior of nickel-doped samples and iron- or titanium-doped samples, is that in the latter cases, the dopant, iron or titanium, was not observed in the high-chromium spinel layer, but, as shown in Figure 4, nickel is present in the high-chromium spinel layer. As previously observed for diffusion couples with Cr_2O_3, the surface of the high-chromium spinel layer is faceted, but in this case 2% nickel was observed at the surface.

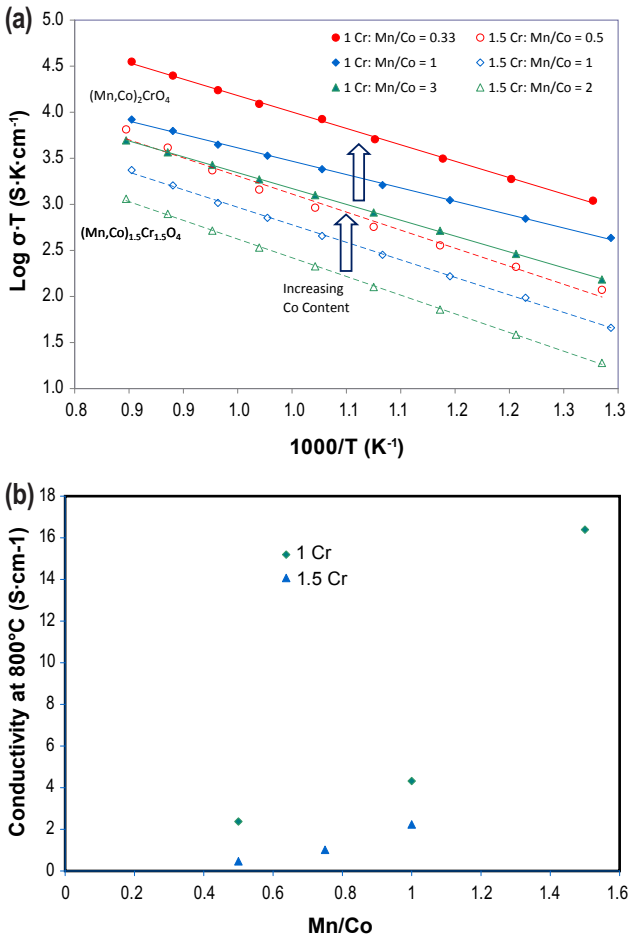

FIGURE 1. Conductivity of $(Mn,Co)_2CrO_4$ and $(Mn,Co)_{1.5}Cr_{1.5}O_4$ in air (a) Arrhenius plot and (b) conductivity at 800°C

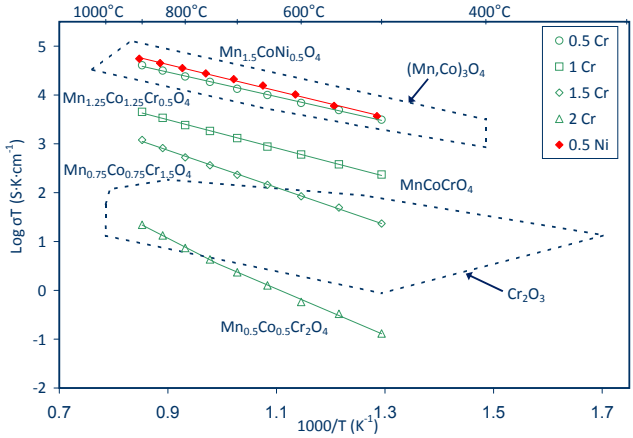

FIGURE 2. Conductivity of $(Mn,Co)_{3-x}Cr_xO_4$, $(Mn,Co)_3O_4$ and $(Mn,Co,Ni)_3O_4$ in air

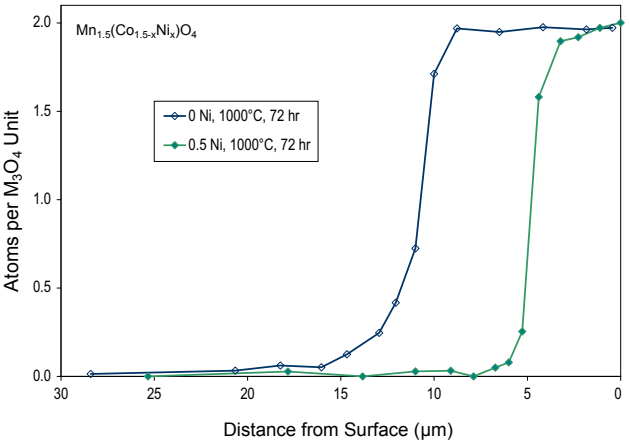

FIGURE 3. Chromium concentration gradient in $Mn_{1.5}Co_{1.5}O_4$ and $Mn_{1.5}CoNi_{0.5}O_4$ after reaction with Cr_2O_3 for 72 hours in air at 1,000°C

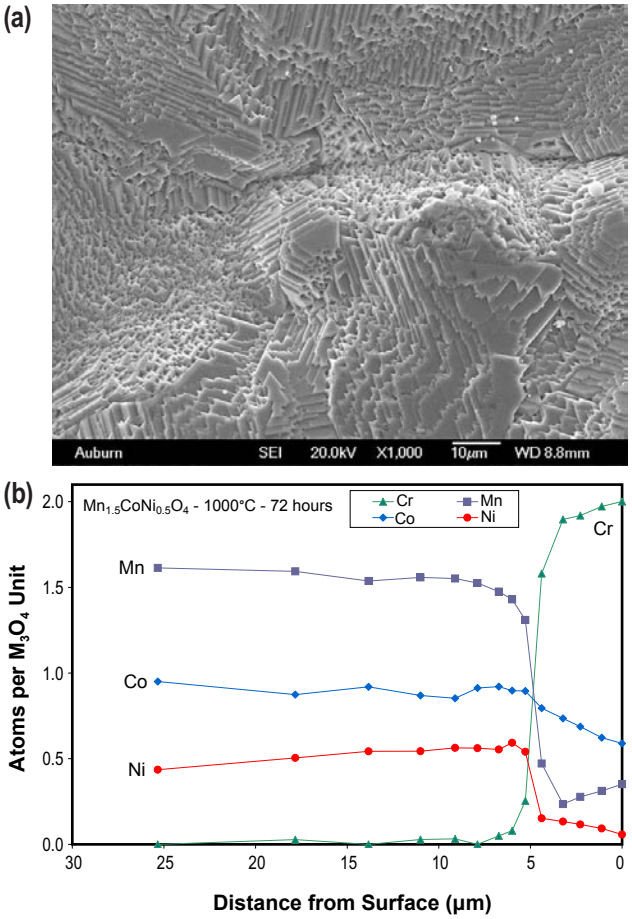

FIGURE 4. Scanning electron microscope micrograph of surface morphology (a) and cross section energy dispersive x-ray spectroscopy composition profile (b) of $Mn_{1.5}CoNi_{0.5}O_4$ after reaction with Cr_2O_3 for 72 hours in air at 1,000°C

The evaluation of the experimental low-chromium alloys provided by Allegheny Technologies Inc. (compositions in Table 1) continued this past year. In particular, the alloys were exposed to dual-atmosphere conditions, in which one side of the alloy was exposed to air and the other side to argon with 5% hydrogen. In each of these experiments a control sample that was exposed to air on all sides was place in the reaction chamber to provide comparison for evaluating the effect of the dual-atmosphere exposure. Figure 5a shows that the iron content in the samples exposed to a dual atmosphere ("air side") is higher than that in the sample exposed only to air ("control"), which is consistent with other reports in the literature [9-11]. The surfaces of the oxide scales contained a network of ridges, which corresponded to the alloy grain boundaries. Figure 5b shows that the manganese concentration in these ridges is higher for both exposure conditions, which suggests that the grain boundaries in the alloy provide a path for manganese diffusion.

TABLE 1. Composition of alloys

Alloy	Concentration (wt%)					
	Fe	Cr	Mn	Si	Ti	Nb
H52	Bal.	13	0.3	0.4	0.2	0.4
H53	Bal.	15	0.3	0.4	0.2	0.4
H54	Bal.	17	0.3	0.4	0.2	0.4
H55	Bal.	18	0.3	0.4	0.2	0.4
AISI 441	Bal.	18	0.4	0.3	0.2	0.5

Some of the alloys were coated with $Mn_{1.5}Co_{1.5}O_4$ at Pacific Northwest National Laboratory using a slurry coating process. The coated alloys were exposed to air at 800°C for 1,600 hours. One notable effect of chromium content shown in Figure 6 was that a significant amount of iron was observed on the surface of the coating for the alloys with low chromium contents (13 and 15 %Cr), while iron was not observed for higher chromium contents (17 and 18 %Cr).

Neutron diffraction of $MnCoCrO_4$ was performed at Oak Ridge National Laboratories to determine the

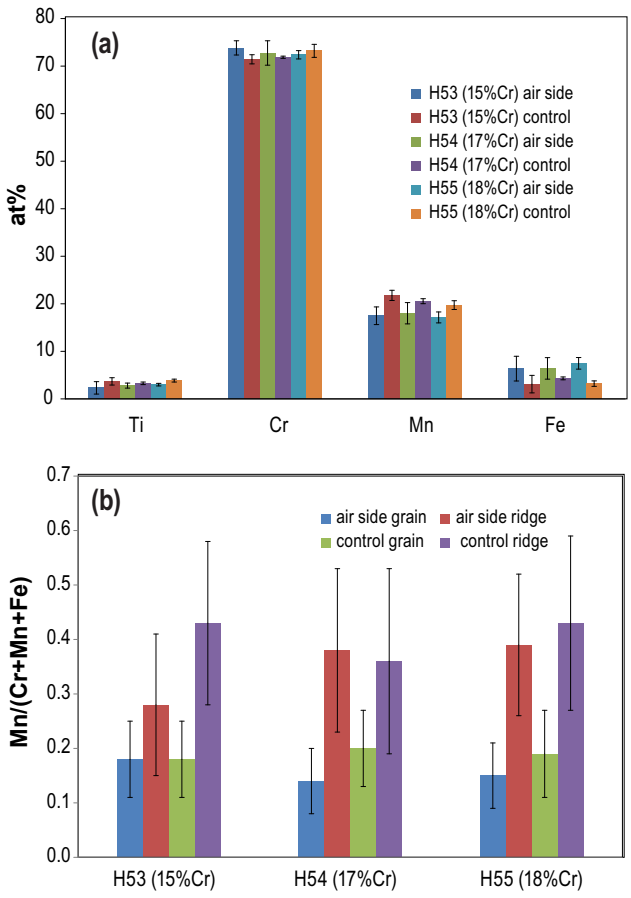

FIGURE 5. Surface composition (a) and manganese proportion (b) in scale formed on alloys with 13-18% Cr after 200 hours in air at 800°C under dual atmosphere (air side) or single atmosphere (control) exposures

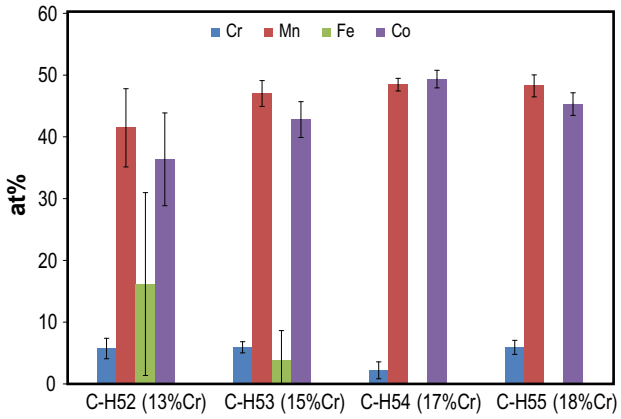

FIGURE 6. Surface composition of $Mn_{1.5}Co_{1.5}O_4$-coated alloys with 13-18% Cr after 1,600 hours in air at 800°C

site occupancy in the spinel structure. Analysis of these results indicated that, as expected, all the chromium occupies octahedral sites, and the occupation on the octahedral sites was 0.50 Cr, 0.39 Mn and 0.11 Co. The occupation on the tetrahedral sites was 0.37 Mn and 0.73 Co. The relative preference of cobalt for the tetrahedral site and manganese for the octahedral site is consistent with previous results [12].

Conclusions and Future Directions

Cobalt and nickel are beneficial to the performance of spinel coating materials and at least 17% chromium in the alloy is needed to minimize outward diffusion of iron.

Work is underway to evaluate the effect of copper additions to the performance of the coating and to compare the reaction of spinel materials with chromia to that with steel. Preliminary results indicate that the presence of dopant materials in the alloy (Mn, Ti) as well and interfacial contact affect the results.

FY 2012 Publications/Presentations

1. K. Wang, Y. Liu, and J.W. Fergus, "Interactions Between SOFC Interconnect Coating Materials and Chromia," *Journal of the American Ceramic Society* 94[12] (2011) 4490-4495.

2. J.W. Fergus, "Solid Oxide Fuel Cells," in *Electrochemical Technologies for Energy Storage and Conversion*, R.-S. Liu, X. Sun, H. Liu, L. Zhang and J. Zhang (Eds.) (Wiley-VCH, 2012) 671-700.

3. Y. Liu, Dileep Kumar C.J., and J. Fergus, "Electrical Properties of Transition Metal-doped $(Mn,Co)_3O_4$ Spinels and Their Interaction with Chromia for SOFC Interconnect Coatings," *Electrochemical Transactions* 45[1] (2012) 421-427.

4. Y. Zhao and J.W. Fergus, "Oxidation Behavior of Stainless Steel 441 and 430 in Dual Atmosphere--Effects of Grain Size," *Electrochemical Transactions* 41[42] (2011) 147-154.

5. J.W. Fergus, Y. Zhao, and Y. Liu, "Optimization of Alloy-Coating Compositions for Use as Solid Oxide Fuel Cell Interconnects," *Materials Research Society Proceedings,* 1384 (2012) b13-22.

6. Dileep Kumar C.J., Y. Liu, J. Ganley, W. Tilson, A. Dekich, and J. Fergus, "Transition Metal Doping of Manganese Cobalt Spinel Oxides for Coating SOFC Interconnects," in *Energy Technology 2012: Carbon Dioxide Management and Other Technologies*, M.D. Salazar-Villalpando, N.R. Neelameggham, D.P. Guilllen, S. Pati and G.K.Krumdick (Eds.), (The Minerals, Metals & Materials Society, 2012) 313-319.

7. Y. Liu, K. Wang, and J.W. Fergus, "Effect of Chromium Doping on the Crystal Structure, Electrical Conductivity and Thermal Expansion of Manganese Cobalt Spinel Oxides," *Advanced in Solid Oxide Fuel Cells VII: Ceramic Engineering and Science Proceedings* 32[4] (2011) 125-129.

8. J.W. Fergus, K. Wang, and Y. Liu, "Effect of Titanium and Iron Additions on the Transport Properties of Manganese Cobalt Spinel Oxide," *Ceramic Transactions* 227 (2011) 33-37.

9. J.W. Fergus, Y. Liu, and Y. Zhao, "Manganese Cobalt Spinel Oxide Based Coatings for SOFC Interconnects," *Ceramic Transactions* [Advanced in Materials Science for Environmental and Energy Technologies] (2012) in press.

References

1. Y. Larring and T. Norby, "Spinel and Perovskite Functional Layers Between Plansee Metallic Interconnect (Cr-5 wt% Fe-1 wt% Y_2O_3) and Ceramic $(La_{0.85}Sr_{0.15})_{0.91}MnO_3$ Cathode Materials for Solid Oxide Fuel Cells," *J. Electrochem. Soc.* Vol. 147, 2000, pp. 3251-3256.

2. Z. Yang, G.-G. Xia, G.D. Maupin, and J.W. Stevenson, "Conductive Protection Layers on Oxidation Resistance Alloys for SOFC Interconnect Applications," *Surf. Coating Tech.,* Vol. 201, 2006, pp. 4476-4483.

3. M.R. Bateni, P. Wei, X. Deng, and A. Petric, "Spinel Coatings for UNS 430 Stainless Steel Interconnects," *Surf. Coating Tech.* Vol. 201, 2007, pp. 4677-4684.

4. M.J. Garcia-Vargas, M. Zahid, F. Tietz and A. Aslanides, "Use of SOFC Metallic Interconnect Coated with Spinel Protective Layers Using the APS Technology," *ECS Trans.* Vol. 7, 2007, pp. 2399-2405.

5. H. Kurokawa, C.P. Jacobson, L.C. DeJonghe, and S.J. Visco, "Chromium Vaporization of Bare and of Coated Iron-Chromium Alloys at 1073 K," *Solid State Ionics* Vol. 178, 2007, pp. 287-296.

6. C. Collins, J. Lucas, T.L. Buchanan, M. Kopczyk, A. Kayani, P.E. Gannon, M.C. Deibert, R.J. Smith, D.-S. Choi, and V.I. Gorokhovsky, "Chromium Volatility of Coated and Uncoated Steel Interconnects for SOFCs," *Surf. Coating Tech.* Vol. 201, 2006, pp. 4467-4470.

7. Z. Yang, G.-G. Xia, H.-H. Li, and J.W. Stevenson, "$(Mn,Co)_3O_4$ Spinel Coatings on Ferritic Stainless Steels for SOFC Interconnect Applications," *Int. J. Hydrogen Energy,* Vol. 32, 2007, pp. 3648-3654.

8. Z. Yang, G. Xia, and J.W. Stevenson, "$Mn_{1.5}Co_{1.5}O_4$ Spinel Protection Layers on Ferritic Stainless Steels for SOFC Interconnect Applications," *Electrochem. Solid-State Lett.* Vol. 8, 2005, pp. A168-A170.

9. Z.G. Yang, M.S. Walker, P. Singh, and J.W. Stevenson, "Anomalous Corrosion Behavior of Stainless Steel under SOFC Interconnect Exposure Conditions," *Electrochem. Solid-State Lett.* Vol. 6, 2003, pp. B35-B37.

10. Z. Yang, G.-G. Xia, M. S. Walker, C.-M. Wang, J.W. Stevenson, and P. Singh, "High Temperature Oxidation/ Corrosion Behavior of Metals and Alloys Under a Hydrogen Gradient," *Int. J. Hydrogen Energy***,** Vol. 32, 2007, pp. 3770-3777.

11. J. Rufner, P. Gannon, P. White, M. Deibert, S. Teintze, R. Smith, and H. Chen , "Oxidation Behavior of Stainless Steel 430 and 441 at 800°C in Single (Air/Air) and Dual Atmosphere (Air/Hydrogen) Exposures," *Int. J. Hydrogen Energy,* Vol. 33, 2008, pp. 1392-1398.

12. A. Purwanto, A. Fajar, H. Mugirahardjo, J.W. Fergus, and K. Wang, "Cation Distribution in Spinel $(Mn,Co,Cr)_3O_4$ at Room Temperature," *J. Appl. Cryst.*,Vol. 43, 2010, pp. 394-400.

III.C.2 Electrodeposited Mn-Co Alloy for Solid Oxide Fuel Cell Interconnects

Heather McCrabb (Primary Contact), Tim Hall
Faraday Technology, Inc.
315 Huls Drive
Clayton, OH 45315
Phone: (937) 836-7749; Fax: (937) 836-9498
Email: heathermccrabb@faradaytechnology.com

DOE Project Manager: Briggs White
Phone: (304) 719-5116
Email: Briggs.White@netl.doe.gov

Subcontractor:
West Virginia University, Morgantown, WV

Contract Number: FE0006165

Start Date: October 1, 2010
End Date: September 30, 2012

Fiscal Year (FY) 2012 Objectives

- Scale-up coating process from 25 cm^2 to 100 cm^2 interconnects.
- Complete process development for planar solid oxide fuel cell (SOFC) interconnects.
- Begin process development for SOFC interconnects with gas flow field structures.

FY 2012 Accomplishments

- Continued optimization of FARADAYIC^{SM} electrodeposition process parameters in order to optimize coating thickness, coating composition and coating adhesion.
- Improved coating uniformity across T441 planar interconnects at the 100 cm^2 scale.
- Demonstrated coating process for 25 cm^2 430 stainless steel interconnect containing gas flow fields.
- Continued refinement of economic analysis to assess economic viability of FARADAYIC^{SM} electrodeposition process for high-volume batch manufacturing.

Introduction

Commercialization of SOFCs requires low-cost components, materials, and manufacturing processes. Specifically, the interconnect material and coating used in SOFCs represent 45% of the total material cost for the typical stack [1]; therefore, it is desirable that new materials and manufacturing technologies be developed that effectively increase system durability while decreasing production costs. The decrease in the SOFC operating temperatures from 1,000ºC to between 800°C and 850ºC has enabled the use of less expensive chromia-forming ferritic stainless steels as interconnects instead of ceramic interconnects. However, even newly developed ferritic alloys such as SS441 cannot completely eliminate the chromia scale growth and chromium evaporation into cells, which can cause unacceptable degradation in the SOFC electrochemical performance. One attractive method to resolve the chromia scale growth and diffusion issues is to electrodeposit a Mn-Co alloy coating onto the interconnect surface and subsequently convert it to a $(Mn,Co)_3O_4$ spinel.

Faraday and West Virginia University are working to develop, optimize, and validate the FARADAYIC^{SM} electrodeposition process as an effective and economical manufacturing method for coating stainless steel interconnects used in SOFC stacks with Mn-Co alloys. The FARADAYIC^{SM} process utilizes pulse and pulse reverse waveforms for manufacturing the interconnect coatings. A preliminary economic analysis based on using batch manufacturing suggests that the innovative coating technology can meet U.S. Department of Energy's high volume target of 1.6 million plates per annum for 250 MW of fuel cell stacks at a cost of ~$1.85 per 625 cm^2 coated interconnect.

Approach

The FARADAYIC^{SM} electrodeposition process is a pulse/pulse reverse plating process that controls the electric field and the boundary layer to reduce gradients (composition, thickness, or morphology) in the formed coating. The novel aspect of this technology is the manner in which the electric field and double layer are controlled and how these parameters can inherently control the properties of the coating. For instance, when using a direct current overpotential for deposition, the composition, thickness, and morphology

of the deposit is controlled by the surface texture of the substrate/electrode. With the use of the FARADAYIC[SM] electrodeposition process, the electric field can be tuned to reduce effects of the substrate and obtain better overall control of the deposit's properties. The main advantages of the proposed technology, as compared to conventional, direct current electrodeposition, are:

- Enhanced process control: because the process proceeds only under the influence of an electric field, the processing time is exact and uniform across the plate.
- Enhanced surface structure and thickness control: the Faradyaic[SM] process parameters can be selected to minimize the diffusion boundary layer, decreasing the effect of substrate surface morphology on the deposit properties across an area.

Results

Mn-Co coatings were electrodeposited using pulse and pulse-reverse waveform parameters, onto 100 cm^2 planar T441 stainless steel substrates (Figure 1) as well as 25 cm^2 430 stainless steel substrates with gas flow field features from a sulfate based electrolyte containing ammonium sulfate, boric acid, and sodium gluconate. The electrolyte flow rate and spacing between the anode and the interconnect substrate (i.e., the cathode) were held constant at 2 GPM and 4 cm respectively. The anode to cathode area ratio was 1:1. Prior to deposition experiments, the T441 stainless steel substrate was grit blasted with alumina followed by an acid pickle to remove the oxide from the surface. Subsequent to the deposition experiments, the coatings were subjected to a ramped heating schedule for spinel growth.

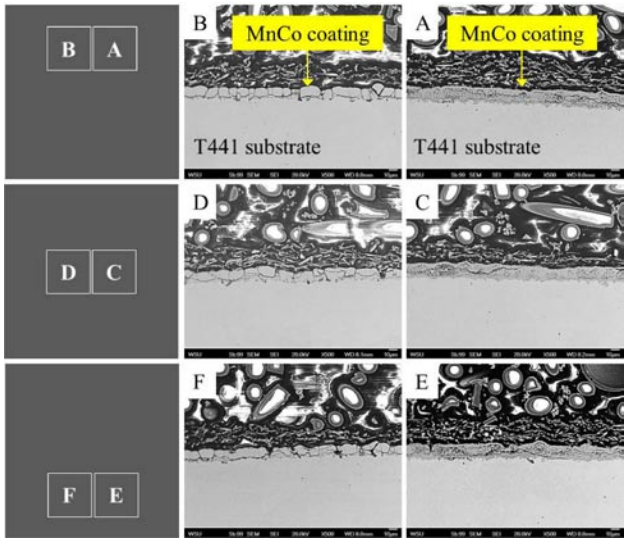

FIGURE 1. SEM images for Mn-Co coating cross sections from selected areas of a 100 cm^2 planar T441 SOFC interconnect. The left column contains a schematic illustration depicting the area of the interconnect analyzed. The Mn-Co coating for sections B, D, and F (center column) was analyzed in the as-deposited state, was ~12 μm thick and contained a dense but vertically cracked coating. The Mn-Co coating for Sections A, C, and E (right column) was analyzed after thermal oxidation at 850°C for 72 hours. The coating was ~15 μm thick and displayed more coating porosity, though vertical microcracks were no longer evident.

Faraday has successfully scaled up the FARADAYIC[SM] electrodeposition process for coating planar T441 SOFC interconnects measuring 26 cm^2 to 103 cm^2 while maintaining both coating thickness and compositional uniformity across the substrate surface. From the scanning electron microscopy (SEM) analysis of a cross section of the coating from various areas of the substrate, it can be seen that the as-deposited coating is relatively uniform in thickness at approximate 12 μm and dense, though with the presence of many vertical micro-cracks. After thermal exposure for spinel conversion, the coating thickness is ~15 μm, and the microstructure becomes highly crystalline with many of the through-cracks closed due to grain diffusion and spinel growth. Energy dispersive X-ray spectroscopy (EDS) indicates that the coating is cobalt rich in both the as-deposited state as well as post-thermal treatment (Figure 2). The chromia layer that grows at the interface between the substrate and the coating is approximately two microns thick after spinel conversion and a thermal soak at 850°C for 72 hours, though the chromium detected at the coating surface is negligible (Figure 2, right). Faraday continues the coating development work to increase the Mn content in the coating to reduce the coating cost and aid in the prevention of outward chromium diffusion.

In addition to coating planar T441 substrates, Faraday performed initial coating demonstration experiments on Stainless Steel 430 patterned interconnect substrates to illustrate the process capability for coating recessed surfaces and sidewalls for gas flow field channels. The channel and landing widths measured 0.85 mm and the channel depth was ~0.5 mm. SEM images of a coated channel and landing are provided in Figure 3. These images suggest that the FARADAYIC[SM] electrodeposition process provides adequate coating coverage of the channels and landings. Interestingly, the coating is thickest in the channel recess and thinner along the top sidewalls and landing surfaces (Figure 3). Work is on-going to improve the coating coverage uniformity across the gas flow field features.

Finally, Faraday continues to examine and refine the preliminary manufacturing throughput and cost analysis for implementing the FARADAYIC[SM] electrodeposition process for high volume manufacturing of Mn-Co spinel interconnect coatings. The cost analysis considers a throughput assessment of a batch manufacturing process for an annual production volume of 250 MW of fuel cell

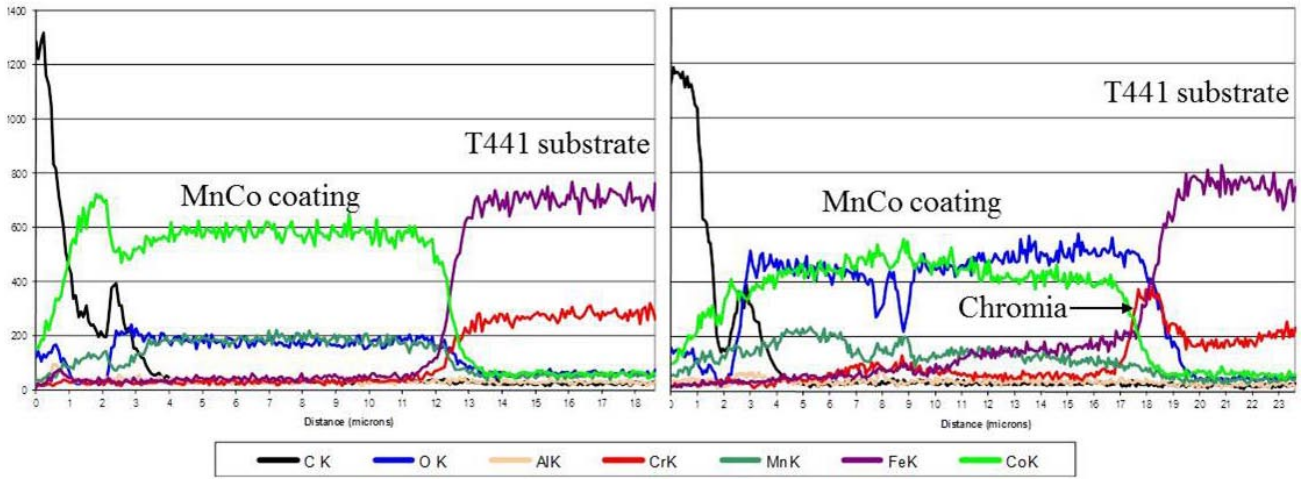

FIGURE 2. Results of EDS line scans for Mn-Co coating cross sections from selected areas of a 100 cm^2 planar T441 SOFC interconnect. In each graph, the coating surface is on the left side at a distance value of zero, and the substrate is on the right side as evident from the sharp increase in the iron signal. The graph on the left is for the as-deposited Mn-Co coating and depicts a coating rich in cobalt. As expected, there is no chromium signal (red line) detected within the coating, only within the substrate. The graph on the right is after thermal oxidation at 850°C for 72 hours. A 2 μm chromia layer is detected at the interface between the coating and the substrate, but the chromium signal at the coating surface is negligible.

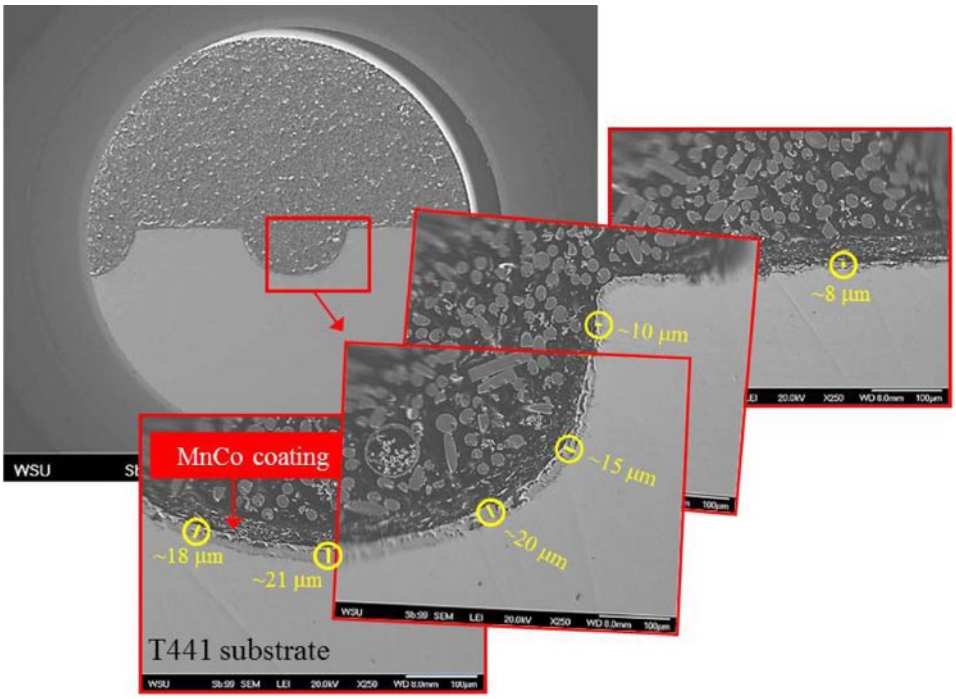

FIGURE 3. SEM images for Mn-Co coating cross sections from a 25 cm^2 SS430 SOFC interconnect containing gas flow fields with channel and landing widths measuring 0.85 mm and a channel depth of 0.5 mm. The upper left image provides a low magnification image of the interconnect channels and landings, but the coating is not visible. The high magnification images stitched together on the bottom right side of the figure show a continuous Mn-Co coating within the channel as well as upon the sidewalls and landings. Interestingly, the coating is thickest in the channel recess and thinner along the top sidewalls and landing surfaces.

stacks. The current cost analysis of the FARADAYIC^{SM} electrodeposition process based upon manufacturing 1.6 million plates per annum was increased from ~$1.23 per coated interconnect reported in FY 2011 to $1.85 per coated interconnect due to revisions in several parameters that comprise the cost analysis. The cobalt

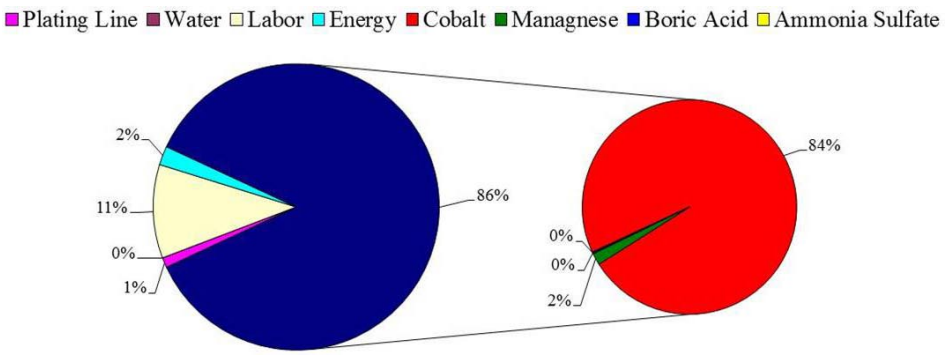

FIGURE 4. Economic assessment of coating process based upon batch manufacturing of 1.6 million plates per annum at a cost of ~$1.85 per 625 cm^2 coated interconnect.

sulfate heptahydrate continues to dominate the coating cost representing 84% of the overall coating cost (Figure 4). It is expected that as Faraday continues to optimize the FARADAYIC^{SM} electrodeposition process for coating the SOFC interconnects, Faraday will to update the cost estimate to reflect changes in the process.

Conclusions and Future Directions

A cost effective process to apply high-quality coatings to SOFC interconnects in a mass production scenario is being developed. The FARADAYIC^{SM} electrodeposition process can be used to deposit a Mn-Co alloy with a controlled composition and thickness that can subsequently be converted to a spinel by thermal exposure at high temperatures in an oxidizing environment. Faraday has scaled its process capabilities from 25 cm^2 to 100 cm^2 SOFC interconnects and demonstrated the ability to coat interconnects containing gas flow field features. Continued analysis and refinement of the economic assessment suggests that the FARADAYIC^{SM} electrodeposition process continues to remain cost competitive with other industrial manufacturing processes under consideration for these types of interconnect coatings.

Development of the FARADAYIC^{SM} electrodeposition process is still in progress with the following activities planned:

- Development, optimization and validation of the FARADAYIC^{SM} electrodeposition process for 100 cm^2 interconnects with gas flow field features.
- Long-term on-cell performance evaluation of button cells.
- Qualification/demonstration of interconnect coating in single cell test rig under ideal SOFC operating conditions by potential commercial partners.
- Continued development of a more comprehensive economic assessment of the electrodeposition coating process as it relates to interconnect manufacturing.

Special Recognitions & Awards/Patents Issued

1. R. Gemmen, T. Hall, C. Johnson, X. Liu, H. McCrabb, J. Wu, "Electroplated Mn-Co Coating for Solid Oxide Fuel Cell Interconnects," National Energy Technology Laboratory, USA, West Virginia University and Faraday Technology, R&D 100 Award, 2011.

FY 2012 Publications/Presentations

1. T.D. Hall, H.A. McCrabb, J. Wu, H. Zhang, X. Liu, J. Kell, B. Kagajwala, S. Snyder, and E.J. Taylor, "Electrodeposited CoMn Alloy onto Stainless Steel Interconnects for Increased Lifetimes in SOFCs," *ECS Trans*. 41 (33), 137, 2012.

2. T.D. Hall, H.A. McCrabb, J. Wu, H. Zhang, X. Liu, J. Kell, B. Kagajwala, S. Snyder, and E.J. Taylor, "Electrodeposited CoMn Alloy onto Stainless Steel Interconnects for Increased Lifetimes in SOFCs," Oral Presentation at the 220th Meeting of the Electrochemical Society, Boston, Massachusetts, October 2011.

3. H.A. McCrabb, T.D. Hall, J.W. Kell, S. Snyder, H. Zhang, X. Liu, E.J. Taylor, "Electrodeposition of SOFC Interconnect Coatings," Oral Presentation at the 12th Annual SECA Workshop, Pittsburgh, Pennsylvania, July 2011.

4. H.A. McCrabb, T.D. Hall, J.W. Kell, S. Snyder, H. Zhang, X. Liu, E.J. Taylor, "Electrodeposited Mn-Co Alloy Coating For SOFC Interconnects," Poster Presentation at the 12th Annual SECA Workshop, Pittsburgh, Pennsylvania, July 2011.

References

1. Eric J. Carlson, Suresh Sriramulu, Peter Teagan, Yong Yang, "Cost Modeling of SOFC Technology," First International Conference on Fuel Cell Development and Deployment, University of Connecticut, Storrs, Connecticut, March 10, 2004.

III.C.3 Development of SOFC Interconnects and Coatings

Jeff Stevenson (Primary Contact), Gordon Xia, and Ryan Scott
Pacific Northwest National Laboratory
P.O. Box 999, MS K2-44
Richland, WA 99352
Phone: (509) 372-4697; Fax: (509) 375-2186
Email: jeff.stevenson@pnnl.gov

DOE Project Manager: Briggs White
Phone: (304) 285-5437
Email: Briggs.White@netl.doe.gov

Contract Number: FWP40552

Start Date: October 1, 2011
End Date: September 30, 2012

Fiscal Year (FY) 2012 Objectives

- Develop cost-effective, optimized materials for intermediate temperature solid oxide fuel cell (SOFC) interconnect applications.
- Identify, understand, and mitigate degradation processes in interconnects and at interconnect interfaces.

FY 2012 Accomplishments

- Evaluated long-term performance of spinel-coated ferritic stainless steel interconnect materials at 800ºC and 850ºC.
- Evaluated performance of protective coatings with reduced (or zero) cobalt content.

Introduction

In previous work at Pacific Northwest National Laboratory (PNNL), $(Mn,Co)_3O_4$ (MC) spinels have been systematically investigated and applied as protection layers on a variety of candidate SOFC interconnect steels. In recent years, the primary emphasis has been on the application of spinel coatings to American Iron and Steel Institute (AISI) 441, ferritic stainless steel. AISI 441 is prepared via conventional melt metallurgy and is therefore less expensive than candidate steels that utilize vacuum processing to reduce the Si content to very low levels. Additions of Nb and Ti to the AISI 441 tie up residual Si in Laves phase at grain boundaries, eliminating the need for expensive processing. To mitigate scale adhesion issues, a Ce-modified MC (Ce-MC) coating, e.g., $Ce_{0.02}Mn_{1.49}Co_{1.49}O_4$, was developed, which combines the advantages of rare earth (RE) surface treatment or bulk addition with those of the MC spinel coating. The stability and electrical performance of AISI 441 coated with Ce-MC protection layers were validated in long-term (>1 year) testing. These tests indicated that the spinel protection layers helped minimize the interfacial electrical resistance and mitigate the scale growth beneath the spinel coatings on AISI 441. In addition, the Ce-modified coatings improved the scale adherence and interconnect surface stability.

Approach

To extend and confirm previous test results, long-term area-specific resistance (ASR) tests are being carried out to evaluate the long-term performance and structural stability of Ce-MC coatings on AISI 441. The AISI 441 was manufactured by Allegheny Ludlum. MC and Ce-MC spinel powders (fabricated at PNNL) were applied to alloy coupons using a slurry-based approach and heat-treated to form protective coatings. The electrical resistance of bare and coated AISI 441 is measured by applying a four-probe direct current measurement technique to simulated interconnect/coating/contact material/cathode structures. In addition to baseline testing of spinel-coated AISI 441 at 800ºC, the effects of (a) physical surface modifications to the AISI 441, and (b) higher exposure temperature (850ºC) are being studied. Alternative protective coating compositions are also being developed and evaluated, with an emphasis on reduction of coating cost, e.g., reduction of Co content.

Results

Figure 1 shows long-term ASR test results for bare (uncoated) AISI 441 and Ce-MC coated AISI 441 at 800ºC. Some tests are still in progress. In contrast to the bare AISI 441, the ASR of the Ce-MC coated AISI 441 remained low over time, indicating good stability of the coated steel coupons. Preliminary oxidation studies were also performed on coated AISI 441 coupons at 800°C and 850ºC. As expected, the oxidation rates were faster at the higher temperature, and spallation was observed at the scale/alloy interface of some coated AISI 441 coupons after heat treatment at 850ºC. No obvious differences in coating/scale/alloy chemistry were observed during post-test scanning electron microscopy (SEM)/energy dispersive spectroscopy (EDS) analysis, suggesting

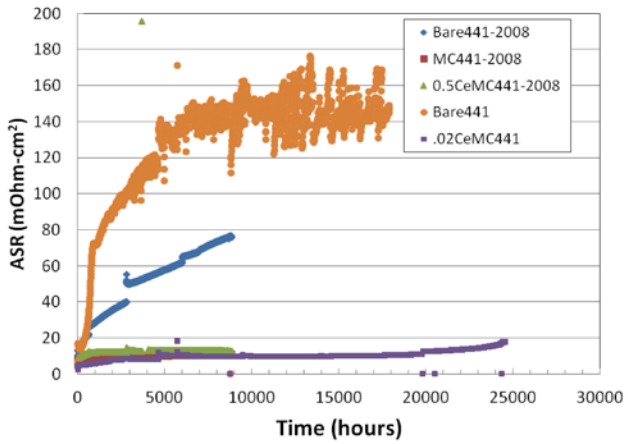

FIGURE 1. Area specific resistance of bare and Ce-MC coated AISI 441 at 800°C in air

that the spallation may have been primarily related to increased thermal stresses due to coefficient of thermal expansion (CTE) mismatch, resulting from increased oxide scale thickness at the higher temperature.

To mitigate possible spallation issues, a variety of physical surface modifications to the AISI 441 are being investigated. Allegheny Ludlum provided sheet stock (0.02" thick) of AISI 441 with the following five surface conditions:

- Mill reference (unmodified)
- De-siliconized (treated to sequester and remove silicon from the near surface of the sheet; an alternative to decreasing the Si content of the alloy)
- Surface blasted (subjected to a grit/shot blast process to produce surface deformation)
- Surface ground (subjected to surface abrasion to produce surface deformation)
- Temper-rolled (subjected to a cold rolling process)

Coupons of the surface-treated steel were coated with Ce-MC spinel and subjected to oxidation testing in air at 800ºC. At 2,000 hour intervals, the coupons were cooled down to room temperature and examined. One coupon from each surface treatment was removed from the study for SEM evaluation, while the rest of the coupons were reheated to 800ºC for continued testing.

After 2,000 hours, no coating/scale spallation was observed on any of the specimens. After another 2,000 hours (total oxidation time of 4,000 hours), the coupons were again cooled to room temperature and examined. Spallation was not observed on any coupons, except for on one (out of 14) mill reference coupon. After another 2,000 hours (total oxidation time of 6,000 hours), the coupons were again cooled and examined. Extensive spallation was observed on the mill reference coupons; in addition, one of the surface-treated coupons (a de-siliconized 441 coupon) exhibited spallation. Also, SEM analysis of the coupons removed from the study at that time revealed complete de-bonding of the oxide scale of the temper-rolled coupon, possibly due to stresses occurring during the metallographic preparation of the sample. After another 2,000 hours (total oxidation time of 8,000 hours), the last of the mill reference coupons exhibited spallation, but no spallation was observed on the surface-modified coupons. Similar to the 6,000-hour results, no spallation was observed during visual examination of the temper-rolled coupon, but SEM analysis revealed complete de-bonding of the oxide scale from the alloy substrate. After another 2,000 hours (total oxidation time of 10,000 hours), no spallation was observed on the samples, although once again cross-section SEM analysis indicated de-bonding at the alloy/scale interface for the temper-rolled coupon. After another 2,000 hours (total oxidation time of 12,000 hours at 800ºC), no spallation was observed, except for localized spallation on one of the remaining surface ground coupons. Localized scale de-bonding was also evident on the surface ground coupon examined with the SEM. After another 2,000 hours (total oxidation time of 14,000 hours at 800ºC), no spallation was observed. Cross-section SEM montages of the coupons removed from the study for SEM/EDS analysis are shown in Figure 2. Localized scale de-bonding was evident for the de-siliconized coupon. SEM/EDS analysis on the 14,000-hour surface-blasted sample indicated minimal diffusion of Cr from the alloy and scale into the protective coating (Figure 3). Table 1 summarizes the 800ºC oxidation results for the various surface treatments. Overall, surface blasting appears to offer the greatest degree of improvement in oxide scale adhesion.

A similar set of coupons of the spinel-coated surface treated steel was subjected to oxidation testing in air at 850ºC. After 4,000 hours of oxidation (performed in two 2,000 hour intervals), no spallation was observed,

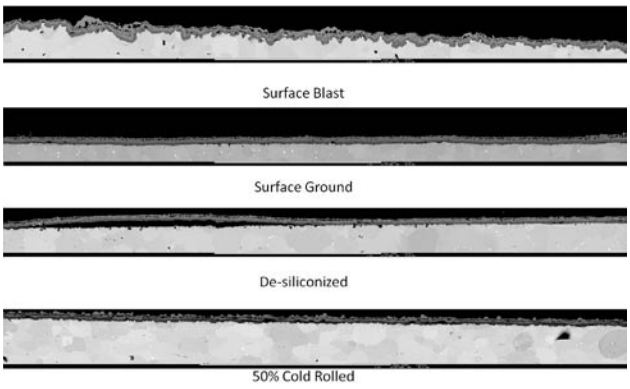

FIGURE 2. SEM cross-section montages of 800°C, 14,000 hour samples

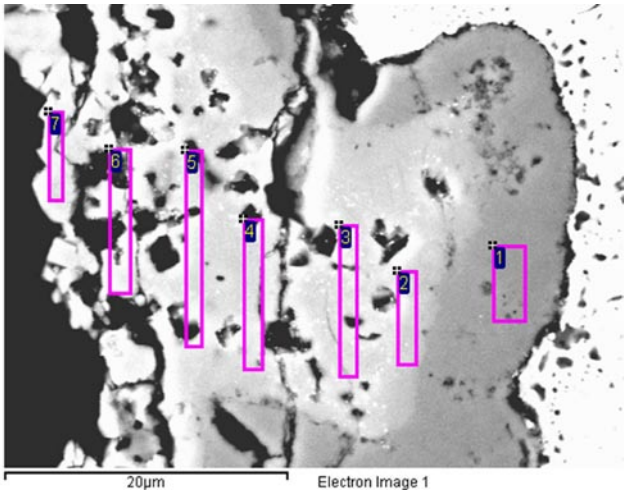

Spectrum	In stats.	O	Si	Ti	Cr	Mn	Fe	Co	Ce
1	Yes	66.09		1.12	**32.56**		0.23		
2	Yes	62.93		0.60	**13.42**	9.97	1.60	11.49	
3	Yes	61.90		1.32	**2.29**	18.45	2.52	13.22	0.30
4	Yes	60.96		1.02	**3.03**	18.77	2.64	13.58	
5	Yes	60.60		0.73	**3.78**	18.14	2.56	13.90	0.29
6	Yes	59.79	0.58	0.62	**2.81**	19.12	2.78	13.94	0.37
7	Yes	61.61	0.24	0.44	**2.24**	19.64	2.39	13.43	
Max.		66.09	0.58	1.32	32.56	19.64	2.78	13.94	0.37
Min.		59.79	0.24	0.44	2.24	9.97	0.23	11.49	0.29

FIGURE 3. SEM/EDS results from cross-sectional analysis of an 800ºC, 14,000 hour surface-blasted coupon (element concentrations in atomic %)

although SEM analysis of a mill reference 4,000 hour coupon removed from the study revealed signs of incipient de-bonding at the scale/alloy interface. After another 2,000 hours (total oxidation time of 6,000 hours), no spallation was observed, although cross-section SEM analysis of a mill reference coupon removed from the study revealed extensive de-bonding at the scale/alloy interface. After another 2,000 hours (total oxidation time of 8,000 hours), no spallation was observed, although cross-section SEM analysis of two coupons (mill reference and de-siliconized) revealed de-bonding at the scale/alloy interface. After another 2,000 hours (total oxidation time of 10,000 hours at 850ºC), spallation was observed on mill reference and temper-rolled coupons. Cross-section SEM montages of the coupons removed from the study for SEM/EDS analysis are shown in Figure 4. Extensive scale de-bonding was evident for the de-siliconized coupon. SEM/EDS analysis on the 10,000 hour surface-blasted sample indicated minimal diffusion of Cr from the alloy and scale into the protective coating (see Figure 5). Table 2 summarizes the 850ºC oxidation results for the various surface treatments. The surface grind and surface blast processing appear to offer improved oxide scale adhesion compared to the other surface modification processes.

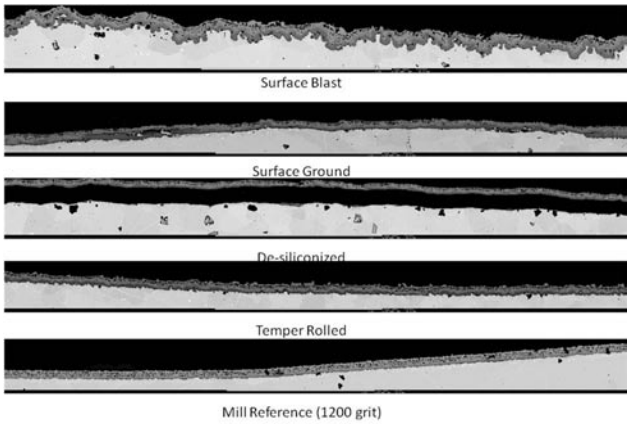

FIGURE 4. SEM cross-section montages of 850ºC, 10,000 hour samples

TABLE 1. Summary of results of 800°C oxidation study

Time (h)	Mill Reference (1200 grit)		Temper Rolled		De-siliconized		Surface Grind		Surface Blast	
	Macroscopic Spallation	Microscopic De-bonding	Macroscopic Spallation	Microscopic De-bonding	Macroscopic Spallation	Microscopic De-bonding	Macroscopic Spallation	Microscopic De-bonding	Macroscopic Spallation	Microscopic De-bonding
2000										
4000	X									
6000	X			C	X					
8000	X			C						
10000	XX			C						
12000	XX						X	L		
14000	XX					L				

X - Spallation on at Least One Coupon
XX - No Unspalled Coupons Left in Study
C - Complete De-bonding of Scale of SEM/EDS Sample
L - Localized De-bonding of Scale of SEM/EDS Sample

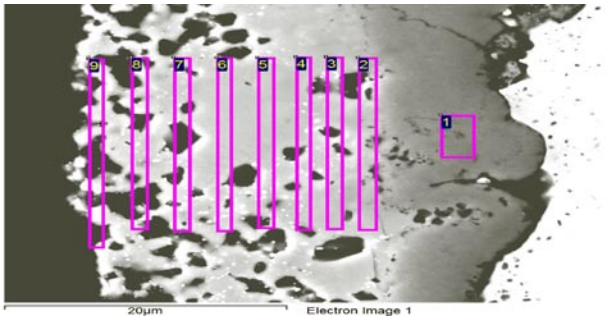

Spectrum	In stats.	O	Si	Ti	Cr	Mn	Fe	Co	Ce
1	Yes	64.99	0.49	0.78	**33.58**		0.16		
2	Yes	63.67	0.96	0.22	**16.91**	7.61	0.86	9.77	
3	Yes	62.05	1.01	0.27	**8.28**	14.05	1.75	12.59	
4	Yes	62.12	0.71	0.32	**5.67**	16.17	1.87	12.85	0.30
5	Yes	62.19		0.31	**5.68**	16.47	1.91	13.20	0.24
6	Yes	62.18		0.31	**4.67**	17.43	1.83	13.58	
7	Yes	59.57	0.71	0.31	**3.75**	19.06	2.11	14.15	0.34
8	Yes	59.72		0.32	**3.49**	19.39	2.14	14.59	0.36
9	Yes	58.86		0.26	**3.69**	19.48	2.27	14.95	0.50
Max.		64.99	1.01	0.78	33.58	19.48	2.27	14.95	0.50
Min.		58.86	0.49	0.22	3.49	7.61	0.16	9.77	0.24

FIGURE 5. SEM/EDS results from cross-sectional analysis of an 850°C, 10,000 hour surface-blasted coupon (element concentrations in atomic %)

As mentioned above, alternative protective coating compositions are also being developed and evaluated, with an emphasis on reduction of coating cost by reducing or eliminating the cobalt content. Preliminary results on cobalt-free Mn-Fe-Cu-O protection coatings demonstrated satisfactory coating densities; and, electrical testing with lanthanum strontium cobalt ferrite (LSCF) as the simulated cathode and contact material indicated relatively low and stable ASR, as shown in Figure 6.

Conclusions and Future Directions

Ce-MC coated AISI 441 is a promising alloy/coating combination for intermediate temperature SOFC interconnect applications. Based on oxidation testing

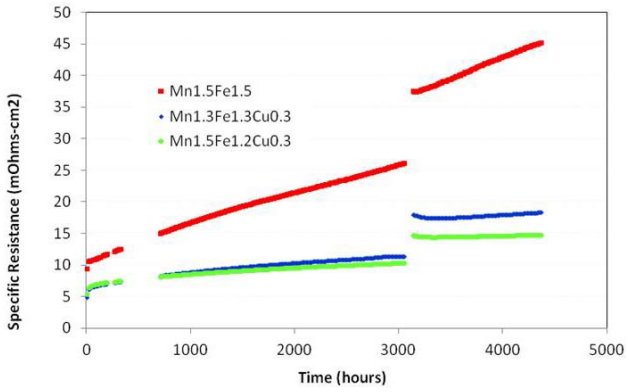

FIGURE 6. Area specific resistance of Mn-Fe-Cu oxide coated AISI 441 with LSCF simulated cathode and contact material at 800ºC in air. The Mn-Fe-Cu protection layers were formed in situ using metal precursor powders. (a) $Mn_{1.5}Fe_{1.5}O_4$ (red line); (b) $Mn_{1.35}Fe_{1.35}Cu_{0.3}O_4$ (blue line); and (c) $Mn_{1.5}Fe_{1.2}Cu_{0.3}O_4$ (green line).

at 800ºC and 850ºC, surface modifications to AISI 441, performed prior to application of the Ce-MC coating, appear to be a viable means of extending interconnect life by delaying the onset of scale/substrate de-bonding. Should it become necessary to avoid the use of cobalt in the protective coatings, due to cost or availability issues, compositions in the Mn-Fe-Cu-O system may prove to be viable alternatives. Future research directions include continued long-term oxidation testing at 800ºC and 850ºC to determine upper service limits for the coated AISI 441, optimization of surface modification process parameters, and optimization of spray-based fabrication processes for protective interconnect coatings.

FY 2012 Publications/Presentations

1. J.P. Choi, K.S. Weil, Y.S. Chou, J.W. Stevenson, and Z.G. Yang, "Development of MnCoO Coating with New Aluminizing Process for Planar SOFC Stacks," Int. J. Hydrogen Energy, 36, 4549 (2011).

TABLE 2. Summary of results of 850ºC oxidation study

Time (h)	Mill Reference (1200 grit)		Temper Rolled		De-siliconized		Surface Grind		Surface Blast	
	Macroscopic Spallation	Microscopic De-bonding	Macroscopic Spallation	Microscopic De-bonding	Macroscopic Spallation	Microscopic De-bonding	Macroscopic Spallation	Microscopic De-bonding	Macroscopic Spallation	Microscopic De-bonding
2000										
4000										
6000		C								
8000		C				C				
10000	X		X			C				

X - Spallation on at Least One Coupon
C - Complete De-bonding of Scale of SEM/EDS Sample

2. J.P. Choi, J.W. Stevenson, R.C. Scott, and Y.S. Chou, "The Effect of MnCoO-CeO Spinel Coating Thickness on Electrical Conductivity at Long-term SOFC Operating Condition," Materials Science and Technology Conference and Exhibition, Columbus, Ohio, October, 2011.

3. Y.S. Chou, E.C. Thomsen, J.P. Choi, G.G. Xia, and J.W. Stevenson, "Long-term Solid Oxide Fuel Cell Candidate Material Evaluation in a 3-Cell Short Stack Geometry at Pacific Northwest National Laboratory," Fuel Cell Seminar and Exhibition, Orlando, Florida, November, 2011.

4. Y.S. Chou, E.C. Thomsen, J.P. Choi, J.W. Stevenson, G.G. Xia, J.F. Bonnett, and W.E. Voldrich, "Long-term Evaluation of Ce-Modified (Mn,Co) Spinel Coating for SOFC Application in a 3-Cell Short Stack Geometry," 36th International Conference and Exposition on Advanced Ceramics and Composites (ICACC), Daytona Beach, Florida, January, 2012.

5. J.P. Choi, J.W. Stevenson, R.C. Scott, and Y.S. Chou, "Coating Optimization of MnCoO-CeO Spinel and the Effect of Thickness on Electrical Conductivity," 36th International Conference and Exposition on Advanced Ceramics and Composites (ICACC), Daytona Beach, Florida, January, 2012.

III. SECA CORE TECHNOLOGY R&D

D. Seals

III.D.1 Viscous Glass/Composite SOFC Sealants

Scott Misture (Primary Contact), James Shelby
NYS College of Ceramics at Alfred University
2 Pine St., Binns-Merrill Hall
Alfred, NY 14802
Phone: (607) 871-2438; Fax: (607) 871-2354
Email: misture@alfred.edu

DOE Project Manager: Joseph Stoffa
Phone: (304)285-0285
Email: Joseph.Stoffa@netl.doe.gov

Contract Number: NT0005177

Start Date: October 1, 2011
End Date: September 30, 2012

Fiscal Year (FY) 2012 Objectives

- Extend glass compositional ranges for study and produce candidate glasses.
- Perform compatibility testing for the sealants in contact with stainless steel (SS) interconnects and zirconia based electrolyte (8YSZ) materials.
- Evaluate the material stability in solid oxide fuel cell (SOFC) operating environments including different operating temperatures/temperature cycles and different atmospheres (air/hydrogen, and water vapor in the atmospheres).

FY 2012 Accomplishments

- Identified four candidate glass compositions for an operating temperature (OT) of ~850°C, eleven compositions for an OT of ~750°C, and six compositions for an OT of ~650°C.
- Down-selected to two glass systems, for operation at two different temperatures, ~850°C (GaBA glasses) and ~750°C (GaSiB glasses), and performed temperature cycling and testing under dry H_2.
- Investigated interactions of the downselected glasses with SS and 8YSZ in dry H_2 (4% in N_2) at 750°C and 850°C.
- Determined the amorphous phase composition for several glasses that crystallize partially. Thus far, one of these remnant glass compositions was melted with promising results and testing is underway.

Introduction

Large scale production of SOFC laminate stacks is complicated by difficulties of sealing the stack components using a reliable method that is robust over the lifetime of the device. Candidate sealants should exhibit high coefficient of thermal expansion (CTE) values near 12 ppm/K, gas impermeability, minimal interaction with SOFC stack components for 40,000 hours between 600°C and 850°C, and a maximum processing temperature of ~950°C [1]. Glass, glass-ceramic, and glass-ceramic composite seals are the best candidates for forming seals due to ease of manufacture and ability to control CTE, viscosity, and sealing temperatures with composition.

Many sealants currently being studied contain large amounts of alkaline earths such as barium or strontium which aid in seal formation below 1,000°C, yet form undesirable crystals when held at temperatures within the SOFC target operating temperature range [2-3]. Some contain undesirable amounts of boron which may partially vaporize during SOFC operation [4]. The current project centers on developing new viscous oxide glass sealants that will flow at the operating temperature to reduce mechanical stresses between components but maintain the required hermeticity. By using glasses with lower alkaline earth content and reduced alkali content as well, we hope to avoid known reactivity issues. Compositions with gallium and germanium additions to silicate based compositions appear to be promising candidates.

Approach

Potential sealing glasses were tested in several stages. The first stage simply tested the behavior of the base glass, where we measured the thermal expansion and glass transition temperatures (T_g) for as-melted glasses and then frit processed samples that were heated to the target sealing temperature.

The second level of testing was focused on interactions of the glass with aluminized SS and YSZ, and this past year we added also spinel coated SS. Testing out to 2,000 hours was undertaken, in increments of 100 h or 500 h. Full characterization of the resulting samples was performed using cross-sectional scanning electron microscopy (SEM) and microprobe elemental mapping, as well as weight loss measurements, measurement of T_g, and diffraction analysis of the phase content.

Finally, temperature cycling and reactive atmospheres have been explored, or are currently under study. For temperature cycling, the critical question is how the glass behaves when repeatedly heated through the glass nucleation curves. In other words, we aimed to determine if any additional crystallization occurs as a result of temperature cycling, which could potentially be a failure mode. Of course, temperature cycling experiments also allow us to evaluate the thermal expansion matching and to easily determine if the YSZ/glass/SS bodies are mechanically sound. Testing under wet hydrogen is also of interest, and we have already completed testing under dry 4% H_2. We are presently working on testing down-selected glasses under wet 100% H_2.

Results

Down-selection from the full range of glasses yielded four glasses for additional detailed study. GaBA1 and GaBA5 glasses showed good bonding with both aluminized stainless steel (Al-SS) and 8YSZ after thermal treatment at 850°C, and the same was true of GaSiB5 and GaSiB9 glasses at their desired lower OT of 750°C. Reactivity testing against Co-Mn oxide spinel coated stainless steel (CoMn-SS) from Pacific Northwest National Laboratory was not as successful, as we found that the coatings debonded from the stainless steel in most cases.

In dry hydrogen, the glasses were tested for 100 h at their respective operating temperatures, on both Al-SS and 8YSZ. Figure 1 shows that there is no difference

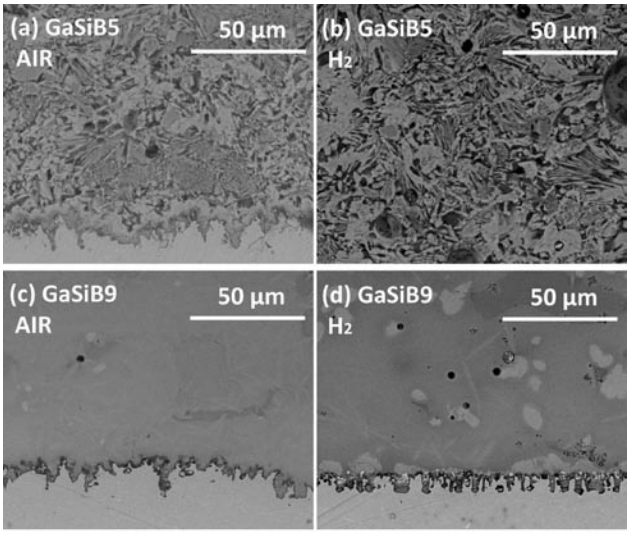

FIGURE 1. SEM images of the GaSiB5/Al-SS and GaSiB9/Al-SS after thermal treatment at 750°C in both air and H_2 for 100 h. The Al-SS substrate is on the bottom of each image.

in microstructure or phase content between the glasses treated in air and 4% H_2. The bonding and crystallization are still robust and only insignificantly affected by hydrogen, a highly encouraging point for this series of glasses.

Figure 2 captures the results of thermal cycling testing. Thermal cycling does not yield observable changes to the highly crystallized compositions such as GaBA1 and GaSiB5. For GaSiB9, which has a large amorphous content, the crystallization is barely

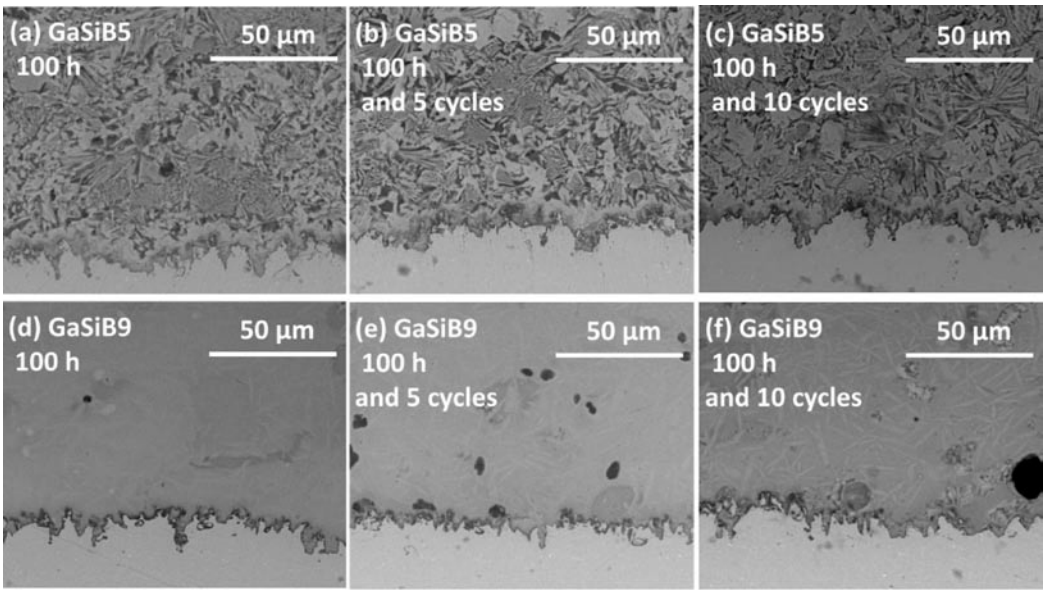

FIGURE 2. SEM images of the GaSiB5/Al-SS441 and GaSiB9/Al-SS441 before and after five and 10 thermal cycles of 10 h at 750°C. The Al-SS441 substrate is on the bottom of each image.

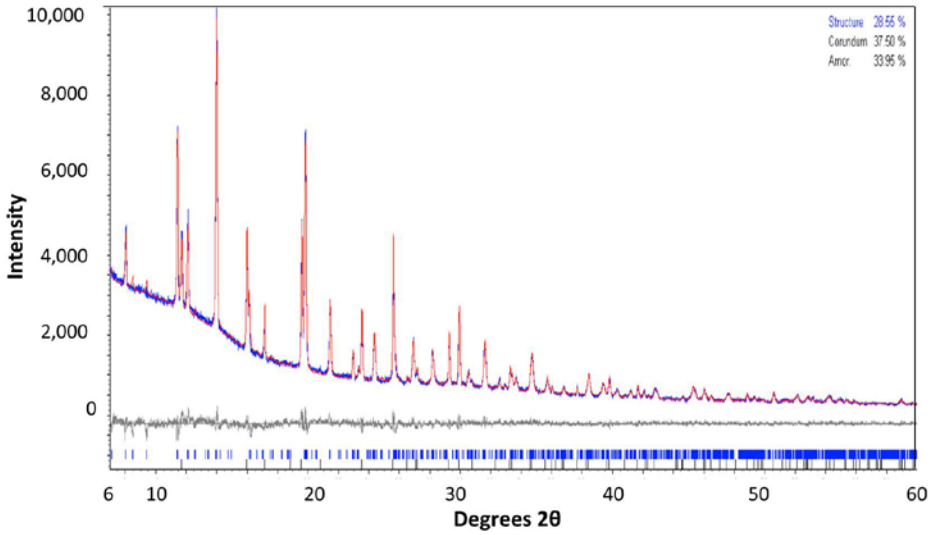

FIGURE 3. Rietveld quantification of the x-ray diffraction pattern of GaBA1 glass-ceramic heated for 500 h at 850°C. The blue line is the measure data, red line is the model, and the grey line is the difference pattern. The diffraction pattern was analyzed for quantification of the phases present, including the internal standard phase, and allows back-calculation of the remnant glass chemistry.

detectable after the first 100 h at 750°C before the thermal cycling. The sealant layer is still transparent on the Al-SS substrate. Only some needle-shaped features can be seen under SEM in the glass phase. After thermal cycling, the needle-shaped crystals may increase slightly in number at the interface, but any changes are minor and cannot be accurately quantified. Again, this is a positive result that indicates that the glasses are largely or wholly insensitive to excursions through the crystal nucleation and growth curves.

A final example of a complex approach to quantification of the remnant glass phase is shown in Figure 3. Using quantitative diffraction analysis, we were able to determine the crystalline phases present, and by difference, the average chemical composition of the remnant glass phase. The remnant glass content of three GaBA series glass-ceramics was calculated and used as a base composition for extending the glass compositional range. With the intent of forming the remnant glass as a starting point, we envision finding new glasses that resist crystallization at the higher temperature of 850°C. We have thus far successfully melted the glasses and are currently heat treating samples for further analysis.

Conclusions and Future Directions

Our initial down-selection, based upon stability against Al-SS and YSZ in air to ~10 glasses per series was effective in identifying top candidates. Additional testing under 4% H_2 and after 10 temperature cycles showed no quantifiable changes in the glass phase content and microstructure. These results demonstrate successful initial performance and therefore the future directions will include:

1. Additional testing under the harsh condition of wet pure H_2.
2. Additional melting and testing of the glasses derived as the remnant glass phase in the top candidate glasses.
3. Full detailed characterization of the glasses and completion of the properties measurements for all down-selected glasses.

Special Recognitions & Awards/Patents Issued

1. U.S. Provisional Application Seriel No. 61/594,062, Mark O. Nalyor, Scott T. Mistuer and James E. Shelby, "Viscous Sealants for Solid Oxide Fuel Cells," February 3, 2012.

References

1. S.C. Singhal and K. Kendall, "High Temperature Solid Oxide Fuel Cells," *Fundamentals, Design, and Applications*, pp. xvi, 405 p. Elsevier, Oxford; New York, 2003.

2. Z. Yang, J.W. Stevenson, and K.D. Meinhardt, "Chemical Interactions of Barium-Calcium-Aluminosilicate-Based Sealing Glasses with Oxidation Resistant Alloys," *Solid State Ionics*, 160 [3-4] 213-25, 2003.

3. M. Brochu, B.D. Gauntt, R. Shah, G. Miyake, and R.E. Loehman, "Comparison Between Barium and Strontium-Glass Composites for Sealing SOFCs," *Journal of the European Ceramic Society*, 26 [15] 3307-13, 2006.

4. A. Flugel, M.D. Dolan, A.K. Varshneya, Y. Zheng, N. Coleman, M. Hall, D. Earl, and S.T. Misture, "Development of an Improved Devitrifiable Fuel Cell Sealing Glass," *Journal of the Electrochemical Society*, 154 [6] B601-B8, 2007.

III.D.2 Development of Glass-Based Seals for SOFC Stacks

Y.S. Chou (Primary Contact) and J.W. Stevenson
Pacific Northwest National Laboratory
P.O. Box 999, MS K2-44
Richland, WA 99352
Phone: (509) 375-2527; Fax: (509) 375-2186
Email: Yeong-Shyung.Chou@pnnl.gov

DOE Project Manager: Briggs White
Phone: (304) 285-5437
Email: Briggs.White@netl.doe.gov

Contract Number: FWP40552

Start Date: October 1, 2011
End Date: September 30, 2012

Fiscal Year (FY) 2012 Objectives

- Evaluate viability of compliant glass as basis for solid oxide fuel cell (SOFC) seals.
- Develop SOFC seal designs based on compliant glass.
- Develop devitrifying glasses with sealing temperatures in the 900°C–1,000°C temperature range with improved wetting/flow behavior and slower devitrification rates compared to previously developed glasses.

FY 2012 Accomplishments

- Evaluated effect of processing conditions (particle size, sintering temperature, ramp rate) on compliant glass microstructure and density.
- Investigated effects of compositional variation on sintering and thermal expansion behavior of devitrifying sealing glasses.

Introduction

To date, most SOFC glass-based seal research has focused primarily on approaches in which, after the sealing process, the glass devitrifies into a rigid or semi-rigid glass-ceramic mixture. In particular, alkaline earth-based aluminosilicate glasses have been extensively studied due to their appropriate coefficient of thermal expansion (CTE) and sealing temperatures. Recently, a novel approach involving a glass resistant to crystallization has been under study. The primary advantage of this type of approach lies in the fact that, in contrast to conventional glass seals that develop a rigid microstructure, a crystallization-resistant sealing glass may retain relatively compliant behavior at SOFC operating temperatures, thereby minimizing thermal stress generation during operation and cool-down. In addition, should cracks form during cooling to room temperature, there is the potential for self-healing during the re-heating portion of the thermal cycle. On the other hand, compliant seals also face a number of potential challenges, including long-term devitrification, enhanced reactivity, temperature-dependent viscosity, and containment issues.

Approach

Compliant Glass Seals

Sealing glass properties were evaluated, in collaboration with Oak Ridge National Laboratory, for possible containment materials and geometries, thermal stresses developed during cooling, and potential chemical reactivity between the glass and other stack materials. Seal designs based on the compliant glass were subjected to post-test characterization techniques, e.g., optical microscopy, scanning electron microscopy (SEM), and energy dispersive spectroscopy (EDS), to evaluate seal performance in terms of leakage, mechanical stability, and reactivity, including interactions with adjacent materials, electrode poisoning due to volatilization, and deposition of glass constituents.

Devitrifying Glass Seals

The group fabricated and evaluated modified refractory glass seal compositions with a primary emphasis on improving wetting/flow behavior and reducing devitrification rates while maintaining stable CTE behavior and sealing temperatures in the desired 950°C–1,000°C temperature range.

Results

Compliant Glass Seals

Previous studies at Pacific Northwest National Laboratory (PNNL) indicated that a candidate commercial sealing glass such as SCN-1 from SEM-COM, Toledo, OH, retained high electrical resistance when sealed to coated stainless steel, although some devitrification was observed. Studies also revealed

the formation of large spherical voids in the glass. Recent work was focused on evaluation of possible processing modifications to minimize the void formation. Several processing parameters including glass particle size, sealing temperature, and ramp rate were studied. The processing optimization was conducted on die-pressed pellets using either as-received (30-40 μm) or attrition-milled glass powders (1-3 μm). The powders were die-pressed and sintered at temperatures ranging from 650°C to 850°C for two hours in air. As shown in Figure 1, the sintered bulk density decreased with increasing sintering temperature.

The sintered pellets were cross-sectioned for SEM microstructural characterization. Figure 2 shows the cross-section microstructure of as-received glass powders sintered at 700°C for two hours, while Figure 3 shows the microstructures of pellets of attrition-milled powders sintered at the same temperature. There were more pores in samples prepared with attrition-milled powders than samples prepared with the as-received powders. The microstructure of a sample sintered at 800°C using as-received powders is shown in Figure 4. It is clear that the pores expanded at the higher sintering temperature, although some pore coalescence also occurred. This pore expansion/bloating are not typically observed with refractory-type sealing glasses, in which rapid crystallization creates a more rigid structure which restricts the expansion of the remaining residual glass. The results suggest that the firing profile for a compliant-type sealing glass needs to be controlled in such a way that maximum densification or particle packing is achieved before pores become sealed off from the outer surfaces. In addition to the sealing temperatures,

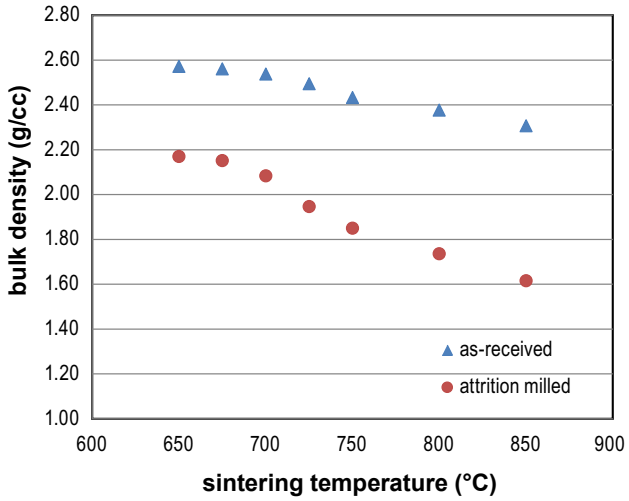

FIGURE 1. Sintered bulk densities of SCN-1 pellets pressed using either as-received or attrition-milled powders at various temperatures

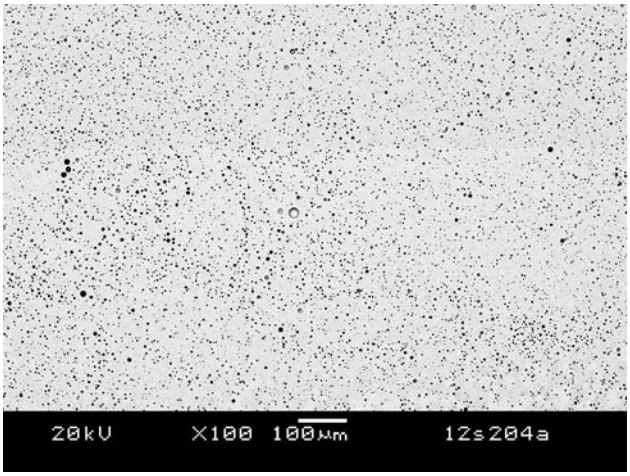

FIGURE 3. Microstructure of the sintered (700°C/2 hours) SCN-1 glass pellet using attrition-milled powder

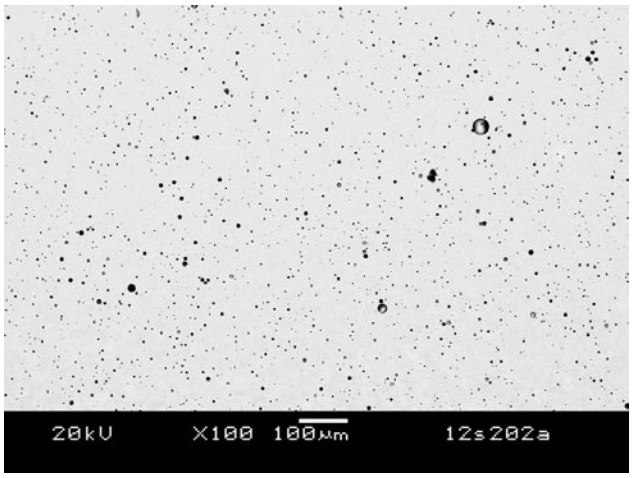

FIGURE 2. Microstructure of a sintered (700°C/2 hours) SCN-1 glass pellet using as-received powder

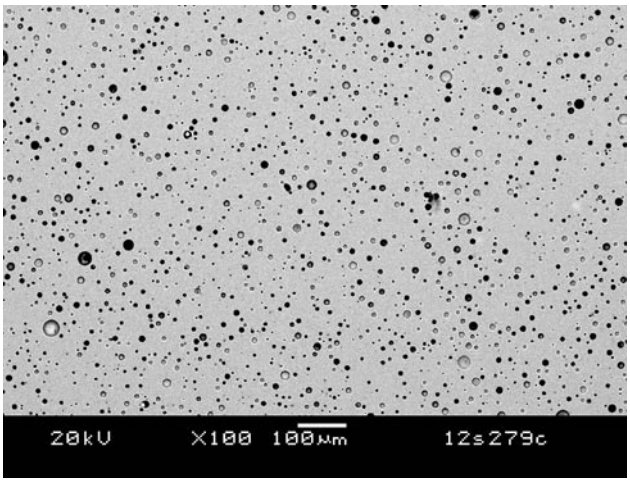

FIGURE 4. Microstructure of a sintered (800°C/2 hours) SCN-1 glass pellet using as-received powder

the effect of heating rate on sintered bulk density was also investigated. For this study, pellets of as-received glass powders were used. Two heating rates were tested: 3°C/min and 1°C/min for three sintering temperatures: 650°C, 675°C, and 700°C. The results of sintered bulk density measurements are listed in Table 1. Clearly, there was no distinct effect of ramp rate on density, as the bulk density was almost identical for the two heating rates.

After identifying the temperature range at which maximum bulk density was obtained for the pressed pellets, simulated seal tests were then conducted on a realistic material set, i.e., aluminized AISI 441 substrate and ceramic bi-layer. The as-received glass powders were mixed with organic binders to form a paste and applied between the bi-layer and aluminized metal coupons. After drying, a small dead weight was applied to ensure contact, and two strips of 0.012 inch thick mica were used as a spacer/stopper so that the glass would not be squeezed out by the dead weight. The specimens were then heated to 650ºC or 700ºC for two hours (the previously identified temperature range for achieving maximum bulk density), and then heated to 800ºC for two hours to simulate stack sealing/operating conditions.

Figure 5 shows the microstructure for a sample heated to 700°C for two hours, then 800°C for two hours in air. It is clear that the voids in the glass were, on average, much larger than the voids in a sample fired at 700ºC only (Figure 2). The results indicate that the residual pores entrapped during the sintering process expanded substantially during the heat-up to the SOFC operating temperature, presumably due to both increased gas pressure (ideal gas law) and reduced viscosity of the glass.

TABLE 1. Effect of heating rate on the sintered bulk density (g/cc) of glass pellets prepared from as-received powder

sintering T, °C	3°C/min	1°C/min
650	2.57	2.57
675	2.56	2.56
700	2.54	2.54

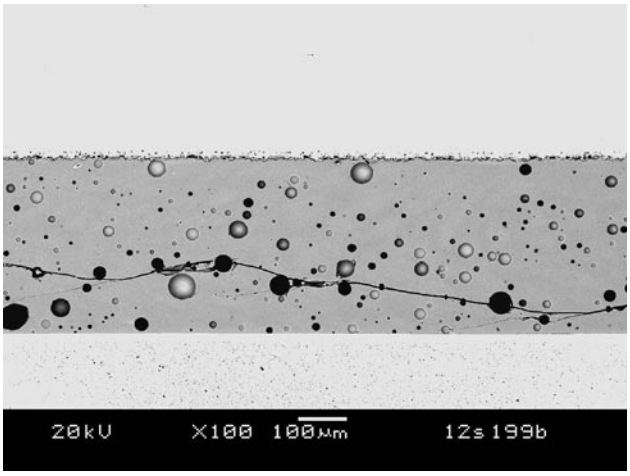

FIGURE 5. Microstructure of SCN-1 (as-received) heated to 700°C for two hours, then 800°C for two hours between aluminized AISI 441 substrate and ceramic bilayer

Devitrifying Glass Seals

In recent years, PNNL has developed a series of sealing glasses covering SOFC stack sealing temperatures between 800°C and 1,000ºC. Compositions for sealing at temperatures greater than 900ºC offer excellent CTE match and stability, but their rapid devitrification kinetics can lead to wetting/flow challenges, particularly for seal/stack designs which are not conducive to the application of a compressive load during the sealing process. Recent efforts are focused on improving the wetting/flow behavior of glasses for relatively high sealing temperatures (≥950°C) with a slightly lower CTE to obtain compatibility with ceramic substrates such as MgO-$MgAl_2O_4$ composites (~11.5 x 10^{-6}/°C) as opposed to ferritic stainless steel interconnects (~12.5 x 10^{-6}/°C). Previously developed sealing glasses were reviewed in terms of glass transition temperature (T_g), dilatometric softening temperature (T_s), and CTE (Table 2), which led to the selection of glass YSO-12 as the basis for further development.

Three approaches were adopted to improve the wetting/flow behavior of the refractory sealing

TABLE 2. Thermal properties of candidate sealing glasses with high sealing temperatures (≥950°C) vib: vibration milled; att: attrition milled

	as-made	as-made	as-made	sintered (vib)	sintered (att)
glass #	Tg	Ts	CTE to Tg	CTE to Ts	CTE to Ts
unit	degree C	degree C	ppm/C	ppm/C	ppm/C
YSO-1	703	---	11.97	---	---
YSO-2	687	734	11.71	---	---
YSO-7	671	725	11.66	---	---
YSO-8	653	712	11.69	---	---
YSO-12	627	662	11.50	11.50	11.43
YSO-47	632	694	11.51	12.10	12.12

glass: (1) increasing the amount of B_2O_3 glass former; (2) increasing the amount of SiO_2 glass former; and (3) changing the alkaline earth from Ca to Mg or Ba. Nine compositions were formulated, as listed in Table 3.

Raw powders (oxides or carbonates) were dry mixed before melting in a Pt crucible at 1,420°C for 0.5 hour in air, followed by casting on a metal plate and annealing at 600°C for six hours. All nine glasses were transparent and homogeneous, and free from precipitation or crystallization, except glass YSO-12-I, which showed some surface precipitation. After glass fabrication, a rectangular bar was cut for thermal property characterization, and the rest of the bulk glass was vibration milled and sieved through a #100 mesh sieve. The sieved glass powders were then die-pressed into bars and fired to a temperature of 975°C/2 hours consistent with SOFC sealing conditions. The results of measurements of T_g, T_s, and average CTE are listed in Table 4. A small increase in B_2O_3 content had a distinct effect in lowering the softening point. For example, the softening point was lowered from the parent glass of 670°C to 653°C for YSO-12-B with a 3% increase in B_2O_3 content, but essentially unchanged at 669°C for YSO-12-D with a 3% increase in SiO_2 content. A small change in B_2O_3 or SiO_2 content did not significantly affect the CTE of the as-made bulk glass. For the sintered glasses, the change in CTE appears rather large as compared to the percentile change in composition. For example, the CTE of the sintered parent glass was 11.50 x 10^{-6}/°C, while it was 12.21 x 10^{-6}/°C for glass YSO-12-B (3% increase in B_2O_3 content), and 10.81 x 10^{-6}/°C for glass YSO-12-D (3% increase in SiO_2 content).

The effect of SiO_2 glass former was further evaluated among glasses YSO-12-E, -F, and -G with a substantial increase in SiO_2 at the expense of $SrCO_3$ content (Table 3). The glass transition point appeared to increase with SiO_2 amount from 627°C (YSO-12) to 652°C (YSO-12-G) while the change in softening point was less linear, from 670°C (YSO-12) to 696°C (YSO-12-G). The increase in SiO_2 clearly had a negative effect on CTE values; the more SiO_2 was added, the lower the CTE for the as-made bulk glasses (Table 4). For example, the CTE of as-made parent glass was 11.69 x 10^{-6}/°C (SiO_2=34%), which decreased to 11.51 x 10^{-6}/°C for glass YSO-12-E (SiO_2=39%), 10.50 x 10^{-6}/°C for glass YSO-12-F (SiO_2=44%), and 9.72 x 10^{-6}/°C for glass YSO-12-G (SiO_2=49%).

TABLE 3. Glass compositions for YSO-12 series (in mole %)

glass #	$SrCO_3$	MgO	CaO	$BaCO_3$	Al_2O_3	$B2O_3$	SiO_2	ZnO
YSO-12	42.5		10		3	7.5	34	3
YSO-12-A	42.5		10		3	9.0	34	1.5
YSO-12-B	42.5		10		3	10.5	34	0
YSO-12-C	42.5		10		3	7.5	35.5	1.5
YSO-12-D	42.5		10		3	7.5	37	0
YSO-12-E	37.5		10		3	7.5	39	3
YSO-12-F	32.5		10		3	7.5	44	3
YSO-12-G	27.5		10		3	7.5	49	3
YSO-12-H	42.5	10	0		3	7.5	34	3
YSO-12-I	42.5		0	10	3	7.5	34	3

TABLE 4. Thermal properties of as-made glass and sintered glasses

	as-made	as-made	as-made	sintered	sintered
glass #	Tg	Ts	CTE to Tg	Ts	CTE to Ts
unit	degree C	degree C	ppm/C	degree C	ppm/C
YSO-12	627	670	11.69	928	11.50
YSO-12-A	609	656	11.66	947	11.39
YSO-12-B	609	653	11.56	942	12.21
YSO-12-C	624	666	11.70	942	11.42
YSO-12-D	628	669	11.61	936	10.81
YSO-12-E	637	667	11.51	869	11.87
YSO-12-F	648	687	10.50	955	11.68
YSO-12-G	652	696	9.72	701	9.67
YSO-12-H	630	665	11.67	840	11.30
YSO-12-I	N/A	N/A	N/A	868	12.81

For wetting/flow behavior characterization, an in situ camera was set up to take photos of the morphology change of the glass powder samples (pressed small cylinders about 0.4-0.5" tall) during heating to 1,050°C in air. The die-pressed glass powder cylinders were placed on a polished $MgO/MgAl_2O_3$ ceramic substrate, a potential high temperature SOFC ceramic substrate. In addition to the in situ observations, the morphology of sintered powder bars (975°C/2 hours) was examined around the corners as an indication of melting, which is critical in determining wetting and flow behavior during the sealing process. Overall, glass YSO-12-F appeared to be the most promising candidate in terms of rounding of corners and CTE (11.68 x 10^{-6}/°C).

Conclusions and Future Directions

A novel approach to sealing of SOFC stacks based on devitrification-resistant glass has the potential to minimize thermal stresses during stack operation and thermal cycling. Several challenges must be overcome for this approach to prove viable, including minimization of porosity in the seal. Future activities will focus on optimization of glass paste properties to obtain improved green density, addition of a small fraction of inert fibers or particles to restrict pore coalescence, and development of seal designs which mitigate issues related to glass reactivity and mobility.

De-vitrifying glass seals developed at PNNL offer effective sealing and stable thermal expansion behavior during SOFC operation. Challenges related to wetting/flow during high temperature sealing processes are being addressed through compositional variation. Future activities will focus on continued evaluation and optimization of glasses based on YSO-12-F.

FY 2012 Publications/Presentations

1. Y.S. Chou, E.C. Thomsen, J.P Choi, and J.W. Stevenson, "Compliant Alkali Silicate Sealing Glass for Solid Oxide Fuel Cell Applications: Combined Stability in Isothermal Ageing and Thermal Cycling with YSZ Coated Ferritic Stainless Steels," *J. Power Sources*, 197, 154 (2012).

2. Y.S. Chou, E.C. Thomsen, J.P. Choi, and J.W. Stevenson, "Compliant Alkali Silicate Sealing Glass for Solid Oxide Fuel Cell Applications: The Effect of Protective YSZ Coating on Electrical Stability in Dual Environment," *J. Power Sources*, 202, 149 (2012).

3. Y.S. Chou, E.C. Thomsen, J.P. Choi, and J.W. Stevenson, "Compliant Glass Seal Development at Pacific Northwest National Laboratory," Fuel Cell Seminar and Exhibition, Orlando, Florida, November, 2011.

4. Y.S. Chou, E.C. Thomsen, J.P. Choi, W.E. Voldrich, and J.W. Stevenson, "Compliant Sealing Glass for SOFC Applications: Electrical Stability with YSZ and Alumina Coating under DC Loading," 36th International Conference and Exposition on Advanced Ceramics and Composites (ICACC), Daytona Beach, Florida, January, 2012.

III. SECA CORE TECHNOLOGY R&D

E. Cross-Cutting Materials, Testing, and Manufacturing

III.E.1 Testing and Evaluation of Solid Oxide Fuel Cells in Extreme Conditions

A. Alan Burke (Primary Contact),
Louis G. Carreiro
Naval Undersea Warfare Center (NUWC),
Division Newport
1176 Howell Street, Bldg. 1302/1
Newport, RI 02841
Phone: (401) 832-6675; Fax: (401) 832-6202
Email: Adrian.Burke@navy.mil

DOE Project Manager: Maria Reidpath
Phone: (304) 285-4140
Email: Maria.Reidpath@netl.doe.gov

Subcontractor:
Delphi Corporation, Troy, MI

Contract Number: NT43247

Start Date: January 1, 2011
End Date: December 31, 2011

Fiscal Year (FY) 2012 Objectives

- Evaluate solid oxide fuel cell (SOFC) system with anode recycle and CO_2 scrubbing using methane and pure oxygen as the reactants for an undersea vehicle application.
- Evaluate CO_2 scrubber in isolated testing and elevated pressure.
- Utilize mass spectrometry to monitor gas composition at various locations in the anode recycle loop.

FY 2012 Accomplishments

- Achieved continuous power output of 800 W (35 A at 24 V) with ~80% methane utilization, >85% oxygen utilization, and >60% gross system efficiency.
- A packed-bed scrubber operated at 20 psig showed prolonged CO_2 removal rate versus ambient pressure testing. Total carbon removal rate was still 40-50% after 150 minutes of operation.
- The mass spectrometer calibration for reformate gas species is sensitive to operating pressure as well as steam levels. Refined software that can consider these sensitivities and use a reference sample gas would make great strides towards more accurate and real time reformate gas analysis.

Introduction

Naval Undersea Warfare Center continues to investigate a zero emission SOFC system for use in unmanned undersea vehicles (UUVs). In past studies, sulfur free fuels such as S-8 and JP-10 were contrasted against methane. With waste heat being at a premium in such a highly efficient system (>60%), it has been determined that steam reforming of liquid fuels will likely require an additional burner or catalytic partial oxidation (CPOX) reforming, which in turn decreases system efficiency and energy metrics. Using liquefied natural gas or liquefied methane as the fuel maximizes the hydrogen-to-carbon ratio, thus decreasing the amount of oxygen storage and carbon dioxide sorbent required on board. In addition, the greatest advantage of using methane might be that waste heat can be used for steam reforming both in the stack and throughout the CO_2 sorbent bed. A gaseous fuel feed is more resilient towards carbon deposition, power transients, and flow disruptions.

Besides providing UUV-specific advantages, wider adoption of natural gas would aid in meeting energy security and conservation goals established by U.S. Navy leadership. Versus diesel or gasoline, methane has a lower carbon footprint and can be synthesized from renewable resources/biomass more sustainably [1]. Natural gas or other light hydrocarbon fuels would also favor SOFC systems that offer higher efficiency than combustion engine generators.

Approach

System tests were assembled as shown in Figure 1. Check valves (2 psi) were used to provide back-pressure to the stack while also preventing excessive pressures that might damage the stack. The main system components were a Delphi Gen 3.2 SOFC stack, an R&D Dynamics' high temperature blower, TDA Research's CO_2 sorbent, and a Delphi Gen 8T fuel processor. In each test, the system was started on hydrogen gas in order to generate steam for methane reforming. Once adequate steam levels were achieved, methane flow was initiated and hydrogen flow was halted. Hydrogen flow was restarted when necessary to help sustain stack voltage.

The CO_2 sorbent supplied by TDA Research, Inc., was baked out at 850˚C prior to its use to ensure maximum amount of CaO was present in the starting

material. Roughly 7.5 liters of the sorbent was used in each test. In the isolated scrubber testing, a needle valve was used to provide back pressure.

In order to gather more information on the anode recycle loop, a Mound Technical Solutions, Inc., mass spectrometer (MS) with heated capillary lines was used to analyze gas composition at various locations in the anode recycle loop. The goal was to attain more accurate determination of scrubber performance, anode recycle flow rate, gas leakage, and reformer operation. The issues associated with steam flooding the MS detector were abated by appropriate heating of the capillary lines, limiting the number of consecutive samples per capillary, and alternating dry gas sampling with wet gas sampling. Steam levels of 20-75% were effectively measured without any instrument error or shut-down during continuous operation.

The MS accuracy was further evaluated during the isolated scrubber testing. While the effluent from the scrubber was monitored to determine CO_2 removal performance over time at both ambient and elevated pressures, a comparison of dry and wet inlet compositions also offered a means of determining steam interference with other species in the MS measurements. Also, addition of an inert gas such as argon to the feed provided a valid reference point for the total flow and composition of the gas stream. Nitrogen does not work as well as argon, because nitrogen and carbon monoxide have the same mass, thus they interfere with each other in the mass spectrometer measurement.

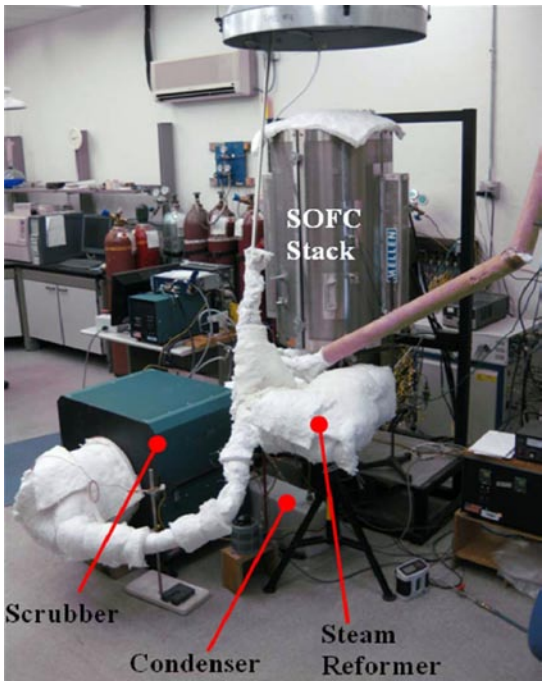

FIGURE 1. Picture of Assembled Hardware in Laboratory. The SOFC stack was mounted on a manifold in the clamshell furnace (top, center). The anode recycle blower to the lower left of the clamshell furnace drove the anode exhaust into the CO_2 scrubber (inside box furnace). The steam reformer to the lower right of the stack manifold was covered with insulation. A water trap/condenser used in the first test is also shown.

Results

Acceptable gross efficiency of 60% based on the lower heating value of methane was achieved in the first system demonstration, albeit at lower power level (800 W, 35 A, 24 V) than the target 1 kW. In addition, there was concern regarding the CO_2 removal rate and steam/carbon ratio at the SOFC. Figure 2 shows that at 40 amps, performance steadily decreased. Adding H_2 to the feed helped stabilize stack voltage, but overall efficiency decreased. For the final segment of testing, the system was adjusted back to 35 amps with pure methane feed. The degradation towards the end of run can be attributed to decrease in scrubber performance, lower pressure operation (2.0 versus 2.5 psig), and possibly dilution of oxygen at the cathode due to impurity accumulation (argon).

During start up, unusually high levels of steam were detected in the anode loop by the MS. The origin of the steam could have been the sorbent material, but the sorbent was pre-fired before the test, so this is not likely. Another explanation is that this steam is a product of oxygen crossover combustion in the anode exhaust manifold. In fact, there was so much steam that the system did not first need to operate on hydrogen gas in order to generate the steam required for methane steam reforming. Instead, methane gas was turned on as current

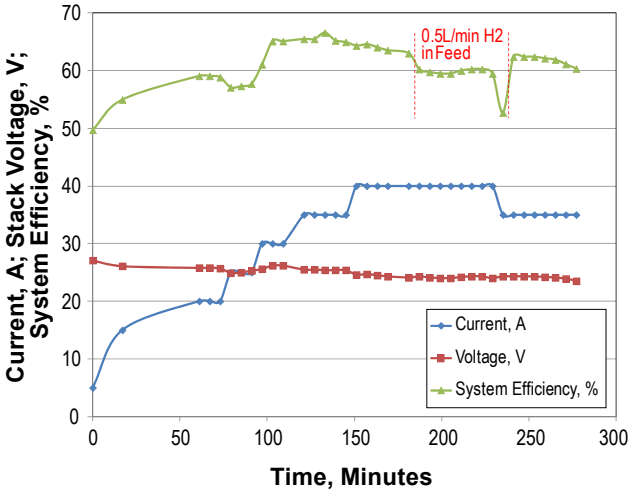

FIGURE 2. Performance of the First System Demonstration in July 2011. Stack current, voltage, and system efficiency are plotted versus time. Supplemental hydrogen flow was added for a brief period to stabilize cell voltages, which were decreasing over time.

was initiated. The lower than normal open circuit cell voltages during pre-run idling also suggested high steam levels in the anode gas stream. The gradual depletion of fuel gas in the anode loop due to crossover combustion could also explain the decline in system efficiency over time while trying to hold the system at steady state as well as the low maximum power level as compared to prior studies. Similar crossover has also been seen by Chick et al. in Delphi Gen 3.2 stack technology [2].

Scrubber Performance

As can be seen in Figure 3, the rate of carbon removal varied greatly, but there was a general downward trend over time. During initial system testing, the scrubber was at too low an operating temperature, which favored $Ca(OH)_2$ formation instead of $CaCO_3$. Moisture could have also been absorbed during cool down if steam/water remained in the anode recycle loop. In a second test, the scrubber furnace temperature was increased to prevent $Ca(OH)_2$ formation; however, the post-run X-ray diffraction analysis indicated that only the inlet and outlet regions of the sorbent were active and that the middle region was actually too hot for either CO_2 or steam absorption. As the scrubber temperature was raised above 850°C, CO_2 was likely driven out of the scrubber (desorption). Very little $Ca(OH)_2$ was detected, and this probably only formed during cool down or upon exposure to the ambient humidity.

In the system demonstrations, the CO_2 removal was far lower than required for sustainable recycle loop operation and high fuel utilization. Although there was a large uncertainty (+/-10%) regarding the MS measurements in the system demonstrations, Figure 3 shows that there was a general trend towards reduced CO_2 removal, and even the higher rates at the beginning of the test were hardly adequate at only 50-60% carbon removal.

In the isolated scrubber tests, the MS measurements were more accurate, and higher percentage carbon removal was attained. Figure 4 gives the performance of the first isolated test, in which a mixture of steam, CO_2, and H_2 was fed to the scrubber. A subsequent test conducted at higher pressure where steam was replaced with argon is shown in Figure 5. The trends in Figures 4 and 5 match fairly well, and it does not appear that steam

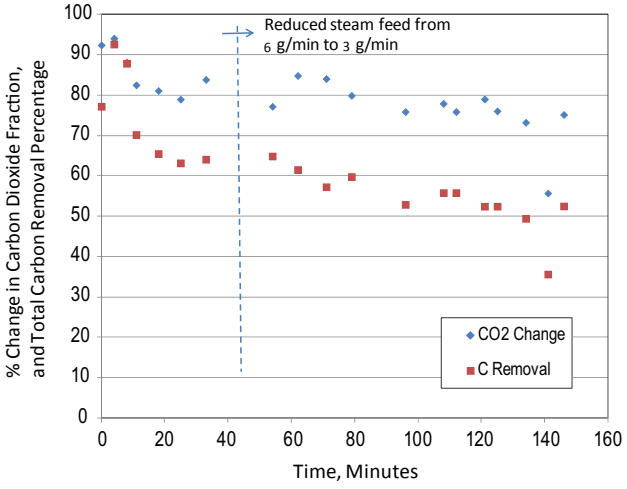

FIGURE 4. Carbon Removal in Scrubber with Steam Present. Feed was 3.2 sL/min CO_2 and 4.8 sL/min H_2 with either 6 g/min or 3 g/min steam.

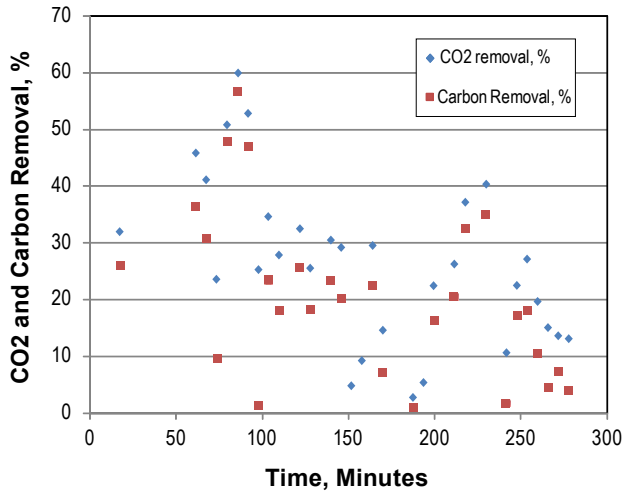

FIGURE 3. Steady Deterioration of Carbon Species Removal in the First System Test. This plot compares CO_2 removal percentage versus total carbon species removal, which is a better indicator of sorbent performance than CO_2 removal alone.

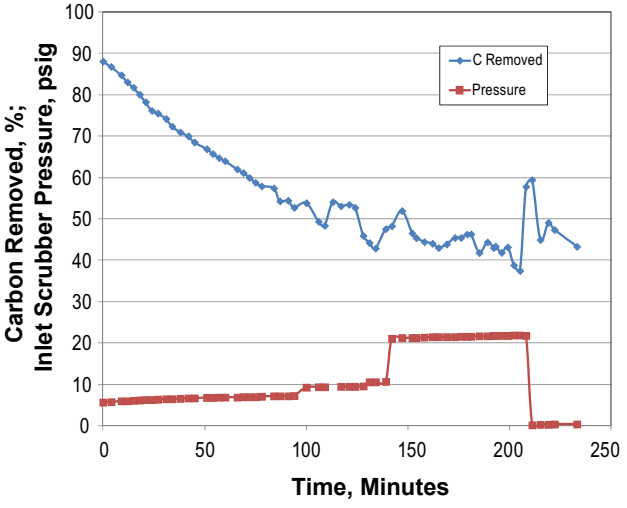

FIGURE 5. Performance of Baffled Scrubber over Time at Furnace Temperature of 700°C. There was a steady decrease in performance until pressure was elevated and the scrubber partially recovered. Constant feed of 3.2 sL/min CO_2, 4.8 sL/min H_2, and 7.66 sL/min Ar was supplied.

has a detrimental effect (versus inert argon) regarding CO_2 removal rate or selectivity. Higher CO_2 partial pressure did partially recover scrubber performance, as is expected by increasing gas density and residence time in the reactor, as well as favoring higher CO_2 sorption by an equilibrium shift. More studies are required to determine optimum pressure for system operation, but it is estimated that 3-10 atm is the range for the UUV system of maximum efficiency and energy density.

Mass Spectrometer Accuracy

Real-time, compositional analysis of high-temperature, wet reformate gas streams continues to be a challenge. The MS was able to run continuously and monitor several sampling locations, completing a cycle every 3-5 minutes. Variation in measured composition can be attributed to fluctuating steam, which is reflective of oscillations in the steam concentration being measured at the MS detector. Regardless of the mechanism causing this oscillation, it appears that time-averaged data acquisition could result in accurate and reliable data; however, the prospect of real-time, instantaneous measurement would be sacrificed for the sake of accuracy.

Concerning the accurate measurement of individual species during the wet sampling tests, the nitrogen reading was low, the CO_2 reading was generally good, and the hydrogen reading was high. The dry input feed was monitored as well and was accurate in all species. While there may have been fluctuations in the steam measurement, the proportions between the other species are also shifted upon introduction of steam. This suggests that the presence of steam is altering the MS sensitivity of the other species being measured. Figure 6 shows the molar ratios in the wet reformate, which should not be affected by steam fluctuations and should match the known dry feed molar ratios. The gas feeds were controlled to deliver molar ratios of $H_2/N_2 = 3.6$, $CO_2/N_2 = 2.4$, and $H_2/CO_2 = 1.5$. While the dry MS measurements did match these ratios, the wet gas samples shown in Figure 6 did not. The mere presence of steam had varying impact on the sensitivity of each species. For instance, the H_2/N_2 ratio is considerably altered upon introduction of steam, such that the H_2 signal appears amplified and the N_2 signal reduced. If the only error was the accuracy of the steam measurement, then these molar ratios should not have been changing between the wet and dry samples.

It was also shown in the pressurized scrubber experiments that sampling pressure can affect each species' calibration. Despite these factors hindering reliable calibration, one approach was found to be effective, at least in the case of the isolated scrubber experiments. By monitoring the controlled inlet gas

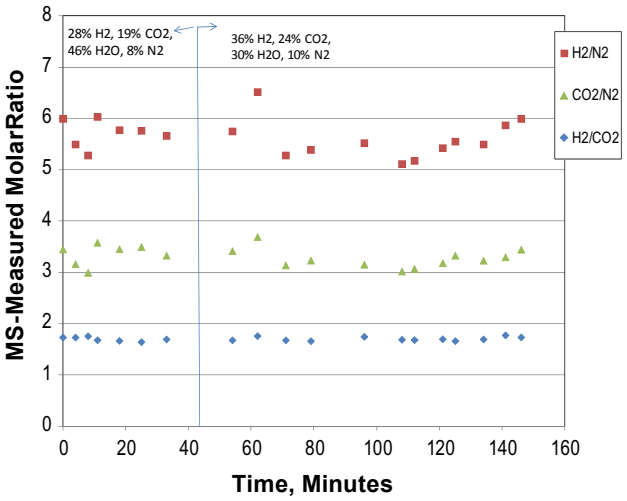

FIGURE 6. Measured Molar Ratios of Gases during the Calibration Run. The gas feeds were controlled to deliver dry molar ratios of $H_2/N_2 = 3.6$, $CO_2/N_2 = 2.4$, and $H_2/CO_2 = 1.5$, but the measured wet molar ratios do not match as they should.

feed of known concentration, continuous verification of the instrument calibration can be established at each operating pressure. At this time, the correction needs to be applied in post-experiment data processing, but the instrument could be programmed to recalibrate in real time according to a reference gas mixture or known pressure dependence. Atomic balances were converged to within +/-5% across the scrubber throughout the test, so the carbon removal trends measured should be reflective of performance.

High Temperature Blower Performance

The blower provided an estimated recycle flow of 25 sL/min while drawing 35 amps from the SOFC stack. Gas composition through the blower was estimated at 16% H_2, 36% CO_2, 6% CO, 41% steam, and 0.5% methane, but there is considerable uncertainty in these estimates because mass balances were dependent upon accurate, MS-measured compositions.

Blower RPM was raised from 60 to 85,000 RPM while stepping from 20 to 40 amps in the system. This seemed to stabilize SOFC cell voltages while minimizing the parasitic power draw. With blower power input proportional to the RPM, the lowest RPM required to stabilize cell voltages results in the lowest parasitic power loss and maximum system efficiency. Pressure differential across the blower was approximately 0.3 psig, with outlet pressure up to 3 psig during the maximum power excursions at 800 W from the SOFC stack.

The blower was in good operating condition after roughly 50 h of run time in the system demonstrations. The second generation blower's quality in terms of

integrity and gastight operation far exceeded the first generation prototype.

Conclusions and Future Directions

Limitations regarding the CO_2 removal rate is a concern in the closed SOFC system intended for UUV application. Evidence from this study shows that pressure and temperature optimization should help increase CO_2 removal rate. By removing CO_2 at an acceptable rate, high anode loop pressure and CO_2 dilution can be mitigated while achieving higher fuel utilization at the system level.

Pressurization needs to be further explored to benefit scrubber performance (and in return system performance); however, any SOFC gas leakage that exists will only be worsened by higher pressure operation. A clear SOFC system design for UUV implementation remains reliant on a rugged SOFC stack that can tolerate targeted operating pressure. Successful operation of SOFC technology at least at moderate pressure (10-20 psig) needs to be developed to realize this high-utilization, anode recycle design with carbon dioxide collection. For planar SOFC stacks, this will involve construction of a pressure vessel for the hot components and a precise method for balancing the anode, cathode, and ambient pressure zones.

The prospect for refined system monitoring via MS has also been challenged by variable interspecies and sampling pressure sensitivities. These phenomena impede a simple, straightforward calibration approach, and ample post-run data analysis is still required to estimate the actual compositions and recycled gas flows during the test.

Despite the significant development still required to render a fleet-serviceable SOFC power system for UUVs, these system demonstrations and isolated scrubber tests were valuable in quantifying recycle gas flows and reformate compositions in a real system. In order to achieve targeted energy system metrics for UUVs, some level of pressurization will likely be required, and future tests will focus on higher pressure operation.

References

1. J. Murphy and T. Thamsiriroj, "What Will Fuel Transport Systems of the Future?" *Materials Today*, 14(11) (2011) 518-524.

2. M. Powell, K. Meinhardt, V. Sprenkle, L. Chick, and G. McVay, "Demonstration of a Highly Efficient Solid Oxide Fuel Cell Power System Using Adiabatic Steam Reforming and Anode Gas Recirculation," *Journal of Power Sources,* 205 (2012) 377-384.

III.E.2 Reliability and Durability of Materials and Components for SOFCs

Edgar Lara-Curzio (Primary Contact),
A. Shyam, R. Trejo, M.J. Kirkham,
V. Garcia-Negron and B. Armstrong
Materials Science & Technology Division
Oak Ridge National Laboratory
1 Bethel Valley Rd.
Bldg. 4515, MS-6062
Oak Ridge, TN 37831-6062
Phone: (865) 574-1749; Fax: (865) 574-4913
Email: laracurzioe@ornl.gov

DOE Project Manager: Patcharin Burke
Phone: (412) 386-7378
Email: Patcharin.Burke@netl.doe.gov

Contract Number: FEAA066

Start Date: October 1, 2000
End Date: September 30, 2012
(annual continuations)

Fiscal Year (FY) 2012 Objectives

- Support the Solid State Energy Conversion Alliance (SECA) industrial teams in the development of reliable and durable solid oxide fuel cells (SOFCs).
- Identify and utilize test techniques to determine the physical and mechanical properties of SOFC component materials and the interfaces between them.
- Characterize candidate glasses developed for SOFC seal applications.
- Develop economically viable sealing materials and concepts.

FY 2012 Accomplishments

- Determined the effect of time of exposure to air and gas mixtures of $H_2 + N_2 + H_2O$ on the viscosity of SCN-1 and G6 glasses.
- Developed engineered glass seals for SOFCs consisting of a crystallization-resistant glass matrix and frangible ceramic particles or ceramic fibers.
- Demonstrated the ability of engineered silicate glass seals to seal surfaces that are not flat and/or parallel and the feasibility of tailoring their viscosity and wetting behavior by changing the concentration of frangible ceramic particles or ceramic fibers.

Introduction

Planar SOFC stacks consist of alternating fuel and air chambers which are sealed from each other and connected to fuel and air delivery manifolds, respectively. Seals must have low electrical conductivity and be chemically and mechanically stable in SOFC operating environments. Fuel leakage should be less than one percent averaged over the seal area, and the seal material must be capable of a service life of more than 40,000 hours and dozens of thermal cycles. Furthermore, seals should have high manufacturability and low cost to meet the SECA program goals.

In previous reports we have presented results from the evaluation and characterization of the physical and mechanical properties of two crystallization-resistant multicomponent silicate glasses (SCN-1 and G6) [1-3]. During FY 2012, Oak Ridge National Laboratory (ORNL) continued investigating the effect of time of exposure to SOFC-relevant environments on the evolution of the microstructure and properties of these glasses. Of particular interest are the kinetics of precipitation of crystalline phases and the evolution of the distribution of pore sizes. This information can only be determined experimentally because to date there are no models to predict these phenomena.

During FY 2012, efforts were also focused to develop engineered silicate glass seals that have controllable levels of viscosity and wetting behavior to address the wide range of temperatures in SOFCs (in-plane temperature gradients in cells and axial temperature gradients along the length of the stack) and the ability to seal surfaces that are not flat and/or parallel, which are likely occurrences for cells with large active area.

Approach

A box furnace and a tubular furnace with environmental control were used for aging studies of SCN-1 and G6 glasses in air and in a gas mixture of $H_2O + H_2 + N_2$. Aging tests were carried out at 800°C and interrupted periodically to remove test specimens for microstructural characterization. Thermal expansion, glass transition temperature and viscosity were determined using a thermomechanical analyzer. The wetting behavior of engineered glass seals, containing different amounts of frangible ceramic particles or ceramic fibers was determined in real time using digital

photography. Infrared imaging was used to assess, non-destructively, the microstructure of engineered glass seals. The hermeticity of these seals was evaluated using a test set-up in which zirconia tubes bonded to zirconia plates using these seals are evaluated under dual environmental conditions (a gas mixture of $H_2O + H_2 + N_2$ inside the zirconia tube and air outside).

Results

The microstructure, chemical composition and properties of test specimens of two multicomponent silicate glasses, SCN-1 and G6 were examined as a function of time of exposure to air and a gas mixture of $H_2O + H_2 + N_2$ at 800°C. The viscosity and glass transition temperature were determined using a thermomechanical analyzer per ASTM-C1351 [4]. Test specimens for viscosity measurements were core-drilled from glass beads that had been sintered onto 300 µm thick 8-mol% yttria stabilized zirconia (8YSZ) substrates. Figure 1 shows the effect of time of exposure on the viscosity of SCN-1 glass. It was found that the viscosity of the glass decreases with temperature but increases with time of exposure. An analysis of the microstructure of SCN-1 glass after exposure revealed the precipitation of crystalline phases, in particular $KAlSi_3O_8$ and BaO. Empirical analysis of the kinetics of precipitation of these phases suggests that after 40,000 hours their concentration will be less than 15%, which is below the percolation threshold. Previously it had been reported that the glass transition temperature of this glass is not affected after 10,000 hours of exposure in these environments [3]. These results are important because they demonstrate that this glass will preserve its ability to heal cracks. At the same time, while the precipitation of these crystalline phases will not compromise the self-healing ability of the glass, it is clear that these phases are responsible for the increase in its viscosity and those changes in viscosity need to be taken into consideration. Similar results were found for G6 glass.

During the reporting period ORNL continued working on the development of engineered glass sealing concepts for SOFCs. Planar SOFC stacks will experience temperature gradients both in-plane in the cells and along the height of the stack. These temperature gradients pose challenges because it is unlikely that a single glass will possess the viscosity characteristics necessary to seal the stack for wide ranges of operating temperatures. ORNL developed engineered glass seals with values of viscosity that can be tailored. One of the concepts under consideration consists in forming composite seals consisting of a crystallization-resistant matrix, e.g., SCN-1, G6, and frangible ceramic particles. Figure 2 shows a scanning electron micrograph of a composite seal consisting of SCN-1 matrix and calcia-stabilized zirconia frangible hollow spheres. The fracture of the hollow spheres under the application of a compressive load gives the composite glass seal the ability of filling uneven spaces, for example when sealing surfaces that are not parallel or flat. An alternative to the use of frangible hollow zirconia spheres is the use of zirconia fibers, which also provide the necessary compliance when sealing surfaces that are not parallel or flat. Such scenario is likely to be encountered in cells with large active area, which are difficult to manufacture with high tolerances of flatness or parallelism. Figure 3 illustrates the procedure used to demonstrate the ability of these composite

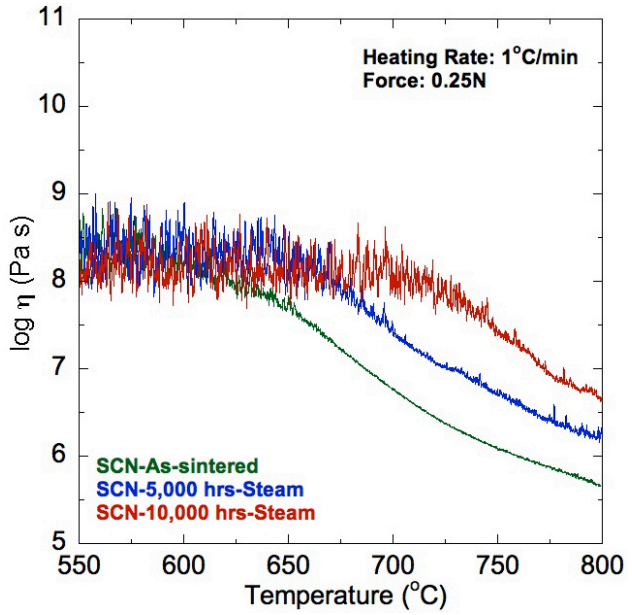

FIGURE 1. Effect of time of exposure in a gas mixture of $H_2 + N_2 + H_2O$ at 800°C on the viscosity of SCN-1 glass

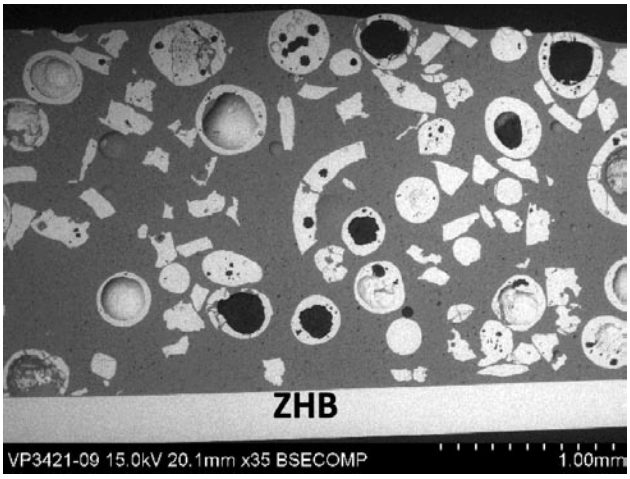

FIGURE 2. Scanning electron micrograph of a composite glass seal consisting of SCN-1 glass and frangible hollow calcia-stabilized zirconia particles

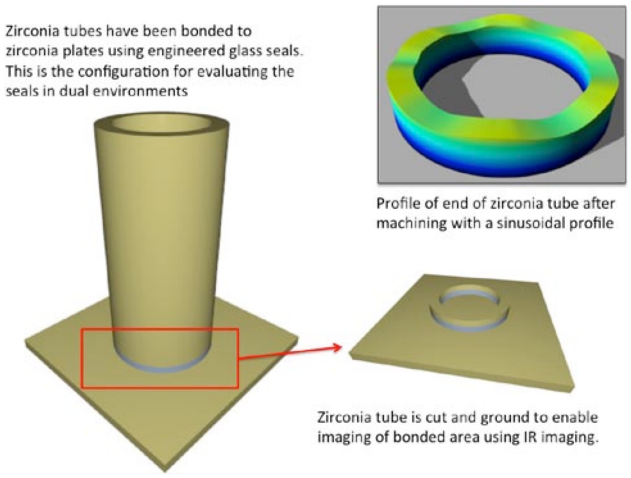

FIGURE 3. Experimental procedure used to demonstrate the ability of engineered glass seals to seal surfaces that are not flat and/or parallel. The inset shows the end of the zirconia tube that had been machined with a sinusoidal profile with an amplitude of 75 μm.

seals to seal surfaces that are not flat or parallel. In this case, the end of a zirconia tube was machined with an arbitrary contour and bonded against a flat zirconia plate. The integrity of the joint was examined by infrared imaging, and its hermeticity was evaluated using a dual environmental test set-up. In this set-up the inside of the zirconia tube (and seal) is exposed to a gas mixture of $H_2 + N_2 + H_2O$ while the outside surface of the tube (and seal) is exposed to air. The flow of the gases and their pressure was monitored throughout the test to quantify the sealing characteristics of the engineered glass seal.

As indicated above, an important feature of these engineered glass seals is the ability of controlling their viscosity. Figure 4 shows the viscosity of composite glass seals consisting of SCN-1 glass reinforced with frangible calcia-stabilized zirconia particles as a function of temperature for various concentration values of particles. These results demonstrate that it is possible to control viscosity of the engineered glass seal by several orders of magnitude over the range of expected operating temperatures in SOFCs. This is an important result because it will be possible to tailor the value of viscosity, depending on the temperature distribution in stacks, by changing the concentration of ceramic particles or fibers.

The addition of ceramic particles into the glass also modifies its wetting characteristics. Figure 5 shows a micrograph showing the effect of concentration of frangible zirconia particles on the contact angle of SCN-1 glass for three different values of particle concentration. It was found that contact angle increases with the concentration of ceramic particles.

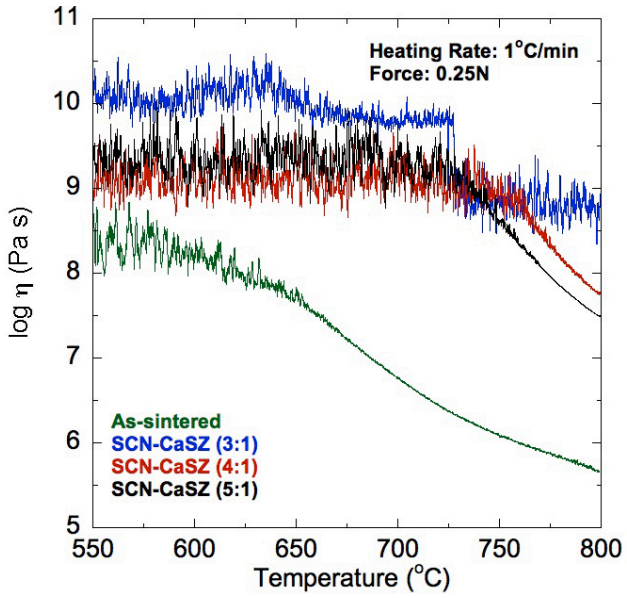

FIGURE 4. Viscosity of engineered glass seals, consisting of SCN-1 glass matrix and frangible hollow calcia-stabilized zirconia particles, as a function of the concentration of particles

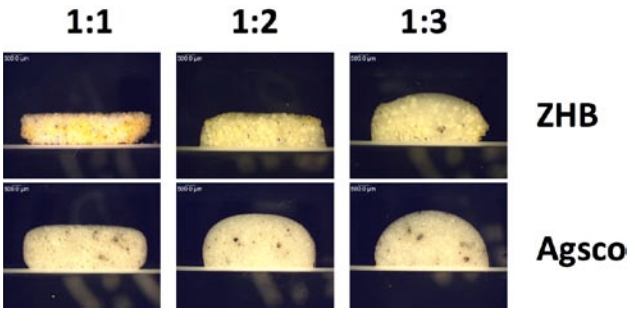

FIGURE 5. Effect of concentration of zirconia particles on the wetting behavior of SCN-1 glass on 8YSZ. The numbers correspond to weight ratios between glass and particles.

Conclusions and Future Directions

Characterization of the physical and mechanical properties of glass specimens of SCN-1 and G6 that have been exposed to air and $H_2O + H_2 + N_2$ environments at 800°C for 10,000 hours was completed. Sets of test specimens continue being exposed to both air and $H_2O + H_2 + N_2$ with the objective of achieving exposure times in excess of 20,000 hours. Future work will be focused on optimizing engineered glass seals, developing low-cost manufacturing processes and transferring the technology to SECA industry teams.

FY 2012 Publications/Presentations

1. Engineered Glass Seals for SOFCs, Presented at 30th SECA Workshop, Pittsburgh, Pennsylvania, July 25, 2012.

2. Silicate Glass Composite Seals for SOFCs, Poster Presentation at 30th SECA Workshop, Pittsburgh, Pennsylvania, July 24, 2012.

3. R. Trejo, E. Lara-Curzio, A. Shyam, M.J. Kirkham, V. Garcia-Negron and Y. Wang, "Physical and Mechanical Properties of Barium Alkali Silicate Glasses for SOFC Sealing Applications," Accepted for publication in *International Journal of Applied Glass Science* (2012).

References

1. ORNL SECA Annual Report for FY 2010, December 2010.

2. "Characterization of a Barium Silicate Glass," ORNL Technical Report TM-SECA-02-09.

3. ORNL SECA Annual Report for FY 2011, December 2011.

4. ASTM-C1351, "Measurement of Viscosity of Glass Between 10^4 Pa·s and 10^8 Pa·s by Viscous Compression of a Solid Right Cylinder," ASTM International, Conshohocken, Pennsylvania.

III.E.3 SOFC Stack Fixture Development and Testing

Y.S. Chou (Primary Contact) and J.W. Stevenson
Pacific Northwest National Laboratory
P.O. Box 999, MS K2-44
Richland, WA 99352
Phone: (509) 375-2527; Fax: (509) 375-2186
Email: Yeong-Shyung.Chou@pnnl.gov

DOE Project Manager: Briggs White
Phone: (304) 285-5437
Email: Briggs.White@netl.doe.gov

Contract Number: FWP40552

Start Date: October 1, 2011
End Date: September 30, 2012

Fiscal Year (FY) 2012 Objectives

- Develop a stack test fixture to validate candidate solid oxide fuel cell (SOFC) materials and processing techniques.
- Evaluate long-term performance of Ce-modified (Mn,Co)-spinel coated American Iron and Steel Institute (AISI) 441 and other stack materials under realistic SOFC test conditions.

FY 2012 Accomplishments

- Completed two long-term (800°C/~6,000 h) performance evaluations of anode-supported cells with candidate (Mn,Co)-spinel coating on AISI 441 interconnect.
- Validated the stability of (Mn,Co)-spinel coating for AISI 441 interconnect.
- Established a generic short-stack test fixture protocol for processing and testing.

Introduction

To date, most SOFC materials development research is conducted on small scale cells, called "button" cell, which typically have an active area of 2 cm^2 or less. The small-sized cells offer rapid turn-around time and require relatively small amounts of materials and equipment, and are therefore well suited for iterative materials optimization studies. However, the electrochemical performance of small-sized cells may not be representative of the larger cells fabricated and tested by industrial developers, due to non-realistic gas composition and flow fields, unrealistic seals and current collectors, and the absence of interconnect materials. To help bridge the gap between button cells and full-sized stacks, Pacific Northwest National Laboratory (PNNL) has developed a generic SOFC stack test fixture. The primary purpose of the fixture is to evaluate new materials and processing techniques in a realistic SOFC stack environment, as a potential step towards transfer of the new technology to the Solid State Energy Conversion Alliance (SECA) industrial teams. In previous studies, (Mn,Co)-spinel coatings were demonstrated to have very stable, high conductivity on AISI 441 stainless steel, a candidate interconnect material, and to block the volatilization of Cr, which can cause severe degradation of cathode performance. The addition of a small amount of Ce to the coating was found to improve the adhesion of the oxide scale that grows under spinel coating to the underlying steel substrate. However, these tests were all conducted on small metal coupons in the absence of a realistic SOFC stack environment. To gain further insight into the performance and stability of the Ce-modified spinel coated AISI 441, 3-cell stack fixture tests were assembled and tested using interconnects fabricated from coated AISI 441.

Approach

Long-term performance of a 3-cell stack fixture with commercial $La_xSr_{1-x}MnO_{3-\delta}$ (LSM)-based anode-supported cells (2"x2") and AISI 441 interconnects was evaluated at 800°C for ~6,000 hours. Ce-modified (Mn,Co) spinel coatings were applied to the cathode region of the interconnect, and reactive air aluminization, also developed at PNNL, was applied to the sealing areas. Refractory glass seals were used to seal the ceramic cells onto aluminized cell frame plates. Hybrid mica seals with glass interlayers were used as perimeter seals. $La_{0.8}Sr_{0.2}MnO_3$ and NiO pastes were used as cathode and anode contact materials, respectively. Ni mesh was spot welded onto interconnect plate as current collector on anode side. The short stack was tested in constant current mode with humidified fuel (H_2:N_2=1:1) and air. Cell voltages were monitored versus time and impedance data was collected periodically. Upon completion of the test, the stack was disassembled and examined. Areas of interest were evaluated with scanning electron microscopy (SEM) and energy dispersive spectroscopy (EDS).

Results

Long-term electrochemical performance

The electrochemical performance of each cell of a 3-cell stack fixture test is shown in Figure 1. From open voltage circuit (OCV) measurements, it was found that there were leaks of the middle and bottom cells after around 2,000 h, while the OCV of the top cell remained fairly constant and close to the theoretical value. In the first 2,000 h the degradation rates of the top, middle, and bottom cell were 1.4%/1,000 h, 5.0%/1,000 h, and 3.3%/1,000 h, respectively. The degradation rates from 2,000 h to ~6,000 h were 2.5%/1,000 h, 22.6%/1,000 h, and 18.5%/1,000 h for the top, middle, and bottom cell, respectively.

Ce-Modified (Mn,Co)-Spinel Coating

Post-test examination indicated that the spinel coating remained intact without de-bonding or spallation from the steel interconnects, indicating that the coating was effective in preventing extensive oxidation of the AISI 441 which can lead to spallation. Figure 2 shows an interfacial region between the cathode contact material (right side of image) and a spinel coated AISI 441 interconnect (left side of image). EDS analysis indicates formation of a Cr-rich oxide scale beneath the coating, with detectable but decreasing Cr content in the coating with increasing distance from the steel interconnect. The Cr content in the contact material appeared to be negligible. Therefore, the spinel appears to have been effective in significantly reducing volatilization/diffusion of Cr from the steel. It should be noted that the spinel coating was very thin in some interconnect regions, probably due to non-homogeneity in the spray-based coating application process. Figure 3 shows the microstructure of one such region; results of EDS spot analysis are shown in Table 1. As expected, Si and Ti, present in the AISI 441, were detected near the coated interface (spots #1 and #2). However, the presence of Si did not result in formation of a continuous silica layer, which would greatly increase the ohmic resistance and thereby reduce stack performance. At the center of the coating (spot #3), EDS showed an Mn/Co atomic ratio of 9.23:6.44=1.43:1, which differs from the nominal ratio of 1:1. The excess Mn likely diffused from the AISI 441 substrate. Note that a discrete thin layer of (Mn,Cr)-oxide is often observed on top of the Cr_2O_3 scale after oxidation of uncoated AISI 441. Although some Cr was detected within the dense coating layer, no Cr was detected

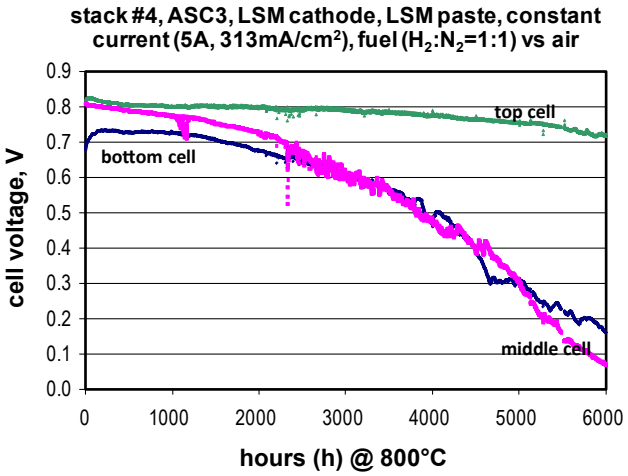

FIGURE 1. Electrochemical performance data of a long-term stack fixture test. The stack was tested at 800°C using diluted fuel (H_2:N_2=1:1) bubbled through water at room temperature.

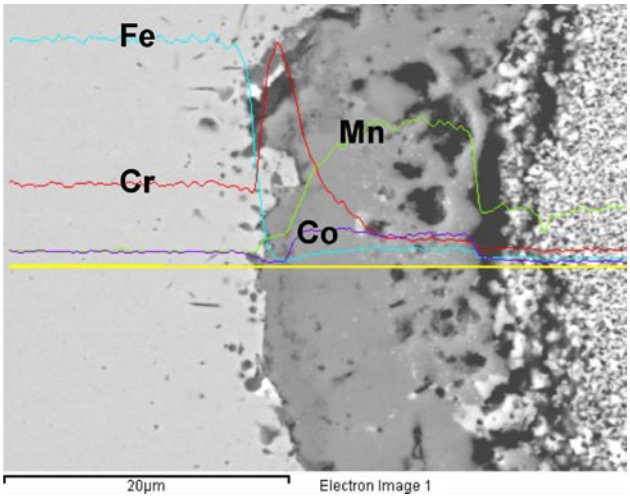

FIGURE 2. Elemental line scan across the Ce-modified (Mn,Co) spinel coating between contact material and AISI 441 substrate

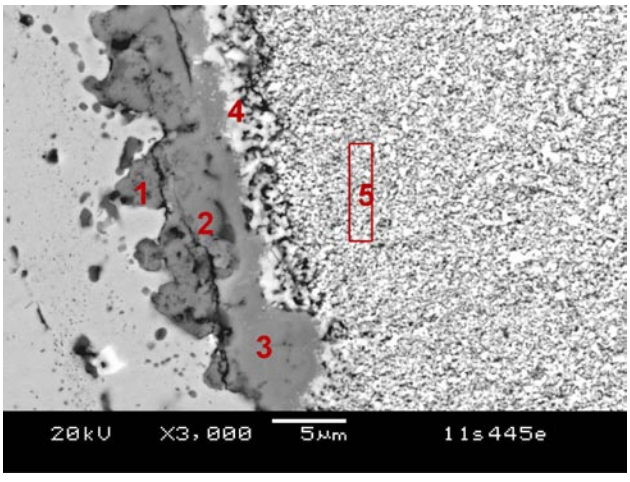

FIGURE 3. Microstructure of a Ce-modified (Mn,Co) spinel coated AISI 441 interconnect and cathode contact material; results of EDS analysis listed in Table 1

TABLE 1. EDS analysis of the indicated regions in Figure 3

spot #	O	Si	Ti	Cr	Mn	Fe	Co	Sr	Nb	La
1	65.05	0.69	3.89	27.08		3.09			0.20	
2	63.55	1.46	1.04	26.02	3.94	0.42	3.56			
3	63.38	0.56		19.85	9.23	0.53	6.44			
4	62.01		1.38	0.61	16.46	0.82	1.26	3.11		14.35
5	60.45				18.25		0.89	3.53		16.88

outside this layer, as Cr content dropped to 0.61 at% at spot #4, and no Cr was detected in the cathode contact material (rectangular area #5). The Fe content in the coating was negligible, indicating effective protection of the steel against runaway oxidation.

Glass Seals

Another important component subjected to analysis was the refractory alkaline-earth silicate sealing glass used for the cell-to-frame seal. Devitrifying glasses are good candidates for sealing because, after the sealing process is complete, they undergo substantial crystallization which stabilizes the microstructure and minimizes seal mobility. In the 6,000-hour tests, a glass developed at PNNL was used to seal the yttria-stabilized zirconia (YSZ) electrolyte of the cell to the surface of an AISI 441 cell frame which had been aluminized using a reactive air aluminization process, which was also developed at PNNL. Previous research at PNNL has shown that aluminized surfaces can substantially improve the interfacial strength and stability compared to non-aluminized surfaces, primarily by minimizing the interaction between Cr in the steel and alkaline earth elements in the glass. Figure 4 shows the microstructure of the glass and aluminized AISI 441 near the air side of a seal. Seven spots were selected for EDS analysis; the results are listed in Table 2. Overall, the sealing glass (about 300-400 microns thick) showed no sign of large pore formation, indicating that any existing defects did not coalescence to form large ones, likely due to the set microstructure which limited migration. Examination of the aluminization/glass interface indicated that the initial dense, continuous alumina layer on the steel was no longer present. Instead the microstructure near the metal/glass interface showed an interaction zone (spots #1-4) that differed from the crystallized glass matrix (spots #5-7). EDS analysis (Table 2) clearly showed substantial diffusion of Al into the glass; a substantial amount of Cr was also detected, e.g., 14 at% of spot #4. Spot #4 has a (Ba+Sr):Cr ratio nearly equal to 1:1, which suggests the possible formation of alkaline earth chromate. Formation of this phase can lead to micro-cracking due to its very large CTE, although no such damage was observed in this sample.

The interfacial microstructure at the fuel side was also examined (see Figure 5). Again the glass was well-bonded to the aluminized AISI 441; cracks from the metallographic preparation occurred away from the glass/metal interface. There were some shallow and discontinuous voids near the glass/metal interface, shown as a dark region in center of Figure 5, but no cracking

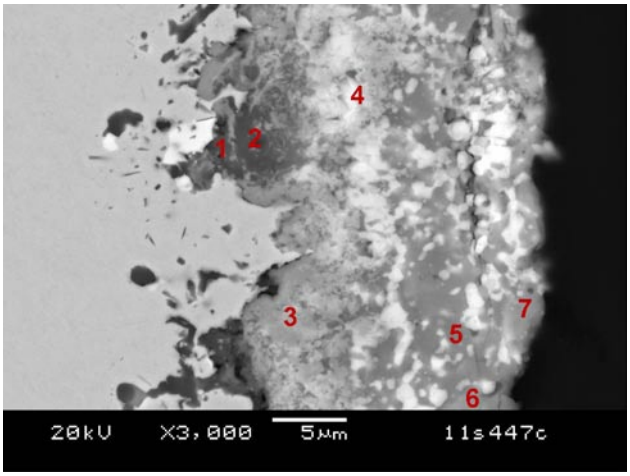

FIGURE 4. Microstructure of the aluminized AISI 441 and sealing glass near the air side of the seal; results of EDS analysis listed in Table 2

TABLE 2. EDS analysis of the indicated regions in Figure 4

spot #	O	Na	Al	Si	Ti	Cr	Mn	Fe	Sr	Ba	Cu	Ce	Nb	K
1	66.74	0.76	26.89	0.94	0.83	1.35	0.12	0.41	1.48				0.47	0.22
2	62.68	0.59	32.13	0.65	0.85	1.63	0.12	0.17	1.17					
3	71.70		2.46		4.81	10.50	5.41	0.36	4.05		0.25	0.46		
4	67.52	0.74	2.11			14.01	1.08	0.26	3.31	10.97				
5	61.55	5.25	14.38	5.82		4.13			7.17	1.49				
6	64.17	1.34	13.19	12.01		1.10	1.07	0.15	2.89	4.08				
7	63.91	3.83	13.99	3.86	0.41	3.05	1.55	0.35	8.25	0.61				0.17

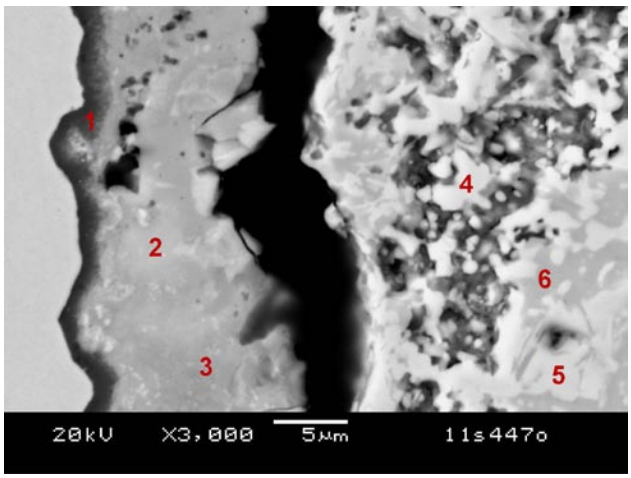

FIGURE 5. Microstructure of the aluminized AISI 441 and sealing glass near the fuel side of the seal; results of EDS analysis listed in Table 3

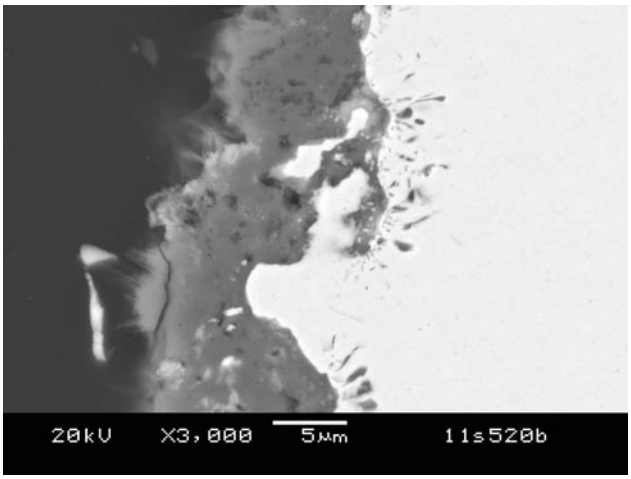

FIGURE 6. Microstructure of aluminized AISI 441 exposed to air during ~6,000 hour stack fixture test

TABLE 3. EDS analysis of the indicated regions in Figure 5

spot #	O	Al	Si	Cr	Mn	Fe	Sr	Y	Ba
1	62.29	31.45		1.50		4.58			0.18
2	63.44	14.01	5.38	4.76	0.32	2.48	3.47	0.43	5.71
3	64.79	8.23	4.53	4.57	0.25	2.58	10.72	1.62	2.72
4	68.62	1.12	7.31	0.13		0.74	12.07	8.46	1.54
5	69.27		5.31				12.13	11.36	1.94
6	63.40		19.43				15.82		1.35

occurred in that region. EDS results for selected spots are listed in Table 3. Unlike the air side, the alumina layer on the steel remained intact and dense. The Cr content (~4.5-4.7 at% in spots #2-3) was lower as compared to the air side (10-14 at%), and little or no Cr was detected within the glass matrix (#4-6).

In addition to the interface between glass and the aluminized AISI 441 substrate, the interface between the glass and the YSZ electrolyte was examined. The glass/YSZ interface appeared to be relatively weak, as evidenced by the fracture which occurred there during metallographic preparation. EDS analysis indicated little or no reaction between the glass and the YSZ.

Aluminized regions of the steel outside of the sealing region were also analyzed. The performance of uncovered aluminized surfaces are of interest not only for stack interconnect applications but also for balance of plant components upstream of the stack. Figure 6 shows a micrograph of an aluminized AISI 441 surface exposed to air during the 6,000-hour test. Overall, the aluminization layer appeared to be dense, homogeneous, and stable, consisting almost exclusively of alumina, as determined by EDS analysis. Similar results were observed for aluminized surfaces exposed to fuel during the test.

Conclusions and Future Directions

A generic stack test fixture was developed and used for long-term evaluation of candidate SOFC stack materials, including modified spinel coatings, aluminization, sealing glass, and AISI 441 interconnects. Post-test analysis after an 800°C/~6,000 h test showed that the Ce-modified spinel coating remained adherent to AISI 441 interconnects. No spallation was observed, indicating good bonding and effectiveness in minimizing oxidation and growth of the underlying Cr oxide scale. EDS analysis revealed some diffusion of Cr and Mn into the spinel coating. In regard to the sealing glass, no distinct reaction was observed at the YSZ electrolyte interface, while some interaction was observed between the glass and the aluminized AISI 441 interconnect surfaces. Overall, the 6,000-hour short stack test validated the stability of Ce-modified spinel coatings, aluminization, refractory sealing glass, and candidate AISI 441 interconnects. Future work will be focused on two areas: evaluation of new candidate materials and processing techniques; and optimization of the test fixture design.

FY 2012 Publications/Presentations

1. Y.S. Chou, J.W. Stevenson, and J.P. Choi, "Evaluation of a Single Cell and Candidate Materials with High Water Content Hydrogen in a Generic Solid Oxide Fuel Cell Stack Test Fixture, Part II: Materials and Interface Characterization," *International J. Appl. Ceram. Tech*., 9, 1 (2012).

2. Y.S. Chou, E.C. Thomsen, J.P. Choi, G.G. Xia, and J.W. Stevenson, "Long-Term Solid Oxide Fuel Cell Candidate Material Evaluation in a 3-cell Short Stack Geometry at Pacific Northwest National Laboratory," Fuel Cell Seminar and Exhibition, Orlando, Florida, November, 2011.

3. Y.S. Chou, J-P Choi, J.W. Stevenson, G-G Xia, J.F. Bonnett, and W.E. Voldrich, "Long-term Evaluation of Ce-modified (Mn,Co) Spinel Coating for SOFC Application in a 3-cell Short Stack Geometry," 36th International Conference and Exposition on Advanced Ceramics and Composites (ICACC), Daytona Beach, Florida, January, 2012.

III. SECA CORE TECHNOLOGY R&D

F. Fuel Processing

III.F.1 Solid Oxide Fuel Cells Operating on Alternative and Renewable Fuels

Chunshan Song (Primary Contact), Serguei Lvov, Xiaoxing Wang, Mamoru Fujii, Jing Xiao, Wenying Quan, Cigdem Sentorun-Shalaby, Debanjan Das, Mark LaBarbera, Sanchit Khurana, Mark Fedkin, and David Johnson

Pennsylvania State University
EMS Energy Institute and Department of Energy and Mineral Engineering
C211 CUL
University Park, PA 16802
Phone: (814) 863-4466; Fax: (814) 865-3573
Email: csong@psu.edu

DOE Project Manager: Joseph Stoffa
Phone: (304) 285-0285
Email: Joseph.Stoffa@netl.doe.gov

Contract Number: NT0004396

Start Date: October 1, 2010
End Date: August 31, 2013

Fiscal Year (FY) 2012 Objectives

- Develop new fuel processing approaches for using selected alternative and renewable fuels--anaerobic digester gas (ADG) and commercial diesel fuel, for solid oxide fuel cell (SOFC) power generation systems.
- Develop and evaluate effective sorbents for contaminants removal including hydrogen sulfide, ammonia, and siloxane for ADG purification.
- Improve the performance of the metal-oxide-based adsorbents for adsorptive desulfurization (ADS) of ultra-low sulfur diesel (ULSD).
- Evaluate the state of materials and material interfaces on a commercial Delphi SOFC stack running on alternative hydrocarbon fuels instead of hydrogen.
- Define the electrochemical processes occurring in the Delphi fuel cell stack, on both the short- and long-term scales.

FY 2012 Accomplishments

- A series of mixed oxide adsorbents have been developed and evaluated for H_2S removal at room temperature. A high sulfur capacity of ca. 4 wt% has been achieved, which is better than the commercial SulfaTrap™ R7 adsorbent under the studied conditions.
- For the mixed oxide adsorbent, various preparation methods including co-precipitation and incipient wet impregnation have been applied. A proper preparation method has been identified for the best result.
- The selected mixed oxide adsorbent has been characterized by N_2 physisorption and H_2 temperature-programmed reduction to fundamentally understand the relationship between the structure and the adsorption performance. The high capacity may be attributed to its higher surface area and high dispersion of active metal oxide phase.
- Based on the concept of molecular basket, a novel solid sorbent (NH_3-MBS) has been developed for ammonia sorption at ambient conditions. The NH_3-MBS was prepared by loading acidic polymer on porous material and evaluated for NH_3 adsorption at ambient conditions. The sorbent can be regenerated at 100°C.
- A preliminary test on siloxane removal has been conducted over the silica gel and lab-prepared mesoporous materials. The mesoporous silica showed a much higher adsorption capacity than silica gel.
- The effect of fuel composition, adsorption temperature and in situ air flow on the ADS performance of Ti-based binary mixed oxide adsorbent have been studied and clarified. A significant increase in the ADS breakthrough capacity from 2.5 to 22.5 g-F/g-sorb was obtained when in situ air was added. The material was further studied by X-ray absorption technique and high resolution transmission electron microscopy (HRTEM) to fundamentally understand the role of CeO_2.
- Another highly efficient adsorbent for deep adsorptive desulfurization of diesel fuel has been developed by loading T-based mixed ternary oxide over mesoporous support, the breakthrough capacity of which reached as high as 95 g-F/g-sorb, indicating a significant promotion role of added silver oxide.
- An SOFC system was tested with hydrogen, ADG, and reformed diesel fuel. A comparative study on the data was carried out. Extended power generation and degradation characterization tests were carried out using ADG as the fuel. Electrochemical impedance spectroscopy (EIS) and equivalent circuit modeling were used to track the degradation of the SOFC performance over a period of 200+ hours.

- In this period, the work has generated seven journal articles and four presentations for the national/ international conferences.

Introduction

The work at Pennsylvania State University (Penn State) focuses on the development of fuel processors for both ADG and commercial diesel fuels for integration with SOFC power generation systems. As scheduled, in this annual report period, our major work focused on (1) preparation and evaluation of novel sorbents including mixed metal oxides adsorbents and molecular basket sorbent (MBS) for ADG cleanup including H_2S removal, ammonia capture and siloxane removal; (2) improving the adsorption performance of mixed Ti-Ce-O-based adsorbents for deep adsorptive desulfurization of ULSD; (3) characterization of above-mentioned adsorbents for better understanding the sorbent materials and guiding the future development; and (4) developing a combined steam reforming-SOFC system to generate electric power from commercial diesel fuel.

Approach

To achieve the FY 2011 objectives, the following approaches have been applied:

1. Among ADG cleanup, the contaminants including H_2S, ammonia and siloxane have been considered. To achieve a better performance and higher capacity, mixed Cu-Ti-Ce metal oxide adsorbents have been explored for H_2S adsorption. For ammonia removal, a novel solid sorbent has been prepared on the basis of molecular basket concept invented by our lab, which may be able to provide a regenerable sorbent material for NH_3 capture. As for the removal of siloxane, silica gel, which is widely suggested, will be explored. Mesoporous molecular sieves such as Mobil Composition of Matter (MCM)-41 and Santa Barbara Amorphous (SBA)-15 are considered good candidates due to high surface area, large pore volume and pore size, and uniform pore structure.
2. For ADS of diesel, it is expected that a high capacity could be achieved by converting sulfur species to sulfur oxide species (e.g., sulfone) over the developed Ti-Ce-O adsorbent. Thus, introducing in situ air during the ADS process as a new approach has been applied and explored for deep removal of sulfur from ULSD.

Results

Development of ADG Fuel Processor Concept (Novel)

Our last report has shown that Cu-Ti-Ce mixed metal oxide adsorbent is superior to the commercial SulfaTrap R7 adsorbent. In this period, we have studied the effect of preparation method including co-precipitation and impregnation method on the performance of the adsorbent. It was found that the adsorbent prepared by co-precipitation method at the pH value of seven has the best capacity. The prepared adsorbents have also been characterized by N_2 physisorption and H_2-TPR. The results suggested that the high capacity may be attributed to the highly dispersed CuO phase and relatively higher surface area. Furthermore, the regenerability of the Cu-Ti-Ce adsorbent has been investigated. Figure 1 shows the adsorption capacity as a function of regeneration cycles in comparison with SulfaTrap R7 adsorbent. Although the capacity decreased with the cycles, the capacity after five cycles still reached 0.95 mmol-H_2S/g-Ads (or 3.2 wt%), about 30% higher than that for the fresh TDA SulfaTrap R7 adsorbent. It implies that the developed CuO-TiO_2-CeO_2 adsorbent in this project is promising for H_2S removal from biogas.

In addition to sulfur compounds, ammonia and siloxanes are two major contaminants in biogas, which are harmful to the environment and detrimental to any devices in the ADG processing, e.g., corrosion, erosion, fouling. As part of the project, a new solid sorbent has been developed on the basis of molecular basket concept for NH_3 sorption at ambient conditions. The material showed good sorption capacity for ammonia removal at the concentrations of 0.05-0.5%. The NH_3-MBS sorbent can be fully regenerated at elevated temperature such as

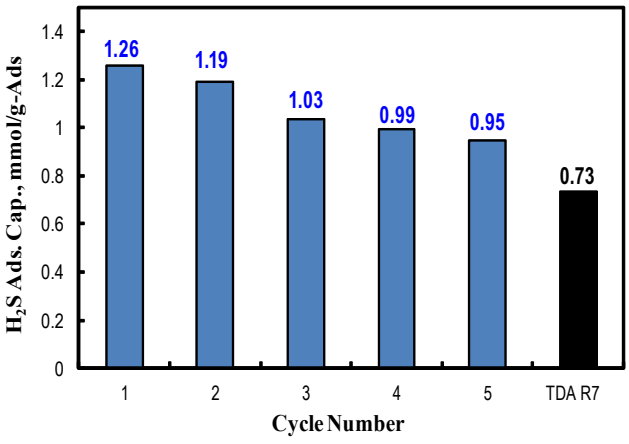

FIGURE 1. H_2S adsorption capacity as a function of regeneration cycle number over the CuOTiO_2-CeO_2 adsorbent. H_2S adsorption and adsorbent regeneration was performed at room temperature and 350°C, respectively.

100°C, and the sorbed NH_3 could be recovered for other usage. Additionally, a primary study was conducted on siloxane removal over commercially available adsorbents such as silica gel and lab-prepared mesoporous molecular sieves including MCM-41 and SBA-15 using hexamethyldisiloxane (L2, or MM) as the model siloxane compound. The silica gel material had a good performance for siloxane capture. MCM-41 and SBA-15 showed a much better capacity (about twice that of silica gel) due likely to their higher surface area and uniform pore structure.

Deep Desulfurization of ULSD

The effect of fuel composition on the performance of Ti-Ce-O adsorbent for adsorptive desulfurization has been studied using a model diesel, which suggested that critical inhibiting or competitive components for ADS are present in real diesel fuel. The selectivity decreased as the order: Indole > $DBTO_2$ > DBT > MDBT > BT > DMDBT > Phe > Flu ~ MNap > Nap. The competitive adsorption of nitrogen compounds may inhibit ADS over the Ti-Ce-O adsorbent. The adsorption temperature influenced the ADS performance. Higher temperature resulted in a lower capacity. Adding in situ air flow greatly improved the ADS performance of Ti-Ce-O adsorbent. The ADS breakthrough capacity increased significantly from 2.5 to 22.5 g-F/g-sorb. The promotion effect can be attributed to the oxidation of sulfur compounds which are more prone to be adsorbed, as proven by gas chromatography flame ionization detector (GC-FID) and S-X-ray absorption near edge structure (XANES). The role of Ce in Ti-Ce-O adsorbent has been studied by X-ray absorption technique and HRTEM. The addition of CeO_2 significantly promoted the adsorption capacity of TiO_2, especially with in situ air flow. Besides, the MCM-48 supported Ti-Ce-O adsorbent has also been studied. By adding small amount of silver oxide, the ADS capacity of Ti-Ce-Ag-O/MCM-48 adsorbent reached as high as 95 g-F/g-sorb, suggesting a promotion role of silver oxide.

Delphi SOFC Stack Running on Alternative Fuels

A combined steam reforming-SOFC test system was developed and used to generate electric power from commercial diesel fuel. The SOFCs used in these experiments were NextCell-B button cells with 1.256 cm^2 active area (Fuel Cell Materials). The SOFC membranes in these cells were 150 µm dense yttria stabilized zirconia (YSZ), 8 mol% yttria. The anode layer was a porous 50 µm Ni-YSZ cermet, and the cathode layer was a porous 50 µm lanthanum strontium manganite (LSM).

Cell performance was tested with hydrogen, ADG, and reformed diesel, and a comparative study on the data was carried out. Extended power generation and degradation characterization tests were carried out using ADG as fuel. EIS and equivalent circuit modeling were used to track the degradation of SOFC performance over a period of 200+ hours. During the extended power generation testing, periodic polarization and EIS tests were carried out in an effort to characterize the nature of SOFC performance degradation. The polarization testing carried out was done by applying a series of decreasing external electronic loads between the SOFC electrodes while monitoring current and voltage responses. Figure 2 shows the change in polarization behavior between 175 and 225 hours of power generation; this time period corresponds to a 20% overall power reduction shown. The EIS Nyquist plots shown in Figure 3 demonstrate separate contributions to overall inefficiencies in the electrochemical system. An equivalent circuit has been developed to fit the measured impedance behavior to individual kinetic, ohmic, and mass transport resistance contributions.

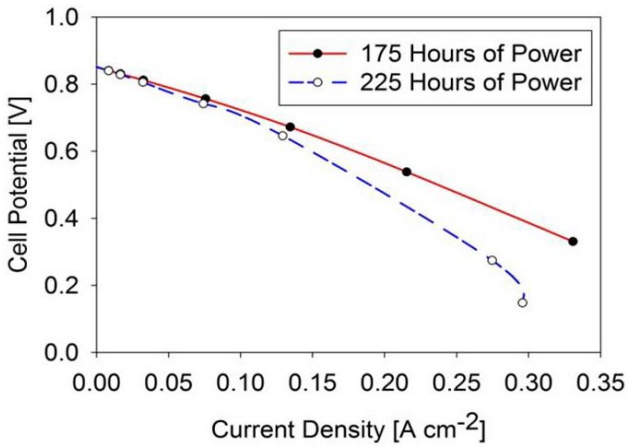

FIGURE 2. Polarization analysis of Ni-YS anode fueled with anaerobic digester gas for 175 and 225 hours

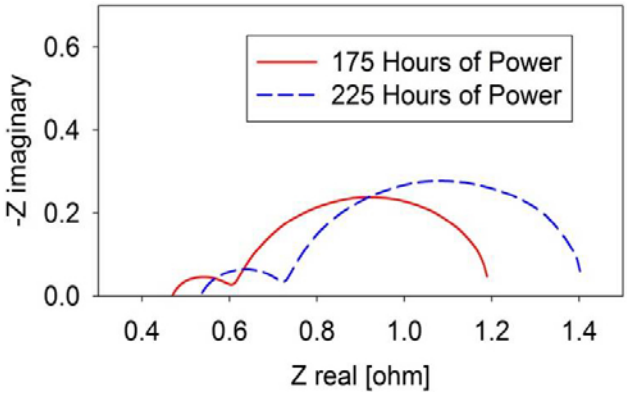

FIGURE 3. Nyquist plot of SOFC system after 175 and 225 hours of power generation from anaerobic digester gas

Conclusions and Future Directions

Within this period, the following conclusions can be drawn:

- A series of Cu-Ti-Ce mixed oxide adsorbents have been developed in this project for ADG cleanup. The Cu-Ti-Ce adsorbent prepared by urea co-precipitation method at pH value of seven exhibited very good performance for ADG cleanup. Before breakthrough, it can treat ca. 150 L-ADG/g or a breakthrough capacity of ca. 4 wt%.
- Cu-Ti-Ce mixed oxide adsorbents have been prepared by co-precipitation at the pH values of seven and 10, and by incipient wet impregnation (IWI) method. The Cu-Ti-Ce adsorbent prepared by co-precipitation method at pH value of seven showed the best, probably because of its higher surface area and high dispersion of CuO phase.
- The regeneration of the Cu-Ti-Ce adsorbent was performed at 350°C using air. A slight decrease in the capacity was observed. After five cycles of regeneration, the Cu-Ti-Ce adsorbent preserved an adsorption capacity of about 3 wt%, indicating the adsorbent is regenerable somehow.
- A novel solid sorbent based on the concept of molecular basket sorbent (NH_3-MBS) has been developed for ammonia sorption at ambient conditions. The NH_3-MBS was prepared by loading 50 wt% of an acidic polymer on fumed silica and was evaluated for NH_3 adsorption at room temperature. The sorbent can be regenerated at 100°C.
- A primary test on siloxane removal has been conducted over the commercial silica gel and lab-prepared MCM-41 and SBA-15. Both MCM-41 and SBA-15 showed a much higher adsorption capacity than silica gel.
- It was found that fuel composition, adsorption temperature and flowing in situ air could greatly affect the ADS performance of the Ti-Ce-O adsorbent. The competitive adsorption of nitrogen compounds may inhibit ADS over the Ti-Ce-O adsorbent. Higher adsorption temperature resulted in a lower capacity. The addition of in situ air flow can greatly improve the ADS performance of Ti-Ce-O adsorbent with a significant increase in capacity from 2.5 to 22.5 g-F/g-sorb.
- The adsorption capacity of Ti-Ce-O/MCM-48 adsorbent for deep adsorptive desulfurization of diesel fuel can be greatly enhanced by incorporating a small amount of silver oxide. Under the same conditions, a breakthrough capacity as high as 95 g-F/g-sorb can be attained over the Ti-Ce-Ag-O/MCM-48 adsorbent.

FY 2012 Publications/Presentations

1. C. Xie, Y.S. Chen, Y. Li, X.X. Wang and C.S. Song, "Influence of Sulfur on the Carbon Deposition in Steam Reforming of Liquid Hydrocarbons over CeO_2-Al_2O_3 Supported Ni and Rh Catalysts," Applied Catalysis A: General, 2011, 394 (1-2), 32-40.

2. J.H. Guo, C. Xie, K.T. Lee, J.T. Miller, N. Guo, M.J. Janik, and C.S. Song, "Improving the Carbon Resistance of Ni-Based Steam Reforming Catalyst by Alloying with Rh. A Computational Study Coupled with Reforming Experiments and EXAFS Characterization," ACS Catalysis, 2011, 1, 574-582.

3. C. Sentorun-Shalaby, S.K. Saha, X.L. Ma, and C.S. Song, "Mesoporous-Molecular-Sieve-Supported Nickel Sorbents for Adsorptive Desulfurization of Commercial Ultra-Low-Sulfur Diesel Fuel," Applied Catalysis B: Environmental, 2011, 101 (3-4), 718-726.

4. M. LaBarbera, M. Fedkin, X. Wang, X. Chao, C. Song, and S. Lvov, "Solid Oxide Fuel Cell Fueled by Diesel Reformate and Anaerobic Digester Gas," ECS Transactions, 2011, 35 (1), 2867-2872.

5. C. Xie, Y.S. Chen, M.H. Engelhard and C.S. Song, "Comparative Study on the Sulfur Tolerance and Carbon Resistance of Supported Noble Metal Catalysts in Steam Reforming of Liquid Hydrocarbon Fuel." ACS Catalysis, 2012, *2*, 1127–1137.

6. S. Sitamraju, M.J. Janik and C.S. Song, "Selectivity of Adsorption of Thiophene and Its Derivatives on Titania Anatase Surfaces: A Density Functional Theory Study," Topics in Catalysis, 2012, 55, 229-242.

7. X.X. Wang, X.L. Ma, V. Schwartz, J.C. Clark, S.H. Overbury, S. Zhao, X. Xu, C.S. Song, "A Solid Molecular Basket Sorbent for CO_2 Capture from Gas Streams with Low CO_2 Concentration Under Ambient Conditions," Physical Chemistry Chemical Physics, 2012, 14, 1485-1492.

8. Xiaoxing Wang, Mamoru Fujii, Wenying Quan, Chunshan Song, "Development of Solid Adsorbents for Biogas Purification," 244th American Chemical Society (ACS) National Meeting, Philadelphia, Pennsylvania, August 19–23, 2012. Accepted.

9. Jing Xiao, Qiujing Yang, Xiaoxing Wang, Chunshan Song, "Air-Promoted Adsorptive Desulfurization (ADS) over TiO_2-CeO_2 Mixed Oxides from Ultra-Low Sulfur Diesel (ULSD) Under Ambient Conditions," 244th American Chemical Society (ACS) National Meeting, Philadelphia, Pennsylvania, August 19–23, 2012. Accepted.

10. Jing Xiao, Xiaoxing Wang, Qiujing Yang, Chunshan Song, "Effect of Support for TiO_2-CeO_2 on Adsorptive Desulfurization (ADS) from Ultra-Low Sulfur Diesel (ULSD) Under Ambient Conditions," 244th American Chemical Society (ACS) National Meeting, Philadelphia, Pennsylvania, August 19–23, 2012. Accepted.

11. Chunshan Song, James J Strohm, Jian Zheng, Yan Li, Chao Xie, Yongsheng Chen, Xiaoxing Wang, "Sulfur-Tolerant and Carbon-Resistant Bimetallic Catalysts for Steam Reforming of Liquid Hydrocarbon Fuels for Fuel Cells," 241st American Chemical Society (ACS) National Meeting, Anaheim, California, March 27–31, 2011.

III. SECA CORE TECHNOLOGY R&D

G. Modeling and Simulation

III.G.1 LG SOFC Model Development

Greg Rush
LG Fuel Cell Systems Inc. (formerly Rolls-Royce Fuel Cell Systems, Inc.)
6065 Strip Ave., NW
North Canton, OH 44720
Phone: (330) 491-4831
Email: greg.rush@lgfcs.com

DOE Project Manager: Patcharin Burke
Phone: (412) 386-7378
Email: Patcharin.Burke@netl.doe.gov

Subcontractor:
BAH Consulting Inc.
Toronto, Canada

Contract Number: FE0000773

Start Date: October 1, 2009
End Date: September 30, 2012

Fiscal Year (FY) 2012 Objectives

- Enhance the LG Fuel Cell Systems Inc., (LGFCS) (formerly Rolls-Royce Fuel Cell Systems) multi-physics code (MPC) to model transient behavior of cells, substrates, and bundles.
- Continue validation of steady-state bundle model predictions.
- Validate transient predictions of MPC cell/substrate/bundle current-voltage measurements during anticipated operational transients.
- Establish and test methodology for code-to-code comparisons with larger scale stack and system level simulation tools.
- Demonstrate MPC capabilities by developing models of specific applications of interest to LGFCS.
- Prepare MPC for use by LGFCS engineers outside of the project team.

FY 2012 Accomplishments

- Completion of MPC code enhancements for time dependent simulations as set out in project objectives.
- Further code enhancements to improve parallel computation efficiency and calculation stability during fuel starvation.
- Development of an acceleration algorithm to greatly reduce time taken to obtain converged solutions on large scale steady-state and transient models.
- Validation of bundle steady-state model predictions.
- Successful testing of transient models of penta (five) cells, substrates, and bundles.
- Development of models for specific LGFCS applications including:
  - Detailed analysis of substrate electrical connections.
  - Flow distribution analysis of bundle and strip.
  - Transient thermal analysis of bundle.
- Successful comparisons between MPC predictions and those made using other LGFCS modeling tools.
- MPC link established with mechanical analysis tools and successful export of MPC model predictions for use in thermal stress analysis.

Introduction

The objective of this project is for LGFCS to develop a multi-physics solid oxide fuel cell (SOFC) computer code for performance calculations of the LGFCS fuel cell structure to support fuel cell product design and development. This work consolidates years of LGFCS investment and research throughout the world as part of its business objective to develop a SOFC product for stationary power generation.

This project has proceeded on schedule and under budget. A one year no-cost project extension was granted that allows the third project year (FY 2012) to focus on developments that were beyond the original project scope. The focus of activity during the first year of the project (FY 2010) was the down-select of a suitable commercially available multi-physics computer code (CD-adapco STAR-CCM+) and commencement of the code enhancement and model verification/validation work required to develop and test the MPC. The second project year (FY 2011) focused on the extension of the MPC from small-scale models to substrate and bundle models and the development of degradation models to enable the prediction of fuel cell durability. The third project year (FY 2012) is focused on the extension of steady-state modeling capabilities to transient analysis, the demonstration of the MPC predictive capabilities for LGFCS engineering applications, and the enhancement of the MPC user interface for use by LGFCS engineers outside of the development team.

Approach

The MPC development project has been split into two work streams: (i) code enhancement and (ii) model verification and validation. A code enhancement methodology has been implemented whereby the MPC comprises three distinct elements, (a) STAR-CCM+, the down-selected, commercially available computational fluid dynamics simulation tool; (b) a Microsoft Excel spreadsheet where all model data is stored; and (c) a set of Java macros to perform all model operations.

This approach has been used to fully automate the process of installing all model features required to perform a SOFC simulation. The starting point is the model geometry, a computer aided design (CAD) fuel cell drawing that has been imported into STAR-CCM+. The MPC automatically configures the mesh, installs existing STAR-CCM+ models, installs the code enhancements required for new models, runs the simulation, and post-processes the results.

The model verification and validation program has run concurrently with the code enhancement program and has involved building and testing SOFC models on a variety of scales including: one, two, and three dimensional models of single cells, penta (five) cells, substrates, and bundles. The validation process involves several steps including comparisons with experimental data and predictions from other models.

Results

The MPC code enhancements for FY 2012 are complete and all model inputs required in addition to the model CAD geometry are stored in a Microsoft Excel spreadsheet. This spreadsheet consolidates the model settings into a single form and facilitates the quick checking and sharing of model data without requiring a STAR-CCM+ license. Figure 1 shows a sample part of this spreadsheet where details of the simulations to be performed are input by the user.

Figure 1 also shows in the "Iteration Schedule …" how the user is able to specify a number of different simulations (steady-state and transient) to run consecutively using the results from one calculation as the starting point for the next. These simulations are performed using a series of Java macros which use the information contained in the spreadsheet to perform the necessary tasks in STAR-CCM+.

The model verification and validation program for FY 2012 has successfully validated three-dimensional steady-state models of bundles and demonstrated the operation of transient penta cell, substrate, and bundle models. Figure 2 shows a plot of predicted steady-state

	A	B	C	
438	**Solver Settings**			
439		Name	Under Relaxation Factor	Time Discre
440		Solv1	0.3	First
441		Solv2	0.7	First
442		Solv3	0.9999	First
443		Solv4	0.99	First
444				
445				
446				
447				
448		Velocity	Pressure	Species
449	1	Solv1	Solv2	Solv2
450				
451				
452	**Iteration Schedule & Stopping Criteria**			
453		Inner Iterations	Time Step (s)	Calculation
454	1	1000	Steady	
455	2	100	0.10	
456	3	100	0.10	
457	4	100	0.10	
458	5	100	0.10	
459				
460				
461				
462				
463				
464				
465				
466				
467				
468				
469				
470				
471				
472				
473		Total Number of Iteration Loops	Physical Time	Total Outer
474	TotalTimes	5	0.80	
475		Start	End	
476	MacrosAtStartEnd			

FIGURE 1. Sample of Excel spreadsheet input file

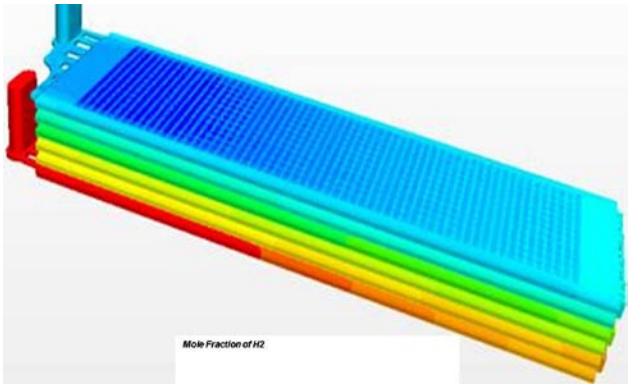

FIGURE 2. Predicted hydrogen mole fraction within a bundle model

hydrogen mole-fraction within a three-dimensional bundle model.

Figure 2 shows that the MPC is able to predict how substrate geometry influences hydrogen mole fraction in the anode of each cell; a lower mole fraction is seen in anode regions that are not directly above fuel channels where the flow path through the substrate is longer.

The MPC is also able to perform transient calculations and Figures 3 through 5 illustrate the predicted evolution of hydrogen mole fraction within a substrate model where there has been a sudden change in fuel input composition.

After reaching the steady-state, the inlet fuel hydrogen composition was reduced by 50% in a step change. Figures 4 and 5 show the transient hydrogen

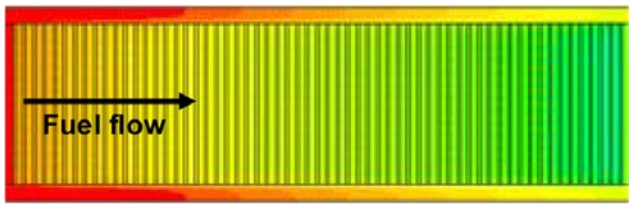

FIGURE 3. Steady-state distribution of hydrogen mole fraction within a three-dimensional substrate model

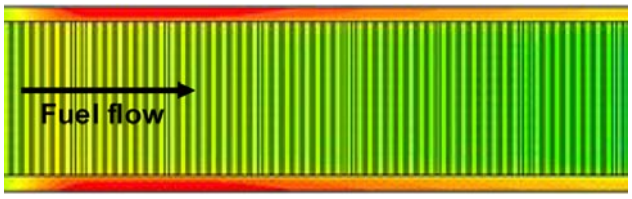

FIGURE 4. Transient distribution of hydrogen mole fraction 0.1 seconds after halving inlet fuel hydrogen composition

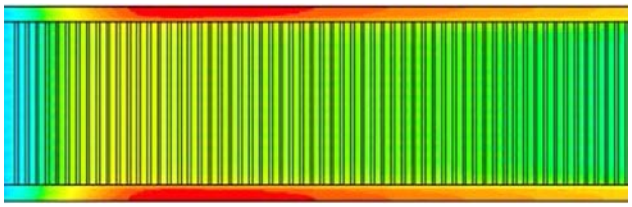

FIGURE 5. Transient distribution of hydrogen mole fraction 0.2 seconds after halving inlet fuel hydrogen composition

distribution calculated after 0.1 and 0.2 seconds following the step change.

In addition to the validation and verification activities described above, the MPC predictive capabilities have also been demonstrated in a wide range of engineering applications. In one application the MPC was used to predict the flow distribution and gas composition in a strip of bundles. Figure 6 shows the predicted distribution of hydrogen mole fraction for this strip model.

Conclusions and Future Directions

The aim of this project is for LGFCS to develop a multi-physics computer code for performance analysis of the LGFCS SOFC structure to support fuel cell product design and development. The MPC is based in the CD-adapco STAR-CCM+ computational fluid dynamics software package. The MPC development is organized into concurrent code enhancement and model verification/validation work programs.

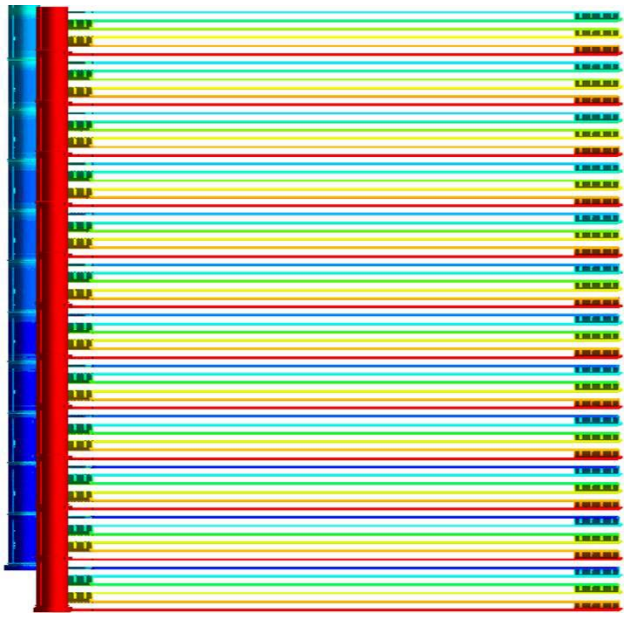

FIGURE 6. Steady-state distribution of hydrogen mole fraction within a three-dimensional strip model

This project has proceeded on schedule and under budget. A one year no-cost project extension was granted that allows the third project year (FY 2012) to focus on developments that were beyond the original project scope.

A code enhancement methodology has been implemented to fully automate all aspects of model generation and to consolidate all model input data into a single Microsoft Excel file. This work has progressed on schedule and the MPC is now capable of performing steady-state and transient simulations of the coupled heat and mass transfer, chemical, electrochemical, current flow, and porous flow processes that occur in SOFCs.

The model verification/validation work program is progressing on schedule. Steady-state MPC models up to the bundle scale have been validated successfully in FY 2012. The validation work is now being extended to transient test cases. The predictive capabilities of the MPC are also being demonstrated for a range of fuel cell engineering applications that are of interest to LGFCS.

This material is based upon work supported by the U.S. Department of Energy under Award Number DE-FE0000773.

III.G.2 SOFC Modeling and Simulation Tools

Moe A. Khaleel (Primary Contact),
Brian J. Koeppel, Elizabeth V. Stephens,
Kurt P. Recknagle, Emily M. Ryan, Kevin Lai,
Wei Xu, Xin Sun, and Hussein Zbib
Pacific Northwest National Laboratory
902 Battelle Blvd.
Richland, WA 99352
Phone: (509) 375-2438; Fax (509) 375-4392
Email: moe.khaleel@pnnl.gov

DOE Project Manager: Briggs White
Phone: (304) 285-5437
Email: Briggs.White@netl.doe.gov

Subcontractor:
E.M. Ryan, Boston University, Boston, MA

Contract Number: FWP40552

Start Date: October 1, 2011
End Date: September 30, 2012

Fiscal Year (FY) 2012 Objectives

- Develop and validate multi-physics modeling tools to simulate solid oxide fuel cell (SOFC) stack performance.
- Utilize computational techniques for the optimization of modular SOFC stack and system designs with mitigation of performance degradation.
- Disseminate/transfer modeling tools to Solid State Energy Conversion Alliance (SECA) industry teams and Core Technology Program (CTP) members.

FY 2012 Accomplishments

- Extended capabilities of the two dimensional (2D) SOFC-multi physics (MP) simulation tool to include effects of temporal degradation behaviors on the long-term electrochemical and thermal performance of large stacks and to automatically seek a desirable operating temperature state by changing various stack input parameters.
- Developed a modeling framework suitable for use in system engineering studies that creates and tests a fast reduced order model (ROM) for the SOFC stack operating space based on simulation results from a detailed numerical model.
- Successfully benchmarked 2D SOFC-MP predictions for an operating SOFC temperature field against a fully instrumented multi-cell stack.
- Developed a graphical user interface (GUI) to create, run, and review model results for the 2D SOFC-MP simulation tool.
- Developed computational models to investigate the effects of degradation on the SOFC electrodes at the cell-, electrode- and surface-levels.
- Investigated sulfur and antimony poisoning in the anode, humidity in the cathode and high fuel water in the anode.
- Developed a two-step mechanistic based time and temperature dependent healing model for self-healing glass.
- Demonstrated the effects of mechanical surface modification on life improvement of coated, 441 stainless-steel interconnect (IC) materials.

Introduction

In order to efficiently develop and optimize planar SOFC stacks to meet technical performance targets, it is desirable to perform numerical experiments on the effects of geometry, material properties, operational parameters, and thermal-mechanical loading. The computations with representative baseline designs, validated by experimental data, have been used to develop a better understanding of the stack behavior while avoiding costly and time-consuming experiments. In order to model the coupled physics associated with an SOFC stack, the simulation tool SOFC-MP was developed. This modeling tool combines the versatility of a commercial multi-physics code and a validated electrochemistry calculation routine to predict the gas flow distributions, current distribution, temperature field, and power output for stack-level simulations. The fundamental building blocks of the modeling and simulation tools are electrochemical models, heat and mass transfer simulations, computational mechanics, and experimental data.

Approach

The following technical approach has been taken in the modeling task to meet program goals.

- Maintain, enhance, and provide guidance for the integrated modeling tools developed under the SECA

CTP for evaluating fuel cell stack design concepts by the industry teams.

- Investigate the effects of materials degradation on cell performance and life.
- Investigate the effects of cell geometric design, material property distributions, and operating conditions on SOFC reliability.
- Perform material experiments for property data essential to constitutive and numerical model development.

Results

Enhancement and Performance Improvement of Modeling Tools

Numerical experiments to study the effects of geometry, material properties, operational parameters, and thermal-mechanical loading on SOFC performance have long been used to supplement the physical experiments used in testing, development, and optimization of SOFC stacks. Such computations with representative baseline designs, validated by experimental data, have provided better understanding of the stack behavior while reducing the number of these costly and time-consuming experiments. The simulation tool SOFC-MP (consisting of both 3D and 2D versions) was developed to model the coupled physics associated with an SOFC stack. These modeling tools are used to predict the gas flow distributions, current distribution, temperature field, and power output for stack-level simulations.

- Since SOFC short-term performance has matured due to materials and design engineering, more emphasis was focused on the SOFC long term performance necessary to realize commercial success. Calculation routines were added to the 2D code to include the effects of degradation over time based on relevant state variables (e.g., scale thickness, electrode porosity, etc.). It was assumed that the degradation process occurs over a long time period such that the stack can still be assumed to be in thermal equilibrium. The capability was demonstrated for the added ohmic loss due to temperature-dependent oxide scale growth on the metallic IC, where accelerated growth on the hottest region of the stack resulted in greater scale thickness and reduced power output (Figure 1). The capability is generic, so any user-defined degradation relationship can be implemented with the appropriate state variables and evolution equations to track how the performance changes with time.
- Based on the degradation simulations, the added losses result in more generated heat that increases the stack maximum temperature. Since the maximum temperature is usually a critical design parameter to ensure acceptable stability of the fuel cell materials, a temperature increase due to the degradation process must be mitigated by changes to the stack operating parameters. This functionality was added to the code so that a selected combination of parameters, e.g., inlet fuel or air temperatures, inlet fuel or air rates, external environment temperatures, etc. are automatically adjusted to indicate how the stack can be best operated over time (Figure 2).
- Typical system models are thermodynamic models, but they have no spatial information for the temperature distribution within the stack. To address this need, a framework for automatic creation of a ROM was developed (Figure 3). This framework samples the desired operating space of the SOFC based on selected input parameter ranges, obtains

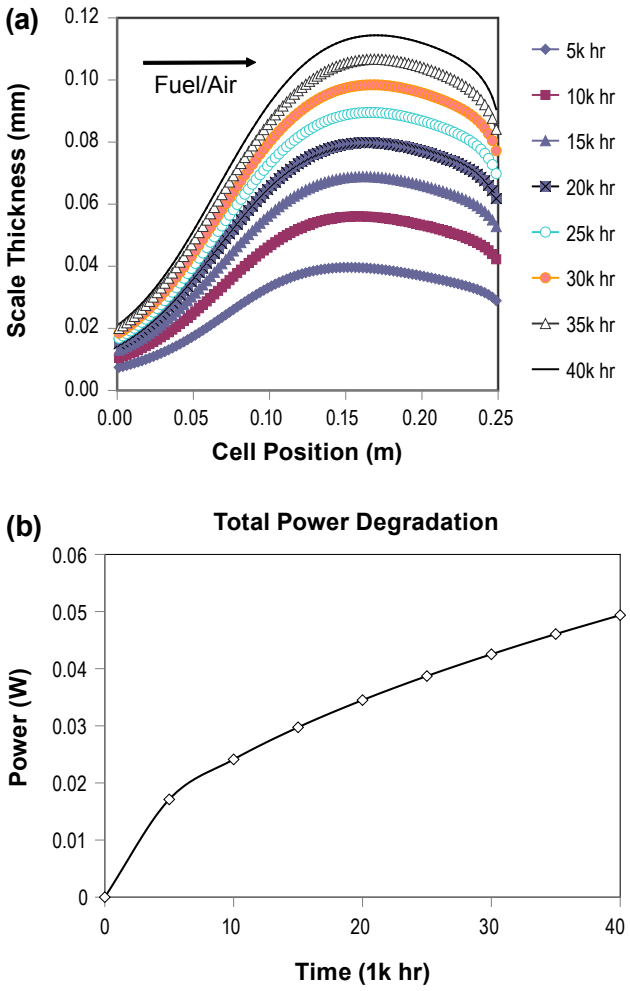

FIGURE 1. Plots of the predicted oxide scale growth along the co-flow cell (a) and the associated stack power loss (b) over the operating lifetime due to increased ohmic loss

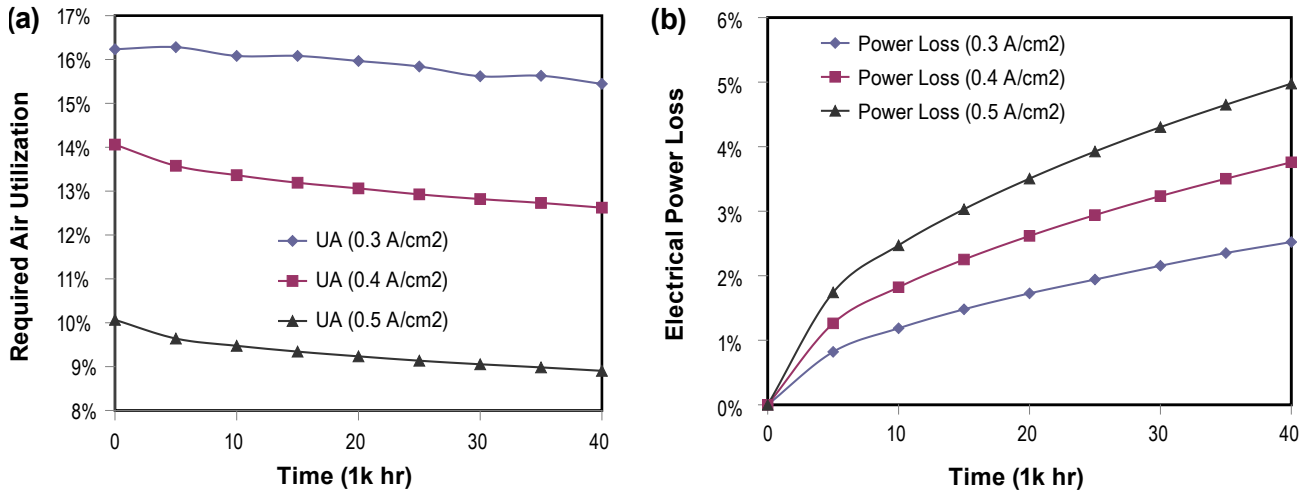

FIGURE 2. Plots of the required air utilization (a) and the corresponding power loss (b) due to oxide scale growth for a 96-cell, 25 kW stack with temperature control to maintain 850°C maximum temperature

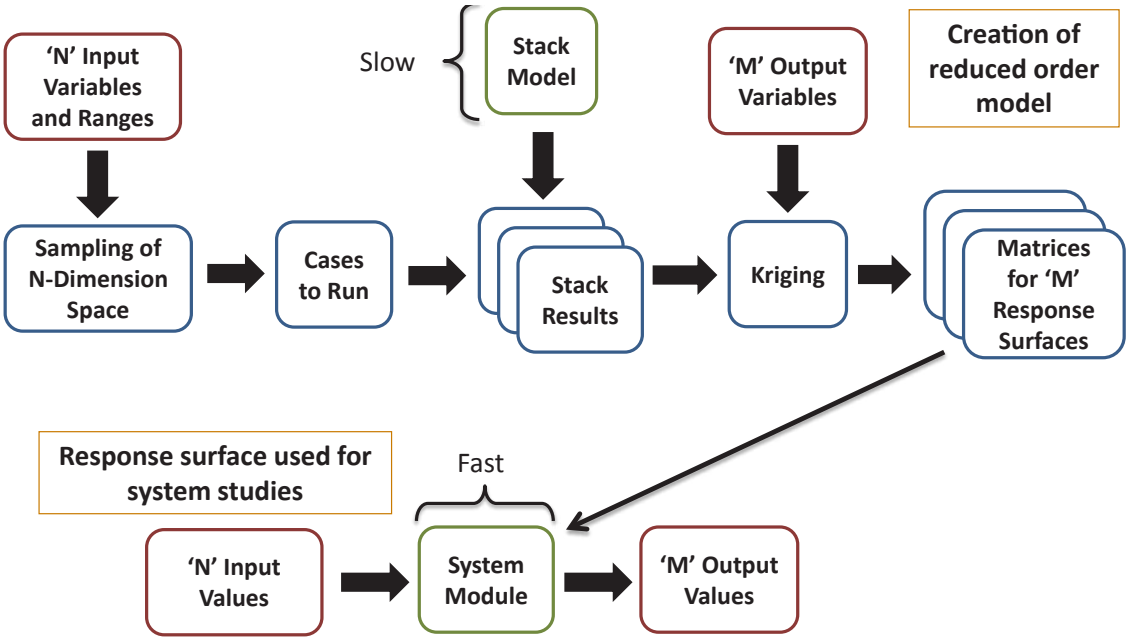

FIGURE 3. Framework for the creation of the SOFC ROM based on response surface analyses

results data for selected output parameters at these points using a detailed model for the user's stack, and performs numerical interrogation of the results to extract response surfaces which describe the complex relationships between the selected input and output variables. These relationships, i.e., the ROM, are then incorporated in a package that interfaces directly with the system modeling tool. Once the ROM is validated against the detailed model to ensure that the approximation error is acceptable, this fast code can well represent the stack across its desired operating window.

- Benchmarking against modern high-performance anode-supported cells was performed. Proprietary experimental data for a state-of-the-art multi-cell planar stack was obtained from a SECA member to facilitate code benchmarking (previously, the 2D SOFC-MP code was benchmarked successfully against simple adiabatic cases from the literature). The test cases consisted of a single stack at ten operating states using different fuel compositions, current densities, and inlet gas temperatures. Model predictions were compared to experimental data for voltage, current, and thermocouple temperature

measurements along the flow direction at various cells along the stack height. The model results well captured the thermal profile along the cells, even with large endothermic contributions from on-cell steam reforming of CH_4.

- A prototype GUI was developed to facilitate simulations with both the 2D and three dimensional (3D) codes based on users' feedback to eliminate the licensing fee and to simplify the analysis process. The initial SOFC-MP framework relied on a costly commercial pre-processor to create the numerical model and review the simulation results. A menu-based interface (Figure 4) was developed to provide the necessary capabilities for model pre-processing such as parameter input, geometry, material properties, boundary conditions, electrochemical relationship, and solution, i.e., job submission and monitoring, and post-processing such as performance metrics, plotting of distributions.

Investigating Electrode Degradation through Computational Modeling

To understand the various degradation mechanisms which affect the long term performance of SOFCs, several computational models which resolve the multi-physics of the SOFC at the cell-, electrode- and surface-levels were developed. The power output and long-term performance and degradation of SOFCs rely heavily on the reactive transport and electrochemical performance within the electrodes. In SOFCs, performance degradation can be caused by a number of factors, including environmental and operating conditions, contaminants in the fuel and air streams, and impurities in materials and balance of plant equipment. These various degradation mechanisms can rapidly reduce the power output of SOFCs, as in the case of sulfur poisoning and redox (reduction-oxidation) cycling, or gradually affect performance over the SOFC's operating lifetime, as with chromium poisoning. To improve the performance and lifetime of SOFCs, it is important to understand the various degradation mechanisms that occur within the electrodes and how they are affected by the local conditions within the electrodes.

- In FY 2012, various degradation mechanisms in the anode and cathode of the SOFC were investigated to better understand the physical mechanisms involved in degradation. In particular, sulfur and antimony poisoning in the anode, humidity in the cathode and high fuel water in the anode were considered. For sulfur poisoning, a damage factor, which is a function of the local partial pressure of H_2S and the operating temperature, was developed based on experimental data. It was used to predict the voltage drop due to sulfur poisoning at various

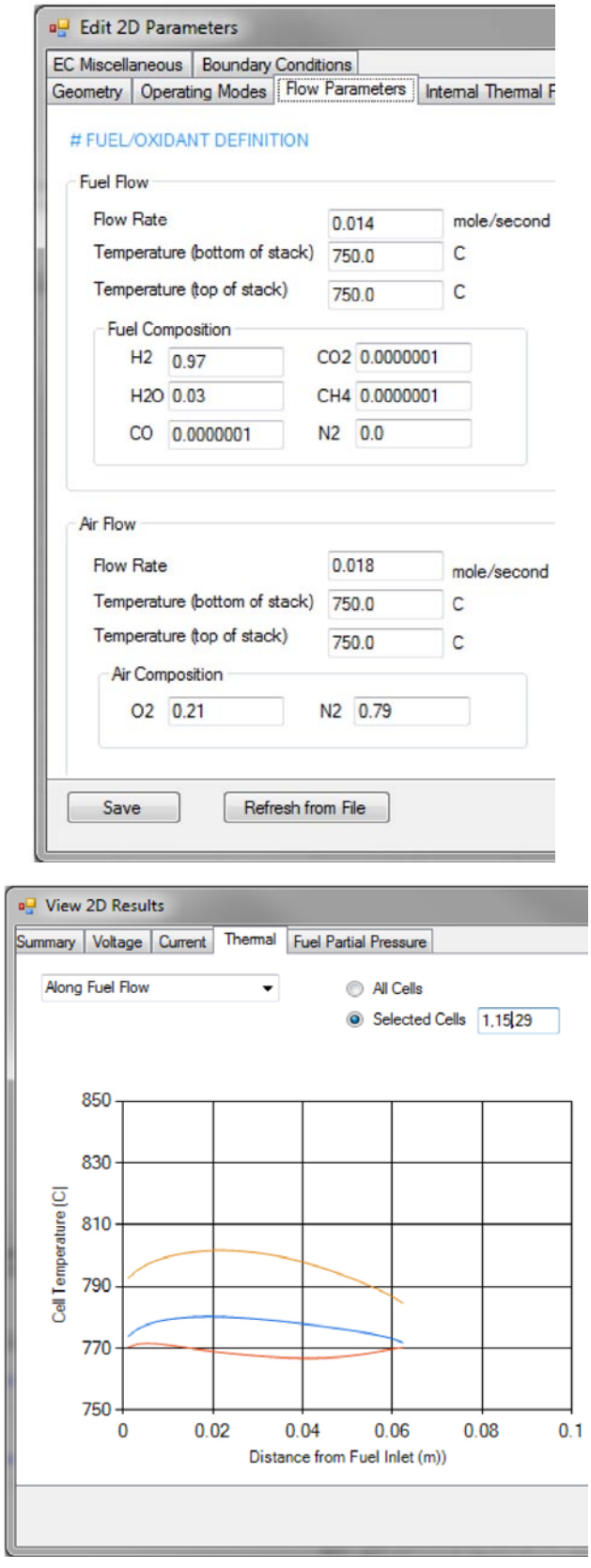

FIGURE 4. Screenshots of the new SOFC-MP GUI for 2D pre- and post- processing

temperatures and concentrations of H_2S. A similar model was developed to investigate the degradation trends in the anode in the presence of antimony. For the humidity in the cathode, smaller scale models are being developed to investigate the reactions of H_2O with the cathode and the local conditions within the cathode that lead to a decrease in the overall SOFC electrochemical performance. For high fuel water in the anode, a model is being developed to examine nickel being volatilized from the anode resulting in damage to the electrochemical performance. Additionally, during long-term operations of commercial SOFC systems, the nickel in the anode may reoxidize due to seal leakage, fuel supply interruption, or system shutdown. Following such an event, the anode must be reduced before operations can continue. This redox cycle can result in significant structural and electrochemical performance degradation. Thus, models to quantify the damaging effects of redox cycling, which can then be used to investigate strategies that will minimize the damage, are being developed.

Computational Investigation of Performance of Self-healing Glass Seals used in SOFC Stacks

A self-healing glass seal has the potential of restoring its mechanical properties upon reheating to SOFC stack operating temperature, even when it has experienced some cooling induced damage/cracking at room temperature. Such a self-healing feature is desirable for achieving high-seal reliability during thermal cycling. On the other hand, self-healing glass is also characterized by its low mechanical stiffness and high creep rate at the typical operating temperature of SOFCs. Therefore, geometry stability and structural integrity of the glass seal system becomes critical to its successful application in SOFCs. It is crucial to be able to predict the effects of sealing system design and their structural stability under long term stack operating conditions, and to guide the design and optimization of a sealing system with a self-healing glass and appropriate containment mechanisms to achieve the ultimate goal of SOFC seal development.

- In FY 2012, a mechanistic-based self-healing model was developed to quantitatively capture and predict the crack healing behavior of SCN-1 glass (an alkali-containing silicate glass). A two-step healing mechanism was developed: crack closure and crack healing. To obtain the model parameters, controlled healing experiments were conducted at different temperatures, followed by four-point bend tests to evaluate the recovery of the material strength. The experimental measurements were used to calibrate a kinetic Monte Carlo (kMC) model methodology applied. The kMC model was then used to extrapolate the experimental results to a wider range of temperatures and to formulate the temperature dependence of the characteristic dwelling time. The effects of various factors such as temperature, stress, and crack characteristics were also evaluated.

Modeling for IC Life Prediction

The interfacial strength between the oxide scale and the substrate is crucial to the reliability and durability of the metallic IC in SOFC operating environments. An integrated experimental/analytical methodology for quantifying the interfacial strength between the oxide scale and the different metallic IC candidates has been developed, therefore being able to predict the life of IC candidate materials under typical SOFC operating conditions. This integrated approach can also be used to quantify the effects of different surface finishes, coating layer thicknesses as well as different coating materials so that an optimized coating thickness as well as surface condition for the IC candidates can be developed to satisfy SECA life requirements.

- In FY 2012, new experimental/numerical methodologies were explored to better quantify the interfacial strength between the oxide and substrate of coated IC materials. Interfacial analysis via micro/nano-indentation was performed. Preliminary results show that direct interface indentation can be performed by targeting the oxide/substrate interface. By measuring the crack length and the load induced by the indenter, the apparent fracture toughness, hence, interfacial strength, of the "interface material" can be determined. The modeling tool will be extended to implement the new experimental methodologies and quantitative measurements to further improve the predicted life-time and life-extension of surface modified, coated IC materials.

Conclusions and Future Directions

During FY 2012, the modeling tools were improved and expanded with additional capabilities developed to address degradation and durability issues. The SOFC-MP modeling tool was improved to address changing modeling needs for the industry teams. The ability to evaluate long-term stack performance was added by including degradation behaviors for the stack electrochemical and thermal performance, and the code was modified to automatically compute the necessary changes in operating conditions over the simulated lifetime. Several models of degradation in the SOFC electrodes were developed. These models will be able to investigate how the local conditions within the electrodes affect the overall electrochemical performance of the SOFC and how various degradation mechanisms

affect the local conditions of the electrodes. Future modeling activities will continue to focus on reliability, degradation, time-dependent response, and code usability:

- Continue to enhance and maintain the modeling tools to meet the needs of the SECA program and continue to promote the usage of the tools by the industry and academic teams.
- Continue to add improved material models and numerical procedures to the modeling tools for simulation of time-dependent mechanical response and reliability.
- Complete the ROM capability.
- Complete the GUI and implement a flexible framework for 3D SOFC-MP analyses to eliminate reliance on costly third party software.
- Validate the enhanced 3D model by benchmarking against multi-cell experimental data.
- Continue to investigate the effects of humidity in the cathode through cell level and smaller computational models. The goals of these models are to understand the physical phenomena which cause degradation and to investigate mitigation strategies to reduce and eliminate degradation.
- Continue to investigate the effects of high fuel water and redox cycling with models that build upon the existing SECA modeling capabilities with the goals of providing operation and design guidance that prevents or minimizes damage to the anode.
- Develop computational models of other degradation mechanisms of interest to industry.
- Continue to support development of a robust test cell design.
- Develop a continuum damage-healing model for self-healing glass.
- Use modeling tools to examine and optimize varying engineering seal design concepts in a multi-cell stack.
- Extend the modeling framework for IC life evaluation to implement new experimental methodologies and quantitative measurements.
- Perform parametric study on the effects of design and operating variables on IC lifetime.

FY 2012 Selected Publications/Presentations

1. B.J. Koeppel, C. Lai, and M.A. Khaleel, 2011, "Effect of Geometry and Operating Parameters on Simulated SOFC Stack Temperature Uniformity," In: *Proceedings of ASME 2011 5th International Conference on Energy Sustainability & 9th Fuel Cell Science, Engineering and Technology Conference,* August 7–10, Washington, D.C., Technical Publication No. ESFuelCell2011-54803.

2. E.M. Ryan, W. Xu, X. Sun, and M.A. Khaleel, 2012, "A Damage Model for Degradation in the Electrodes of Solid Oxide Fuel Cells: Modeling the Effects of Sulfur and Antimony in the Anode," *Journal of Power Sources* 210(0):233-242.

III.G.3 Development of a Mechanistic-Based Healing Model for Self-Healing Glass Seals

Wei Xu, Xin Sun, Hussein Zbib,
Elizabeth Stephens, and Moe A. Khaleel
(Primary Contact)
Pacific Northwest National Laboratory
902 Battelle Blvd
Richland, WA 99352
Phone: (509) 375-2438; Fax: (509) 375-4392
Email: moe.khaleel@pnnl.gov

DOE Project Manager: Briggs White
Phone: (304) 285-5437
Email: Briggs.White@netl.doe.gov

Contract Number: FWP40552

Start Date: October 1, 2011
End Date: September 30, 2012

Fiscal Year (FY) 2012 Objectives

- Quantify the self-healing mechanism of SCN-1 glass seals.
- Determine the thermo-mechanical dependence of the self-healing behavior to assist the development of a reliable glass sealing system design within solid oxide fuel cells (SOFCs).

FY 2012 Accomplishments

- Developed a two-step mechanistic-based time and temperature dependent healing model.
- Predicted the healing behavior of the SCN-1 glass seals under various healing conditions.
- Examined effects of thermo-mechanical conditions on the healing behavior.

Introduction

Self-healing glass, a recent development of hermetic sealant materials, has the ability to effectively repair damage when heated to elevated temperatures, and thus, is able to extend its service life. Since crack healing morphological changes in the glass material are usually temperature and stress dependent, quantitative studies to determine the effects of thermo-mechanical conditions on the healing behavior of the self-healing glass sealants are extremely useful to accommodate the design and optimization of the sealing systems within SOFCs.

The goal of this task is to develop a mechanistic-based healing model to quantify the stress and temperature dependent healing behavior. A two-step healing mechanism was developed and implemented into finite element (FE) models through user-subroutines. Integrated experimental/kinetic Monte Carlo (kMC) simulation methodology was taken to calibrate the model parameters. The crack healing model is able to investigate the effects of various thermo-mechanical factors and is, therefore, able to determine the critical conditions under which the healing mechanism will be activated. Furthermore, the predicted results can be used to formulate the continuum damage-healing model and to assist the SOFC stack level simulations in predicting and evaluating the effectiveness and the performance of various engineering seal designs.

Approach

The following approaches have been taken in FY 2012 to meet the overall goals:

- Developed a two-step healing mechanism (crack closure then heal) concept.
- Implemented a mechanistic-based model into FE simulations to perform thermo-mechanical stress analyses.
- Integrated an experimental/kMC model calibration methodology.
- Investigated the effects of various operating factors through FE parametric studies.

Results

Effects of temperature conditions

The influence of the operating temperatures on the healing behavior was investigated using FE analysis. A 100 mm × 100 mm, two dimensional (2D), plane strain numerical model with a 10 mm long, V-type edge crack, as shown in Figure 1, was used to represent the cross-section of a glass sealant. The crack tip opening considered was 0.1 mm. All displacements of the bottom side were fixed and a uniform pressure of 5 MPa was applied onto the top surface, resulting in a Mode-I crack. The gravity effect of the material was also included. The thermo-mechanical stress analyses were performed using the commercial FE software package ABAQUS.

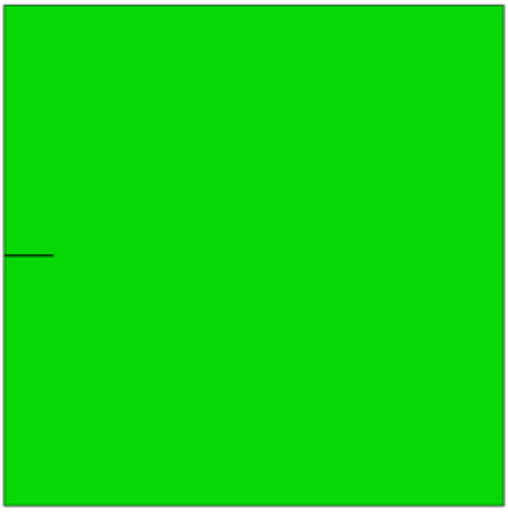

FIGURE 1. FE model of the two-step healing mechanism

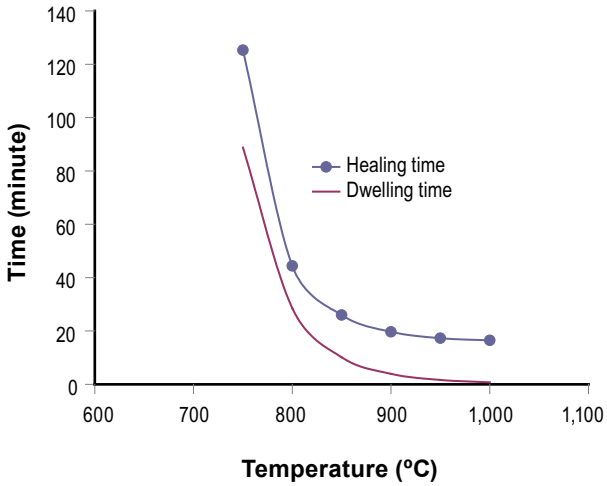

FIGURE 2. Effects of temperatures on the healing behavior

Figure 2 shows the variation of the total healing time (the sum of the duration of both the crack closure and the healing stages) versus temperature and its comparison with the temperature dependent variation of the characteristic dwelling time. The dwelling time represents the intrinsic healing time for initially closed cracks.

It was found that, similar to the temperature dependence of the dwelling time, the total healing time increases as the temperature decreases, indicating that lower temperatures reduce the healing rates. It can also be seen that at high temperatures (>900°C), the total healing time is mostly determined by the crack closure time. The cracks almost instantly heal once the crack surfaces are in contact, while at low temperatures (<800°C) where diffusion rate is considerably low, the dwelling time becomes more dominant. The predicted results for the states of stress that have been studied further indicate that a small reduction in the operating temperature is not likely to lead to a drastic increase in healing time.

Effects of external pressure loading conditions

To evaluate the effects of externally confining pressure on the healing behavior of the SCN-1 glass sealant, two different levels of external pressure (5 MPa and 10 MPa) were applied onto the top surface of the model. A stress factor, defined as the healing time of the case of 10 MPa divided by the healing time of the case of 5 MPa, was used to quantify the stress-induced change in healing time.

It was found that higher confining pressure generally shortens the healing process because more creep strain produced by the high confining stress leads to faster crack closure. However, as the temperature decreases, the stress-induced healing efficiency enhancement becomes less effective. This is due to the fact that both crack closure and healing are primarily thermally driven processes. When temperature further decreases and approaches the glass transition temperature, the molecular motion is restricted, leading to the greatly reduced diffusion rate and increased viscosity. As a result, both crack closure and healing process prolong even under high-pressure conditions.

Effects of activation energy on healing rates

Since the environmental or crack surface conditions are also considered to have influence on the healing behavior, the dependence of the healing rates in the activation energy was studied. The kMC model, an effective technique to simulate the time evolution of natural physical processes in dynamical systems, was developed to simulate the interfacial diffusion-driven healing process. Figure 3a shows the 2D lattice kMC model with the lattice spacing Δl representing the glass bond length. The 1 Δl height rectangular hole in the middle represents the crack. Since the typical glass bond length is known to be between 0.5 nm and 0.8 nm, the model actually describes the situation where a crack has been already closed yet unhealed. A broken bond ratio, the number of remaining broken bonds divided by the initial number of broken bonds, was used to measure the healing behavior. The whole healing process was considered to be completed when no broken bond was left, as shown in Figure 3b. To ensure numerical convergence, a 1,000 × 1,000 lattice square was used in the simulation.

Figure 4 shows the healing curve for three different activation energy values, including the baseline value of 2.5215 eV and values with ±5% variations. It can be

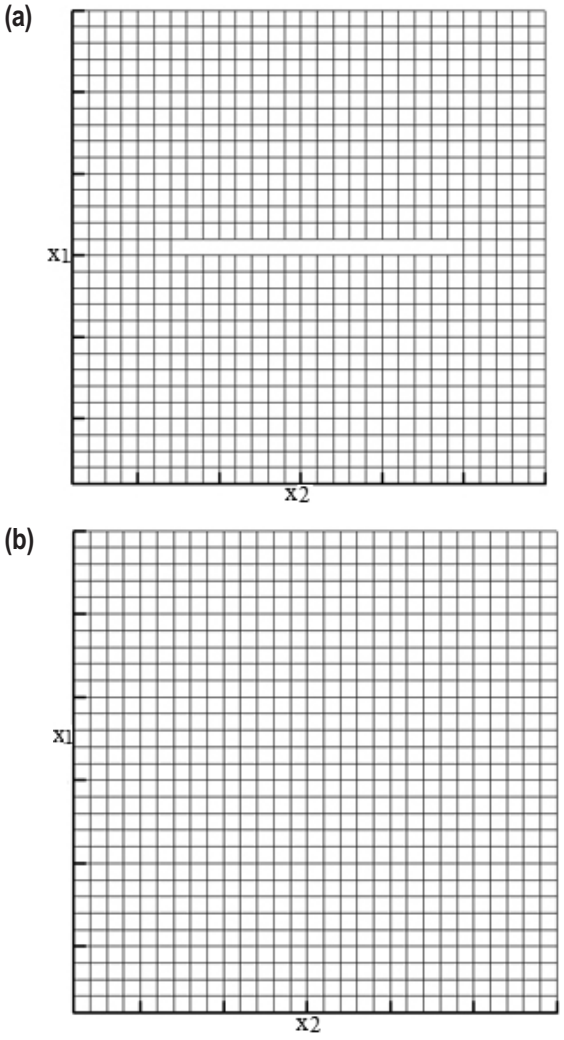

FIGURE 3. The kMC model for diffusion-driving crack healing before (a) and after (b) healing

seen that the healing time drastically changes for the three cases, indicating that the healing behavior is highly sensitive to the activation energy. Moreover, the results show that higher activation energy prolongs the healing process while lower activation energy shortens the healing time.

Conclusions and Future Directions

During FY 2012, the seal modeling work has been focused on quantifying the self-healing mechanisms with a mechanistic-based model and investigating the effects of various thermo-mechanical operating conditions. Based on the simulation results to date, several conclusions can be made as follows:

- High operating temperature shortens the healing time. For the cases being considered, it was found that the crack closure is mostly dominant at extremely high temperatures (>900ºC), while the crack healing stage primarily determines the total healing time at low temperatures (<800ºC) when the interfacial diffusion is considerably slow.
- High external confining pressure accelerates the crack healing. However, such influence becomes less effective as the temperature decreases because the stress primarily takes effect in the crack closure stage, which is found to be less influential on the total healing time as temperature decreases.
- The healing rate is highly sensitive to the healing activation energy, which may be affected by environmental or surface chemical conditions. Higher activation energy hinders the healing process while lower activation energy shortens the healing time.

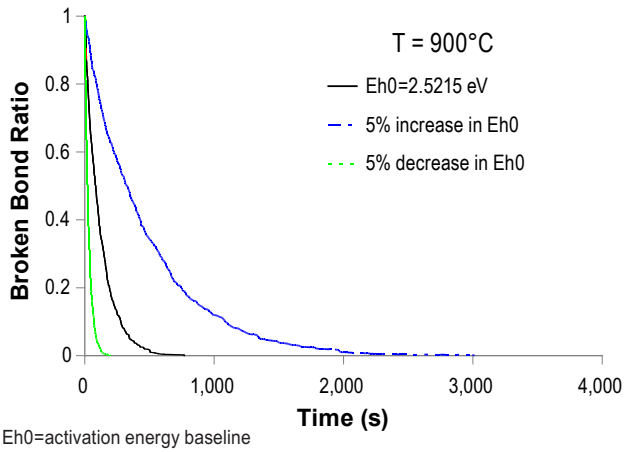

FIGURE 4. Effects of the activation energy on the healing behavior

Future work in the seal modeling will continue in the following areas:

- Develop a continuum damage-healing model by incorporating the findings from the meso-scale healing modeling and simulations
- Continue to work with seal materials development teams in improving and optimizing the engineering seal design.

FY 2012 Publications/Presentations

1. W. Xu, X. Sun, H. Zbib, E. Stephens, I. Mastorakos, and M.A. Khaleel, 2012. "A Mechanistic-Based Healing Model for Self-Healing Glass Seals Used in Solid Oxide Fuel Cells," *Journal of Power Sources,* 218: 445-454.

2. W. Xu, X. Sun, H. Zbib, E. Stephens, and B.J. Koeppel, 2011, "Quantify the Self-healing Behavior of Engineering Seal Designs in SOFC Stacks," Presented at SECA-NETL Review Meeting, November 8–9, 2011, Pacific Northwest National Laboratory, Richland, Washington.

III.G.4 Investigating Electrode Degradation through Computational Modeling

Emily M. Ryan, Kurt P. Recknagle, Wei Xu, Moe A. Khaleel (Primary Contact)
Pacific Northwest National Laboratory
902 Battelle Blvd.
Richland, WA 99352
Phone: (509) 375-2438; Fax (509) 375-4392
Email: moe.khaleel@pnnl.gov

DOE Project Manager: Briggs White
Phone: (304) 285-5437
Email: briggs.white@netl.doe.gov

Subcontractor:
E.M. Ryan, Boston University, Boston, MA

Contract Number: FWP40552

Start Date: October 1, 2011
End Date: September 30, 2012

Fiscal Year (FY) 2012 Objectives

- Determine degradation mechanisms of interest to Solid State Energy Conversion Alliance (SECA) industry partners.
- Demonstrate cell level modeling of performance degradation.
- Apply the cell level model and continuum damage model to a degradation mechanism of interest to industry.

FY 2012 Accomplishments

- Investigated sulfur poisoning in the anode using the continuum damage model and cell level distributed electrochemistry (DEC) model.
- Investigated the effects of antimony on the anode microstructure's electrical conductivity and Joule heating.
- Began studying the effects of high fuel water and reduction-oxidation (redox) cycling on the anode and humidity on the cathode.

Introduction

Solid oxide fuel cells (SOFCs) are a promising alternative energy device that are being developed for stationary and auxiliary power applications, which require a 40,000 hour or more lifetime [1]. The power output and long-term performance and degradation of SOFCs rely heavily on the reactive transport and electrochemical performance within the electrodes. In SOFCs, performance degradation can be caused by a number of factors including environmental and operating conditions, contaminants in the fuel and air streams, and impurities in materials and balance of plant equipment. These various degradation mechanisms can rapidly reduce the power output of SOFCs, as in the case of sulfur poisoning [2,3] and redox cycling [4], or gradually affect performance over the SOFC's operating lifetime, as with chromium poisoning [5].

To improve the performance and lifetime of SOFCs, it is important to understand the various degradation mechanisms that occur within the electrodes and how they are affected by the local conditions within the electrodes. This work investigates various degradation mechanisms in the anode and cathode of the SOFC to better understand the physical mechanisms involved in degradation. Experimental studies of degradation mechanisms focus on the effects of overall performance without resolving the physics within the electrodes and electrolyte of a working fuel cell [2,6]. In SOFCs, the high operating temperatures and complex, compact geometry make it difficult for experimentalists to get detailed data on the conditions within the fuel cell. Computational modeling is able to simulate the multi-physics occurring within the electrodes and investigate the local physical mechanisms that cause the degradation in overall SOFC performance. The SECA modeling team has used various computational models to investigate several degradation issues of interest to industry.

Approach

To investigate degradation in the SOFC electrodes several different computational models are used considering the SOFC at different scales. Depending on the degradation mechanism of interest, different computational models can be used to investigate the mechanism's effects on the local conditions within the electrode, and/or the mechanism's effects on the overall

electrochemical performance of the SOFC. Before computational modeling could begin, a framework for classifying degradation based on its effects on the electrodes was developed. The framework helps to identify what reaction, structural, and materials properties are affected by the degradation mechanism and how to incorporate their effects into our computational models.

Several different models are used to consider the various degradation mechanisms. The cell-level DEC model [7,8] is used to simulate the SOFC's performance. The DEC model simulates the multi-physics of the SOFC, including the electrochemistry, through the thickness of the electrodes and electrolyte. The properties of the electrodes, such as the triple phase boundary (TPB) length, are allowed to vary spatially in the DEC model. A continuum damage model is overlaid on the DEC model to consider degradation within the SOFC electrodes. The SECA modeling team also has a smaller electrode scale reactive transport model which simulates the reactive transport within the porous media of the electrode. This model is able to resolve the detailed surface reactions occurring within the electrodes and the effects of the microstructure on the reactions. Also available to the SECA team are models capable of investigating the detailed surface reactions in the electrodes. These models use molecular dynamics and density functional theory to consider the energy associated with surface reactions and transport by studying the interactions of individual molecules in the system.

Results

Five different degradation mechanisms are considered in this report: sulfur poisoning, antimony poisoning, humidity effects in the cathode, high fuel water in the anode, and redox cycling in the anode. The computational models and results for each of these degradation mechanisms are discussed below.

Sulfur Poisoning

To investigate the effects of sulfur poisoning on SOFC performance, a degradation model was developed based on applying a damage factor to the triple phase boundary (TPB) length in the anode. H_2S has been shown to adsorb to the surfaces of the anode and block H_2 adsorption [9,10]. This reduces the surface area available for the electrochemical reactions in the anode, causing a reduction in the SOFC's overall performance. In SOFC modeling, the surface area available for electrochemical reactions is represented by the TPB length. A continuum damage model of the degradation in TPB length with H_2S was developed based on experimental data [3]. The TPB length varies throughout the anode based on the local H_2S concentration and the operating temperature of the SOFC. The varying TPB length was integrated into the DEC model and the SOFC performance with the degraded TPB length was predicted. The continuum damage model was fit to data [3] at 1,073 K and was used to predict the performance at temperatures between 973 K and 1,173 K as shown in Figure 1.

The sulfur degradation model is able to predict the performance decrease with an average relative difference of 3.6%. The DEC model can resolve the local conditions within the electrodes, such as the H_2S concentration shown in Figure 2 for the cases at 1,073 K and with 10 and 2 ppm H_2S/ppm H_2. As shown in Figure 2, the mass fraction of H_2S varies significantly through the thickness of the anode, which will lead to different levels of damage to the TPB length. Also, the mass fraction of H_2S of the 10 ppm H_2S/ppm H_2 differs from that of the 2 ppm H_2S/ppm H_2 by almost an order of magnitude, resulting in a roughly 4% difference in performance drop (Figure 1).

Antimony

When gasified coal is used as a fuel in SOFCs, volatized antimony (Sb) will strongly interact with the Ni-YSZ anode. After an initial stage of a reversible antimony diffusion/adsorption-driven poisoning, prolonged exposure to Sb results in extensive formation of nickel antimonide compounds (such as NiSb and Ni_5Sb_2) inside the anode, which coalesces and eventually reduces the electrical percolation of the anode, leading to an abrupt performance loss in SOFCs [11]. Because

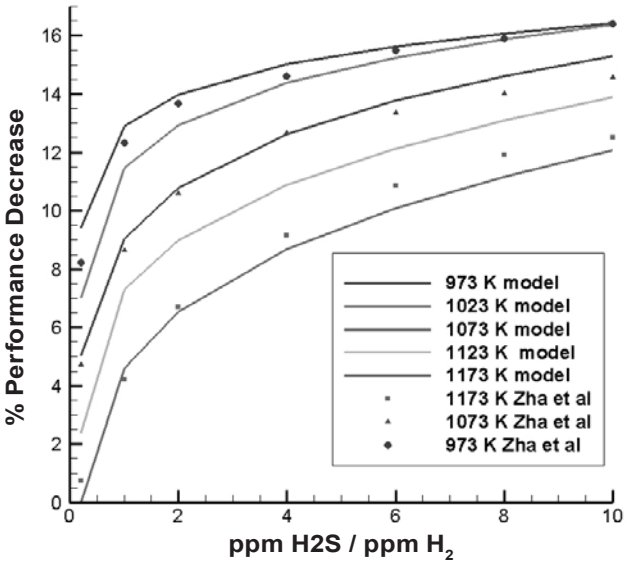

FIGURE 1. Plot of the percent of SOFC performance decrease due to sulfur poisoning. The lines represent the results of the degradation model, while the symbols are the experimental data from Zha et al. [3]

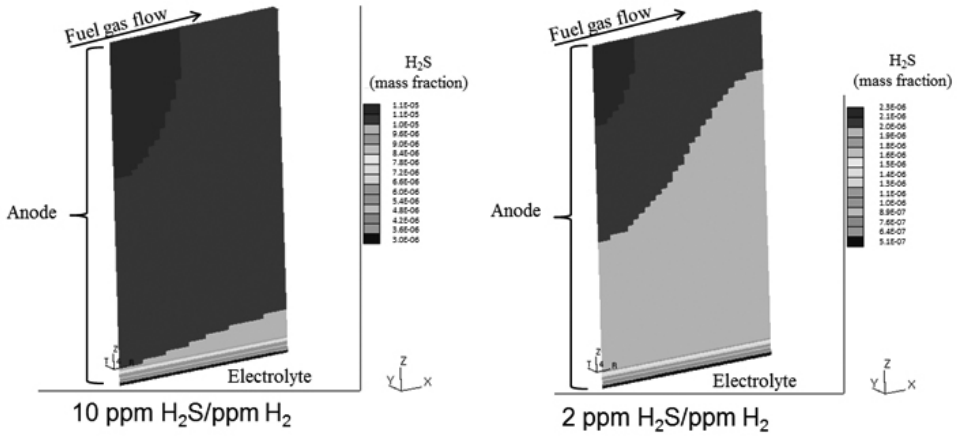

FIGURE 2. Mass fraction of H_2S in the anode for 10 ppm H_2S/ppmH_2 (left) and 2 ppm H_2S/ppmH_2 (right) at 1,073 K. H_2S enters the anode with the fuel from left to right along the top of the anode. Note the order of magnitude difference in mass fraction of H_2S between the two cases.

yttria stabilized zirconia (YSZ) is an electrical insulator, the percolation loss can be described as Ni depletion. Removing Ni reduces the electrical conductive paths (electrical percolation) available between particles and causes a reduction in the effective electrical conductivity of the anode, leading to the SOFC's performance degradation. A finite element model of the anode is used to investigate the effects of Ni removal from the anode on the electrical conductivity. As with the sulfur model, the continuum damage approach is used to model a reduction of the volume fraction of Ni in the anode. The removal of Ni due to Sb is approximated as a step function based on the penetration of Sb into the anode over time.

To investigate Sb poisoning, six simulations were performed considering the effects of different patterns and magnitudes of Ni depletion in the anode. Three cases were run to investigate the effects of anode thickness (D_o) on Ni depletion, and three cases were run with a linear depletion ($F(x) = F_o + ax$) of Ni with various F_o and a values. For all simulations, the top and bottom sides of the simulation domain are kept at a constant temperature of 1,123 K, and a 1.0 V operating voltage is applied to the anode. Antimony is introduced to the anode with the gas flow at the top surface of the anode ($x = 0$).

Figure 3 shows the change in conductivity over time for four cases considering a linear depletion of Ni. Two of the four cases considered in Figure 3 use a uniform degradation function, where $a = 0$. The other two cases exhibit linearly decreasing degradation along the penetration depth, causing the electrical conductivity to more rapidly reach their respective steady-state plateaus. These results are similar to the experimentally observed effects of Sb poisoning [11]. If the Ni depletion is allowed to increase further with time, it is expected that the Sb poisoning eventually will lead to the ultimate failure of the SOFC.

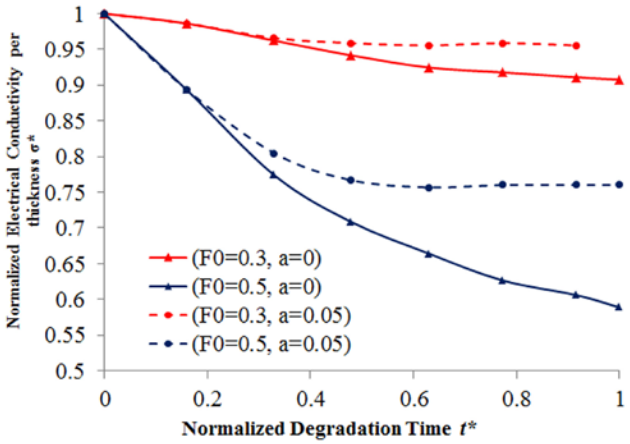

FIGURE 3. Plot of the electrical conductivity degradation of the Ni-YSZ anode supports under different environmental Sb concentration conditions

Cathode Humidity

It has been shown that humidity in the air flow in the cathode can cause significant degradation in the electrochemical performance of the SOFC. The physical mechanisms of the humidity degradation are being investigated through a small scale model. This includes the investigation of the reaction mechanisms of water with LSM through quantum mechanical modeling. The goals of these models are to understand the exact reactions of H_2O with the cathode; it has been suggested that H_2O reacts with either the lanthanum or manganese in the cathode. The modeling will help to distinguish the most plausible reaction mechanism. Additionally, a cathode scale model is being developed to investigate the reactive transport of H_2O in the cathode. This model is based on a previous cathode level model [12] and expands on the model to include the effects of ion and electron transport. Both models are still under development.

High Fuel Water

During the most efficient fuel cell operations, the hydrogen utilization is high resulting in high concentrations of water that can cause long-term damage to the electrochemical performance of the cell. Water concentrations are highest in the regions where the electrochemical reactions are concentrated. The water reacts with and volatilizes nickel from the anode to create $Ni(OH)_2$ gas. This gas can then be swept out of the anode thus decreasing the nickel content and reaction sites available for the electrochemical reactions. The nickel volatilization kinetics and pore transport properties are being considered in a model that is coupled to the multi-physics DEC model. This combined model is used to calculate the distribution and amount of nickel volatilized and the effect on the electrochemical reactions throughout the volume of the anode.

Redox Cycling

During long-term operations of commercial SOFC systems, the nickel in the anode may reoxidize due to seal leakage, fuel supply interruption, or system shutdown [4]. Following such an event, the anode must be reduced before operations can continue. This redox cycle can result in significant structural and electrochemical performance degradation. Again, the DEC model is being exercised by this task, this time being coupled to a sub-model that considers the nickel oxidation kinetics and pore transport properties to predict the damage to electrochemical properties of the anode. The model being developed calculates the transport of intrusive oxygen gas through the anode where it oxidizes the nickel resulting in increased nickel particle size, decreased porosity for gas transport, and decreased area for electrochemical reactions.

Conclusions and Future Directions

The research presented in this report discusses the development of several computational models to investigate degradation in the SOFC electrodes. The models are able to resolve the local conditions within the electrodes that occur during degradation and show how those local conditions affect the overall performance of the SOFC.

Future work in this area will continue the development of computational models of humidity in the cathode and the effects of high fuel water and redox cycling on the stability and performance of the anode.

FY 2012 Publications/Presentations

1. E.M. Ryan, W. Xu, X. Sun, and M.A. Khaleel, 2012, "A Damage Model for Degradation in the Electrodes of Solid Oxide Fuel Cells: Modeling the Effects of Sulfur and Antimony in the Anode," *Journal of Power Sources* 210(0):233-242.

References

1. M.C. Williams, J.P. Strakey, and W.A. Surdoval. 2005. *Journal of Power Sources* 143:191-196.

2. O.A. Marina, C.A. Coyle, E.C. Thomsen, D.J. Edwards, G.W. Coffey, and L.R. Pederson. 2010. *Solid State Ionics* 181:430-440.

3. S. Zha, Z. Cheng, and M. Liu, 2007, *Journal of the Electrochemical Society* 154:B201-B206.

4. D. Waldbillig, A. Wood, and D.G. Ivey, 2005, *Journal of Power Sources* 145:206-215.

5. T. Cruse, M. Krumpelt, B. Ingram, S. Wang, and P.A. Salvador. 2009. *Ceramic Engineering and Science Proceedings* 29:147-158.

6. O.A. Marina, L.R. Pederson, C.A. Coyle, E.C. Thomsen, and G.W. Coffey, 2009, In: 11th International Symposium on Solid Oxide Fuel Cells (SOFC-XI)- 216th ECS Meeting, Electrochemical Society Inc., Vienna, Austria, 2125-2130.

7. E.M. Ryan, K.P. Recknagle, and M.A. Khaleel. 2011. In: Twelfth International Symposium on Solid Oxide Fuel Cells (SOFC-XII), Montrael, California.

8. K.P. Recknagle, E.M. Ryan, and M.A. Khaleel, 2011, In: ASME 2011 International Mechanical Engineering Congress & Exposition, Denver, Colorado.

9. O.A. Marina, L.R. Pederson, C.A. Coyle, E.C. Thomsen, and D.J. Edwards, 2011, *Journal of the Electrochemical Society* 158:36-43.

10. L. Yang, Z. Cheng, M. Liu, and L. Wilson, 2010, *Energy and Environmental Science* 3:1804-1809.

11. O.A. Marina, L.R. Pederson, C.A. Coyle, E.C. Thomsen, P. Nachimuthu, and D.J. Edwards, 2011, *Journal of Power Sources* 196:4911-4922.

12. E.M. Ryan, A.M. Tartakovsky, K.P. Recknagle, C.H. Amon, and M.A. Khaleel, 2011, *Journal of Power Sources* 196:287-300.

IV. INNOVATIVE CONCEPTS

IV.1 Performance Degradation of LSCF Cathodes

Matthew Alinger
GE Global Research
1 Research Circle, MB277
Niskayuna, NY 12309
Phone: (518) 387-5124; Fax: (518) 387-5403
Email: alinger@ge.com

DOE Project Manager: Joseph Stoffa
Phone: (304) 285-0285
E-mail: Joseph.Stoffa@netl.doe.gov

Subcontractors:
- Rensselaer Polytechnic Institute, Troy, NY
- NexTech Materials, Lewis Center, OH

Contract Number: NT0004109

Start Date: October 1, 2008
End Date: June 30, 2012

Fiscal Year (FY) 2012 Objectives

- Develop a thermal sprayed ceria barrier layer coating process to address cell degradation challenges.
- Optimize thermal sprayed structures on 25 cm^2 (2 in. x 2 in.) cells to achieve >0.5 W/cm^2.
- Develop thermo-mechanical models of cells during the manufacturing process.
- Develop a low-cost metal supported substrate for thermal spray to meet Solid State Energy Conversion Alliance (SECA) cost targets.

FY 2012 Accomplishments

- Developed a smooth anode thermal spray process to enable hermetic electrolytes.
- Demonstrated hermeticity of 25 cm^2 thermal spray manufactured cells.
- Demonstrated performance of 25 cm^2 thermal spray manufactured cells.

Introduction

Through research and development efforts conducted within the U.S. Department of Energy's SECA fuel cell program, considerable progress has been made towards the realization of current solid oxide fuel cell (SOFC) stack cost goals. However, performance degradation of high-performance SOFC cathodes, in particular $La_{1-x}Sr_xCo_{1-y}Fe_yO_{3-\delta}$ (LSCF), remains a technical barrier to the commercial viability of SOFC technology. An objective of this project is to identify the dominant degradation mechanisms, and to develop and implement cost-effective mitigation strategies to retain high electrochemical performance in LSCF-based cathodes over the operational lifetime of an SOFC stack (>40,000 hours). The project goal is to reduce power density degradation rates to less than 1% per 1,000 hours, while maintaining high initial power densities (>0.75 W/cm^2). Performance degradation has been investigated on a fundamental materials level to identify mechanisms and to propose and implement solutions to improve chemical and structural stability.

Another key barrier to the commercialization of SOFCs is the excessively high capital cost involved with developing a manufacturing infrastructure for fabricating sufficient quantities of the multilayered cells for demonstration units. GE Global Research has been developing solutions to address these manufacturing costs using thermal spray processing which offers a new, lean manufacturing paradigm for the production of SOFC electrolytes and electrodes.

Approach

The LSCF-based cathode degradation mechanisms will be identified and evaluated using the state-of-the-art SOFC characterization laboratory at the GE Global Research Center in Niskayuna, New York. The approach relies on the electrochemical testing of SOFCs under realistic operating conditions. However, given the complexity of SOFCs, off-line laboratory testing including sintering studies, contact resistance, and diffusion couples will be leveraged to isolate and understand specific mechanisms under representative conditions. The structural and chemical degradation components will be identified using advanced characterization techniques such as high-resolution transmission electron microscopy (TEM), scanning electron microscopy (SEM) microprobe, and high-angular resolution synchrotron X-ray diffraction.

Alternative cell manufacturing approaches will also be evaluated. In particular, approaches will be evaluated for improved barrier layers to provide enhanced cathode interfacial strength. In addition, low-cost thermal spray manufacturing approaches will be developed for electrodes and electrolytes and evaluated with respect to cost-effectiveness as well as cell performance.

Results

A key barrier to the commercialization of SOFCs is the high capital cost involved with developing a manufacturing infrastructure for fabricating sufficient quantities of the multilayered cells for demonstration units. In addition, to accommodate low initial rates of market adoption, low-cost manufacturing is imperative to establishing a commercially viable fuel cell technology business. Recent progress on this program in thermal spray manufacturing technology at GE Global Research is very promising for dramatically reducing low-volume manufacturing costs. Thermal spray processing offers a new, lean manufacturing paradigm for the production of planar SOFCs (see Figure 1).

Planar thermal spray manufactured cells require a metal substrate to support the electrodes and electrolyte. Typically, a porous metal foam is used to provide support in addition to permitting fuel/air access to the electrodes. This sort of cell design is referred to as a planar, metal-supported SOFC. Figure 2 compares the schematic of this concept with the schematic of a more traditional planar design with anode supported cells. In addition to significantly diminished initial capital costs, several additional advantages of thermal spray manufacturing are listed below.

1. An integrated electrolyte-to-metal seal is formed during thermal spray deposition, eliminating the need for the traditional post-fabrication glass sealing methods used for sintered cells.
2. The thermal spray manufacturing process is scalable to a large cell area that reduces part count, and is a modular process that allows flexibility in accommodating production volume and design changes that are critical for demonstration/prototype units. Larger cell sizes are directly related to a decreased part count, and thereby play a major role in reducing the stack cost through reduced materials and labor.
3. A successful thermal spray manufacturing process is inherently modular and investment in manufacturing capacity can grow as the market develops. This approach enables the commercial introduction of prototype units and low-volume production as the technology finds market acceptance with significantly reduced capital risk.

Recent efforts on this program at GE Global Research have been devoted to the development of suitable substrate and thermal spray process parameters to produce hermetic YSZ electrolytes. Due to the highly localized thermal energy directly under the

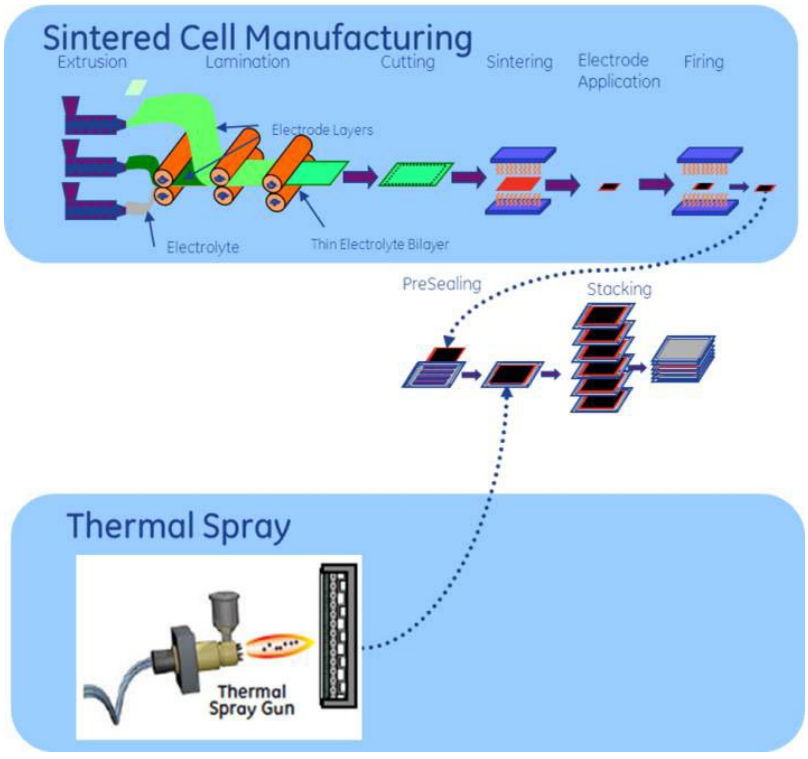

FIGURE 1. SOFC manufacturing process map comparing a traditional sintering approach with thermal spray manufacturing

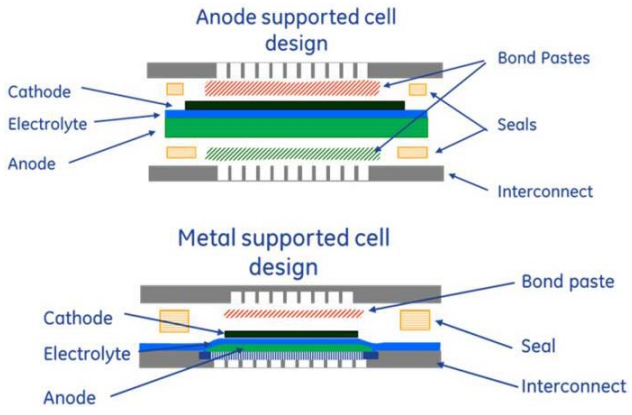

FIGURE 2. Planar SOFC designs showingtraditional anode supported design compared to metal supported cell design

thermal spray jet on the substrate, design of a substrate to dissipate this energy is critical. If local regions of the substrate are significantly hotter than adjacent regions, thermal expansion will cause excessive strains, leading to cracking of the electrolyte coating. To better understand this challenge, thermal heat flux modeling was employed to support thermal management on current 25 cm^2 designs and future scale-up to large area cells. Heat transfer simulations were used to determine the local temperatures and determine the resulting strains in the substrate to evaluate the process and optimize the substrate geometry, architecture and thermal spray conditions. Figure 3 shows the thermal modeling results as well as the evaluation of the strain during thermal spraying.

Optimization of the substrate and the thermal spray conditions have for low-strain conditions, the coatings is critical to enabling hermetic thermal spray manufactured electrolytes. An important measure of hermeticity at operational temperatures is the open circuit voltage (OCV). The theoretical OCV for the conditions tests in this work is 1.059 V. An OCV of >95% of theoretical is sufficient to enable high-efficiency commercially feasible SOFC stacks. As can be seen in Figure 4, the OCV is >97% of theoretical. This validation of the ability to produce hermetic electrolytes with thermal spray manufacturing is a very significant development. In addition to hermetic electrolytes, the manufacturing approach is capable of producing electrolytes that are sufficiently thin and conductive for commercial applications. Figure 4 also shows a thermal sprayed cell with 0.25 W/cm^2 at 0.7 V and a second cell with a 2X improvement in the power density resulting from improved electrode and electrolyte sprayed structures. High OCV and good power density are significant milestones on the path to manufacturing thermal sprayed stacks and systems.

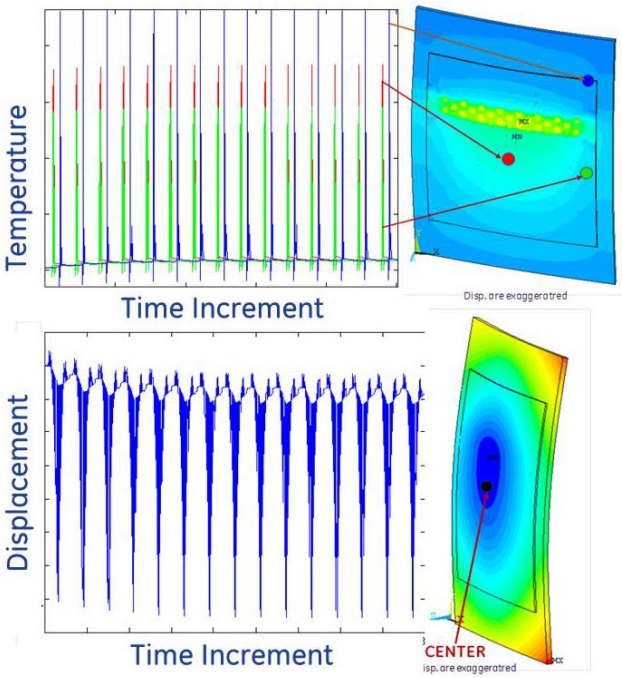

FIGURE 3. Thermal and strain history of a thermal sprayed 25 cm^2 SOFC single cell

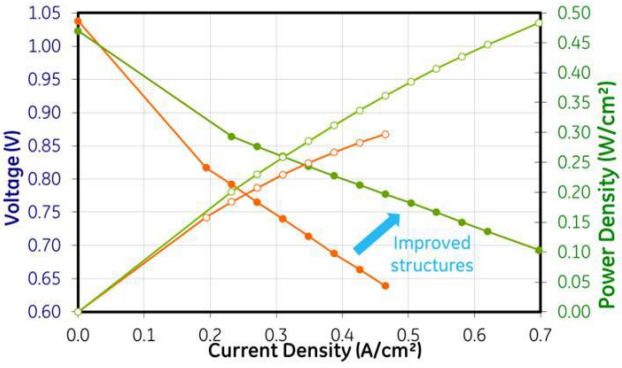

FIGURE 4. Performance curves (I-V curves) at 800°C for thermal sprayed 25 cm^2 cells showing improvement in performance with optimized structures

Conclusions and Future Directions

Thermal spray manufacturing offers a new, lean manufacturing paradigm for the production of planar SOFCs. Continued development of substrate design and thermal spray conditions will ultimately lead to the required innovation to overcome the commercialization barrier for solid oxide fuel cells with the ability to meet SECA cost targets at much lower production volumes.

Special Recognitions & Awards/Patents Issued

1. A. Kebbede, G.K. Ofori-Okai, F.J. Klug, M.J. Alinger, D.J. Lewis, Barrier Coatings for Interconnects, Related Devices, and Methods of Forming, US8163434 B2, issued 2012.

FY 2012 Publications/Presentations

1. Quarterly Report for 4th calendar quarter 2011, January 30, 2012.

2. Quarterly Report for 1st calendar quarter 2012, April 30, 2012.

3. M.J. Alinger, "Degradation of LSCF Cathodes," 12th Annual SECA Workshop, Pittsburgh, PA, 2011.

4. M. Casteel, D. Lewis, P. Willson and M. Alinger, "Ionic Conductivity Method for Measuring Vaporized Species from Solid Oxide Fuel Cell Interconnects," *International Journal of Hydrogen Energy*, Vol. 37 No. 8 (2012) 6818-6829.

IV.2 Improved Flowfield Structures for Direct Methanol Fuel Cells

Michele Tague (Primary Contact), Lloyd Ploense, Bogdan Gurau, Corey Grice, Mohammad Taslim, Mehdi Abedi, Eugene Smotkin

NuVant Systems, Inc.
130 N. West Street
Crown Point, IN 46307
Phone: (219) 644-3231; Fax: (219) 644-3682
E-mail: m.tague@nuvant.com

DOE Project Manager: Maria Reidpath
Phone: (304) 285-4140
E-mail: Maria.Reidpath@netl.doe.gov

Contract Number: FE0000982

Start Date: August 1, 2009
End Date: December 31, 2012

Fiscal Year (FY) 2012 Objectives

- Improve methanol flow to the anode by preferentially coating the patterned integrated flowfield diffusion layer (IFDL).
- Mathematically model the fuel cell using Comsol software as a means to optimize the operating parameters for increased gross fuel energy density (GFED) and fuel utilization.
- Construct a short stack consisting of two cells and design a configuration that increases the overall power output.

FY 2012 Accomplishments

- A Teflon® coating was applied to the anode side of the IFDL plate.
- A short stack has been constructed and initial performance testing was performed.
- Two dimensional modeling of the fuel cell has commenced and preliminary results are in progress.

Introduction

Direct liquid fuel oxidation fuel cells hold great promise for portable power sources and even intermediate power sources (low hundreds of watts) because the fuels have high energy density. An example of a high energy density fuel is methanol (synthesized from gasified coal), which has an energy density of 3,780 kcal/L versus 947 kcal/L for hydrogen at 400 atm. Currently, state-of-the-art direct methanol fuel cells (DMFCs) have acceptable degradation rates, but the excessive crossover of the fuel diminishes the ability to fully harvest the energy contained in the fuel. The crossover impediment can be mitigated by the use of diluted fuel; but, this decreases heavily the GFED—the energy produced per unit of fuel solution (the largest volume component for a long-term power system)—and brings about a complex and bulky balance of plant, which impacts the final energy and power density of the system. If the DMFCs are going to be successful in coming years, an alternative approach that uses concentrated fuel is required.

Approach

Methanol crossover is a challenge to DMFC development that NuVant proposes to mitigate by employing highly porous structures at the DMFC anode which enable controlled delivery of highly concentrated or neat methanol to the anode catalytic layer. NuVant's fuel cell design employs the back-diffusion of water from the cathode to the anode to supply water supply for dilution of the methanol fuel for optimal kinetics at the anode. This in situ dilution at the anode decreases the methanol crossover and thus increases the GFED. Fuel delivery to the anode is controlled by the structure of the porous material, where the pore diameter and total porosity are very important factors to be considered. Various hydrophilic and/or hydrophobic treatments of the porous substrate impact the way methanol distributes over the entire geometric area of the electrode. Also, these treatments impact the way reaction products are exhausted. In order to control the methanol flow through the IFDL to the reaction site and the exhaust, a patterned polytetrafluoroethylene (PTFE), or Teflon®, impregnation applied on the catalyst side of the IFDL plate has been proposed to permit selective permeation of methanol. The hydrophobic Teflon® will also serve to direct gaseous products to escape the cell system more readily. The implementation of the Teflon® coating will coincide with the computational fluid dynamics (CFD) modeling of the fuel through the IFDL. Further mathematical modeling of the entire fuel cell will accelerate the optimization of the fuel cell operating parameters. Initial results will be discussed. NuVant will construct single and multiple cell fuel cell stacks that incorporate the IFDL plates that are strategically modified by Teflon® impregnation. Operating parameters will be adjusted as per modeling results.

Results

CFD modeling using Fluent software demonstrated that the optimal configuration of the IFDL has a square pin grid as a flowfield on both sides but offset such that the square pins do not overlap (Figure 1). According to the CFD results, this configuration was predicted to allow a more uniform flow distribution across the fuel side of the plate and eliminated regions of fuel depletion on the membrane electrode assembly (MEA)-side. The square pins on the catalyst side are predicted to enable CO_2, a byproduct of methanol oxidation, to be easily removed from the anode electrode. A Teflon® coating on the channels of the catalyst side can further enhance the CO_2 removal from the system. NuVant is in the process of developing a method to Teflon®-ize strategic areas of the finished IFDL plates.

Single fuel cells were tested using the porous graphite non-Teflon® coated IFDL plates with a 25 cm^2 DMFC MEA. Operating parameters, such as cell temperature, fuel flow rate, method of fuel delivery (continuous flow or discrete doses), fuel concentration, and air flow rate, were varied to achieve a maximum of 781 Wh/L of GFED at a fuel utilization of 79.4%. These values are approaching the goal of 1,000 Wh/L and 100% fuel utilization. Cells were operated up to 80 hours continuously without significant loss of power output, but longer experiments are planned (several 100s of hours) to confirm the stability of the IFDL arrangement. The Teflon® coating on the IFDL is predicted to improve the current GFED and fuel utilization. Mathematical modeling is underway to optimize the following parameters: the cathode GDL hydrophobicity, porosity of the IFDL plate, thickness of the ionomer membrane, fuel and air flow rates, thickness of the cathode GDL, cell current, state of hydration, and cell temperature.

A stack consisting of multiple cells electrically connected in series was tested for proof of concept with the non-Teflon® coated IFDL plates. With this arrangement, a greater power output can be attained, and, if compared to a commercial power system, at least 10 or more cells would be needed to supply meaningful current and voltage. A small stack, consisting of two cells, was constructed (Figure 2). Fluctuations in the open circuit potential and lower operating currents instigated the redesign of the bipolar plate arrangement to allow the IFDL plate to perform normally. Figures 3 and 4 show the redesigned anode composite plate and cathode current collector plate. The fuel cell stack will be tested with the Teflon®-coated IFDL plates and their performance monitored over time.

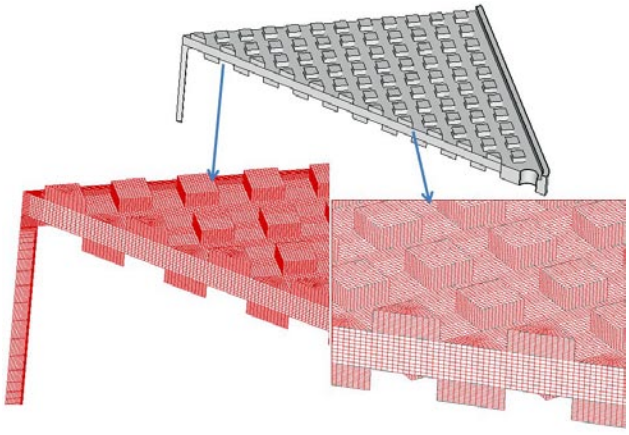

FIGURE 1. A mesh depiction of the IFDL plate with equal depth channels

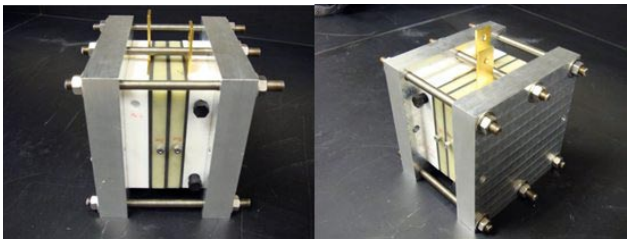

FIGURE 2. Photographs of an assembled two-cell IFDL stack. Electrical connections are made at gold plated terminals. Air flow connections are made to PTFE endplate (white) and fuel solution inlet and effluent connections are made to stainless steel fittings in garolite anode plates (light yellow).

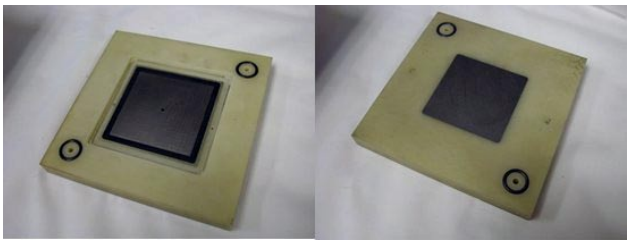

FIGURE 3. Photographs of a composite anode plate showing one side machined to mate with porous IFDL plate and sealing gasket (left) and flat surface to allow electrical contact with cathode current collector (right)

FIGURE 4. Photographs of a cathode current collector plate showing three-channel serpentine flow field (left) and flat surface for electrical connection to anode composite plate (right)

Conclusions and Future Directions

CFD modeling of the IFDL porous plate contributed to the current design of the fuel cell for even distribution of the highly concentrated methanol to the anode. In order to correlate the model to the experimental setup, a hydrophobic Teflon® coating should be applied to the channels in the patterned IFDL plate for the CO_2 to readily exit the fuel cell. A Teflon® coating/impregnation method is being developed to evenly coat the IFDL porous plate. GFED have been demonstrated as high as 781 Wh/L with fuel utilizations up to 79.4% with cells that have operated up to 80 hours in duration. Mathematical modeling of the entire fuel cell is being employed to rapidly optimize the GFED and fuel utilization by varying fuel cell parameters. These results will be correlated with experiment and can help predict the appropriate configurations to improve the GFED to 1,000 Wh/L or greater without significant losses in fuel utilization. The IFDL strategy could prove promising for the oxidation of other small organic molecules such as ethanol, formic acid, etc. Furthermore, other fuel cell materials can be incorporated into this system such as alkaline electrolyte membranes and non-noble metal catalysts. NuVant plans to commercialize the DMFC, and this will entail decreasing the size and complexity of this system.

FY 2012 Publications/Presentations

1. Staser, J., Grice, C., Taslim, M., Abedi, M., "Direct Methanol Fuel Cell Operating with Concentrated Methanol," NETL 12th Annual SECA Workshop, July 26–28, 2011, Pittsburgh, Pennsylvania, U.S. (Poster).

IV.3 Small Scale SOFC Demonstration Using Bio-Based and Fossil Fuels

Michael Petrik (Primary Contact),
Dr. Robert C. Ruhl, and Dr. Christopher Milliken
Technology Management, Inc.
9718 Lake Shore Boulevard
Cleveland, OH 44108
Phone: (440) 995-9500
Email: mpetrik@anywherenergy.com

DOE Project Manager: Maria Reidpath
Phone: (304) 285-4140
Email: Maria.Reidpath@netl.doe.gov

Contract Number: FE0005132

Start Date: October 1, 2010
End Date: March 31, 2012

Fiscal Year (FY) 2012 Objectives

- Complete fabrication of two 1-kW Technology Management, Inc., (TMI) solid oxide fuel cell (SOFC) systems.
- Site and test systems at potential end-user location for less than 30 days to obtain operating and customer interaction data.
- Identify long-term risks associated with commercialization and prepare a preliminary product/market roll-out plan.

FY 2012 Accomplishments

- Completed fabrication of two 1-kW TMI SOFC systems.
- Demonstrated operation of system for approximately 45 days at end-user location, generating valuable operating data and end-user feedback.
- Evaluated commercialization risks and preliminary product roll-out plans.

Introduction

TMI is working to develop and demonstrate a residential-scale prototype fuel cell system that will provide the basis for a new paradigm of power production and integration to utility Smart Grids (Figure 1) Massively Distributed Generation. These small scale systems will operate 24/7, producing electric power for on-site use and grid export with the option for recovered heat for cogeneration, thereby transforming today's residential power grid. Small, on-site generation provides a critical missing component to the Smart Grid equation—intelligent on-site power generation that can adapt to user loads, including electric and plug-in hybrid vehicles. The systems would operate on both conventional and renewable biofuels, providing cost-effective, uninterruptible whole-house power with major environmental and reliability advantages. The critical component to point-of-use distributed power generation is the unique TMI SOFC integrated module, which would operate on whichever fuel is used for an adjacent furnace. Most residential systems would use multiple 1-kW modules to provide continuous service to all of the electric power needs, including power to charge plug-in hybrid and electric vehicles, and hot water needs of the home, and surplus heat for space heating. Excess electricity would be available to be exported to the grid whenever necessary or economically prudent, thus providing the equivalent of massively distributed power storage. During grid outages, the system would continue to provide uninterruptible power, with a battery bank supplying surge power needs.

Relative to the primary mission of the U.S. Department of Energy Fuel Cell Program, the TMI SOFC system is potentially a 'drop-in' distributed generation subsystem that can be grid-independent and/or grid-connected operating on fossil fuels as well as on various bio-based fuels, with zero water consumption and no air pollutants. The expected outcome would be technical feedback for TMI engineers to begin to optimize the system for a commercial product application. There are few practical alternatives for ordinary consumers to obtain all *their home electric energy from zero carbon biofuels.* Actual operating experience in a non-laboratory setting is crucial to establishing viable pathways to market for future product embodiments.

Approach

The program offers the opportunity to evaluate early generation engineering prototypes in a realistic, non-laboratory environment. Two identical 1-kW modular systems would be fabricated, benchmarked on available fossil and biofuels, and then moved to an end-user site for long term (>30 days) testing and observation. Evaluation

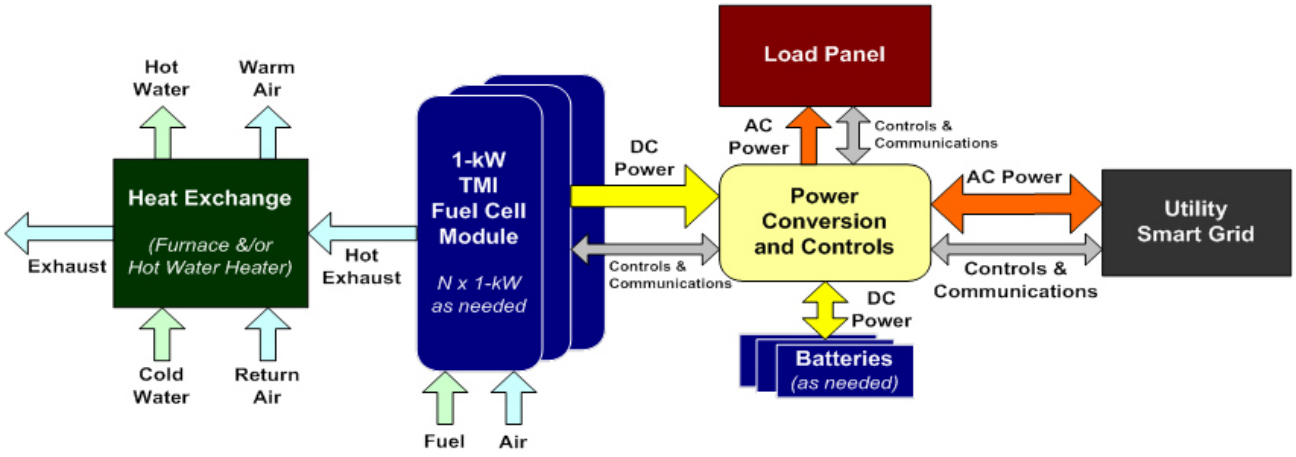

FIGURE 1. Residential fuel cell-grid interconnection system schematic

of system performance, operational issues, and end-user interactions would provide improvements for potential future product design iterations.

Results

Site preparation was completed at the primary demonstration site, Patterson's Fruit Farm, in Chesterland, Ohio. Issues were encountered relative to the use of available natural gas from an on-site gas well due to communication problems with the well operator. To expedite the testing, bottled industrial propane was selected as a replacement, and a secure storage and manifold system was fabricated (Figure 2). In addition, as a part of the overall project management task, product and market evaluations were completed.

Systems engineering and fabrication were completed for two 1-kW systems. The systems were designed to accommodate both fossil and bio-based fuel operation and loads associated with the site. The TMI SOFC system consists of hot subassembly, balance of plant (BoP) components, and ancillary systems. The fuel cell system design, particularly with respect to the hot subassembly, is directly leveraged to existing systems that are currently being developed for military applications in conjunction with funding from the Ohio Third Frontier (OTF) Fuel Cell Program through Lockheed Martin (Akron, Ohio). The hot subassembly system provides the stack with the proper operating environment for optimal performance through the integration of multiple complex functions. This subassembly mechanically holds the stack in place, removes heat to maintain stack temperature, heats the incoming air prior to entering the stack, heats the reformer and vaporizer entirely by exhaust heat to provide gaseous-state fuel to the stack, and provides the electrical connections to the stack. All heat required for air pre-heating, steam production, and

FIGURE 2. Location of Patterson Fruit Farm Market (propane closet)

steam reforming is provided by the hot subassembly's integrated internal heat exchange. To facilitate this simple implementation, TMI has developed a reforming catalyst capable of continuous operation on sulfur-bearing heavy hydrocarbons.

The BoP consists of the water/fuel subsystem, exhaust condensers, power conditioning, and data acquisition/control systems. The water/fuel subsystem for operation on liquid fuels utilizes small variable-speed positive displacement pumps to deliver variable flows for both fuel and water. A mass flow controller is used for gaseous fuels. A fan-cooled exhaust condenser provides the required reforming water from the hot exhaust stream and recycles the water to the vaporizer assembly. Careful thermal packaging ensures the system is water neutral under a wide range of conditions. Power conditioning utilizes custom electronics to convert stack DC power into useable voltages for on-board components. A microprocessor controller provides the overall operational logic and data acquisition functions.

For this program, design work was performed on the BoP systems, overall system layout, and control interface with particular consideration given to the needs of the customer site in regards to safety and fuels availability. The current design of the system places the hot subassembly side by side with the BoP components and the overall size of the system is 16" x 32" x 36"—approximately the size of a two-drawer file cabinet. Figure 3 shows the external view of the demonstration systems.

FIGURE 3. External view of demonstration systems

Ancillary systems include start up components, DC-AC inverter, packaging/structure and external interfacing for electrical load, fuel supply, and safety systems. These components were included inside the overall system box to ensure the fuel cell system has minimal impact to site operations and provides a high degree of system safety.

The demonstration was conducted using two 1-kW systems over the first quarter of 2012 at Patterson's Fruit Farm in Chesterland. Figure 4 shows the two systems running in the farm store powering multiple on-site loads during a visit by Congressman Steven LaTourette of the 14th Congressional District. Table 1 shows a summary of the peak performance of the first system on natural gas. This test indicates that the TMI SOFC has the potential to achieve the necessary high net efficiencies (>30%) to be viable in the stationary distributed generation market. Owing to limited maturity of the system, a number of electrical and flow problems compromised the ultimate system efficiency.

FIGURE 4. Two systems at Patterson's Farm Market with Rep. Steven LaTourette

TABLE 1. Peak system performance

Gross Power (W)	Net Power (W)	NG Flow (lpm, corrected)	DC Eff (%)	Net Eff (%)
759	570	2.9	43.0%	32.3%
895	710	4.3	34.3%	27.2%
1099	836	5.4	33.5%	25.5%
Maximum Projected Performance				
1355	1092	5.4	41.3%	33.3%

Both 1-kW systems were ultimately benchmarked on both propane and biodiesel. Performance on propane, as expected, was very similar to natural gas. On biodiesel, the system demonstrated a performance of 713 W at approximately 80% of full flow with 62% fuel utilization. BoP issues relating to thermal management and heat exchange caused difficulties in achieving the full target operation. Additional technical issues included handling of electrical noise, non-uniform flow and heat distribution, and water pump failures. All of these issues will be tackled in future designs.

In addition, end-user comments and feedback identified audible noise as a concern. The unit uses vane compressors for both reactant and cooling air. Although quiet (64 dB at 1 meter) compared to compressors (70+ dB at 7 meters), the noise level was sufficiently high to interrupt the normal atmosphere of the farm shop and bakery. The design had not actively attempted to minimize sound, but after the feedback was received, alternative compressors were identified to further reduce the sound to <60 dB at 1 meter in future prototypes.

Conclusions and Future Directions

Technology Management, Inc., of Cleveland, Ohio, engineered and demonstrated two 1-kW fuel flexible solid oxide fuel cell systems operating on both traditional fuels and environmentally friendly biodiesel under the project entitled "Small Scale SOFC Demonstration using Bio-based and Fossil Fuels." Operation of several systems occurred primarily on bottled propane and biodiesel. A two month demonstration at Patterson's Farm Market of Chesterland, Ohio, a local, environmentally-conscious business, was completed, and quantitative and qualitative metrics were evaluated. This demonstration supported the mission of developing an efficient, cost effective electricity source with near-zero water consumption and low atmospheric emissions of CO_2 or other air polutants.

As a result of this demonstration, TMI has initiated several engineering modifications, particularly to reduce the acoustic signature of the system. This change is expected to enhance customer acceptance and will be completed in 2012. Additionally, TMI has begun to reassess all fluid pathways to improve stack-to-stack performance reproducibility. Based on the test results, TMI still believes >30% net electrical efficiency at 1 kW on both traditional and renewable fuels with a reasonable entry price is obtainable.

FY 2012 Publications/Presentations

1. Milliken, Christopher; Petrik, Michael; and Ruhl, Robert, "Technology Management Inc. Solid Oxide Fuel Cell Demonstration Systems," poster presentation, 2011 Fuel Cell Seminar, Orlando, FL, November 1–3, 2011.

IV.4 Techno-Economic Analysis of Scalable Coal-Based Fuel Cells

Steven S.C. Chuang (Primary Contact), Felipe Guzman, Tritti Siengchum, Jelvehnaz Mirzababaei, Azadeh Rismanchian, and Brian Mohrman
The University of Akron
Department of Chemical and Biomolecular Engineering
230 E. Buchtel Commons
Akron, OH 44325-3906
Phone: (330) 972-6993; Fax: (330) 972-5856
Email: schuang@uakron.edu

DOE Project Manager: Maria Reidpath
Phone: (304) 285-4140
Email: Maria.Reidpath@netl.doe.gov

Contract Number: FE0000528

Start Date: September 1, 2009
End Date: August 31, 2013

Fiscal Year (FY) 2012 Objectives

Demonstrate the technical and economic feasibility of building a kW scale pilot-plant coal-based fuel cell with participation by industries. This project will address initial development, scaling, and manufacturing of the core technology. Objectives for 2012 include the following:

- Design and fabricate a preliminary fuel cell stack.
- Improve the durability and reduce the resistance of the current collectors and interconnects used for the fuel cell stack.
- Demonstrate the operation of fuel cell stack with hydrocarbon and solid carbon fuels.
- Study the effect of type of carbonaceous fuels on the performance of the fuel cell.

FY 2012 Accomplishments

- Developed an integration of Ni/yttria stabilized zirconia (YSZ) anode-supported fuel cells in series configuration and evaluated the performance of the fuel cell operated in H_2 fuel and hydrocarbon fuel.
- Improved the performance of the cathode current collectors by coating of a highly conductive layer on a low cost metal alloy.
- Determined the effect of surface functional groups present in various types of carbonaceous solid fuels on the fuel cell performance.
- Evaluated the operating efficiency of the fuel cell operated with fresh biomass to emulate the environment of solid biomass/coal during their injection to the high temperature fuel cell and evaluate the fuel cell performance without ash interference.

Introduction

The direct use of coal in a coal-based solid oxide fuel cell (SOFC) is an innovative concept for electric power generation. The coal-based fuel cell could offer significant advantages: (i) minimization of NOx emissions due to its operating temperature range of 700–1,000°C, (ii) high overall efficiency because of the direct conversion of coal to CO_2, (iii) production of a nearly pure (>99%) CO_2 exhaust stream for direct CO_2 sequestration, and (iv) low investment and maintenance costs due to the simplicity of the power generation process.

This project is expected to develop a scalable coal fuel cell manufacturing process through testing and simulation, demonstrating the feasibility of building a large-scale coal fuel cell power plant. The success of this project will further attract industrial investment for the commercialization of this technology for applications ranging from small-scale battery replacement to megawatt scale power generation. Ultimate success of this technology will reduce the nation's dependence on foreign oil, reduce pollution and CO_2 emission, and increase power generation efficiency above 50%, meeting the U.S. Department of Energy clean coal technology performance target.

Approach

A set of experiments was conducted aiming at (i) development of integrating Ni/YSZ anode-supported fuel cells in parallel and series configuration, (ii) determination of the effect of carbonaceous fuel sources on the performance of the fuel cell, and (iii) evaluation of the fuel cell performance under the environment of solid biomass/coal with and without ash interference. Ni/YSZ anode-supported fuel cells were fabricated in a large-scale production with tape casting technique. Tape casting formulations contain fuel cell materials, i.e., NiO and YSZ, organic additives, and different concentrations of pore formers. Testing of the fuel cell was performed with an in-house made fuel cell

reactor accompanied with gas chromatography and mass spectrometry (MS) to quantify the product. The study of the fundamental reaction pathway was performed by in situ infrared (IR) study.

Results

The integration of individual fuel cells

The integration of fuel cells in series configuration was designed to achieve high fuel cell voltages and was tested for the series of three and five Ni/YSZ anode-support fuel cells. The series configuration was achieved with a metal alloy connecting the anode of each cell to the cathode of the adjacent cell. The fuel cell and the metal alloy interconnect were attached to a steel frame, serving as the anode chamber with the aid of a ceramic seal. The fuel cells were reduced by heating at 750°C in flowing H_2/He (100 sccm, 50 vol% H_2). Figure 1a shows the V-I curves of a three-cell series stack in H_2 and CH_4, displaying an open circuit voltage (OCV) of 3.0 V. Drawing current from the fuel cell stack caused a rapid drop in voltage, evidencing the presence of large fuel cell losses. The high fuel cell losses could be attributed to contributions from the metal alloy current collectors, as discussed in this report. The V-I curves show that individual fuel cells in the three-cell series stack produced maximum current densities in the range of 300–350 mA/cm^2. Figure 1b shows a five-cell series stack and the corresponding V-I curves for each individual cell and the five cells connected in series configuration in H_2 fuel. Operating the five cells in series produced an OCV of 4.6 V, close to the expected fuel cell Nernst potential.

Improvement of current collectors

The improvement of metal alloy current collectors was tested on three configurations with the purpose of reducing the ohmic losses and increasing the fuel cell power output. The three current collector configurations included (i) a metal alloy strip coated with a thin layer of a conductive paste on one side, (ii) a metal alloy strip coated with a thin layer of conductive paste on both sides, and (iii) two alloy strips with one layer of conductive paste between the strips. The current collectors were connected to a 4,700 µF capacitor in parallel resistance circuit (RC) to measure the ohmic resistance via electrochemical impedance analysis, shown in Figure 2a. The semicircle diameter represents the resistance element R of the circuit. The non-coated alloy showed the highest resistance close to 4.2 Ω. A thin layer of conductive paste reduces the ohmic resistance by as much as 25%.

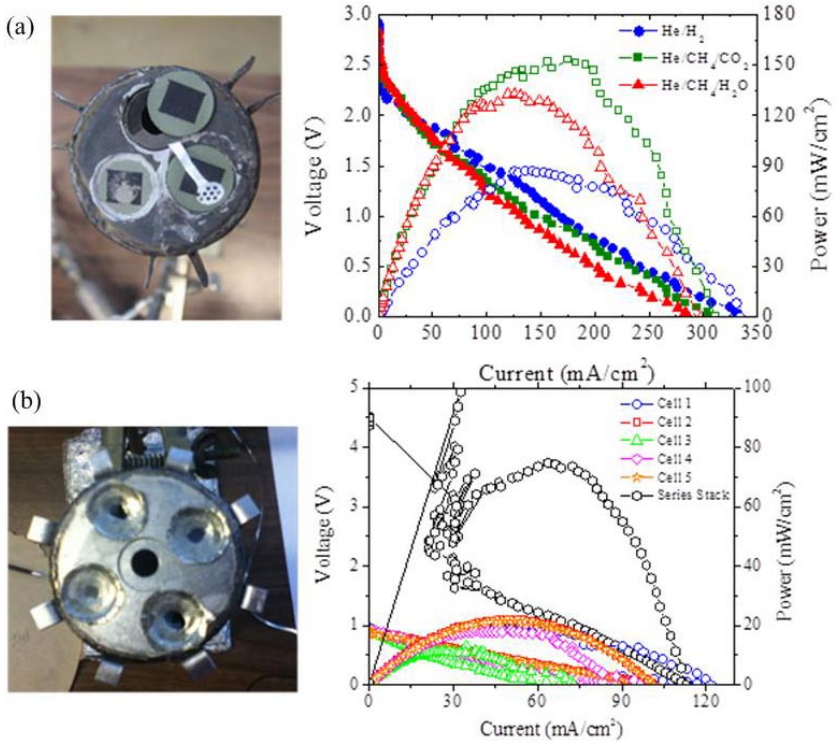

FIGURE 1. (a) Three fuel cells connected in series configuration using a metal alloy interconnector and voltage-current characteristics of the stack at 750°C in H_2 and CH_4 fuel, and (b) five fuel cells connected in series configuration and voltage-current characteristics of each individual cells and series configuration at 750°C in 100 sccm He/H_2 (50 vol% H_2)

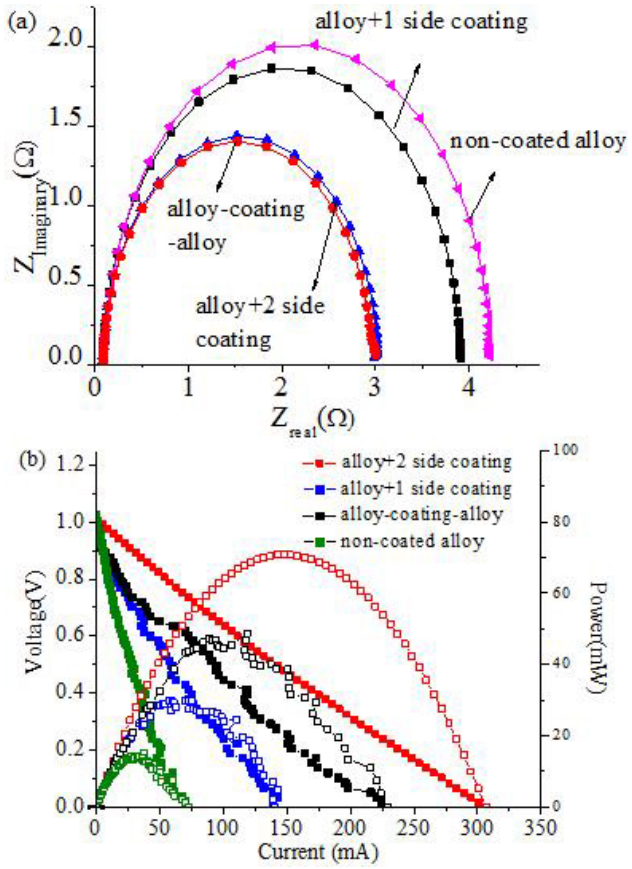

FIGURE 2. (a) Impedance spectra of the RC circuit composed of a 4,700 μF capacitor and the three cathode current collector configurations: alloy +1 side coating, alloy +2 side coating, and alloy-coating-alloy, and (b) V-I curve of a Ni/YSZ anode supported fuel cell recorded at 750°C using different cathode current collector configurations. The resistance of three cathode current collector configurations was compared with that of a non-coated alloy strip.

The current collectors were then attached to the cathode electrode of a fuel cell and tested in H_2 to quantify their contribution to the cell power generating ability. Figure 2b shows the V-I curves of the fuel cell in which the cathode was attached to the modified current collectors recorded at 750°C in H_2 fuel. The alloy +2 sides (with conductive paste on both sides) produced the highest maximum power density of 78 mW/cm^2. Although the alloy-coating-alloy current collector showed similar ohmic resistance at room temperature to that of the alloy with both sides coated, shown in Figure 2a, its performance in the fuel cell differed. The difference could be related to changes in electronic conductivity due to delamination of the conductive layer during long-term heating at 750°C. Therefore, protecting the conductive paste layer in between two alloy strips is considered the most suitable approach for achieving high durability and low resistance in the fuel cell cathode current collector.

Study of the effect of carbon surface functional group

IR absorbance spectra of coconut carbon and petcoke before and after the gasification are shown in Figure 3. Coconut carbon possesses more organic surface functional groups, i.e., C-H, C-O-H, and O-H, than petcoke. Following the gasification with a 3-cc pulse of CO_2 and O_2 at 600°C, the intensity of C-H, C-O-H, and O-H peaks on coconut carbon decreased, indicating that these functional groups participated in gasification that produced CO. The results from previous quarterly reports show that fuel cells operating in coconut carbon exhibit a maximum current density of 19% of that operated in H_2/He, while the fuel cell operated in petcoke produced only 9% of that in H_2/He. The higher performance of the fuel cell operated in coconut coke is due to the formation of CO through the gasification which can be further electrochemically oxidized on the anode generating electricity.

Efficiency of the fuel cell in biomass

Figure 4 shows the MS profiles of the fuel cell effluent and the current generated by the fuel cell operated in coconut shell under 10 cm^3/min He at a voltage of 0.4 V at 750°C. The active cathode area is 0.5 cm^2. Injection of coconut shell in the anode chamber at 750°C caused a rapid increase in the MS intensities of CO, CO_2, CH_4, and H_2 (m/e = 28, 44, 15, and 2, respectively). This increase was the result of pyrolysis of the coconut shell. Injection of the coconut shell accompanied with the production of CO, CH_4, and H_2 increased the current produced by the fuel

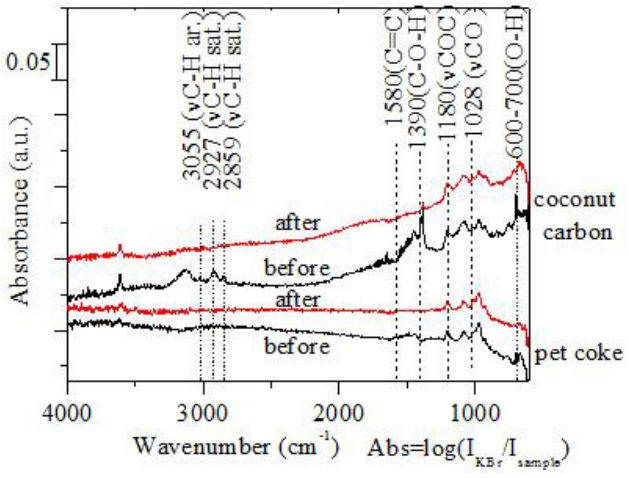

FIGURE 3. Absorbance spectra of coconut carbon and petcoke (5 wt% in KBr) before and after gasification with 3-cc pulse of CO_2 and O_2 at 600°C. Absorbance was obtained by Abs = log(I_0/I) where I is single beam spectra of the sample at room temperature and I_0 is single beam of KBr at room temperature.

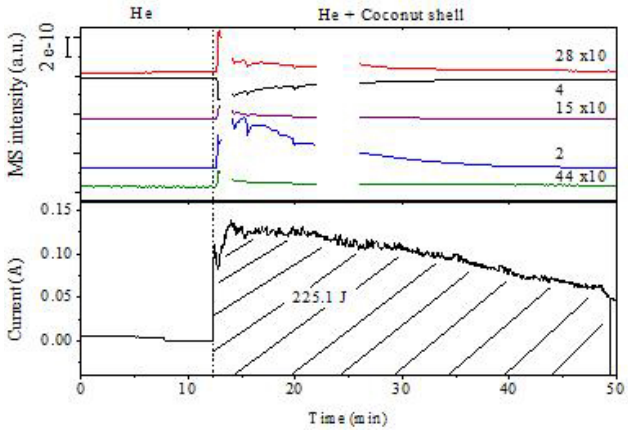

FIGURE 4. MS profiles of the fuel cell effluent and the current generated by the fuel cell operated in coconut shell under 10 cm^3/min He at 750°C

cell to a maximum of 0.14 A at two minutes after the injection. Operation of the fuel cell in coconut shell gradually decreased the current to 0.08 A in 37 min, and the operation was stopped to determine the effective efficiency. The operating efficiency was calculated by relating the electric power produced by the fuel cell at the operating voltage, W_e, and the energy provided from the consumption of the coconut shell, resulting in the operating efficiency of 1.2%. The low operating efficiency of the fuel cell operated in coconut shell can be attributed to the majority of the gaseous product generated by the fast pyrolysis leaving the anode chamber prior to the electrochemical oxidation.

Conclusions and Future Directions

Results from these experimental studies provide experimental evidence supporting the feasibility of developing a coal-based fuel cell manufacturing technology. Milestones achieved during FY 2012 demonstrated that (i) integration of the fuel cells in series increases the fuel cell voltage, (ii) durability and conductivity of the current collectors can be improved by coating of a highly conductive paste, (iii) surface functional groups on carbonaceous fuel can increase the performance of the fuel cell, and (iv) the operation of the fuel cell with solid fresh biomass was demonstrated.

Future studies will focus on:

- Modification of the anode catalyst to increase the activity toward carbonaceous fuels and its gasification products.
- Evaluation of the efficiency of the fuel cell stack in carbonaceous fuels.
- Integration of multiple fuel cell stacks and design of a kW scale pilot plant.
- Cost analysis of a kW scale fuel cell stack.

FY 2012 Publications/Presentations

1. Tritti Siengchum, Felipe Guzman, and Steven S.C. Chuang, "Analysis of Gas Products from Direct Utilization of Carbon in a Solid Oxide Fuel Cell," *Journal of Power Sources* **2012,** *213* (0), 375-381.

V. SMALL BUSINESS INNOVATION RESEARCH

A. Cathodes

V.A.1 Solid Oxide Fuel Cell Cathode Enhancement Through a Vacuum-assisted Infiltration Technique

Greg Tao
Materials & Systems Research Inc.
5395 West 700 South
Salt Lake City, UT 84104
Phone: (801) 530-4987 ext. 30; Fax: (801) 530-4820
Email: gtao@msrihome.com

DOE Project Manager: Briggs White
Phone: (304) 285-5437
Email: Briggs.White@netl.doe.gov

Subcontractor:
Argonne National Laboratory, Argonne, IL

Contract Number: SC0006374

Start Date: June 17, 2011
End Date: March 16, 2012

Fiscal Year (FY) 2012 Objectives

- Fabricate planar anode-supported solid oxide fuel cells (SOFCs) for nano-catalyst infiltration evaluation and performance characterization.
- Optimize cathode backbone microstructures to improve the catalyst infiltration efficiency.
- Develop a cost-effective, one-step nano-catalyst infiltration technique.
- Construct SOFCs and experimentally characterize the cathode enhancement via the one-step infiltration.

FY 2012 Accomplishments

- Planar, anode-supported SOFCs (as baseline cells) were fabricated with the engineered cathode microstructures suitable for an efficient infiltration of catalyst precursor solutions.
- A one-step vacuum-pressure-infiltration-thermal (VPIT) treatment process and apparatus were developed and implemented successfully on scalable cells with per-cell active area varying from 2 cm^2 to 100 cm^2.
- An infiltration matrix was defined and related key parameters determining the infiltration efficiency were investigated.
- Nano-sized (Sm,Sr)CoO_3 catalyst loading level was efficiently increased from 1 mg/cm^2 to 2.5 mg/cm^2 after the one-step infiltration process.
- Proof-of-concept tests were performed on both button cells and a short stack by demonstrating cell performance improvement over 45% after nano-sized $Sm_{0.6}Sr_{0.4}CoO_3$ (SSC) catalyst infiltration.
- A strategy to mitigate the nano-sized catalyst coarsening/growth issue was developed and implemented successfully.
- Long-term stability tests of button cells with catalyst infiltration were performed at 800ºC and demonstrated a degradation rate less than 2.5%/1,000 hrs over a 2,500 hour test.
- A hybrid stack (100 cm^2/cell) comprising a combination of a baseline cell and four catalyst-infiltrated cells was constructed and tested over 1,100 hours, demonstrating a stack degradation rate less than 5.4%/1,000 hrs and all catalyst-infiltrated cells outperforming the baseline cell.

Introduction

SOFC technology promises to provide an efficient method by which electricity can be generated from coal-derived syngas, biofuels, and natural gas, while increasing energy security and reducing greenhouse gas emissions. The large capital costs attributed to the cathode low performance and long-term stability issues are a leading limitation of SOFC technologies that must be addressed before commercial SOFC power generation can be realized. A state-of-the-art SOFC composite cathode, typically consisting of an ionic conducting electrolyte material and a mixed ionic-electronic conducting perovskite oxide, possesses excellent performance characteristics, but it is subject to chemical stability issues during manufacturing and power generation operation at elevated temperatures. Additionally, the mismatch of thermal expansion coefficients (TECs) between the SOFC electrolyte (i.e., YSZ-based electrolyte) and an adjacent barrier layer (i.e., a doped ceria layer) often causes delamination issues.

An alternative approach to enhancing the SOFC performance is to develop an advanced cathode deposition process via nano-sized catalyst impregnation. It enables the suppression of deleterious reactions during the conventional cathoding process at elevated temperatures and elimination of thermal expansion mismatching between adjacent layers, while it also enables the increasing of surface areas and triple-phase

boundary lengths substantially. Typically, the infiltration can be realized through impregnating a catalyst precursor solution in a form of an aqueous nitrate salt solution, a colloid suspension solution, or a molten nitrate salt mixture [1] into either pre-formed oxygen ion-conducting scaffolds [2-5] or pre-formed cathode backbones [6-12] consisting of an electron conductor material, a mixed ionic-electronic conductor material, or a composite (two phases). Infiltrating a solution of nitrate salts into pre-formed porous electrolyte backbones is simple and effective, however forming a continuous structure and getting a certain level of perovskite (catalyst) loading normally involves multiple sequential steps of infiltration followed by heat-treatment at high temperatures, sometimes over 20 infiltrations [2-5]. Such a multitude of infiltrations is not economical and impedes its use in practical applications. On the contrary, with assists of a surfactant and surface tension modification, the approach of infiltrating a catalyst directly into the cathode backbones has attracted considerable attention and shows much promise.

Materials & Systems Research, Inc. (MSRI), teaming with Argonne National Laboratory (ANL), has developed a single-step, vacuum-assisted infiltration technique to enhance SOFC cathode performance and longevity through the impregnation of an inexpensive electro-catalyst precursor into a preformed cathode backbone. Upon calcination at reduced temperatures, a thin but continuous network of nano-sized catalysts was formed and covered the cathode backbone with enlarged catalytic surface area and heterogeneous microstructure, thus enhancing both the oxygen exchange rate and oxygen ions transport rate on the cathode surface.

Approach

Development of an infiltration process has been reported vastly at a lab-scale and demonstrated on button-sized cells successfully; however, lack of a technically and economically sound fabrication process and lack of repeatability and long-term stability evaluation impedes its use in large-scale applications. From the industrial-scale manufacturing standpoint, MSRI developed a cost-effective, sequential single-step VPIT treatment process, and successfully implemented and evaluated this unique VPIT process on scalable planar cells (as large as 100 cm^2). The development approach followed the defining and investigating key parameters that determine the success of the one-step infiltration process, which include the adaptability to the pre-established cathode backbones, precursor solution concentration for the one-step process, surfactant loading level for assisting the correct perovskite phase formation, evenness of solution distribution across cells with large active areas, and thermal-treatment (gelation/ decomposition temperature and rate, and calcination temperature).

Planar, anode-supported cells were fabricated using MSRI's proven SOFC fabrication techniques and widely adopted industry material sets. Baseline cells, including button-sized cells and internally-manifolded square cells with a respective per-cell active area of 2 cm^2 (2.7 cm diameter) and 100 cm^2 (outer dimension 15 cm x 15 cm), were fabricated from the same batch of green tapes comprising NiO and 8 mole % yttria stabilized zirconia (8YSZ) to eliminate any possible variations among different batches. 8YSZ was deposited via air-spraying as the electrolyte, and the $(La,Sr)MnO_3$-8YSZ based composite was screen-printed onto the electrolyte as the cathode backbones. In order to increase the infiltration efficiency, pore formers with different sizes were blended into the cathode inks to engineer the backbone microstructures, thus allowing the active catalyst to be loaded heavily enough to cover the cathode grains along the triple-phase boundaries but lightly enough along the other cathode layers to save material costs.

Strontium-doped samarium cobaltite ($Sm_{0.6}Sr_{0.4}CoO_3$), possessing the most desirable properties (high adsorption/desorption rates and an oxygen ion diffusion coefficient), was used as the electrocatalyst for this infiltration study. Aqueous solutions of SSC precursor was prepared by dissolving the nitrates of $Sm(NO_3)_3 \cdot 6H_2O$, $Sr(NO_3)_2$, and $Co(NO_3)_2 \cdot 6H_2O$ in de-ionized water at a proper molar ratio. The effects of the precursor concentrations on the infiltration efficiency and cell performance were investigated respectively via scanning electron microscopy (SEM) and voltage-current (VI) sweeps along with the electrochemical impedance spectrum (EIS) measurements. Proof-of-concept tests were performed on both button cells and a short stack to demonstrate SOFC cathode enhancement via the proposed one-step VPIT infiltration technique.

Results

Phase Formation

Urea (a surfactant) was added to the aqueous SSC precursor solution as a complex agent to assist the perovskite phase formation. The molar ratios of urea to SSC cations were varied from 5:1 to 15:1 in order to study the effects on the correct phase formation. Representative SSC powders were prepared from three precursor solutions with urea to SSC ratios set to 5:1, 10:1, and 15:1. Powders were calcined in air at 800ºC and 850ºC for two hours. X-ray diffraction (XRD) pattern studies of those SSC powders showed that a correct perovskite phase was formed when the urea loading level was high enough (urea/SSC ratio >10/1), which is consistent with the results of literature [12].

SSC precursor concentration effects

The SSC catalyst infiltration was performed on a home-built apparatus based on a concept of the vacuum pressure impregnation process used by the electronic packaging industry. An SSC precursor solution was introduced to the cathode backbone under vacuum by a needle valve that was adjusted to control the solution flow rate. Depending on the concentrations of precursor solutions, typically ~50 µL and 2,500 µL of a solution were used to infiltrate a button cell and a large cell, respectively. Upon finishing the delivery of the precursor solution, the vacuum was then released and the cell was pressurized to 3 psig. The cell was then removed and placed on a hot plate for a few minutes or until the solution gelled, followed by calcination at 850ºC for two hours. The local flooding issue, which may lead to cathode delamination due to mechanically weak cathode structures, was avoided with the use of a built-in sprinkler-like device with a rotation mechanism, which assisted in distributing the precursor solution evenly onto the cathode surface. The effects of SSC precursor concentrations on the infiltration efficiency were investigated via SEM evaluation. Figure 1 shows the SEM characterizations of cathode interlayers (CIL) of four post-test 1" button cells, which were respectively infiltrated with four different SSC precursor solutions having concentrations of 0.5 M, 0.94 M, 1.14 M, and 1.4 M as measured. As clearly shown in the figure, highly concentrated precursor solutions are much desirable to cover sufficient LSM cathode grains so that the catalytic surface area and/or heterogeneous microstructures can be enlarged. This hypothetically leads to an enhancement of both the oxygen exchange rate and oxygen ions transport rate on cathode surfaces.

Electrochemical characterization

Button cells infiltrated with catalysts were tested on MSRI's standard button-cell testing fixtures, which were spring-loaded to ensure constant loading and to minimize interfacial contact resistances. No metallic interconnects, typically used in planar stacks, were used, and thus the effects of oxidation and associated resistances of the metallic interconnects and Cr poisoning were eliminated from testing. Both the ceramic-based air and fuel manifolds had been machined with flow patterns assisting the reactants distribution. Dry contact

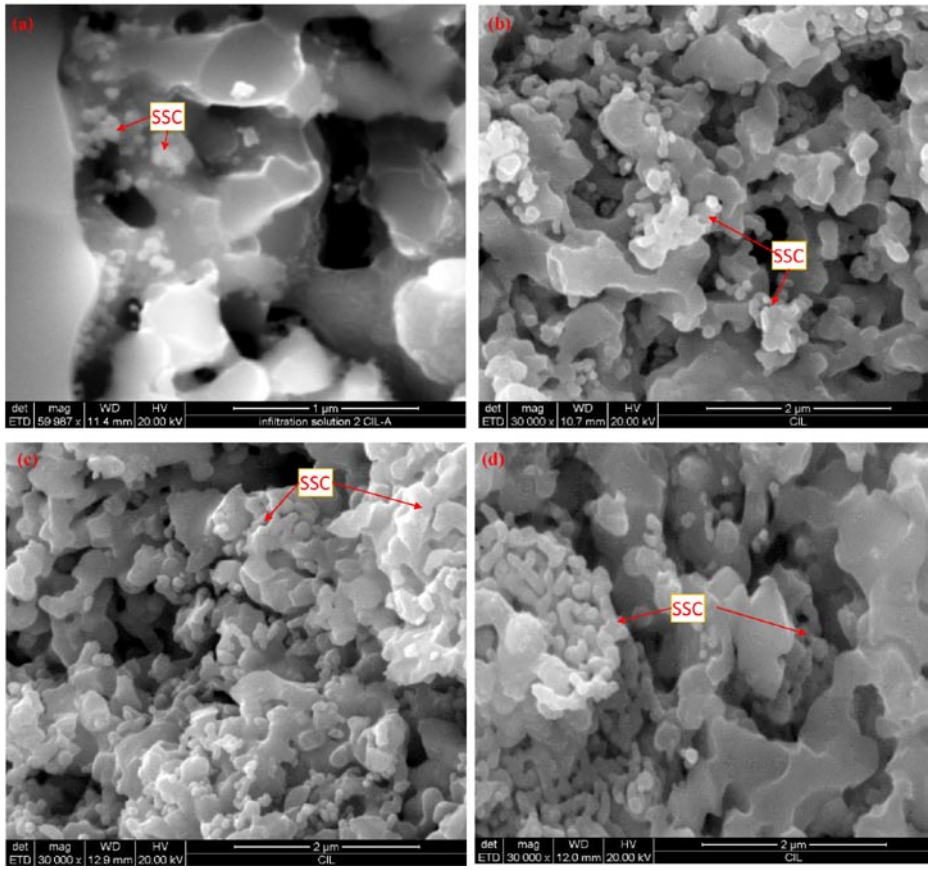

FIGURE 1. SEM characterizations of the SSC precursor solution concentration effects on infiltration efficiency: (a) 0.5 M, (b) 0.94 M, (c) 1.14 M, (d) 1.4 M as measured

aids (meshes) were used to reduce contact resistance. A standard four-probe configuration with two voltage leads and two current leads were used for an accurate measurement by eliminating many of the secondary losses that could occur in stack tests. A shielded/grounded K-type thermocouple was inserted inside the air manifold to monitor and record the cell temperature.

Figure 2 shows the electrochemical characterization results of cells infiltrated with precursor solutions having different concentrations. The performance of a baseline cell was also shown in the same figure for comparisons. In order to eliminate any possible variations among the different testing stations, all the cells shown in the figure were tested on the same testing fixture under the same operating conditions. Evidently, significant performance improvement was observed for cells infiltrated with highly concentrated precursor solutions, such as cells infiltrated with the S3-5 solution (1.4 M). At 0.7 V, the power density of the S3-5 cell (1.4 M) was 0.6 W/cm^2, outperforming the baseline cell by nearly 40%. The performance improvement was attributed mostly to a reduced polarization overpotential loss, which was confirmed from the EIS measurements.

It has been a known issue that the nano-sized catalyst particles tend to grow or coarsen during power generation at elevated operation temperatures. A strategy to mitigate the issue was developed in Phase I by properly organizing the catalysts at desirable deposition locations; the resulting cells (S3-5-s) were evaluated, where they showed significant improvement from the standpoint of short-term VI performance and long-term stability. As shown in the same Figure 2, the power density of a representative specially-treated cell (S3-5-s) increased by nearly 63% compared to the baseline cell.

Long-term tests were conducted on several selected S3-5-based cells, as well as a baseline cell, for degradation evaluation of cathode enhancement via the VPIT process. All the long-term tests were performed at a current-control mode (constant currents) such that the cell initial voltages were set to around 0.73~0.74 V. In order to investigate any possible degradation mechanisms, the long-term tests were interrupted weekly for scheduled operations, which included VI sweeps and EIS measurement under the open circuit voltage conditions. Figure 3 summarizes the test results. Over a 2,100-hour test, the baseline cell (shown in a red line) demonstrated a degradation rate of ~1.16%/1,000 hrs (linear fitting of the power density line). All three button cells infiltrated with a S3-5 solution (1.4 M) showed much better performance than the baseline cell. However, the performance improvement was not sustainable long enough before all three cells started degrading, as shown in dark, wine, and blue color lines in the same plot. Moderately large SSC particles and agglomerates were observed along the cathode grains from the post-test SEM studies, indicating the possible degradation mechanism. It is suspected that the coarsening or particle growth of nano-sized SSC catalysts may have resulted from a high current operation (probably leading to excessive heating locally).

As discussed previously, a solution to mitigate the particle growth issue was implemented, and the resulting button cells were tested to evaluate the long-term stability improvement. The test results of a representative cell (SSC-S3-5-s) were also shown in an orange line in the same Figure 3. Clearly, the cell performance enhancement and longevity improvement are far more profound when the mitigation solution is implemented. In excess of 2,500-hour tests (currently, this test is still on-going), this cell showed remarkable stability with a degradation rate less than 2.5%/1,000 hrs. Periodically,

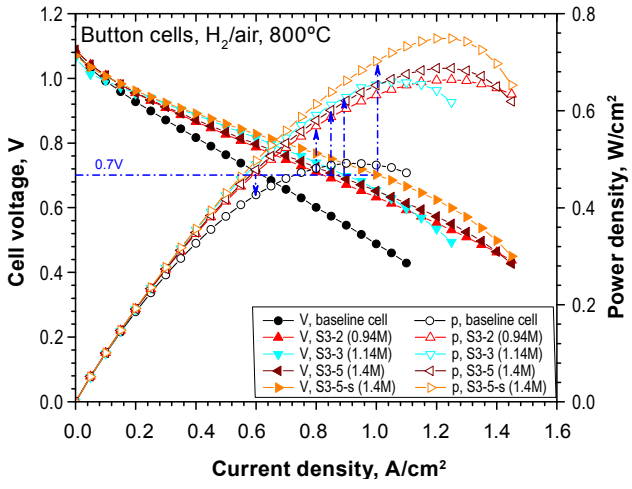

FIGURE 2. Performance of five representative button cells tested at 800ºC

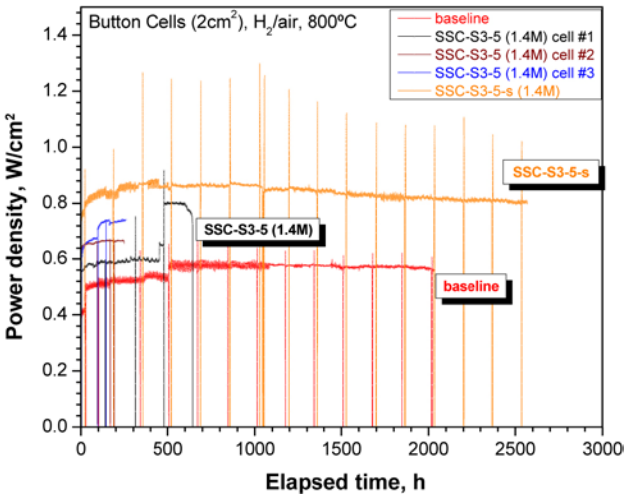

FIGURE 3. Long-term stability test comparisons among a baseline cell, three SSC-S3-5 cells (1.4 M), and a specially-treated SSC-S3-5-s cell (1.4 M)

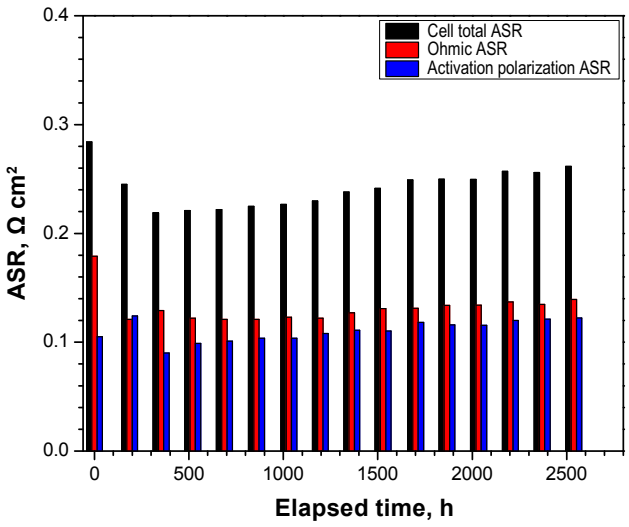

FIGURE 4. ASR breakdown of the same specially-treated SSC-S3-5-s cell obtained at different time (weekly base)

throughout the long-term test, VI sweeps and EIS measurements were performed weekly to study possible degradation mechanisms. Assuming the concentration polarization losses were negligible (this can be confirmed from Nyquist plots), the activation polarization losses were obtained by deducting the ohmic-ASR from the total ASR. Figure 4 shows the histogram of the ASR breakdown. The degradation evidently attributed from the growth of the ohmic losses more than that of activation polarization losses, partially suggesting that the mitigation solution retains the activity of the infiltrated nano-sized SSC catalysts effectively.

While the button-cell tests provided the most cost-effective means for evaluating the advanced VPIT infiltration methodology and for validating the process, the Phase I efforts were also extended successfully towards large cells and stacks for the proof-of-concept demonstration. Internally-manifolded cells with a per-cell active area as large as 100 cm^2 were randomly picked from a pool of 35 baseline cells and then infiltrated with precursor solutions of SSC-S3-5 and SSC-S3-5-s. A hybrid stack comprising a baseline cell, two SSC-S3-5 cells and two SSC-S3-5-s cells was constructed and tested over 1,100 hours under a constant current (40 A). The stack demonstrated a degradation rate of 5.4% with the catalyst infiltrated cells outperforming the baseline cells.

Conclusions and Future Directions

- Successfully met all the critical milestones set for Phase I.
- Modification of the LSM-8YSZ-based cathode backbones sufficiently furnished an efficient catalyst infiltration.
- Developed and implemented a one-step VPIT process for infiltrating the nano-sized SSC catalyst into pre-established cathode backbones.
- Key parameters determining the infiltration efficiency were investigated; successfully increased the loading of the nano-sized SSC catalyst from 1 mg/cm^2 to 2.5 mg/cm^2.
- Cells with a catalyst infiltration outperformed the cells without infiltration by at least 40% (at 0.7 V), mainly attributed to the activation polarization reduction from cathodes.
- Long-term tests of a baseline cell (w/o catalyst infiltration) showed a degradation rate of -1.16%/1,000 hrs over the 2,100-hour test.
- Mitigating the nano-structured catalyst coarsening issue showed much promise.
- Long-term tests of a treated cell (SSC-S3-5-s) showed an overall degradation of 2.5%/1,000 hrs over the 2,500-hour test.
- The scheduled VI sweep tests and EIS measurements suggested that the mitigation solution retains the activity of the infiltrated nano-sized SSC catalysts effectively.
- Overall, the one-step VPIT process offers much flexibility of highly active catalysts selection and materials combination for the cathode enhancement. Further development efforts will be needed to perfect the one-step VPIT process before being implemented for large-scale SOFC applications, as well as proof-of-concept demonstration at 1 kW-class stack level.

FY 2012 Publications/Presentations

1. G. Tao and M. King, "Solid Oxide Fuel Cell Cathode Enhancement Through a Vacuum-assisted Infiltration Technique," 221st Electrochemical Society Meeting, May 6–11, 2012, Seattle, Washington.

References

1. Y. Huang, J.M. Vohs, and R.J. Gorte, "SOFC Cathodes Prepared by Infiltration with Various LSM Precursors," *Electrochemical and Solid-State Letters*, 9 (5) (2006) A237-A240.

2. F. Bidrawn, S. Lee, J.M. Vohs, and R.J. Gorte, "The Effect of Ca, Sr, and Ba Doping on the Ionic Conductivity and Cathode Performance of $LaFeO_3$," *J. Electrochem. Soc*., 155 (2008) B660-B665.

3. J.M. Vohs and R.J. Gorte, "High-Performance SOFC Cathodes Prepared by Infiltration," *Adv. Mater.*, 21 (2009) 943-956.

4. S. Lee, M. Bevilacqua, P. Fornasiero, J.M. Vohs, R.J. Gorte, "Solid Oxide Fuel Cell Cathodes Prepared by Infiltration of $LaNi_{0.6}Fe_{0.4}O_3$ and $La_{0.91}Sr_{0.09}Ni_{0.6}Fe_{0.4}O_3$ in Porous Yttria-Stabilized Zirconia," *J. of Power Sour*ces, 193 (2009) 747-753.

5. R. Küngas, F. Bidrawn, J.M. Vohs, and R.J. Gorte, "Doped-Ceria Diffusion Barriers Prepared by Infiltration for Solid Oxide Fuel Cells," *Electrochemical and Solid-State Letters*, 13 (2010) B87-B90.

6. K. Yamahara, C.P. Jacobson, S.J. Visco, X. Zhang, L.C. De Jonghe, "Thin Film SOFCs with Cobalt-Infiltrated Cathodes," *Solid State Ionics*, 176 (2005) 275–279.

7. T.Z. Sholklapper, V. Radmilovic, C.P. Jacobson, S.J. Visco, and L.C. De Jonghe, "Synthesis and Stability of a Nanoparticle-Infiltrated Solid Oxide Fuel Cell Electrode," *Electrochemical and Solid-State Letters*, 10 (2007) B74-B76.

8. X. Lou, S. Wang, Z., L. Yang, M. Liu, "Improving $La_{0.6}Sr_{0.4}Co_{0.2}Fe_{0.8}O_{3-\delta}$ Cathode Performance by Infiltration of a $Sm_{0.5}Sr_{0.5}CoO_{3-\delta}$ Coating," *Solid State Ionics*, 180 (2009) 1285–1289.

9. L. Nie, M. Liu, Y. Zhan, M. Liu, "$La_{0.6}Sr_{0.4}Co_{0.2}Fe_{0.8}O_{3-\delta}$ Cathodes Infiltrated with Samarium-Doped Cerium Oxide for Solid Oxide Fuel Cells," *J. Power Sources*, 195 (2010) 4704–4708.

10. J.D. Nicholas and S.A. Barnett, "Measurements and Modeling of $Sm_{0.5}Sr_{0.5}CoO_{3-x}$–$Ce_{0.9}Gd_{0.1}O_{1.95}$ SOFC Cathodes Produced Using Infiltrate Solution Additives," *J. Electrochem. Soc*., 157 (2010) B536-B541.

11. S. Lee, N. Miller, H. Abernathy, K. Gerdes, and A. Manivannan, "Effect of Sr-Doped $LaCoO_3$ and $LaZrO_3$ Infiltration on the Performance of SDC-LSCF Cathode," *J. Electrochem. Soc*., 158 (2011) B735-742.

12. X. Lou, Z. Liu, S. Wang, Y. Xiu, C.P. Wong, and M. Liu, "Controlling the Morphology and Uniformity of a Catalyst-Infiltrated Cathode for Solid Oxide Fuel Cells by Tuning Wetting Property," *J. Power Sources,* 195 (2010) 419–424.

V. SMALL BUSINESS INNOVATION RESEARCH

B. Seals

V.B.1 High-Temperature Viscous Sealing Glasses for Solid Oxide Fuel Cells

Cheol-Woon Kim
MO-SCI Corporation
4040 Hy Point North
Rolla, MO 65401
Phone: (573) 364-2338
Email: ckim@mosci.com

DOE Project Manager: Joseph Stoffa
Phone: (304) 285-0285
Email: Joseph.Stoffa@netl.doe.gov

Subcontractor:
Richard K. Brow
Missouri University of Science & Technology,
Rolla, MO

Contract Number: SC0002491

Start Date: August 15, 2011
End Date: August 14, 2013

Fiscal Year (FY) 2012 Objectives

- Refine and optimize the crystallization-resistant glass compositions, developed in Phase I, with the requisite thermal and physical properties, e.g., glass transition temperature (T_g), softening point (T_s), liquidus temperature (T_L), and coefficient of thermal expansion (CTE), for making viscous seals for solid oxide fuel cells (SOFCs).
- Evaluate viscosity-temperature characteristics of new glass compositions using high temperature rheometry and parallel plate viscometry.
- Determine glass stability against volatilization by weight loss measurements under SOFC operational conditions (650-850°C, wet reducing and dry air conditions).
- Characterize the thermochemical reactions that occur at the seal/SOFC material interface under the operating conditions.
- Conduct hermetic seal tests and evaluate the self-healing performance of candidate viscous glass seals under the operating conditions.

FY 2012 Accomplishments

- Forty-three new viscous glass compositions (Glass 42 to 84) were formulated and melted, and their thermal and physical properties (T_g, T_s, T_L, and CTE) were measured. These alkali-free glasses have compositions from the BaO-RO-Al_2O_3-B_2O_3-SiO_2 system where RO represents other alkaline earth oxides or ZnO. Additional compositions will be formulated and evaluated.
- The dilatometric softening points (T_s) and the glass transition temperatures (T_g) of the favored glasses meet the requirements for use in SOFC viscous seals operating at temperatures as low as 650°C.
- The favored glasses do not crystallize in a differential scanning calorimeter (DSC) when heated at a rate of 10°C/min up to 1,000°C, indicating much greater stability against crystallization than conventional glass-ceramic sealing compositions.
- Three glass compositions (Glass 73, 75, and 77) were selected from the 43 different compositions based on their desirable thermal and physical properties. Glass 73, 75, and 77 have relatively low liquidus temperatures ($T_L \leq 810$°C) and so can form viscous seals that do not substantially devitrify under SOFC operational conditions.
- The CTEs of Glass 73, 75, and 77 are greater than that of Glass 28, developed in Phase I.
- Viscosity-temperature curves for Glass 73, 75 and 77 were obtained using the rotating spindle and parallel-plate viscometry techniques and were analyzed using the Corning viscosity equation. Based on these results, the self-healing behavior could be expected at temperatures above about 675°C, the temperature of the Littleton softening point (viscosity $10^{6.6}$ Pa-s).
- The interfacial reactions of the candidate sealing glasses with aluminized 441 stainless steel (SS441) and a Ni/ yttria-stabilized zirconia (YSZ) bilayer were studied using scanning electron microscopy (SEM) for sandwich seals held in air at 800°C. Glass 73 has good thermo-chemical compatibility with SS441 and YSZ.
- Glass stability against volatilization was determined by weight loss measurements. Weight loss measurements were conducted as a function of time (up to 2,000 hours) at 750°C. The total weight loss of Glass 73 was estimated, by extrapolation, to be 4.5% under flowing wet forming gas and 1.9% under stagnant dry air at 40,000 hour design lifetimes.
- Hermetic seal tests were conducted using a newly constructed horizontal test manifold. A hermetic seal between SS441 and a YSZ bilayer with Glass 73 has survived 80 thermal cycles (room T-750ºC) to date under dry air over the course of >2,500 hours

without failure. Another Glass 73 seal has survived 48 thermal cycles to date under wet forming gas. Both tests are still continuing.

- Self-healing of glass seals that were intentionally cracked by thermal shock was observed in a SS441/Glass 73/YSZ-bilayer sample. The glass in a seal originally found to be hermetic was cracked upon quenching at ~25°C/s from 800°C. When re-heated to 800°C for two hours then slowly cooled to room temperature, the seal was again hermetic, holding 1.5 psi overpressure. This test has been successfully repeated two more times.

Introduction

Solid oxide fuel cells require hermetic seals to prevent mixing of the fuel and oxidant streams within the cell stack and to seal the stack to the system manifold. Reliable sealing materials must (a) possess viscosity-temperature characteristics that are compatible with sealing requirements and that allow for stress relaxation and self-healing without excessive flow, under pressure, that would compromise seal integrity; (b) be chemically compatible with SOFC components and so not alter the long-term thermo-mechanical stability of the seal by forming deleterious interfacial reaction products; (c) avoid the significant volatilization of glass constituents under the SOFC operational conditions that has been associated with other sealing materials, and so alter the viscous properties of the seal or the performance of the SOFC; and (d) possess dilatometric properties that are compatible with other SOFC components and stable over the course of the SOFC lifetime (≥40,000 hours).

Approach

The use of viscous glass seals provides one means of reducing the risk that thermal stresses will result in catastrophic failures and may provide a means for the seal to recover if cracks do form. Some of the early work at Argonne National Laboratory identified compositions in the alkaline earth lanthanum aluminoborate system that remained viscous ($\eta > 10^3$ Pa-s) under operational conditions [1]. More recently, Singh [2,3] has proposed that SOFC seals be made from stable (non-crystallizing) glass compositions with glass transition temperatures (T_g) well below the SOFC operational temperature. On heating the seal above T_g, the rigid glass becomes viscous and any flaws within the seal (or at a seal interface) will heal because of viscous flow. In addition to providing a means to repair cracks in a seal caused by thermal stresses, the use of a viscous seal could also reduce the magnitude of those stresses compared with a rigid glass seal with the same thermal expansion characteristics since the stresses will be relieved at temperatures above T_g in the viscous glass seal, reducing the effective ΔT over which thermal stresses develop.

The Phase I research successfully identified and tested several glass compositions that could be used as viscous seals for SOFCs. The Phase II activities described in this report build on the Phase I accomplishments by optimizing the glass compositions and address the unresolved technical issues identified in Phase I, including the long-term performance of the seals.

Results

Forty-three new viscous glass compositions (Glass 42 to 84) were formulated and prepared, and their thermal and physical properties (T_g, T_s, T_L, and CTE) were measured. These alkali-free glasses have compositions from the BaO-RO-Al_2O_3-B_2O_3-SiO_2 system where RO represents other alkaline earth oxides or ZnO. The dilatometric softening points and the glass transition temperatures of the new glasses are generally under 650°C, the lower bound of the SOFC operating temperature. The glasses generally do not crystallize in a DSC when heated at a rate of 10°C/min up to 1,000°C. The CTE values (40-500°C) of Glass 73, 75, and 77 are 8.5×10^{-6}/°C, 8.2×10^{-6}/°C, and 9.3×10^{-6}/°C, respectively, and these values are greater than those of the preferred glasses identified in Phase I. The liquidus temperatures of Glass 73, 75, and 77 are 800 ± 10°C, 810 ± 10°C, and 810 ± 10°C, respectively, so these glasses can form viscous seals that do not substantially devitrify under SOFC operational conditions. Glass 73, 75, and 77 were selected for further tests and evaluation. Glass 46 and 52 were chosen earlier in this reporting period, but they were replaced by the newer compositions which exhibit better thermo-chemical compatibility with SS441 and YSZ.

The viscosities of candidate glass melts were measured at intermediate temperatures using a cylinder compression technique with a dynamic-mechanical analyzer and at high temperatures using a rotating spindle technique. Figure 1 summarizes the viscosity data collected for Glass 73, 75, and 77 with their respective fits to the Corning Viscosity Model (CVM) [4]. Table 1 shows the isokom data for the glasses. Glass 73 has the greatest silica content and possesses the greater isokom temperatures. Based on these viscosity results, the self-healing behavior could be expected at temperatures above about 675°C, the temperature of the Littleton softening point (viscosity $10^{6.6}$ Pa-s).

The interfacial reactions of sealing Glasses 73 and 75 with aluminized SS441 and a Ni/YSZ bilayer were studied using SEM for sandwich seals held in air at

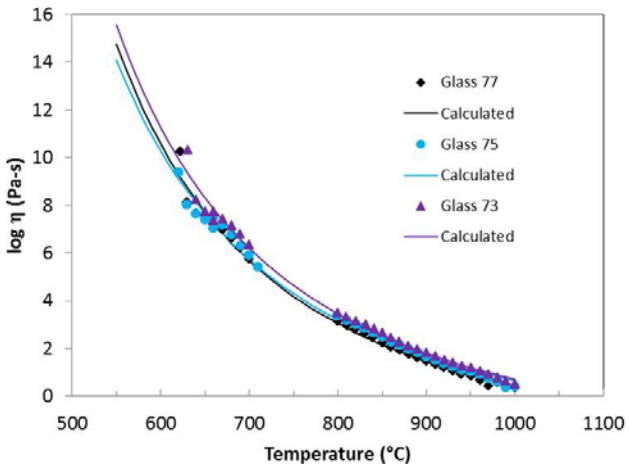

FIGURE 1. Viscosity data for candidate glasses and the corresponding CVM fitted lines

800°C. Figure 2 shows cross-sections of sandwich seals made with Glass 73 after seven days at 800°C in air. The energy dispersive spectroscopy (EDS) line-scans indicate that there are no elements that have diffused from either SS441 (Fe and Cr) or YSZ (Y, Zr). Al-rich and Si-rich needle-shape crystals were observed near the metal interface of the seal with Glass 73. The formation mechanism of these crystals is still not clear. Because of the high aluminum content and their presence only near the metal/glass interface, these crystals may form when aluminum is released from the Al-rich scale on the SS441 surface. Glass 73 and 75 both have good chemical stability in the sandwich seals, but the thermal expansion coefficient (CTE) and T_L of Glass 73 (8.5×10^{-6}/°C; 800°C) are more appropriate for seals than Glass 75 (8.2×10^{-6}/°C; 810°C). So, Glass 73 was selected to be the baseline glass for further tests, described below.

Glass stability against volatilization was determined by weight loss measurements at elevated temperatures. Weight loss measurements were conducted as a function of time (up to 2,000 hours) at 750°C in flowing wet reducing conditions (5% H_2 and 95% N_2 plus water) and stagnant dry air conditions (Figure 3). The total weight loss of Glass 73 after 40,000 hours (the design lifetime) was estimated, by extrapolation, to be 4.5% under flowing wet forming gas and 1.9% under stagnant dry air (Table 2).

Hermetic seal tests were conducted using a newly constructed horizontal test manifold (Figure 4). Coupon sealing was conducted by sandwiching Glass 73 paste between an aluminized SS441 disc (3.2 cm diameter and 1 mm thick) with a central hole (1 cm diameter) and

TABLE 1. Isokom data points according to the CVM for Glasses 73, 75, and 77

Glass	Fitting Parameters		Measured T_g(°C)	Isokom T(°C), log(η) (Pa·s)				
	m	T_g(°C)	(dilatometer)	11	9	6.6	4	2
Glass 73	44.76	590	624	604	637	689	776	885
Glass 75	43.36	575	623	589	622	675	763	875
Glass 77	46.09	581	625	594	625	675	757	861

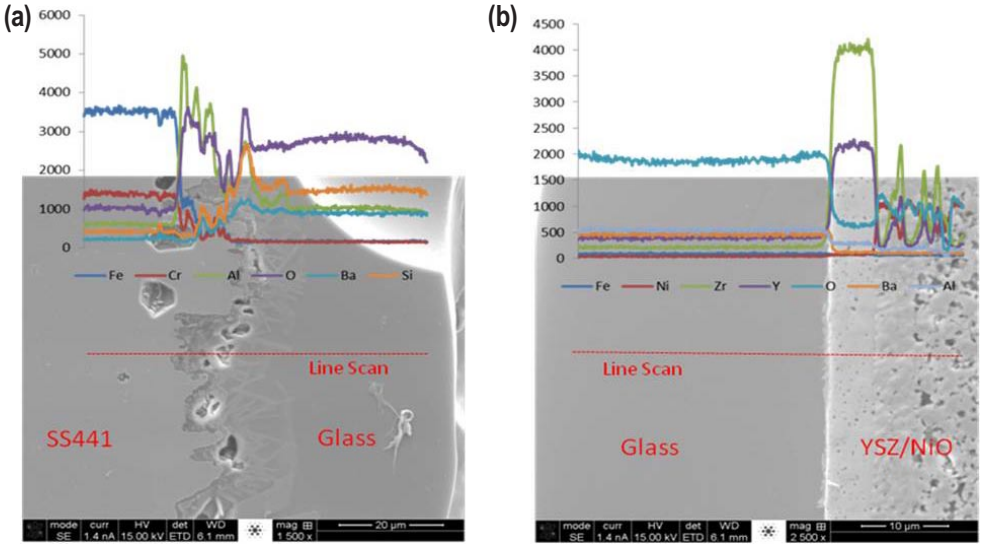

FIGURE 2. Energy dispersive spectroscopy (EDS) line-scans of Glass 73 seal heat treated at 800°C in air for seven days; (a) metal/glass, (b) glass/ceramic

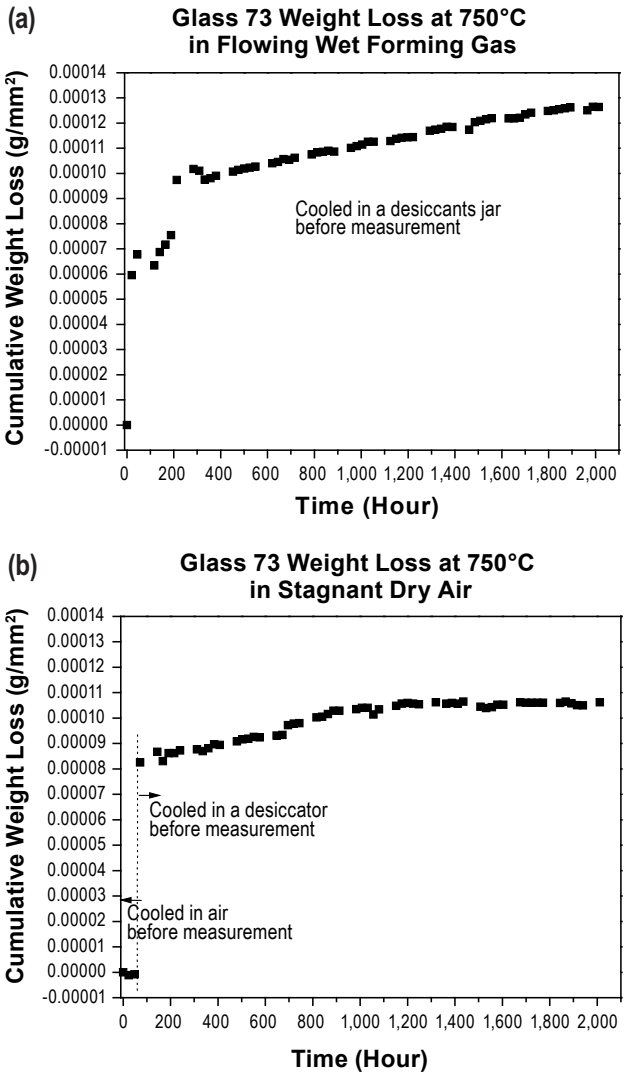

FIGURE 3. Volatility measurements for Glass 73 at 750°C: (a) in flowing wet forming gas, (b) in stagnant dry air

TABLE 2. Measured volatility rate and calculated total weight loss of Glass 73 at 750°C

Test Condition at 750°C	Volatility Rate ($g/mm^2/hr$)	Total Weight Loss (%) at 40,000 hrs
Flowing wet forming gas	2.0×10^{-8}	4.5
Stagnant dry air	1.7×10^{-8}	1.9

an anode-supported (NiO/YSZ) thin electrolyte (YSZ) bilayer square (2 cm side). To date, the Glass 73 seal has survived 80 thermal cycles (room temperature - 750ºC) in dry air at a differential pressure of 0.5 psi (26 Torr) over the course of >2,500 hours without failure (Figure 5). The Glass 73 seal has also survived 48 thermal cycles under wet forming gas. Both tests are still continuing.

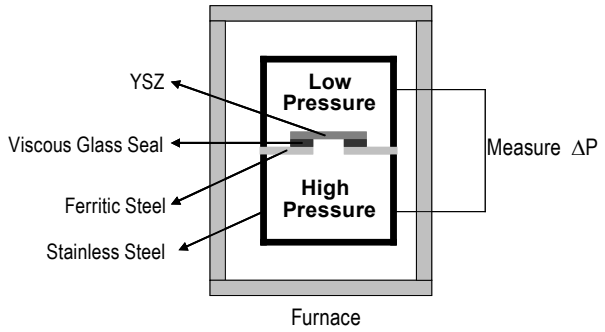

FIGURE 4. Schematic of the new horizontal seal performance test system

Self-healing of glass seals that were intentionally cracked by thermal shock was observed in a SS441/Glass 73/YSZ-bilayer sample. The glass in a seal originally found to be hermetic was cracked upon quenching at ~25°C/s from 800°C. When reheated to 800°C for two hours then slowly cooled to room temperature, the seal was again hermetic, holding 1.5 psi overpressure. This test has been successfully repeated two more times.

Conclusions and Future Directions

New viscous sealing glasses designed for hermetic SOFC seals have been developed and tested. The glasses possess desirable thermo-mechanical and thermo-chemical characteristics and exhibit promising hermetic sealing and self-healing behavior under SOFC operational conditions. Future work will focus on the long-term behavior of candidate glasses, including viscosity stability and interfacial reactions after extended times (≥2,000 hours) under SOFC conditions. Based on these results, optimized glass compositions will be developed for commercialization. Additional tests of the self-healing characteristics for thermally shocked coupon seals are underway. The favored glass seal will be tested at Pacific Northwest National Laboratory using their standard test fixtures to evaluate thermal cycle in dual environments and stack configurations.

FY 2012 Publications/Presentations

1. C.W. Kim and R.K. Brow, et al., "Development of Viscous Sealing Glasses for Solid Oxide Fuel Cells," 36th International Conference and Exposition on Advanced Ceramics and Composites (ICACA12), Daytona Beach, Florida, January 22–27, 2012.

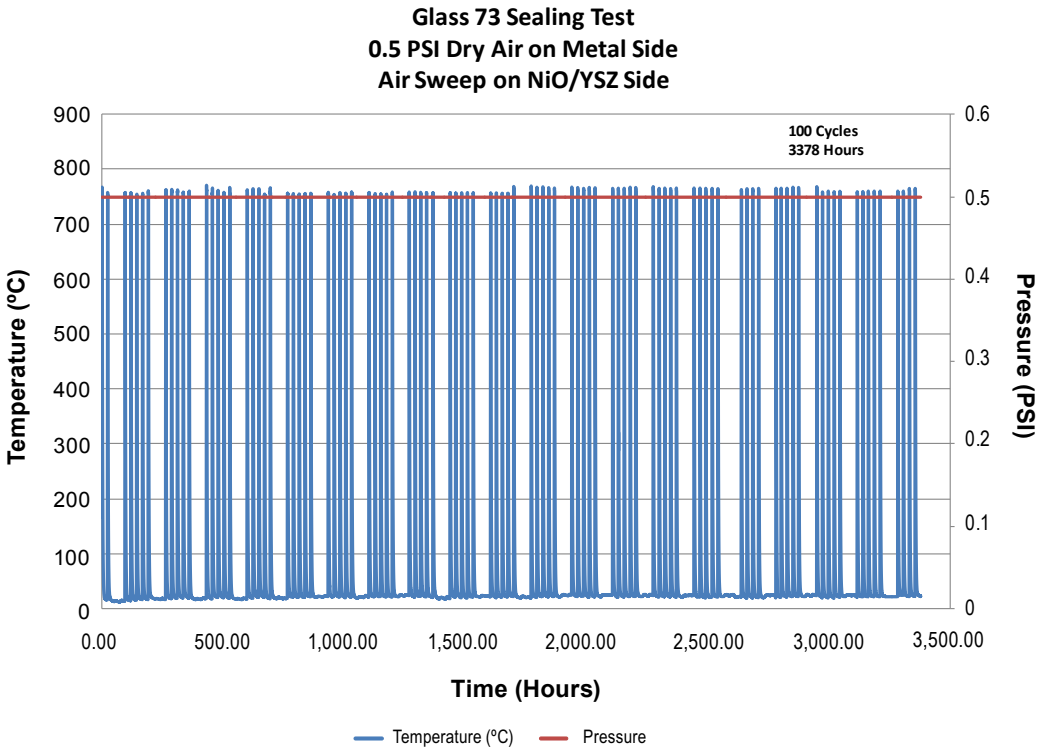

FIGURE 5. Demonstration of a hermetic seal made from SS441/Glass 73/NiO-YSZ bilayer—this seal has survived 80 thermal cycles (room temperature - 750°C) in dry air at a differential pressure of 0.5 psi (26 Torr) over the course of more than 2,500 hours (still ongoing as of June 8, 2012)

References

1. I. Bloom and K.L. Ley (1995), "Compliant Sealants for Solid Oxide Fuel Cells and Other Ceramics," U.S. Patent 5,453,331, issued September 26, 1995; K.L. Ley, M. Krumpelt, R. Kumar, J.H. Meiser, and I. Bloom, "Glass-Ceramic Sealants for Solid Oxide Fuel Cells: Part I. Physical Properties," *J. Mat. Res.,* 11, 1489-1493.

2. R. Singh (2004), "High Temperature Seals for Solid Oxide Fuel Cells," Proceedings of SSM International Conference, Columbus, Ohio, October 18-20, 2011.

3. R. Singh (2008), "Innovative Seals for Solid Oxide Fuel Cells (SOFC)," Final Progress Report, DOE Award DE-FC26-04NT42227.

4. J.C. Mauro, et al. (2009), *PNAS,* 106 (47), 19780-4.

V. SMALL BUSINESS INNOVATION RESEARCH

C. Materials, Testing & Manufacturing

V.C.1 Manufacturing Analysis of SOFC Interconnect Coating Processes

Matthew Seabaugh (Primary Contact), Sergio Ibanez, Kellie Chenault, Lora Thrun, Neil Kidner, and Scott L. Swartz
NexTech Materials Ltd.
404 Enterprise Drive
Lewis Center, OH 43035
Phone: (614) 842-6606; Fax: (614) 842-6607
Email: m.seabaugh@nextechmaterials.com

DOE Project Manager: Briggs White
Phone: (304) 285-5437
Email: Briggs.White@netl.doe.gov

Contract Number: SC0001208

Start Date: May 2010
End Date: May 2012

Fiscal Year (FY) 2012 Objectives

- Quantify the production yields and robustness of the pilot-scale aerosol-spray deposition (ASD) coating process for metallic interconnects (ICs) and identify potential failure modes for the process through a comprehensive process failure modes and effects analysis (PFMEA).
- Translate the baseline, pilot-scale ASD coating process to a high-volume production process and refine the manufacturing system design (MSD) and cost analysis to reflect the high-volume production process.
- Based on the results of the MSD and cost analysis at high-volumes, identify the lowest cost manufacturing route and create a comprehensive manufacturing strategy to reduce volume production manufacturing costs.
- Demonstrate the performance and value proposition of the coating process through stack performance demonstrations of coated interconnect (IC) components and complete post-mortem analysis of the coating.

FY 2012 Accomplishments

- Manufacturing assessment of the pilot-scale ASD coating process determined the process was robust and able to achieve greater than 97% production yield (based on over 500 coated ICs).
- Coating process was translated from a pilot-scale to a high-volume production process. Manufacturing system design and cost analysis were refined to incorporate optimized high-volume production process operations.
- Process options for adding production capacity were defined and evaluated against the cost model to identify the lowest cost manufacturing route at high-volume production. The analysis showed high volume manufacturing process projected to be less than $2/part within Solid State Energy Conversion Alliance (SECA) targets.
- A manufacturing strategy and roadmap to reduce high-volume production manufacturing costs and outlining equipment specification and selection at different volume levels was created.
- Demonstrated lifetime interconnect coating performance of over 10,000 hours with no degradation in electrical performance (area-specific resistance [ASR] testing). Microstructural characterization of the coating post long-term testing quantified the effectiveness of the coating as a barrier to chromium diffusion and evaporation.
- Stack performance validation of ASD based coating was demonstrated for manganese cobalt oxide (MCO) coated vs. uncoated interconnects in 3-5 cell short-stacks and long term (>1,000 hours) stability stack tests. Post-mortem characterization of coated IC components was completed.

Introduction

The adoption of oxidation resistant, high-temperature alloys as alternatives to traditional ceramic interconnect materials for intermediate solid oxide fuel cells (SOFC) provides a path for U.S. Department of Energy SECA teams to meet the aggressive cost targets for SOFC stacks (the interconnect cost has been targeted at approximately 20% of SOFC stack cost). To meet the required lifetime performance targets, protective coatings for the metallic components are necessary. This project was focused on developing a commercially viable, ASD based process for applying protective oxide coatings to metallic interconnects.

Current coating processes cost tens to hundreds of dollars per part, which has impeded the widespread adoption of metallic interconnects and highlights the need for the manufacturing assessment and optimization of the low-cost ASD coating process which was undertaken in this project.

Approach

To align objectives and allow for a complimentary analysis of cost versus performance, this project was structured into two parallel tracks, cost modeling/product planning (Track I) and application-scale performance validation (Track II). Data-exchange between the two tracks facilitated optimization of the coating process and maintained focus on achieving a high performance coating through a high-volume manufacturing scalable and cost-competitive coating process. All three attributes are required for a successful coating product.

During FY 2011, a baseline MSD and cost analysis for the pilot-scale ASD coating process was conducted, and nominal performance metrics for the coating were defined. Using this baseline process as a guide, FY 2012 was focused on translating the process to higher volume production and identifying opportunities for both cost reduction and process scale-up. These opportunities were systematically analyzed and performance validated to develop a manufacturing strategy to reduce volume manufacturing costs.

Results

Translating the baseline, pilot-scale ASD coating process to high-volume manufacturing required, for each of the key process operations (clean, suspension preparation, spray-dry, firing, and inspection), identification of approaches to increase capacity and reduce cycle time. These approaches included larger equipment, faster equipment for reduced cycle time, and transferring the processes from batch-based processes to continuous-based processes. Process options were analyzed with respect to the baseline cost model to down-select the lowest manufacturing route for each operation and develop an optimized high-volume process. The manufacturing system design was refined and the cost model was updated to incorporate the high-volume process changes.

In addition to equipment selection, careful analysis of part handling and automation was performed. The baseline process is labor intensive, with parts manually transferred from batch operation to batch operation. To increase throughput and reduce labor requirements, conveyor based systems (cleaning, spray coating and drying) are utilized to transfer parts through the high production process. A roadmap for increasing the level of automation as the high volume process is ramped up was developed and the cost models updated to allow for various scenarios with different levels of automation.

To enable expeditious validation of the coating performance and stability, high temperature testing protocols were developed to accelerate oxidation kinetics and the corresponding failure mechanisms of the coating. Figure 1 shows the long-term electrical ASR performance of two MCO coated ferritic stainless steel (AL 441-HP) samples. For the first 1,600 hours the test temperature was 800°C, before being increased to 900°C to accelerate thermally driven failure mechanisms. To investigate the integrity of the coating interface, both samples were subjected to multiple thermal cycles, corresponding to the vertical bars in Figure 1. Thermal cycles were performed in sets of 10 from test temperature to room temperature with a ramp rate of 10°C/min and dwell of one hour.

The ASR electrical testing is able to detect several failure mechanisms associated with the MCO coated interconnects directly. For example, oxidation driven growth of the resistive native chromia oxide correlates to the measured ASR. Growth of the native scale also leads to a reduction in interfacial strength and getter susceptibility of the coating to spall. Spallation leads to a reduction in the electrode active area and therefore is also readily detected in the ASR measurement. The two samples demonstrate excellent performance with low and extremely stable ASR values. The behavior indicates that the MCO coating is highly effective at improving the oxidation resistance of the metallic component.

Correlation of the long-term ASR performance under accelerated high-temperature conditions, with oxidation based acceleration factors determined from isothermal oxidation weight-change experiments at different temperatures were used to predict the effective long-term oxidation behavior of the coatings. For example, the 3,800 hours the samples spent at 900°C corresponds to approximately 75,000 equivalent hours at 800°C. Although care must be taken in extrapolating accelerated testing results, as the performance of the coatings

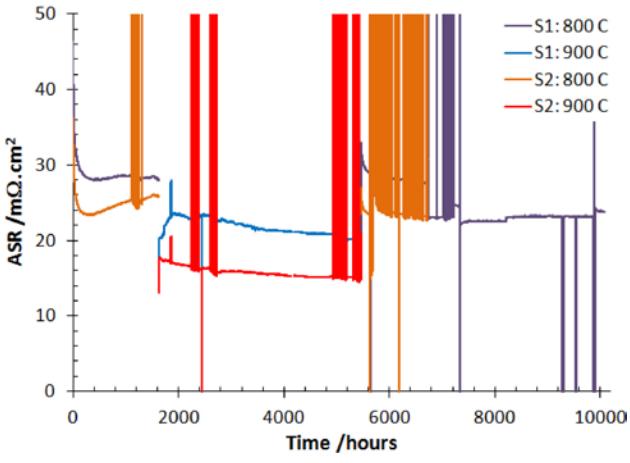

FIGURE 1. Long-term ASR behavior of two MCO coated AL 441-HP substrates. Test conditions were 800°C or 900°C in humidified air with an applied current density of 0.5 A/cm^2.

continues to remain stable for increasingly longer times, confidence in the predicted oxidation-based lifetimes increases.

Chromium evaporation is a significant failure mechanism for chromium-containing stainless steel ICs as it can lead to poisoning of the cathode. After 6,700 hours on test, Sample 2 was removed and the coating microstructure characterized by cross-section scanning electron microscopy (SEM) and energy dispersive spectroscopy (EDS) to enable an assessment of the effectiveness of the coating to act as a chromium diffusion barrier to be made. Figure 2 shows a representative SEM cross-section overlayed with the false color EDS compositional map. The coating microstructure appears relatively unchanged, indicating that the coating is stable at these operating temperatures. Chromium is primarily constrained within the chromia scale at the coating/substrate interface. There is only limited diffusion of chromium within the coating. The separation between the coating and substrate observed was believed to be derived from SEM sample preparation, not as a result of the testing.

Stack validation of the coating process was performed with 160 cm^2 area interconnect components coated with 10 µm thick MCO coatings using nominal processing conditions and integrated into short stacks (3-5 cells). Cell stability data comparing MCO coated and uncoated interconnect components under constant load show that the uncoated cell had a degradation rate (234.8 µV/hr) which was 3.5 to 5.5 times larger than the cells with coated interconnect components. It is believed this increased degradation was due to chromium evaporation from the uncoated components and poisoning of the cell.

The long-term stability of a stack running with MCO coated interconnect components is shown in Figure 3. The average cathode ASR remains stable with no signs of degradation over the 1,000 hours under standard operating conditions. Post-mortem SEM/EDS characterization of the coated interconnect components was performed at the completion of the stack test. The stack was systematically disassembled and samples from various locations on the ICs were cross-sectioned and the coating microstructure examined. Figure 4 shows a representative SEM image of the coating, Limited chromium diffusion into the coating is evident, supporting the conclusion that the MCO coating is acting as an effective chromium barrier under realistic SOFC application conditions.

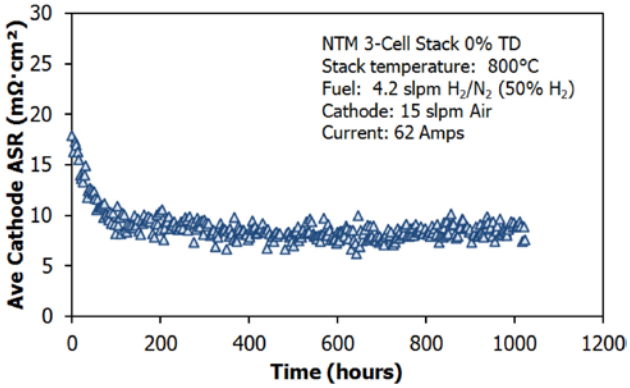

FIGURE 3. Long-term average cathode ASR (incorporating degradation from the MCO coated interconnect) for a three-cell stack operating under constant current (62 Amps) at a temperature of 800°C and 0% turndown. Operating conditions were fuel 4.2 lpm H_2/N_2 (50% H_2) and cathode 15 lpm air.

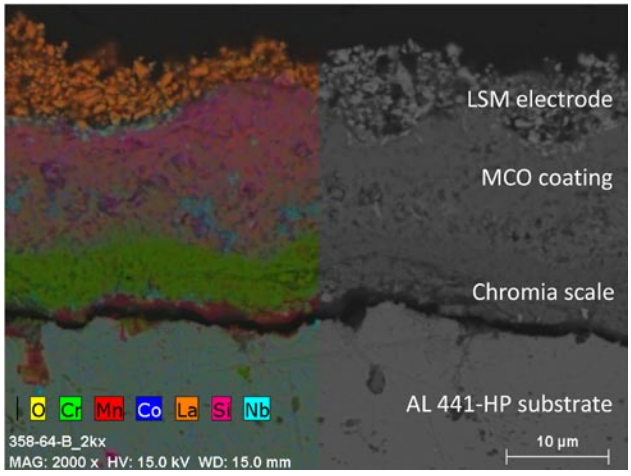

FIGURE 2. Cross-section SEM image and false-color EDS composition map of the MCO coating on AL 441-HP substrate after 7600 hours of testing at 800/900°C in humidified air with an applied current density of 0.5 A/cm^2.

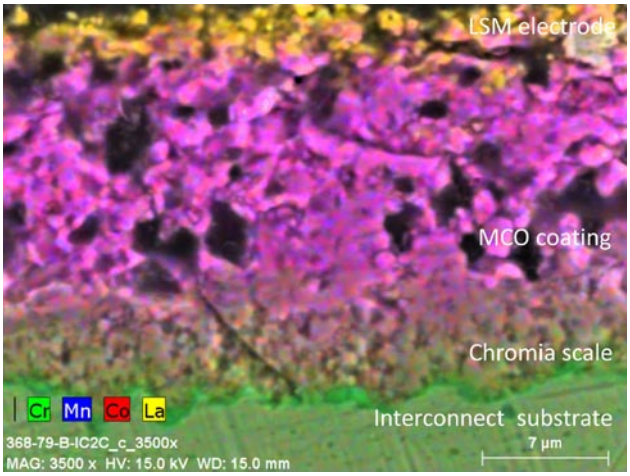

FIGURE 4. Cross-section SEM/EDS composition micrograph of the MCO coating on IC components removed post-test from the stack in Figure 4.

Conclusions and Future Directions

- MSD and cost analysis have been refined and used to identify an optimized ASD coating process for high volume production. Manufacturing strategies have been developed to reduce volume manufacturing costs and outline a roadmap to achieving the less than $2/part cost target for the coating.
- The ASD coating process has been performance validated in both long-term electrical testing and stack testing of coated IC components.
- Coating lifetimes in excess of the 40,000 hour target at 800°C have been predicted through accelerated high-temperature testing protocols developed to expeditiously validate coating performance and stability. Post-test characterization of the coating indicates the coating is effective at reducing chromium diffusion and evaporation from the metallic IC.
- Future work is focused on further increasing the value proposition of the coating product by integrating multiple coatings with different functionalities on the IC and developing a co-processing manufacturing route. For example, with suitable masking, the conductive MCO coating can be applied to the active-region of the IC and a different, less reactive insulating coating can be selectively applied to the non-region areas. The two coatings can then be fired together.

FY 2012 Publications/Presentations

1. N. Kidner, et al., "Oxide Coatings for Metallic SOFC Interconnects," 12th Annual SECA Workshop, Pittsburgh, PA, July 27, 2011.

2. N. Kidner, et al., "High Performance Oxide Protective Coatings for SOFC Components," MS&T, Columbus, OH, October 12, 2011.

3. M. Seabaugh, et al., "High Performance Oxide Protective Coatings for SOFC Components," 10th CMCee, Dresden, Germany, May 20, 2012.

V. SMALL BUSINESS INNOVATION RESEARCH

D. Fuel Processing

V.D.1 Novel Water-Neutral Diesel Fuel Processor and Sulfur Trap

Subir Roychoudhury (Primary Contact), Christian Junaedi, Jeff Weissman and Dennis Walsh
Precision Combustion, Inc. (PCI)
410 Sackett Point Rd.
North Haven, CT 06473
Phone: (203) 287-3700 ext. 267; Fax: (203) 287-3710
Email: sroychoudhury@precision-combustion.com

DOE Project Manager: Joseph Stoffa
Phone: (304) 285-0285
Email: Joseph.Stoffa@netl.doe.gov

Contract Number: ER84674

Start Date: August 15, 2008
End Date: December 14, 2012

Fiscal Year (FY) 2012 Objectives

- Continue development of low pressure drop fuel injector/nozzle to demonstrate stable, durable, and efficient autothermal reformer (ATR) operation capable of fueling fuel cell stacks from diesel fuels.
- Continue developmental efforts to demonstrate the benefits of Rh-pyrochlore catalysts for diesel reforming, gearing towards commercialization and high-volume reforming applications. Compare different catalyst options and evaluate their performance to determine the optimal catalyst for reforming application to meet commercially-viable auxiliary power unit (APU) system targets.
- Demonstrate fuel flexibility of Precision Combustion, Inc.'s (PCI's) fuel processor to advance PCI's reformer development towards specific value-added fuels and operating conditions as well as towards supporting designs for a variety of fuel cell stack opportunities.
- Integrate balance of plant components to develop integrated reformer systems for H_2 production for fuel cell application.
- Demonstrate operation of fuel processor system integrated with a solid oxide fuel cell (SOFC).

FY 2012 Accomplishments

In the fourth budget period of this Phase II project, PCI successfully demonstrated performance of the low pressure drop nozzle for a total of about 300 hours in order to evaluate and demonstrate the long-term durability under water-neutral condition. Additionally, PCI continued the developmental efforts to demonstrate the benefits of Rh-pyrochlore catalyst for diesel reforming. Testing of PCI's fuel reformer unit with different blends of biodiesel (B-20, B-50, B-73, and B-99) was completed to evaluate fuel flexibility of the fuel processor. Finally, a full balance of plant (BOP) system was integrated with a 5 kW_{th} ATR and was utilized to perform steady state reactor operation at 3–5 kW_{th} power levels.

- Continued development of low pressure drop fuel injector/nozzle and demonstrated durability. PCI has successfully developed a novel low-pressure nozzle that operates with an air pressure drop of <1 psi, with cold-start and turndown capability, and has demonstrated an ATR operation with Tier II diesel for about 300 hrs.
- Continued washcoat formulation and coating methodology optimization for an alternative catalyst and performed diesel autothermal reforming. PCI utilized previously scaled-up preparation method for National Energy Technology Laboratory's (NETL's) Rh-pyrochlore catalyst (as reported in 2011 annual report) to evaluate and demonstrate benefits of NETL's Rh-pyrochlore catalyst for practical, cost-effective diesel fuel ATR operation.
- Evaluated and demonstrated reformer fuel flexibility. Testing of PCI's fuel reformer unit with different fuels, including biodiesels (B-20, B-50, B-73, and B-99 blends), synthetic fuels, and distillate fuels has been performed. Stable reformer performance was obtained from all these tests, which demonstrates fuel flexibility of the reformer system.
- Integrated balance of plant (BOP) components. The full BOP system was integrated with a 5 kW_{th} ATR and was utilized to perform steady state reactor operation at 3–5 kW_{th} power levels.

Introduction

The U.S. Department of Energy (DOE) Solid State Energy Conversion Alliance (SECA) goals are to develop fuel cell technology suitable for large coal-fueled central generation applications and to provide similar technology to enable grid-independent distributed power generation. Fuel cells are capable to meet the cost reduction and performance advancement targeted by SECA teams for central generation and is aligned with the near term distributed generation goals of industry. It has become

increasingly apparent that reforming of hydrocarbon fuels to produce hydrogen in situ is a practical approach for operating the fuel cells for distributed power generation applications. Development of a compact, economical, and durable diesel fuel processor capable of operating under a water neutral condition, i.e., very low steam to carbon ratios, while being resistant to coke formation and sulfur poisoning will provide the required impetus for fuel cell commercialization for the industrial teams.

Another important parameter to drive forward the viability of the technology is low operational parasitics of the fuel processor which requires low pressure nozzle/injector development. However, reformer inlet feed preparation at low air-pressure drop could suffer from lack of good mixing and resultant reactor non-uniformities leading to coke formation, among other things.

Toward achieving these goals, PCI is developing its Microlith® fuel processor technology to reform conventional fuels such as diesel, gasoline, distillate fuels, and liquid biofuels to sulfur-free, hydrogen-rich reformate required by fuel cells. By avoiding the need for a hydrogen fueling infrastructure, PCI's technology offers a major advance toward a vital, self-sustaining, American fuel cell industry. Additional attributes of the fuel processor, i.e., ultra-compactness, high sulfur tolerance, and fuel flexibility, are in coherence to the DOE objectives of economical and efficient clean energy. Through DOE Small Business Innovative Research Phase II supplemental effort (awarded in 2010), PCI has demonstrated this technology, along with improved catalyst effectiveness; water neutral operation; fuel flexibility; and substantially improved fuel injection pressure drop without performance loss, reducing parasitic losses of the overall system. The resulting fuel processor enables fuel cell use of wide range of fuels including medium sulfur JP-8, ultra-low sulfur diesel (ULSD)/medium sulfur diesel, and biodiesels. This system and BOP simplification will allow for cost optimization to meet commercially viable targets for the entire APU fuel cell system.

Approach

Practical portable systems mandate fuel processor operation under water neutral or waterless conditions by avoiding the need for external water addition while maintaining stable fuel cell quality reformate. While lower water usage can lead to faster transient behavior during start-up, it is also fraught with the risk of increasingly higher hydrocarbon production, potentially coking the fuel cell stacks. It is important, therefore, to demonstrate long-term reformer operation at water neutral condition using feasible water recovery approaches without catalyst degradation and coke formation.

The concept developed in this project builds upon PCI's Microlith® reforming technology which employs a mesh-based, short-contact-time catalyst as an integrated component of a novel reformer system involving fuel injector, reactor, steam generator, and sulfur trap. PCI's existing 5 kW_{th} system size is approximately 5 L and weighs about 5 kg. This reactor starts up in partial oxidation mode and then transitions to ATR mode upon introduction of steam, operating at low steam-to-carbon (H_2O/C) ratios. The limited water requirement can be satisfied either via a direct anode gas recycling approach or a condenser approach, while performing efficient fuel reformation without performance degradation and coke formation. Moreover, the lower water content of the reformate stream allows sulfur compounds to be readily adsorbed in a downstream desulfurizer bed. High level of sulfur tolerance built into the fuel processor avoids any upstream sulfur removal approaches, further improving the system power density and simplicity. Development of a low pressure drop injector is critical to minimize the parasitic system losses. Appropriate thermal integration of the reformer, fuel cells, water recovery unit, and other BOP components in the APU system are also necessary to maximize the overall system efficiency as well as power density and has been explored using ASPEN process simulation software. Different catalyst options were weighed and compared to determine the optimal catalyst for reforming application to meet commercially viable APU system targets, gearing towards commercialization and high-volume reforming applications.

Results

Key results from the fourth budget period of this Phase II project include (i) the durability testing for up to 300 hrs of low pressure nozzle for fuel processor operation under water neutral condition; (ii) continued development of alternative catalysts and demonstration of its applicability for practical, cost-effective diesel fuel reformer operation; (iii) demonstration of fuel flexibility of PCI's fuel processor; and (iv) integration of BOP components to develop integrated reformer system.

Durability Testing of PCI's Low Pressure Drop Fuel Injector

To minimize the parasitic system losses for on-board fuel reforming, it is prudent to develop a low air pressure drop nozzle. Although a lower pressure drop injector reduces parasitic losses of the overall APU system, a critical challenge is achieving uniform mixing of fuel, air, and steam prior to entering the reactor. Imperfect

mixing could result in pre-reactor ignition, higher catalyst peak temperatures due to local unmixedness and higher propensity for catalyst deactivation due to sintering and coke formation. In this Phase II effort, PCI has successfully developed a novel low-pressure nozzle with cold-start and turndown capability. This result is significant because it reduces parasitic power requirements while providing uniform flow and consistent performance over wide operating range. Throughout this program, the low pressure nozzle has undergone several design iterations and tests to achieve stable reformer operation with an air-side pressure drop of ≤1 psi for the 3–5 kW_{th} ATR system.

To date, this low pressure nozzle has been tested with an ATR comprised of PCI's standard reforming catalyst using Tier II diesel for a total of about 300 hrs in order to evaluate and demonstrate the long-term durability under water neutral condition. Test results showed relatively stable catalyst temperature profile and comparable reformate composition to PCI's high pressure nozzle. During the 300-hr test with Tier II diesel, the reformer was operated at a H_2O/C ratio of 0.90 and an average catalyst temperature of ~880°C while varying the oxygen-to-carbon (O/C) ratio accordingly. Complete fuel conversion to C1 products with ~80% reforming efficiency was achieved throughout the test. The reformate stream consisted of ~44-47 mol% (dry basis) of H_2 + CO with trace amounts of methane. No coke formation or defects were observed in the low pressure drop nozzle after the 30-hr test. The reformer and nozzle were operated for additional 50 hrs with Tier II diesel to confirm the reproducibility of the test results.

Alternative Catalyst Development for Water Neutral Diesel Reformation

Investigating DOE NETL catalysts is a path toward comparing different catalyst options to determine the optimal catalyst for the fuel reformer application and commercialization. DOE NETL's Rh-pyrochlore has potential for same activity/durability level at much less Rh usage, thereby lowering the fuel processor cost. In parallel to demonstrating the potential benefits of the Rh-pyrochlore catalyst, PCI has also been working to optimize its catalyst formulation by reducing the metal loading, to lower material and processing costs.

During FY 2010, the feasibility of integrating NETL catalyst on PCI's Microlith® reactor to perform ATR operation with diesel and logistic fuels was demonstrated. The use of Rh-pyrochlore material as an ATR catalyst is attractive due to its potential to lower costs associated with devices requiring reformers due to a significant reduction in Rh content as compared to more conventional ATR Rh-alumina catalysts. To demonstrate the benefits of Rh-pyrochlore catalysts for diesel reforming gearing towards commercialization and high-volume reforming applications, PCI conducted a detailed investigation of the synthesis, substrate coating, and application method of Rh-pyrochlore catalysts for diesel fuel autothermal reforming, with the goal of using the material in high-volume reforming applications. Both the performance and durability of the pyrochlore-Microlith® ATR have been improved over multiple iterations. A washcoat formulation and coating technique was specifically developed to coat the alternative catalyst on the Microlith® substrate. PCI successfully prepared both the 2 wt% and 5 wt% Rh-pyrochlore materials. The 2 wt% and 5 wt% Rh-pyrochlore catalysts were tested in an ATR reactor operating at H_2O/C ratio of 1.3 with low sulfur JP-5 (resembles Tier II diesel, but with a lower aromatics content) from 3.5 kW_{th} to 5 kW_{th} input (based on fuel energy content). The average O/C ratios for the 2 wt% and 5 wt% Rh-pyrochlore catalysts were 1 and 1.03, respectively, with corresponding average catalyst temperature of 880°C and 860°C, respectively. The 5 wt% Rh-pyrochlore catalyst showed improvement over the 2 wt% batch, yielding ~78.8% reforming efficiency (lower heating value-based) with ~200 ppm_v of hydrocarbons, i.e., potential coke precursor, in the reformate stream. In comparison, the 2 wt% Rh-pyrochlore catalyst achieved only 74% reforming efficiency and ~1460 ppm_v of higher hydrocarbons in the reformate stream.

Rh-pyrochlore/Microlith® catalyst (5 wt% batch) was tested along with PCI's catalyst at a similar Rh content, i.e., same weight hourly space velocity based on Rh metal, for comparison of catalyst activity. Note that the Rh-pyrochlore catalyst operated more optimally at a H_2O/C ratio of 1.3, higher than PCI's typical H_2O/C ratio of 0.9. This resulted in the requirement of a higher O/C ratio for maintaining the catalyst temperature at the desired optimum value. Thus, the reforming efficiency (78.8%) was lower than the expected >80% due to the oxidation of some amounts of the H_2 and CO products to H_2O and CO_2, respectively. At these conditions, ~200 ppm_v (wet basis) of higher hydrocarbons were observed in the reformate stream. For comparison, operating the ATR consisting of PCI's Rh catalyst formulation at a similar Rh content resulted in superior performance. Even at a lower H_2O/C ratio (preferred for a water neutral operation), no higher hydrocarbons were observed. Additionally, the ability to operate the reformer at a lower H_2O/C ratio resulted in a lower O/C ratio and a higher reforming efficiency (83.1%). PCI is currently working with NETL team to further evaluate the Rh-pyrochlore catalyst to increase its performance and to optimize the coating procedure on the Microlith® substrate. We expect to achieve the catalyst performance targets with further catalyst optimization effort to be continued throughout the remaining Phase II effort.

Reformer Fuel Flexibility: Testing with Biodiesels and Tier II Diesel

To demonstrate the fuel flexibility of PCI's ATR, tests were performed using bio-fuels to identify the optimum operating for the reactor and injector to enable optimum production of fuel-cell quality reformate under water neutral condition. Biodiesel 99 (B-99) fuel was acquired from a local residential heating oil company. In order to achieve a different biodiesel mix, e.g., B-50 or B-73, the B-99 was blended with Tier II diesel accordingly. The previous annual report (2011) presents the results from testing PCI's standard ATR catalyst with B-50 for 28 hrs. After the completion of the ATR testing with B-50, the ATR reactor consisting of the same catalyst was tested using B-99 biodiesel for 24 hrs. Relatively stable reformate composition throughout the test, consisting of 30 mol% H_2 and 14 mol% CO (dry basis) with less than 40 ppm_v (dry basis) of total higher hydrocarbons was observed. Near complete fuel conversion and reforming efficiency of ~74% was maintained throughout the test. After completing the testing with B-99 fuel, the ATR consisting of the same catalyst was tested with B-73 fuel for ~12 hrs. Similar to the earlier tests (with B-50 and B-99 fuels), relatively steady temperature profile was observed. The higher hydrocarbon concentration (dry basis) was ~20 ppm_v in the reformate stream. Results from these tests showed potential for PCI's Rh catalyst and ATR for highly efficient, durable biodiesel reforming to syngas with complete fuel conversion, high reforming efficiency, and minimization of coke precursors in the reformate stream.

In addition to testing PCI's standard Rh catalyst formulation, tests were also performed on the low loading version of PCI's Rh catalyst using Tier II diesel (baseline fuel) and B-50 fuel to examine the fuel flexibility and long-term durability. The low loading Rh catalyst was first tested with JP-5 for 28 hrs and results demonstrated stable performance with complete fuel conversion to C1 products and >80% reforming efficiency without any detectable higher hydrocarbons in the reformate stream. Following that test, the same catalyst was operated with Tier II diesel containing ~10% aromatics and <15 ppm_w sulfur for 27 hrs. Reformate composition was stable throughout the test, with a total H_2 and CO of ~46 mol% (dry basis). Near complete fuel conversion to C1 products and ~80% reforming efficiency was observed throughout the test. After completion of the 27-hr test with Tier II diesel, the same catalyst was operated with B-50 biodiesel fuel for ~5 hrs. In the first three hours of testing, the reformate composition was stable; however, it started to degrade, i.e., C2s increased from ~400 ppm_v to ~700 ppm_v, and the test was stopped after five hours of operation. Note that PCI's standard reforming catalyst (with higher metal loading) showed no performance degradation while reforming B-50 fuel. Further catalyst development is ongoing to evaluate the optimum Rh content in PCI's reformer catalyst that has potential to offer a combination of cost savings, fuel flexibility, and long-term performance durability.

Integration of BOP Components

The BOP for PCI's 5 kW_{th} ATR reactor seeks to provide an accurate and reliable supply and control of air, water, and fuel through a system that is both highly efficient (<100 W_e parasitic load) and inexpensive (commercial off the shelf components). The full BOP system was integrated with a 5 kW_{th} ATR and was utilized to perform steady state reactor operation at 3–5 kW_{th} power levels. Gas chromatography samples of the reformate stream were taken periodically throughout the test and showed no significant deviation when compared to the ATR operation with mass flow controllers. Results from the 5 kW_{th}-scale ATR testing were utilized to design and size the BOP components for larger scale systems.

Conclusions and Future Directions

PCI successfully demonstrated efficient, durable, fuel flexible autothermal reformer (ATR) operation under water neutral condition via both, direct anode recycle approach and condensation approach. A novel low-pressure nozzle prototype capable of cold-start and turn-down was also demonstrated. The parasitic losses related to the operation of the fuel processor unit were minimized by utilizing this low pressure nozzle for the introduction of fuel, air, and steam to the catalyst in the reformer unit. The durability of the nozzle was demonstrated for over 300 hrs by integrating it with an ATR fuel processor and operating it with Tier II diesel.

In an effort to lower the precious metal content in the reformer, alternative catalysts were evaluated to develop a highly selective, sulfur tolerant multifunctional reforming catalyst for reformation of logistics fuels at low cost. Results from preliminary catalyst testing demonstrated potential for a reduced-cost, highly efficient reformer system that can accomplish complete fuel conversion and >80% reforming efficiency for reformation of diesel fuel. Tests are ongoing to develop the performance maps and to optimize the operating conditions and durability for both NETL's Rh-pyrochlore catalyst and PCI's Rh catalyst formulation. Finally, testing of PCI's fuel reformer using biodiesels and other fuels was successfully performed to demonstrate fuel flexibility of the reformer.

In summary, PCI demonstrated a novel fuel reformer technology, along with improved catalyst effectiveness,

demonstrated water neutral operation, and substantially improved fuel injection pressure drop without performance loss, reducing parasitic losses of the overall system. The resulting fuel processor enables fuel cell use of widely available conventional fuels including ULSD/ medium sulfur diesels and medium sulfur logistic fuels.

FY 2012 Publications/Presentations

1. 2012 World Renewable Energy Forum in Denver, Colorado.

2. 2012 DOE SECA Meeting in Pittsburgh, Pennsylvania.

3. Submitted abstract for 2012 Fuel Cell Seminar in Uncasville, Connecticut.

V. SMALL BUSINESS INNOVATION RESEARCH

E. Balance of Plant

V.E.1 High Performance Catalytic Heat Exchanger for SOFC Systems

Stephen Jolly
FuelCell Energy, Inc.
3 Great Pasture Road
Danbury, CT 06813
Phone: (203) 830-7519; Fax: (203) 825-6273
Email: sjolly@fce.com

DOE Project Manager: Travis Shultz
Phone: (304) 285-1370
Email: Travis.Shultz@netl.doe.gov

Subcontractor:
Modine Manufacturing Company,
Racine, WI 53403

Contract Number: SC0006282

Start Date: June 17, 2011
End Date: March 16, 2012

Fiscal Year (FY) 2012 Objectives

- Screen candidate materials for oxidation resistance by reviewing previous long-term high temperature gas exposure tests under oxidizing conditions, conducted by FuelCell Energy, Inc. (FCE) and Modine Manufacturing Company.
- Perform high temperature oxidation resistance testing on selected material samples in a flow furnace with high moisture content gas.
- Analyze candidate materials for mechanical strength, creep resistance, stress relaxation, and manufacturability.
- Leverage previous work (BASF) to select appropriate combustion catalyst washcoating and preparation techniques based on application requirements.
- Using selected material(s), design a conceptual catalytic heat exchanger (HX) for a 60 kWe solid oxide fuel cell (SOFC) power plant to meet process requirements for design temperature, pressure drop (dP), effectiveness, and reliability.
- Estimate the budgetary HX cost (±25%) at a high-volume production rate of 1,000 units per year.
- Design and fabricate a lab-scale HX (~0.75-5 kWt) with a combustion catalyst washcoated on the source-side substrate, and conduct performance testing under simulated SOFC conditions.
- Perform a post-mortem analysis of the test unit to validate design features and identify potential design improvements for implementation in a future prototype demonstration.

FY 2012 Accomplishments

- Prior testing results and cost comparison data from FCE and Modine were reviewed, resulting in the selection of two alloys (310S and 347) for further oxidation resistance testing.
- Samples of 310S and 347 were tested in a 14% H_2O environment at 755°C for 2,000 hours. 310S was selected as the primary material of construction (MOC).
- 310S was compared to ferritic stainless steels in terms of mechanical strength. Modine and FCE experience has demonstrated the manufacturability and joinability of 310S. 310S was determined to have sufficient creep resistance to significantly exceed the required HX 40,000 service life.
- BASF's COM-10 catalyst was selected for this application. BASF's proven catalyst deposition method was utilized to successfully deposit the catalyst on a Fecralloy® substrate.
- A 60 kWe catalytic HX concept was designed to meet all process requirements. A 3D computer aided drafting (CAD) model was also developed. Computational fluid dynamics (CFD) simulations were performed to analyze the flow distribution within the HX.
- A lab-scale (3 kWe) catalytic HX was designed, fabricated, and tested to validate the design features developed for the 60 kWe unit. The 3 kWe HX exceeded the thermal performance requirements (when corrected for test facility temperature limitations) and demonstrated low dP. The robustness of the design to self-regulate maximum temperature even at up to twice the design fuel flow rate was demonstrated.
- The estimated high production volume capital cost for a 60 kWe catalytic HX represents an estimated 80% savings compared to the conventional approach of a separate oxidizer and HX.

Introduction

Recuperation of heat at high temperatures (up to 800°C) is a crucial component of an SOFC system. In a typical SOFC system, hot effluent gas from a

catalytic combustor is piped to the source-side of a high temperature recuperator, preheating fresh air for the cathode. To create a competitive market-entry SOFC product (60 kWe nominal rating), balance of plant (BOP) costs must be reduced. The catalytic combustor and the cathode air preheater represent 25-40% of the BOP cost, and therefore represent the largest opportunity for cost reductions.

FCE, in partnership with Modine and BASF Catalysts, have teamed up to develop a novel catalytic HX which combines the functionality of the separate catalytic combustor and cathode air preheater into a single multi-functional unit. Applying this innovative technology to SOFC power systems has the potential to significantly reduce BOP costs while also increasing plant performance.

Approach

The overall objective of this project is the development of a highly effective catalytic cathode air preheater for a 60 kWe SOFC power plant to increase plant performance and to reduce the BOP cost. The project approach was designed to address technical challenges related to material strength and stability, catalyst selection, manufacturability, combustion temperature control, and cost reduction. Candidate MOC were screened based on mechanical strength, creep resistance, stress relaxation, manufacturability, and cost. High temperature oxidation resistance testing was then performed on selected material samples in a flow furnace with high moisture content gas. Using the selected material(s), the engineering design of a conceptual catalytic HX for a 60 kWe SOFC power plant to meet process requirements for design temperature, dP, effectiveness, and reliability was developed. A 3D CAD model of the 60 kWe design was created. This design was utilized to estimate the budgetary HX cost (±25%) at a high-volume production rate of 1,000 units per year.

To validate the design principle and features of the 60 kWe catalytic HX, a lab-scale unit (3 kWe) was designed, fabricated, and tested under simulated SOFC operating conditions. After the testing was complete, a post-test teardown analysis of the test unit was performed to validate design features and identify potential design improvements for implementation in a future prototype demonstration.

Results

Material of Construction Selection

The objective of this task was the down-selection of a suitable MOC for the catalytic HX. FCE and Modine both have extensive experience in materials testing for high temperature applications. Therefore, the first step was to perform a review of existing FCE/Modine testing results and select two candidate materials for further evaluation. The two materials selected from the screening process were then subjected to high temperature oxidation resistance testing. The testing results were then used to down-select the preferred MOC for the catalytic HX.

Key criteria for the catalytic HX MOC selection included:

- Oxidation resistance
- Suitability for catalyst washcoating
- Joining via conventional methods
- Acceptable strength
- Availability
- Cost

Due to HX design features, the maximum HX design temperature is limited to 800°C. Therefore, primary focus was on austenitic stainless steels, not high-nickel content super alloys. Previous testing by FCE and Modine showed that 310S stainless steel displays excellent oxidation resistance at temperatures up to 700°C, in both steady and cyclic operation. FCE's testing showed that 347 displayed good oxidation resistance in a high temperature moist environment, whereas results from Modine show rapid weight loss (spallation) for 347 under similar conditions. To clarify this discrepancy between the FCE and Modine results, 310S and 347 were chosen as candidates for additional testing. The testing was performed at 755°C in a flow furnace with a gas composition of 14% H_2O, 5% O_2, 5% CO_2, with the balance N_2.

After 2,000 hours of testing, the weight gain of 347 was 642% greater than for 310S. Minimal oxide layer spallation was observed for both alloys. 310S was down-selected as the primary MOC due to its excellent oxidation and spallation resistance, acceptable strength at high temperatures, widespread availability, and cost that is significantly lower than that of high-Ni super alloys.

Fecralloy® (specifically ThyssenKrupp Aluchrome YHf) was selected as the substrate material for the exhaust fins, which are coated with catalyst. This material is a proven substrate for catalyst coating and readily forms the necessary alumina blooms for catalyst adhesion.

60 kWe Catalytic HX Conceptual Design

The objective of this task was to develop the conceptual design of a catalytic HX for integration with FCE's 60 kWe SOFC power plant. Key specifications include the maximum design temperature of 800°C, achieving the required cathode inlet temperature of ~700°C, and low total HX dP (cold side + hot side).

Drawing from past work on HXs with reacting surfaces, the overall design principle was to ensure that the non-reacting heat transfer surface (cold-side) had the capacity to accept heat at the same rate it is produced from the combustion reaction on the hot side.

A sensitivity study was performed to determine the effect of HX dP allowance on capital costs, system efficiency, and cost of electricity. Detailed process simulations of an SOFC power plant were performed. Correlations between HX capital cost and dP allowance were also developed. The outputs from the system simulations (efficiency, fuel consumption, net power output, etc.) and the HX capital cost correlation was then fed into FCE's models for plant capital cost and cost of electricity. Power plant efficiency decreases from 61.3% (lower heating value natural gas) at a dP specification of 10" H_2O to 59.5% at a dP specification of 68" H_2O. The levelized cost of electricity produced by the plant is estimated to be 2.35% higher if the allowable dP is increased from 10" to 68" H_2O. The contribution of increased fuel costs at lower efficiency operation superseded the effects of slightly lower plant capital cost. For this reason, the decision was made to keep the dP specification low despite the impacts on HX size and capital cost.

The 60 kWe catalytic HX concept is based on a cross-counterflow arrangement in which the cold-side flow (air) passes through oval tubes in a single pass. The hot side of the HX, which is coated in catalyst to promote the combustion of anode exhaust gases, is arranged in four passes. CFD flow analysis of the design was performed to identify areas for improvement in terms of flow distribution. Figure 1 shows the air-side and exhaust-side flow distribution results. Although the center portion of the HX receives a marginally greater portion of the air flow, the exhaust gases also preferentially flow towards the center cores, creating a balance in terms of thermal performance.

The catalytic HX was designed for integration with the "hot box" module that also houses the SOFC stacks. This design feature reduces the length of hot piping runs, utilizes the existing module insulation, and significantly reduces process heat losses. It also allows for a more compact BOP. Figure 2 shows a CAD rendering of the 60 kWe SOFC module with integrated catalytic HX.

Lab-Scale (3 kWe) Catalytic HX Design, Fabrication and Testing

The primary objective of this task was to design and fabricate a lab-scale (~3 kWe) catalytic HX for performance testing to validate the design principle and concepts developed for the 60 kWe HX. The key technical success criteria was to create a HX design style that would transfer heat into the non-reacting fluid as rapidly as it was created by the catalytic reaction in order to avoid "hot-spots" within the HX.

The HX core was fabricated by Modine, sent to BASF for washcoating with COM-10 combustion catalyst, and then sent to FCE for performance testing. Figure 3 shows a photograph of the completed lab-scale HX, with locations of thermocouples noted.

Testing results showed that the hot-in to cold-out approach temperature was only 19.4°C with fuel flow

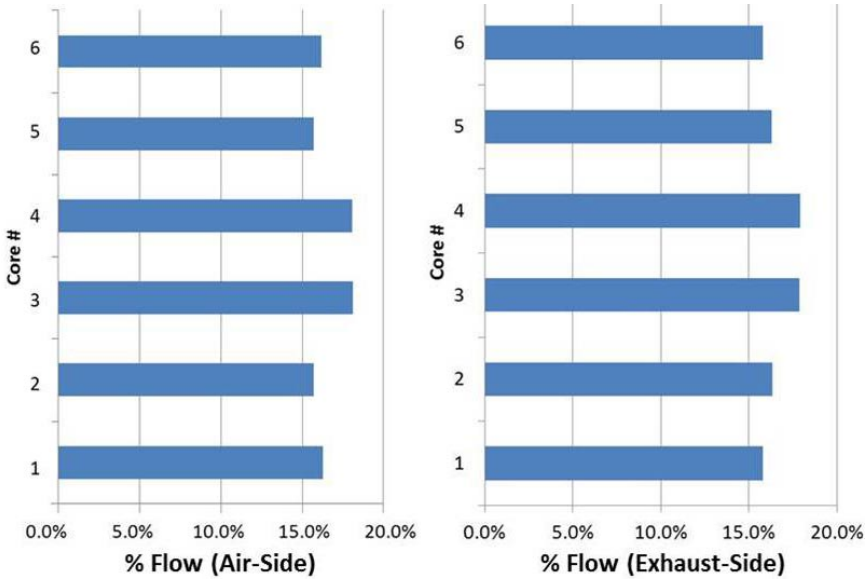

FIGURE 1. CFD results of flow distribution across the HX core sections—air-side (left) and exhaust-side (right)

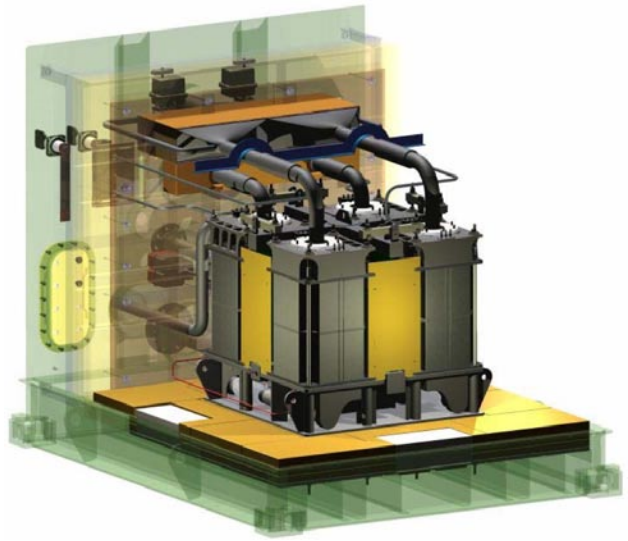

FIGURE 2. CAD rendering of catalytic heat exchanger integrated with 60 kWe SOFC module—heat exchanger located above SOFC stacks

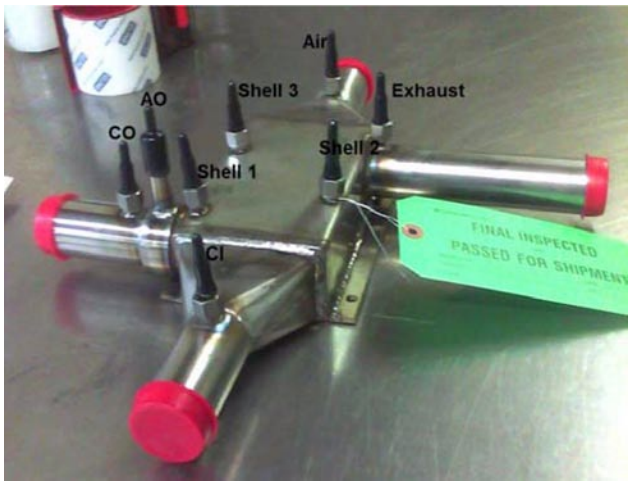

FIGURE 3. Photograph of lab-scale (3 kWe) catalytic heat exchanger prior to testing, thermocouple locations noted

(catalytic mode), significantly better than the 94°C approach observed without fuel flow (non-catalytic mode). The heat duty at normal operating conditions as tested was 2.85 kW. While this is lower than the 3 kWe design target, the heat duty was limited by the test facility temperature for the cathode outlet stream. When corrected for the test facility limitations, the heat duty is actually expected to exceed the design target. The measured total dP through both the hot and cold sides was 7.8" H_2O, significantly below the 10" H_2O target for the lab-scale unit. Furthermore, there was no pre-ignition of the anode exhaust gas upstream of the catalyst surface. Preventing pre-ignition is crucial for limiting the maximum

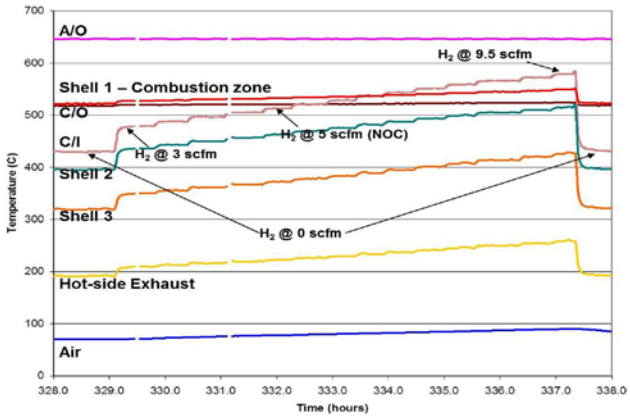

FIGURE 4. Catalytic HX testing results; effect of hot-side fuel flow on thermal performance

temperature based on the design principle of matching cold-side heat removal to hot-side heat generation. Figure 4 shows the HX thermal performance as the H_2 flow to the hot-side was ramped from 3 scfm to 9.5 scfm, nearly double the design flow rate. No temperature run-away was observed, indicating the robustness of the design to self-regulate maximum temperature.

Post-test teardown of the test article showed minimal debris, good catalyst adhesion with minimal sintering, and no signs of fuel pre-ignition prior to the catalyst-coated section. Two small leaks were discovered in the casing seem welds, likely due to poor weld penetration. Improved process control and weld validation is expected to resolve this issue on subsequent builds.

Conclusions and Future Directions

The conceptual design of a 60 kWe catalytic HX was developed. The design is expected to meet all process requirements in terms of thermal performance and dP, and is sufficiently compact that it can be integrated directly into the hot box module which houses the SOFC stacks. This will result in a significantly smaller BOP and also increased plant performance due to less heat loss and dP associated with longer piping runs. The estimated high production volume capital cost for a 60 kWe catalytic HX represents an estimated 80% savings compared to the conventional approach of a separate oxidizer and HX. A lab-scale (3 kWe) catalytic HX was designed, fabricated, and tested to validate the design features developed for the 60 kWe unit. The 3 kWe HX exceeded the thermal performance requirements (when corrected for test facility temperature limitations) and demonstrated significantly lower dP than required. The robustness of the design to self-regulate maximum temperature at up to twice the design fuel flow rate was demonstrated.

Prior to implementation of the 60 kWe catalytic HX design in an SOFC power plant, additional future development work is required. A comprehensive CFD analysis of the reactant diffusers and plenums must be performed to ensure adequate mixing of the anode and cathode exhaust gases upstream of the HX. Also, a finite element analysis is required to assess the durability of the design when subjected to cyclical thermal stresses. The detailed design must also include analysis of the nozzle loads and bellows requirements for interconnecting piping within the SOFC module. Overall, the feasibility of a catalytic HX for SOFC systems was demonstrated. FCE intends to utilize the developed design on future 60 kWe SOFC system demonstrations. The next steps are to finalize the 60 kWe catalytic HX detailed design for fabrication and validation testing.

FY 2012 Publications/Presentations

1. S. Jolly, H. Ghezel-Ayagh, J. Valensa, "High Performance Catalytic Heat Exchanger for SOFC Systems," Poster presented at 12th Annual SECA Workshop, Pittsburgh, Pennsylvania, July 26–28, 2011.

VI. Acronyms and Abbreviations

-	Minus
#	Number
%	Percent
@	At
~	Approximately
+	Plus
<	Less than
>	Greater than
±	Plus or minus
≈	Equals approximately
≤	Less than or equal to
≥	Greater than or equal to
°	Degree
°C	Degrees Celsius
1D	One dimensional
2D	Two dimensional
2PB	Two phase boundary
3D	Three dimensional
3PB	Triple phase boundary
8YSZ	8-mol% yttria-stabilized zirconia
A	Ampere(s), amp(s)
Abs	Absorbance
AC	Alternating current
ACC	Anode current collector
ACS	American Chemical Society
ADG	Anaerobic digester gas
ADIS	Analysis of difference in impedance spectra
ADS	Adsorptive desulfurization
Adv.	Advanced
afm	Atomic force microscopy
AIChE	American Institute of Chemical Engineers
AISI	American Iron and Steel Institute
AISI 441	A ferritic stainless steel
Al	Aluminum
AL	Alabama
Al_2O_3	Alumina, aluminum oxide, sapphire
Al-SS	aluminized stainless steel
ANL	Argonne National Laboratory
ANSYS	A computer modeling code
Appl.	Applied
APS	Air processing system
APS	Advanced Photon Source (at ANL)
APU	Auxiliary power unit
ARRA	American Recovery and Reinvestment Act
ASD	Aerosol spray deposition
ASME	American Society of Mechanical Engineers
ASR	Area specific resistance
ASTM	American Society for Testing and Materials
ASU	Air separation unit
At%	Atomic %
ATI	Allegheny Technologies, Inc.
atm	Atmosphere(s)
ATR	Autothermal reformer
Au	Gold
Ba	Barium
BaO	Barium oxide
Bara, bara	Bar absolute
Bi	Bismuth
Bldg.	Building
Blvd.	Boulevard
BOP	Balance of plant
Br	Bromine
C	Carbon
C_2H_4	Ethylene
Ca	Calcium
CA	California
CAD	Computer aided design
CBS	Coal based system
cc	Cubic centimeter(s)
CCM	Cathode contact material
CCS	Carbon capture and sequestration
CD-adapco	A provider of CFD-focused engineering simulation software
Ce	Cerium
Ce-MC	Cerium modified spinel (Mn,Co)3O4
CeO_2	Ceric oxide
Ceram.	Ceramics
CFD	Computation fluid dynamics
CH_4	Methane
Chem.	Chemistry
CHP	Combined heat and power

CIL	Cathode interlayer
Cl	Chlorine
cm	Centimeter(s)
cm^2	Square centimeter(s)
CMU	Carnegie Mellon University
Co	Cobalt
CO	Carbon monoxide
CO	Colorado
CO_2	Carbon dioxide
COE	Cost of electricity
COS	Carbonyl sulfide
CPOx, CPOX	Catalytic partial oxidation
Cr	Chromium
CT	Connecticut
CTE	Coefficient of thermal expansion
CTP	Core Technology Program
Cu	Copper
CuO	Copper oxide
D.C.	District of Columbia
DBT	Dibenzothiophene
DC	Direct current
DEC	distributed electrochemistry
DMFC	Direct methanol fuel cell
DOE	U.S. Department of Energy
DOE FE	U.S. Department of Energy Office of Fossil Energy
DOI	U.S. Department of Interior
dP	Pressure drop
e.g.	Exempli gratia, for example
ECL	Electrochemical looping
ECR	Electrical conductivity relaxation
ECS	The Electrochemical Society
ed.	Edition
EDAX	Energy dispersive X-ray analysis
EDS	Energy dispersive spectroscopy
Eds.	Editors
Eh0	Activation energy baseline values for healing behavior
EIS	Electrochemical impedance spectroscopy
EISA	Evaporation induced self assembly
Electrochem.	Electrochemical
E-MRS	European Materials Research Society
EMS	Exhaust management system
EPSCOR	Experimental Program to Stimulate Competitive Research
et al.	et alii, and others
etc.	et cetera, and so on
eV	electron volt(s)
EXAFS	Extended X-ray absorption fine structure
F	Fluorine
FA	Functional analysis
FC	Fuel cell
FCE	FuelCell Energy, Inc.
FE	Finite element
Fe	Iron
FEA	Finite element analysis
FIB	Focused ion beam
FIB-SEM	Focused ion beam-scanning electron microscopy
FMEA	Failure mode and effects analysis
FPS	Fuel processing system
FT	Fourier-transformed
FTT	Florida Turbine Technologies
FY	Fiscal year
g	Gram(s)
g(t)	Normalized conductivity
g/min	Gram(s) per minute
Ga	Gallium
GA	Georgia
GC	Gas chromatography
GC-FID	Gas chromatography flame ionization detector
GDC	Gadolinia doped ceria
GE	General Electric
Gen	Generation
Gen2	Second generation
Georgia Tech	Georgia Institute of Technology
GFED	Gross fuel energy density
GLAM	Geballe Laboratory for Advanced Materials
GPa	Gigapascal(s)
GPM	Gallon per minute
GT	Gas turbine
GUI	Graphical user interface
H	Hydrogen
h, hr	Hour(s)
H_2	Diatomic hydrogen
H_2O	Water
H_2S	Hydrogen sulfide
HA	Hazard analysis

HAZOP	Hazard and pperability
HBE	Higher binding energy
Hg	Mercury
HHV	Higher heating value
HR	High resolution
HRTEM	High resolution transmission electron microscopy
HX	Heat exchanger
I	Iodine
i.e.	Id est, that is
IC	Interconnect
ICACC	International Conference and Exhibition on Advanced Ceramics and Composites
IFDL	Integrated flowfield diffusion layer
IGCC	Integrated gasification combined cycle
IGFC	Integrated gasification fuel cell
IL	Illinois
in	Inch(es)
Inc.	Incorporated
Int.	International
IP-SOFC	Integrated planar solid oxide fuel cell
IR	Infared
IWI	Incipient wet impregnation method
J.	Journal
K	Kelvin
K	Potassium
k_{chem}	Chemical surface exchange coefficient
kg	Kilogram(s)
kMC	Kinetic Monte Carlo
kW	Kilowatt
kWe	Kilowatt electric equivalent basis
kWth, kW_{th}	Kilowatt(s) thermal
L	Liter(s)
La	Lanthanum
lb	Pound
LBNL	Lawrence Berkeley National Laboratory
LCC	Cathode material with chemical formula La0.4875Ca0.0125Ce0.5O2-δ
LCM	Calcium doped lanthanum manganite
LDC	Lanthanum doped ceria
Lett.	Letter
LFO	Lanthanum ferrite oxides
LGFCS	LG Fuel Cell Systems, Inc.
LHV	Lower heating value
LLC	Limited liability company
LNG	Liquefied natural gas
lpm	Liter(s) per minute
LSC	Lanthanum strontium cobalt oxide $(LaSr)CoO_3$
LSCF	Lanthanum strontium cobalt ferrite, $(LaSr)(CoFe)O_3$
LSCo	Lanthanum strontium cobalt oxide
LSCuF	Lanthanum strontium copper ferrite, lanthanum strontium copper iron oxide
LSF	Lanthanum strontium ferrite
LSGM	Lanthanum strontium gallate magnesite
LSM	Lanthanum strontium manganite
LSM'V	Manganese-doped lanthanum strontium vanadate
LSMV	Magnesium-doped lanthanum strontium vanadate
LSV	Lanthanum strontium vandate
m	Meter(s)
M&EB	Mass and energy balance
MA	Massachusetts
mA	Milliampere(s)
Mat., Mater.	Material
MBS	Molecular basket sorbent
MC	Manganese cobalt oxide, (Mn,Co)3O4
MCM-41	Mobil composition of matter No. 41
MCM-48	Mobil composition of matter No. 48
MCO	Manganese cobalt oxide
MEA	Membrane electrode assembly
Meet.	Meeting
mg	Milligram(s)
Mg	Magnesium
MgO	Magnesium oxide
MI	Michigan
MIT	Massachusetts Institute of Technology
mL	Milliliter(s)
mm	Millimeter(s)
Mn	Manganese
MN	Methylnapthalene
MnCo	Manganese cobalt
Mn-Co-Cu	Manganese cobalt copper
MnO_3	Manganate
Mo	Molybdenum
MOC	Materials of construction
mol	Mole(s)
mol%	Mole percent
MP	Mesoporous particles

MP	Multi-physics
MPa	MegaPascal
MPC	Multi-physics computer code
MR	Mill reference
MS	Mass spectrometry
MS	Mail stop
MS&T	Materials Science and Technology
MSD	Manufacturing system design
MSRI	Materials Systems and Research, Inc.
MT	Montana
mTorr	Millitorr(s)
MTTF	mean-time to failure
mV	Millivolt(s)
MW	Megawatt(s)
mW	Milliwatt(s)
MWe	Megawatt(s) electric
MWh	Megawatt hour
mΩ	Milli-ohm(s)
N	Nitrogen
N_2	Diatomic nitrogen
NASA	National Aeronautics and Space Administration
Nb	Niobium
NETL	National Energy Technology Laboratory
NG	Natural gas
NGCC	Natural gas combined cycle
NGFC	Natural gas fuel cell
NGO	Neodymium gadolinium oxide, NdGaO3
Ni	Nickel
NIFT	National Institute of Fuel Cell Technology
NiO	Nickel oxide
NOC	Normal operating conditions
NOx	Oxides of nitrogen
NP	Nanoparticles
NRCCE	National Research Center for Coal and Energy at WVU
NUWC	Naval Undersea Warfare Center
NV	Nevada
NW	Northwest
NY	New York
NYS	New York State
O	Oxygen
O_2	Diatomic oxygen
OCV	Open circuit voltage
OEM	Original equipment manufacturer
OH	Ohio
OPPA	Office of Program Planning and Analysis at NETL
ORNL	Oak Ridge National Laboratory
ORR	Oxygen reduction reaction
OSR	Oxidative steam reforming
OT	Operating temperature
P	Pressure
P	Phosphorus
PA	Pennsylvania
Pa	Pascal(s)
PBN	Pyrolytic boron nitride
PCC	Pulverized coal combustion
PCI	Precision Combustion, Inc.
PCM	Proof-of-concept module
PEM	Proton exchange membrane
PFMEA	Process failure modes and effects analysis
PH_3	Phosphine
Phys.	Physics
PLD	Pulsed laser deposition
PNNL	Pacific Northwest National Laboratory
pO_2	Partial pressure of oxygen
pp.	Pages
ppm	Part(s) per million
Proc.	Proceedings
PSCM	Cathode material with chemical formula PrSrCoMnO5+δ
psi	Pound(s) per square inch
PSM	Praseodymium strontium manganite
PSU	Pennsylvania State University
Pt	Platinum
PTFE	Polytetrafluoroethylene
PVL	Process verification line
RC	Resistance circuit
RE	Rare earth
Redox	Reduction-oxidation
Rh	Rhodium
rms	Root-mean-square
ROM	Reduced order model
R_p	Polarization resistance
S	Sulfur
Sb	Antimony
SBA-15	Santa Barbara amorphous type material
SBIR	Small Business Innovation Research
sccm	Standard cubic centimeter(s) per minute

SDC	Samaria doped ceria
SECA	Solid-state Energy Conversion Alliance
SEM	Scanning electron microscopy
SERS	Surface enhanced Raman spectroscopy
SI	Similarity index
SMR	Steam-methane reformation
SOFC	Solid oxide fuel cell
SOFC-MP	Solid oxide fuel cell multi-physics modeling software
SPU	Stationary power unit
Sr	Strontium
SS	Stainless steel
SSC	Strontium samarium cobalt oxide
ST	Steam turbine
STM	Scanning tunneling microscopy
STO	Strontium titanate, SrTiO3
STS	Scanning tunneling spectroscopy
STTR	Small Business Technology Transfer
Surf.	Surface
Symp.	Symposium
T	Temperature
Ta	Tantalum
TBC	Thermal barrier coating
TEC	Thermal expansion coefficient
Tech.	Technology
TEM	Transmission electron microscopy
TEM	Tunneling electron microscope
T_g	Glass transition temperatures
Ti	Titanium
TMI	Technology Management, Inc.
TN	Tennessee
TPB	Triple-phase boundary
TPBL	Triple-phase boundary layer
TRL	Technology readiness level
TSC	Tape-casting, screen-printing, and co-firing
TXRF	Total reflection X-ray fluorescence
U	Uranium
U.S.	United States
UHV	Ultra high vacuum
UK	United Kingdom
ULSD	Ultra-low sulfur diesel
UNLV	University of Nevada, Las Vegas
USAXS	Ultra small angle x
UT	Utah
UTC	United Technologies Corporation
UTRC	United Technologies Research Center
UTSR	University Turbine Systems Research
Uuv	Unmanned undersea vehicles
V	Vanadium
V	Volt(s)
VA	Virginia
VI, V-I	Voltage current
VPIT	Vacuum-pressure-infiltration-thermal
VPS	Versa Power Systems, Inc.
W	Tungsten
W	Watt(s)
WA	Washington
wt	Weight
wt%	Weight percent
WV	West Virginia
WVU	West Virginia University
x	Times
XANES	X-ray absorption near edge structure
XAS	X-ray adsorption spectroscopy
XES	X-ray emission spectroscopy
XPS	X-ray photoelectron spectroscopy
XRD	X-Ray diffraction & X-ray diffractometer
XRR	X-ray reflectivity
Y	Yttrium
YCCC	$Y_{0.8}Ca_{0.2}Cr_{0.8}Co_{0.2}O_3$
Y-P-O	Yttrium-phosphorus-oxygen
YSZ	Yttria stabilized zirconia
Zr	Zirconium
Δ	Change, delta
η	Viscosity
μg	Microgram(s)
μm	Micrometer(s), micron(s)
σ	Conductivity
Ω	Ohms

VII. Primary Contact Index

VIII. Organization Index

IX. Contract Number Index

X. Index of Previous Projects

Projects Discontinued Since the FY 2011 Annual Report

Contract Number	Performer	Project Topic
ER85006	CellTech Power LLC	Liquid Tin Anode Direct Coal Fuel Cell
ER85020	R&D Dynamics Corporation	Foil Gas Bearing Supported High Temperature Cathode Recycle Blower (Large Size Cathode/Anode Recycle Blower)
ER85202	Materials & Systems Research, Inc.	Glass Composite to Coated Interconnect Seals for Long-Term Chemical Stability
FE0001390	University of Cincinnati	Innovative Self-Healing Seals for Solid Oxide Fuel Cells (SOFCs)
NT0004111	CellTech Power LLC	Liquid Tin Anode Direct Coal Fuel Cell
NT0004113	NexTech Materials, Ltd.	Validation of Novel Planar Cell Design for MW-Scale SOFC Power Systems
NT41246	Delphi Automotive Systems LLC	Solid State Energy Conversion Alliance Delphi SOFC
NT42513	Allegheny Technologies, Inc.	Evaluation of a Functional Interconnect System for SOFCs
PPM 300.02.08	Walt Harrison/Stanford University	Electronic Structure of Cathode Materials
SC0004380	TDA Research	Post-SOFC Residual Fuel Oxidizer for CO_2 Capture
SC0004582	CellTech Power LLC	Liquid Tin Anode Direct Coal Fuel Cell
SC0004845	NexTech Materials	Manufacturing System Design Analysis of SOFC Stacks

Projects Discontinued Since the FY 2010 Annual Report

Contract Number	Performer	Project Topic
ER84394	Eltron Research and Development Inc.	Reformer for Conversion of Diesel Fuel into CO and Hydrogen
ER84590	Acumentrics Corporation	Hybrid Ceramic/Metallic Recuperator for SOFC Generator
ER84595	Ceramatec, Inc.	Proton Conducting Solid Oxide Fuel Cell
ER84616	R&D Dynamics Corporation	Foil-Bearing Supported High-Speed Centrifugal Cathode Air Blower
NT0006343	Treadstone Technologies, Inc.	Investigation of Modified Ni-YSZ-Based Anode for High Impurities Containing Syngas Fuels
NT43042	National Institute of Standards and Technologies	Advanced Power Conditioning System (PCS) Technologies for High-Megawatt Fuel Cell Power Plants
SC0000871	Eltron Research and Development Inc.	Perovskite Adsorbents for Warm-Gas Arsenic and Phosphorus Removal
SC0000872	Eltron Research and Development Inc.	First Principles Identification of New Cathode Electrocatalysts for Fuel Cells
SC0001492	TDA Research, Inc.	Sorbents for Warm Temperature Removal of Arsenic and Phosphorous from Coal-Derived Synthesis Gas
SC0001659	Materials & Systems Research, Inc.	Novel SOFC Anodes with Enhanced Tolerance to Coal Contaminants
SC0002491	Mo-Sci Corporation	High-Temperature Viscous Sealing Glasses for Solid Oxide Fuel Cells

Note: Previous contract number ER86387 (Faraday Technology) is now reported under FE0006165.

Projects Discontinued Since the FY 2009 Annual Report

Contract Number	Performer	Project Topic
41567	Virginia Polytechnic Institute and State University	A Low-Cost Soft-Switched DC-DC Converter for Solid Oxide Fuel Cells
41817	American Society of Mechanical Engineers (ASME)	SOFC Design Basis Development Project
41817	Carnegie Mellon University	TEM Investigations of SOFCs: Stability of LSCF-based Cathodes
41817	University of California	High Efficiency Coal Gasification-Based SOFC Power Plants
42219	Georgia Institute of Technology	Novel Sulfur-Tolerant Anodes for Solid Oxide Fuel Cells
42533	Tennessee Technological University	Novel Composite Materials for SOFC Cathode-Interconnect Contact
42613	Siemens Energy, Inc.	Coal Gas-Fueled SOFC Hybrid Power Systems with CO_2 Separation
42735	Georgia Institute of Technology	Characterization of Atomic and Electronic Structure of Electrochemically Active SOFC Cathode Surfaces
43063	University of Texas at San Antonio	Novel Low Temperature Solid State Fuel Cells
44036	Montana State University	SECA Coal-Based Systems Core Research – Montana State University
84209	Phoenix Analysis & Design Technologies	Anode and Cathode Blower Systems for SOFC
84210	R&D Dynamics Corporation	Foil Gas Bearing Supported High-Speed Centrifugal Anode Gas Recycle Blower

Note: Previous contract number FWP44036 (Pacific Northwest National Laboratory) is now reported under FWP40552. Contract number NT0003893 [Rolls-Royce Fuel Cell Systems (U.S.) Inc.] has been changed to FE0000303.

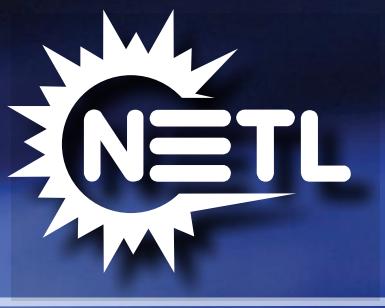

National Energy Technology Laboratory

1450 Queen Avenue SW
Albany, OR 97321-2198
541-967-5892

3610 Collins Ferry Road
P.O. Box 880
Morgantown, WV 26507-0880
304-285-4764

626 Cochrans Mill Road
P.O. Box 10940
Pittsburgh, PA 15236-0940
412-386-4687

Dr. Daniel Driscoll
Technology Manager - Fuels/Fuel Cells
304-285-4717
daniel.driscoll@netl.doe.gov

Visit the NETL website at:
www.netl.doe.gov

Customer Service:
1-800-553-7681

DOE/NETL-2012/1584